Spatial and temporal patterns of crop yield and marginal land in the Aral Sea Basin: derivation by combining multi-scale and multi-temporal remote sensing data with a light use efficiency model

Dissertation zur Erlangung des naturwissenschaftlichen Doktorgrades der Julius-Maximilians-Universität Würzburg

Vorgelegt von Sebastian Fritsch

Würzburg, Februar 2013

Eingereicht am: 18.02.2013
von: Sebastian Fritsch
am: Lehrstuhl für Fernerkundung der Julius-Maximilians-Universität Würzburg, in Kooperation mit dem Deutschen Zentrum für Luft- und Raumfahrt (DLR)

Mentoren: Prof. Dr. Christopher Conrad, Dr. Gerd Rücker

1. Gutachter: Prof. Dr. Christopher Conrad
2. Gutachter: Prof. Dr. Heiko Paeth

1. Prüfer: Prof. Dr. Christopher Conrad
2. Prüfer: Prof. Dr. Jürgen Rauh

Tag der mündlichen Prüfung:
Urkunde ausgehändigt am:

Abstract

Agriculture in the Khorezm region in the arid inner Aral Sea Basin faces enormous challenges due to a legacy of cotton monoculture, non-sustainable water use and future uncertainties concerning climate-induced changes to water supply. Regional crop growth monitoring and yield estimation continuously gain in importance, especially with regard to climate change and food security issues. Remote sensing is the ideal tool for regional-scale analysis, especially in regions where ground-truth data collection is difficult and data availability is scarce. New and operational satellite systems and technologies promise high spatial and temporal resolutions as well as applicability due to specific spectral characteristics, thus providing greater benefit for the potential users. So-called light use efficiency (LUE) models are based on the fraction of photosynthetic active radiation absorbed by vegetation (FPAR), a biophysical parameter that can be derived from satellite measurements. The general objective of this thesis was to use satellite data, in conjunction with an adapted LUE model, for inferring crop yield of cotton and rice at field (6.5 m) and regional (250 m) scale for multiple years (2003-2009), in order to assess crop yield variations in the study area. Validation of the input data (satellite measurements) as well as the results (crop yields) was essential for the approach.

Intensive field measurements of FPAR were conducted in the Khorezm region during the growing season 2009. The sampling design was implemented according to international standards. RapidEye imagery was acquired approximately bi-weekly during the growing season 2009 and also covered the period of ground sampling. Image acquisition failed only in the beginning of the season (April and early May). The normalized difference vegetation index (NDVI) was calculated for all images. Afterwards, image segmentation of the RapidEye data was conducted and the NDVI was additionally calculated for each resulting image object. Linear regression between image-based NDVI and field-based FPAR was conducted. The analyses resulted in high correlations. The resulting regression equations were used to generate field and image-based time series of FPAR. RapidEye-based FPAR was subsequently aggregated to the MODIS scale and used to validate the existing MODIS FPAR product. This step was carried out to evaluate the applicability of MODIS FPAR for regional vegetation monitoring. The validation revealed that the MODIS product generally overestimates RapidEye FPAR by about 6 to 15 %. More problematic was the pixel size of the MODIS product. At the 1 km scale, sub-pixel mixture of crop types is large and prevents the use of the MODIS FPAR product for crop-specific analyses. Mixture of crop types was found to be less severe at the 250 m scale, which allowed identifying

spatial patterns in the study region much more clearly. Consequently, high resolution FPAR was used to calibrate 250 m MODIS vegetation index data, this time by linear regression of RapidEye-based FPAR against MODIS-based NDVI. A comparison of different MODIS vegetation index products showed that the NDVI, calculated from the 8-day MODIS surface reflectance product, was best suited for vegetation monitoring in Khorezm.

The established FPAR datasets, for both RapidEye and MODIS, were subsequently assimilated into a light use efficiency model as the driving variable. This model operated at both satellite scales, and both required an estimation of the photosynthetic active radiation (PAR) and the actual light use efficiency (LUE_{act}). PAR was calculated based on *in situ* meteorological data, geographical location of the region and time of year. LUE_{act} depends on the maximum light use efficiency (LUE_{max}) of each crop and stress factors that constrain LUE_{max} to LUE_{act}. For this study, it was assumed that crops are subject to temperature and especially water stress. While the first was calculated from meteorological measurements, the latter was derived as the ratio between the actual crop evapotranspiration (ET_{act}) and the potential crop evapotranspiration under optimal conditions (ET_c). ET_{act} was estimated using a modified version of the remote sensing-based evapotranspiration algorithm SEBAL. ET_c was calculated by the Penmain-Monteith approach in combination with seasonal parameters from remote sensing data. Besides LUE_{max}, the models depended on the harvest index (H_i) to determine the ratio between end-of-season biomass and final crop yield. The initial values for H_i were taken from literature. Afterwards they were down-regulated based on the mean water stress during the season. Finally, crop maps were used to apply the crop-specific parameters of the model to single fields or pixels. The RapidEye and MODIS time series were interpolated to daily data for use in the LUE model. At the MODIS scale, the start and end of the season (SoS and EoS) were estimated using the TIMESAT software to constrain the seasonal calculation period of the model runs for the years 2003 to 2009.

The variation of the parameters used in the model was investigated at the MODIS scale. The estimated start and end of the season were relatively stable throughout the years. According to the estimates, the cotton season starts in May and ends in late September. The season for rice starts in June and also ends in September. Comparison with published values indicated that the seasonal parameters were estimated with acceptable accuracy, but that the end of the season (corresponding to the time of harvest) of rice was underestimated by nearly a month. Water stress typically occurred between the beginning of May and mid-September and beginning of May and end of July for cotton and rice crops, respectively. The mean water stress showed only minor differences between years. Exceptions occurred in 2008 and 2009, where the mean water stress was higher and lower, respectively. In 2008, this was likely caused by generally reduced water availability in the whole region. There was more variation between years for LUE_{act}, caused by regional temperature variations. However, the overall variation of LUE_{act} was still

small.

Model estimations were evaluated using field-based harvest information (RapidEye) and statistical information at Rayon level (MODIS). The results showed that the model at both the RapidEye and the MODIS scale can estimate regional crop yield with acceptable accuracy. The RMSE for the RapidEye scale amounted to 0.73 $t \times ha^{-1}$ for cotton and 0.98 $t \times ha^{-1}$ for rice, respectively. At the MODIS scale, depending on the year and evaluated at Oblast level, the RMSE ranged from 0.4 $t \times ha^{-1}$ to 0.67 $t \times ha^{-1}$ for cotton and from 0.68 $t \times ha^{-1}$ to 1.13 $t \times ha^{-1}$ for rice. Altogether, the RapidEye scale model slightly underestimated cotton (bias = 0.22) and rice yield (bias = 0.11). The MODIS scale model, on the other hand, also underestimated official rice yield (bias from 0.01 to 0.87), but overestimated official cotton yield (bias from -0.28 to -0.6). Evaluation of the MODIS scale revealed that predictions were very accurate for some Rayons, but less for others. The correlation of the results at the RapidEye and MODIS scales was high, with correlation coefficients ranging from 0.75 to 0.86 for cotton and from 0.64 to 0.79 for rice. The variation depended on the percentage of sub-pixel crop cover. A simple sensitivity analysis at the RapidEye scale showed that different initial values for H_i and LUE_{max} would have led to an altogether slightly lower RMSE.

At the RapidEye scale, mean cotton yield was estimated to be 1.81 $t \times ha^{-1}$. Mean rice yield was estimated to be 3.61 $t \times ha^{-1}$. Mean cotton yield at the MODIS scale ranged from 2.7 $t \times ha^{-1}$ (2008) to 3.1 $t \times ha^{-1}$ (2005, 2007, and 2009), while rice yield ranged from 3.2 $t \times ha^{-1}$ (2008) to 3.9 $t \times ha^{-1}$ (2005). The produced crop yield maps indicated that crop yield generally decreases with distance to the river. The lowest yields can be found in the southern districts, close to the desert. An exception is the Pitnak district, which directly borders the river but is characterized by low yields nonetheless. The found patterns were also confirmed by a geostatistical hot spot analysis. From a temporal point of view, there were areas characterized by low crop yields over the span of the seven years investigated. This information was used as the main input to a GIS-based multicriteria analysis that was conducted to identify marginal land in the Khorezm region. Additional GIS data used in the process consisted of the occurrence of unused land, canal and collector density, groundwater depth and salinity and soil bonitet, which represents a local indicator of land quality.

The study at hand showed that light use efficiency-based modeling, based on remote sensing data, is a viable way for regional crop yield prediction. The found accuracies were acceptable within the boundaries of related research. Although additional validation and slight modifications to the model are necessary, it can be used with its constraints in mind. The model itself was adapted to the study area by incorporating parameters that represent the prevailing agricultural and environmental conditions. Many existing studies on LUE-based crop yield modeling incorporate different parameters in their models, and it is important that certain parameterizations are

not only copied from literature. From a methodological viewpoint, the work carried out made several improvements to the existing LUE models reported in the literature. These improvements included the use of annual crop yield maps in the modeling process, the calibration of FPAR for the study region using *in situ* and high resolution RapidEye imagery, the use of 250 m, 8-day MODIS data for crop yield modeling, the incorporation of crop-specific water stress in the calculation and the implementation for multiple years. Most important of all, this study presented the first application of LUE modeling at the field scale based on RapidEye imagery. New generations of satellite sensors, like RapidEye and the future Sentinel sensors, will open up new possibilities of field-based crop yield studies. Yet both the RapidEye and the MODIS scale are important for agricultural research. As mentioned above, sensors like RapidEye bring new options to the table. But MODIS is still best suited for large-scale investigations, and it additionally allows the view back in time.

Zusammenfassung

Die Landwirtschaft in der Region Khorezm im inneren Aralseebecken sieht sich enormen Herausforderungen gegenüber, ausgelöst durch den langjährigen Anbau von Baumwolle in Monokultur, eine nicht nachhaltige Wassernutzung sowie ungewissen Änderungen des regionalen Wasserangebots im Zuge des Klimawandels. In diesem Zusammenhang gewinnen die satellitengestützte überwachung der Landwirtschaft sowie regionale Ernteabschätzungen immer mehr an Bedeutung, besonders mit Blick auf die regionale Nahrungssicherheit und dem Handel mit landwirtschaftlichen Produkten. Die satellitenbasierte Fernerkundung ist ein ideales Werkzeug für regionale Analysen, vor allem in datenarmen und schwer zugänglichen Regionen. Neue und operationelle Satellitensysteme und -Technologien versprechen potentiellen Nutzern eine höhere räumliche und zeitliche Auflösung, sowie verbesserte Anwendbarkeit aufgrund ihrer spektralen Charakteristika. Sogenannte Lichtnutzungseffizienzmodelle (im Englischen "Light Use Efficiency (LUE) Models" genannt) basieren auf dem Anteil der photosynthetisch aktiven Strahlung, der von Pflanzen für ihr Wachstum aufgenommen wird (FPAR: "Fraction of Photosynthetic Active Radiation"). Dieser wichtige biophysikalische Parameter kann aus Satellitenmessungen abgeleitet werden. Das allgemeine Ziel der vorliegenden Arbeit war die Nutzung von Satellitendaten für die Ableitung der Erntemengen von Baumwolle und Reis. Dazu wurde ein Modell entwickelt, das sowohl auf der Feldebene (Auflösung von 6,5 m) als auch auf der regionalen Ebene (Auflösung von 250 m) operieren kann. Während die Ableitung der Erntemengen auf der Feldebene nur für ein Jahr erfolgte (2009), wurden sie auf der regionalen Ebene für den Zeitraum 2003 bis 2009 modelliert. Damit soll eine Beurteilung des Produktivität der Landwirtschaft im Studiengebiet ermöglicht werden. Besonderes Augenmerk wurde dabei auf die Validierung der Eingangsdaten (Satellitenmessungen und -Produkte) sowie der Ergebnisse (Erntemengen) gelegt.

Intensive Feldmessungen von FPAR wurden im Studiengebiet, der usbekischen Region Khorezm, während der Wachstumssaison 2009 durchgeführt. Die Messungen richteten sich dabei nach internationalen Standards. Bilddaten der RapidEye-Sensoren wurden in diesem Zeitraum ebenfalls mit zweiwöchentlichem Abstand aufgenommen. Diese Aufnahmen misslangen lediglich ganz am Anfang der Saison (April und Mai-Beginn). Ein erster Vorverarbeitungsschritt war die Berechnung des "Normalized Difference Vegetation Index" (NDVI) für alle vorhandenen Bilder. Danach wurde eine Bildsegmentierung der RapidEye-Daten durchgeführt, wodurch spektral homogene Bildobjekte generiert wurden. Für diese wurde ebenfalls ein separater NDVI-Wert ermittelt. Anschliessend wurden lineare Regressionsanalysen zwischen dem bildbasierten NDVI

und den FPAR-Feldmessungen durchgeführt. Die Analysen ergaben eine sehr hohe Korrelation der Daten. Die ermittelten Regressionsgleichungen wurden benutzt um FPAR-Zeitserien sowohl auf Objekt- als auch auf Pixel-Ebene zu generieren. Die Ergebniskarten auf Pixel-Ebene wurden dann auf die MODIS-Skala aggregiert (250 m und 1 km) und zur Validierung des existierenden MODIS FPAR-Produkts genutzt. Dieser Schritt war notwendig, um die Anwendbarkeit dieses Produkts für das Vegetations-Monitoring im Studiengebiet zu überprüfen. Die Validierung zeigte, dass das MODIS-Produkt im Allgemeinen die RapidEye-basierten FPAR-Werte um 6 bis 15 % überschätzt. Als problematisch erwies sich auch die Pixelgrösse des MODIS-Produkts. Auf der 1 km-Skala gibt es häufig Mischpixel, die verschiedene Bedeckungsgrade unterschiedlichster Feldfrüchte beinhalten. Dadurch ist das Produkt für feldfrucht-spezifische Analysen nur eingeschränkt nutzbar. Die Anzahl der Mischpixel, sowie deren Mischungsgrade, waren deutlich niedriger auf der 250 m-Skala. Dadurch konnten räumliche FPAR-Muster im Studiengebiet wesentlich deutlicher identifiziert werden. Als Resultat wurden anschliessend die hochaufgelösten FPAR-Karten für die Kalibrierung von 250 m MODIS Vegetationsindizes genutzt. Dieser Schritt erfolgte nun über eine lineare Regression des RapidEye-basierten FPAR mit MODIS-basiertem NDVI. Der Vergleich verschiedener MODIS-basierter Vegetationsindex-Produkte zeigte, dass der auf 8-tägigen Oberflächen-Reflektanzen basierende NDVI am besten für das Vegetations-Monitoring in Khorezm geeignet war.

Die FPAR-Datensätze auf RapidEye- und MODIS-Ebene wurden anschliessend als Haupteingangsparameter in das LUE-Modell integriert. Beide Modellebenen benötigten eine Abschätzung der photosynthetisch aktiven Strahlung ("Photosynthetic Active Radiation", PAR) sowie der tatsächlichen Lichtnutzungseffizienz ("Actual Light Use Efficiency", LUE_{act}). Die Berechnung von PAR basierte auf *in situ* aufgezeichneten meteorologischen Daten, der geographischen Lage des Studiengebietes und dem Tag im Jahr. Der Parameter LUE_{act} basiert auf der maximalen Lichtnutzungseffizienz (LUE_{max}) einzelner Feldfrüchte. LUE_{max} wird dabei dynamisch durch Umweltstressfaktoren auf LUE_{act} reduziert. Für die vorliegende Arbeit wurde davon ausgegangen, dass Feldfrüchte im Studiengebiet vor allem Temperatur- und Wasserstress ausgesetzt sind. Der Temperaturstress der Pflanzen wurde aus meteorologischen Messungen abgeleitet. Der Wasserstress hingegen wurde berechnet als das Verhältnis von tatsächlicher Evapotranspiration (ET_{act}) zu potentieller, feldrucht-spezifischer Evapotranspiration unter optimalen Bedingungen (ET_c). ET_{act} wurde mit Hilfe einer modifizierten Version des SEBAL-Modells ermittelt, eines satellitenbasierten Evapotranspirationsalgorithmus. ET_c wurde berechnet mittels des Penman-Monteith-Ansatzes, kombiniert mit aus MODIS-Zeitserien abgeleiteten saisonalen Parametern. Beide Modellebenen hängen neben dem Parameter LUE_{max} vor allem stark vom sogenannten Ernteindex ("Harvest Index", H_i) ab. Dieser drückt das Verhältnis von absoluter Biomasse am Ende der Saison zum tatsächlichen Ernteanteil aus. Die Startwerte des Ernteindex wurden der Literatur entnommen. Danach erfolgte eine dynamische Regulierung in Abhängigkeit des durchschnittlichen Wasserstresses während der Wachstumssaison. Schliesslich wurden Land-

nutzungskarten benötigt, um die feldfrucht-spezifischen Parameter der Modelle einzelnen Pixeln oder Feldern zuordnen zu können. Die RapidEye- und MODIS-Zeitserien wurden durch lineare Interpolation auf tägliche Zeitschnitte gebracht, eine Voraussetzung für die Anwendung des LUE-Modells. Für die MODIS-Skala wurden Start (SoS) und Ende der Saison (EoS) mittels des Programms TIMESAT abgeschätzt. Beide Parameter wurden anschliessend genutzt um die Berechnungszeiträume für die Jahre 2003 bis 2009 auf die tatsächliche Wachstumssaison zu begrenzen.

Die Variation der im Modell benutzten Parameter wurde vor allem auf der MODIS-Ebene untersucht. Abgeleitete Werte für den Start und das Ende der Saison waren für alle Jahre relative stabil. Den Schätzungen zufolge beginnt die Baumwollsaison im Mai und endet im September. Für Reis hingegen startet die Saison im Juni und endet ebenfalls im September. Ein Vergleich mit Literaturwerten deutete auf eine akzeptable Genauigkeit der abgeschätzten Werte hin. Dabei wurde jedoch das Ende der Reis-Saison (gleichgestellt mit dem Erntezeitpunkt) um bis zu einem Monat zu früh geschätzt. Wasserstress bei Baumwollpflanzen trat typischerweise zwischen Anfang Mai und Mitte September auf, bei Reis hingegen zwischen Anfang Mai und Ende Juli. Der durchschnittliche Wasserstress schwankte nur geringfügig von Jahr zu Jahr. Ausnahmen traten in den Jahren 2008 und 2009 auf. Im Jahr 2008 war der durchschnittliche Wasserstress höher als in anderen Jahren, im Jahr 2009 hingegen niedriger. Im Jahr 2008 lag dies mutmasslich an der generell geringeren Wasserverfügbarkeit in der gesamten Region. Der Parameter LUE_{act} zeigte grössere Schwankungen von Jahr zu Jahr, was auf regionale Temperaturschwankungen zurückgeführt werden kann. Die absolute Schwankung von LUE_{act} war jedoch immer noch gering.

Die Modellschätzungen wurden durch feldbasierte Ernteinformationen (RapidEye-Ebene) sowie regionale statistische Daten (MODIS-Ebene) evaluiert. Die Ergebnisse zeigten, dass beide Modellskalen regionale Ernteerträge mit akzeptabler Genauigkeit nachbilden können. Der RMSE für das RapidEye-basierte Modell betrug 0,73 $t \times ha^{-1}$ für Baumwolle und 0,98 $t \times ha^{-1}$ für Reis. Die Genauigkeiten für das MODIS-basierte Modell variierten, in Abhängigkeit des betrachteten Jahres, zwischen 0,4 $t \times ha^{-1}$ und 0,67 $t \times ha^{-1}$ für Baumwolle und zwischen 0,68 $t \times ha^{-1}$ und 1,13 $t \times ha^{-1}$ für Reis. Insgesamt gab es eine leichte Unterschätzung der Baumwoll- (Bias = 0,22) und Reisernte (Bias = 0,11) seitens des RapidEye-Modells. Das MODIS-Modell hingegen unterschätzte zwar auch die (offizielle) Reisernte (mit einem Bias zwischen 0,01 und 0,87), überschätzte jedoch die offiziellen Erntemengen für die Baumwolle (Bias zwischen -0,28 und -0,6). Die Evaluierung der MODIS-Skala zeigte dass die Genauigkeiten extrem zwischen den verschiedenen Rayonen schwankten. Die Korrelation zwischen den Ergebnissen auf RapidEye- und MODIS-Ebene war sehr hoch, mit Korrelationskoeffizienten zwischen 0,75 und 0,86 für Baumwolle und zwischen 0,64 und 0,79 für Reis. Die Koeffizienten schwankten dabei in Abhängigkeit des tatsächlichen Bedeckungsgrades eines MODIS-Pixels mit Baumwolle oder Reis.

Eine einfache Sensitivitätsanalyse auf RapidEye-Ebene zeigte dass unterschiedliche Startwerte für H_i und LUE_{max} insgesamt zu leicht niedrigeren Fehlern geführt hätte.

Die Modellläufe ergaben eine durchschnittliche Baumwollernte auf RapidEye-Skala von 1,81 $t \times ha^{-1}$, und eine mittlere Reisernte von 3,61 $t \times ha^{-1}$. Die durchschnittliche Baumwollernte auf der MODIS-Skala reichte von 2,7 $t \times ha^{-1}$ (2008) bis zu 3,1 $t \times ha^{-1}$ (2005, 2007 und 2009), während die Reisernte zwischen 3,2 $t \times ha^{-1}$ (2008) und 3,9 $t \times ha^{-1}$ (2005) schwankte. Die erstellten Karten zeigten dass Erntemengen grundsätzlich mit der Distanz zum Fluss abnehmen. Die niedrigsten Erntemengen traten in den südlichsten Distrikten auf, in der Nähe der Wüste. Eine Ausnahme bildet der Distrikt Pitnak, welcher trotz direkter Nähe zum Fluss von sehr niedrigen Erntemengen gekennzeichnet ist. Die ermittelten Muster wurden auch unterstützt durch eine geostatistische Hot Spot-Analyse der Ergebniskarten. Betrachtet man die Ergebnisse über die Zeit hinweg, gab es Gebiete die über den gesamten Zeitraum von sieben Jahren stets von niedrigen Erntemengen gekennzeichnet waren. Die Information über die Verteilung dieser Gebiete wurde als Haupteingangsdatensatz für eine GIS-basierte Multikriterienanalyse zur Identifikation von marginalem Land in Khorezm genutzt. Weitere GIS-Daten die für diesen Schritt genutzt wurden bestanden aus der Häufigkeit von Brache, den Dichten von Kanälen und Kollektoren, der Grundwassertiefe und -Salinität und der Bodengüte, die einen örtlichen Indikator für die Qualität von Land darstellt.

Die vorliegende Studie zeigt dass satellitenbasierte Lichtnutzungseffizienzmodelle ein geeignetes Werkzeug für die Ableitung und die Analyse regionaler Erntemengen in zentralasiatischen Bewässerungsregionen darstellen. Verglichen mit verwandten Studien stellten sich die ermittelten Genauigkeiten sowohl auf der RapidEye- als auch auf der MODIS-Skala als gut dar. Leichte änderungen an den Modellparametern (LUE_{max}, H_i) sowie eine weitere Validierung des Modells (Felddaten) sind notwendig. Trotzdem kann das Modell im derzeitigen Zustand eingesetzt werden, wenn man sich der Einschränkungen bewusst ist. Das Modell selbst wurde für das Studiengebiet kalibriert indem Parameter integriert wurden, die die lokalen agronomischen und umweltbedingten Gegebenheiten widerspiegeln. Viele existierende Studien zum Thema Erntemodellierung mit LUE-Modellen integrieren andere Parameter in ihren Modellen, und es ist von grösster Wichtigkeit dass bestimmte Modellparametrisierungen nicht einfach aus der Literatur übernommen werden. Von einem methodischen Standpunkt aus gesehen ergänzte diese Arbeit vorhandene LUE-Modelle um einige Neuerungen und Verbesserungen. Dazu zählen: die Nutzung jährlicher Landnutzungskarten für die Modellierung, die Kalibrierung von FPAR für die Studienregion mittels Feld- und hochaufgelösten RapidEye-Daten, die Nutzung von 8-tägigen MODIS-Daten mit einer räumlichen Auflösung von 250 m, der Einbezug von feldfruchtspezifischem Wasserstress in die Modellierung sowie die Anwendung über mehrere Jahre. Der wichtigste Punkt in dieser Arbeit ist allerdings die Nutzung neuartiger RapidEye-Daten für die feldbasierte Erntemodellierung. Neue Generationen von Satellitensensoren, wie etwa RapidEye

oder der kommende Sentinel-2-Sensor, eröffnen neue Möglichkeiten der feldbasierten Erntemodellierung. Trotzdem ist und bleibt auch die MODIS-Skala wichtig für landwirtschaftliche Studien, da diese Daten am besten geeignet sind für grossflächige Anwendungen und vor allem für Studien, die vergangene Zeiträume betreffen.

Contents

List of Abbreviations

AGBM	Aboveground Biomass
APAR	Absorbed Photosynthetically Active Radiation
ASB	Aral Sea Basin
AVHRR	Advanced Very High Resolution Radiomter
AWIFS	Advanced Wide Field Sensor
BPLUT	Biome Properties Look-Up Table
CAM	Crassulacean Acid Metabolism
CART	Classification and Regression Trees
CASA	Carnegie Ames Stanford Approach
CASI	Compact Airborne Spectrographic Imager
CRI	Cotton Research Institute
CV	Coefficient of Variation
DAO	Data Assimilation Office
DLR	Deutsches Zentrum für Luft- und Raumfahrt (German Aerospace Agency)
EF	Evaporative Fraction
EOS	End of Season
ESU	Elementary Sampling Unit
ET	Evapotranspiration
ET_{act}	Actual Evapotranspiration
ETM	Enhanced Thematic Mapper
ET_{pot}	Potential Evapotranspiration
ET_{ref}/ET_0	Reference Evapotranspiration
EU	European Union
EVI	Enhanced Vegetation Index
FAO	Food and Agricultural Organization
FIPAR	Fraction of Intercepted Photosynthetically Active Radiation
FPAR/FAPAR	Fraction of Absorbed Photosynthetically Active Radiation
FSU	Former Soviet Union
G_0	Ground Heat Flux
GDD	Growing Degree Days
GDP	Gross Domestic Product
Geo-TIFF	Geographic Tagged Image File Format

GIS	Geographic Information System
GLO-PEM	Global Production Efficiency Model
GPP	Gross Primary Productivity
GPS	Global Positioning System
H	Sensible Heat Flux
HDF	Hierachical Data Format
H_i	Harvest Index
H_{iact}	Actual Harvest Index
H_{imax}	Maximum Harvest Index
IDW	Inverse Distance Weighted
IPAR	Intercepted Photosynthetically Active Radiation
IPCC	Intergovernmental Panel on Climate Change
JRC	Joint Research Center
K_c	Crop Coefficient
L1B	Level 1 B
LAI	Leaf Area Index
λE	Latent Heat Flux
LSWI	Land Surface Water Index
LUE	Light Use Efficiency
LUT	Look-Up Table
MARS	Monitoring Agriculture with Remote Sensing
MCA	Culticriteria Analysis
MOD09GQ	MODIS Daily Surface Reflectance Product
MOD09Q1	MODIS 8-day Surface Reflectance Product
MOD12Q1	MODIS Land Cover Product
MOD13Q1	MODIS 16-day Vegetation Index Product
MOD15A2	MODIS LAI/FPAR Product
MOD17A2	MODIS GPP Product
MODAPS	MODIS Adaptive Processing System
MODIS	Moderate Imaging Spectroradiometer
MRT	MODIS Reprojection Tool
MVC	Maximum Value Composite
NASA	National Aeronautics and Space Administration
NDVI	Normalized Difference Vegetation Index
NEP	Net Ecosystem Productivity
NIR	Near Infrared
NPP	Net Primary Productivity
PAR	Photosynthetically Active Radiation
PE	Percentage Error

PEM	Production Efficiency Model
P_n	Net Photosynthesis
PRI	Photochemical Reflectance Index
P_s	Gross Photosynthesis
PS	Photosynthesis
QA-SDS	Quality Assessment Science Data Set
QB	Quickbird
R_a	Autotrophic Respiration
RE	RapidEye
RESA	RapidEye Science Archive
R_{glob}	Global Radiation
RH	Relative Humidity
R_h	Heterotrophic Respiration
R_m	Mitochondrial Respiration
RMSE	Root Mean Square Error
R_n	Net Radiation
R_p	Rate of Photorespiration
RS	Remote Sensing
RTM	Radiative Transfer Model
RUE	Radiation Use Efficiency
SANIIRI	Central Asian Research Institute of Irrigation
SEBAL	Surface Energy Balance Algorithm for Land
SoS	Start of Season
SPOT	Satellite Pour l'Obsérvation de la Terre
SR	Simple Ratio
SRTM	Shuttle Radar Topography Mission
STD	Standard Deviation
SWIR	Shortwave Infrared
T	Temperature
T_{base}	Base Temperature
TM	Thematic Mapper
T_{max}	Maximum Temperature
T_{opt}	Optimal Temperature
T_s	Temperature Stress
T_{savg}	Average Temperature Stress (during growing season)
UN	United Nations
UNESCO	United Nations Educational, Scientific and Cultural Organization
UTM	Universal Transverse Mercator
VALERI	Validation of European Remote Sensing Instruments

VI	Vegetation Index
VPD	Vapor Pressure Deficit
VPM	Vegetation Productivity Model
WCA	Water Consumers Association
WDRVI	Wide Dynamic Range Vegetation Index
WFP	World Food Programme
WFS	World Food Summit
WGS	World Geodetic System
W_s	Water Stress
WUA	Water Users Association
ZEF	Zentrum für Entwicklungsforschung (Center for Development Research)

List of Figures

List of Tables

1 Introduction

1.1 Background and motivation

Altogether 12 % of the earths ice free land surface today is covered by cropland. The global area of croplands and pastures increased by 3 % between 1985 and 2005 (Foley et al. 2011). Global croplands form the basis of our daily food supply and large parts of the population depend on smallholder and subsistence farming. In developing countries, smallholder agriculture makes up to 50 % of all agricultural activities (Morton 2007). Agriculture is thus a key element for rural livelihoods. Furthermore many countries also rely on agricultural exports to receive foreign currency. Yet one can observe negative tendencies concerning agricultural land at the global scale. Despite climatic conditions that are similar to countries with higher yields, many countries have crop yields far below the global average (Licker et al. 2010). A high percentage of agricultural land is not in use at all due to political transformation processes, especially in some parts of Eastern Europe (Prishchepov et al. 2012). Finally, many croplands are either physically marginal (Cassel-Gintz et al. 1997) or in danger of degradation due to a general intensification of agriculture (Foley et al. 2011).

Consequently, a functioning agricultural sector is important for income generation, at the state and at the local level, but at the same time global croplands show subpar performance, are not in use at all or are in danger of being marginalized. In the light of a growing world population, the strife to achieve food security while protecting the environment and sustainably use land resources becomes paramount. Food security can be defined as the 'condition in which a population has physical, social, and economic access to sufficient safe and nutritious food over a given period, to meet dietary needs and preferences for an active life' (Justice & Becker-Reshef 2007, p.11). The Global Hunger Index 2008 demonstrated that undernourishment is still a prevalent issue worldwide, especially in developing countries and countries in transition (von Grebmer et al. 2008, FAO 2006). Furthermore, changing dietary patterns due to economic growth leads to a higher demand for feed instead of food production (Licker et al. 2010).

Cropland is thus experiencing more and more pressure to increase its productivity, as a further expansion of agricultural area is an unsustainable option (Foley et al. 2011). Although average yields have increased around 20 % between 1985 and 2005, there is little potential for further increases in many developed countries (Foley et al. 2011). The combination of population

growth, economic interest, land use change, cultivation of biofuels and environmental problems are predicted to cause serious problems by 2050 (Hertel 2011).

On top of these existing burdens, climate change will have a substantial influence on agriculture in the next decades, which, in the major part of the world, will most likely be negative (Schmidhuber & Tubiello 2007). Some negative influences of temperature trends on maize and wheat production have already been observed for the period 1980 to 2008 (Lobell et al. 2011). According to the Fourth Assessment Report of the Intergovernmental Panel on Climate Change (IPCC), agriculture in developing countries is much more exposed to the effects of climate change than agriculture in developed countries (Parry et al. 2007). Whether induced by climate change or recurring natural variability, droughts can have severe effects on vegetation and agriculture (Gobron et al. 2005). Regional patterns differ, but drought events will likely occur more often in the future (Battisti & Naylor 2009). These developments are problematic, as nowadays already approximately 85 % of all water resources are consumed by agriculture (Gleick 2003). Irrigated areas already make up 17 % of global agriculture (Seckler et al. 1998), and this number is likely to grow in the future (Lobell et al. 2008). Crop yields have shown to drop considerably without irrigation, especially in arid and semi-arid regions (Siebert & Döll 2010). Yet at the same time irrigation is responsible for vast environmental problems in many parts of the world (Dougherty et al. 1995), which is partly because irrigation systems are also ineffective and often perform below their potential (Bos et al. 2005).

Despite irrigation, the difference between actual and potential yield is still large in many emerging and developing countries. This difference is also called the 'yield gap' (Lobell et al. 2009, Licker et al. 2010). The fact that there are still large yield gaps worldwide (Lobell et al. 2009), and the limited availability of land that can be utilized for agricultural production, demonstrates the need for a sustainable management of existing resources. Arid and semi-arid areas are especially vulnerable to global climate and environmental change in this context. Climatic conditions lead to agriculture being dependent on irrigation, with high water withdrawals but low yields, and the danger of land degradation (e.g., Saiko & Zonn 2000). Studies have shown that, in order to meet future water demands, severe changes in water use efficiency (WUE) and water allocation are required (Ragab & Prudhomme 2002). Yet a higher WUE is not easily obtained and requires continuous training and education of all involved stakeholders (Gleick 2003). All these factors add to the general vulnerability of semi-arid and arid regions and are largely responsible for the general underperformance of agriculture in those regions (Cassel-Gintz et al. 1997). Amongst those physically marginal areas, characterized by a long history of human mismanagement and political changes that highly influenced the economic and ecological situation, Central Asia is a prime example of the interdependency of all above-mentioned processes.

Central Asia comprises the countries of Uzbekistan, Kazakhstan, Tajikistan, Kyrgyzstan, and Turkmenistan. Its climate, especially in the inner Aral Sea Basin, is dry and continental (figure 1.1). Extensive regional irrigated crop production has led to immense ecological problems and depleted water resources to the point where the two Aral Sea tributaries, the Amu Darya and the Syr Darya, hardly reach their downstream regions in years of water scarcity (FAO/WFP 2000). Central Asia is nowadays infamously known for the Aral Sea disaster, which was a result of expanding cotton production since the 1960s (Micklin 2010) and will be further described in chapter 2. Central Asian countries display an increased natural vulnerability, owing to the highly variable (semi-)arid climate, the subsequent insufficient precipitation during the growing season and the resulting dependency on river water for the vast irrigation systems in the region (Ososkova et al. 2000). The problem is that the region is also one of the current and future 'hot spots' of climate change (Parry et al. 2007). Its population is mainly working within the primary sector and country exports rely on agricultural goods (FAO 2012).

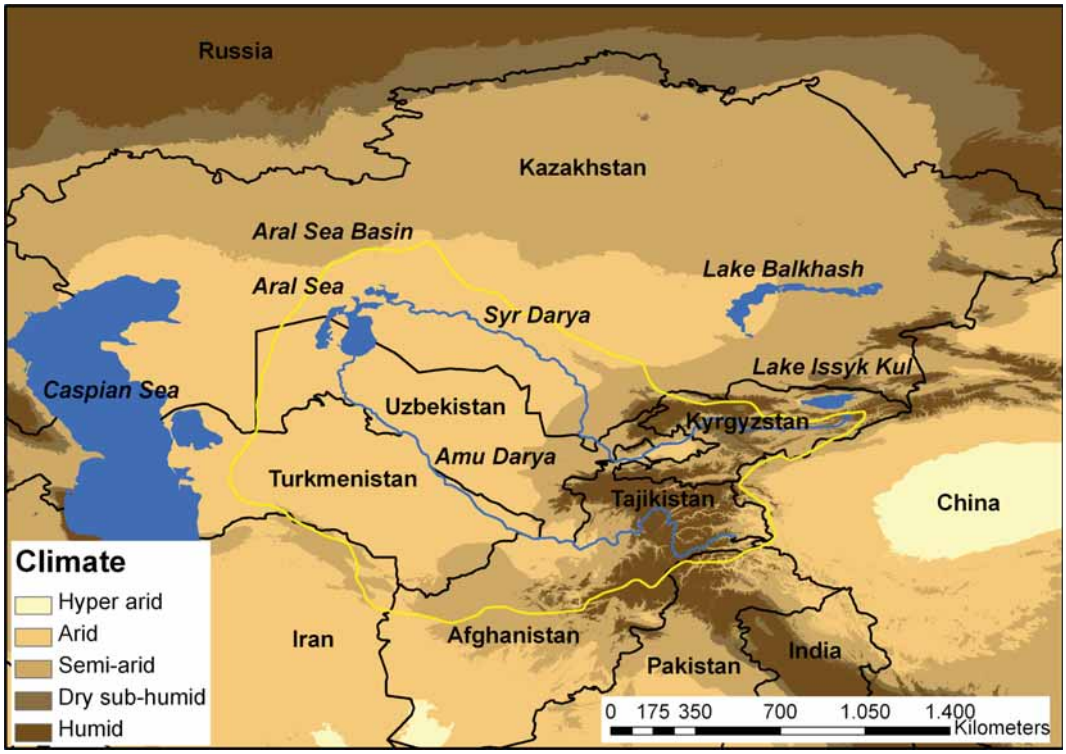

Figure 1.1: Climatic conditions in Central Asia and neighboring countries. The map is based on the Aridity Index described by (Zomer et al. (2008)).

The consequences of climate change will amplify current problems in the region. The Third IPCC Assessment Report states that the water situation will only worsen in the course of global climate change (Ragab & Prudhomme 2002, Parry et al. 2007). The projected (2080-2099) temperature increase will be 3.7 °C and the projected precipitation decrease will be 3 mm (Parry et al. 2007). The vulnerability of the local population in the light of climate change is high

and mainly concerns the areas of food security, water availability as well as human health and diseases (Lioubimtseva & Henebry 2009). Water availability and water stress, already frequent in many parts of Central Asia, are likely to worsen with climate change. Available water is supposed to decrease, which increases the risk of hydrological droughts. River discharge is also supposed to become more variable (Lioubimtseva & Henebry 2009). The food situation supposedly worsened in parts of Central Asia in previous years, for example in Uzbekistan (FAO 2006). The country experienced most severe setbacks compared to the WFS goals. In 2008, the situation of food security in Uzbekistan was still declared as 'serious' (von Grebmer et al. 2008). Although nowadays self-sufficient in terms of wheat production (Kienzler et al. 2011), the problems lie in rural poverty and unsustainable rural livelihoods.

A variety of facts contribute to Uzbekistan's current situation. The overall agricultural area, compared to population growth, was declining between 1992 and 2009 (see figure 1.2). Agriculture is the most important economic sector of Uzbekistan, contributing nearly one third to the annual Gross Domestic Product (GDP) and sustaining about 60 % of the rural population (Abdullaev et al. 2009). Exports of raw cotton are strongly needed to earn foreign currency (Roll et al. 2006, Bekchanov et al. 2010). Yet the agricultural productivity of the country is low. Compared to China for example, which has similar climatic conditions but a much more intensified primary sector, cotton yields are markedly lower (WFP 2008). Agriculture plays a major role in Uzbekistan, for the economy as well as in everyday life. For example, farmers and farm workers heavily depend on the cultivation of cotton and rice in Uzbekistan. While cotton production is state-controlled and profits are low, it employs many laborers and secures a livelihood for them and their families. Rice cultivation is solely of commercial nature, and farmers can sell their production freely in the markets. The revenues are highest for rice crops, and workers in the rice sector also receive higher payments (Veldwisch & Spoor 2008). Either way, the cultivation of both cotton and rice sustains rural livelihoods and thus also contributes to local food security. Agricultural production of fiber and food, however, depends on fluctuating and uncertain water resources and water availability. It also takes place on a limited amount of arable land per capita (Bloch 2002), of which more than 80 % must be irrigated (FAO 2011). A wide range of problems is connected to the management of water resources in this region, which are of economic, ecological and structural nature (Vlek et al. 2001, Martius et al. 2012).

One intensively explored study region in Uzbekistan is Khorezm, which is situated in the upper Amu Darya delta in the inner Aral Sea Basin. Many typical problems of Central Asian irrigation systems can be found in this rural region: high groundwater tables, increased soil salinity, insufficient fertilizer amount, unreliable water supply and inadequate distribution (Martius et al. 2005, Martius et al. 2012 see section 2). The result of these influences are crop yields that vary strongly throughout the region (Shi et al. 2007). Water supply and distribution is the

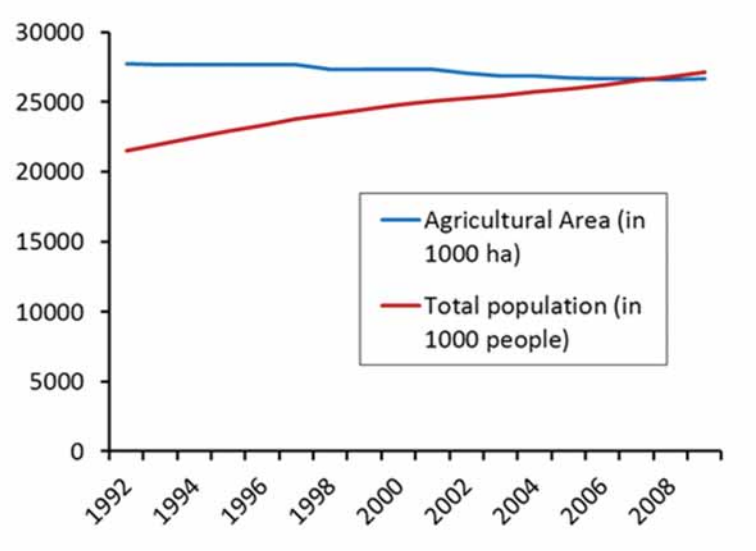

Figure 1.2: Development of agricultural area and total population in Uzbekistan from 1992 to 2009 (source: FAO 2012).

factor that contributes the most to this spatial variability of crop yields and, thus, planning insecurity (Wegerich 2004).

An improved management of limited resources is the most efficient way to tackle current and future challenges of crop production. Besides improved irrigation management an increased agricultural resource efficiency, stopping areal expansion of agriculture, a change of diets, a reduction of the waste of food, and the closing of existing yield gaps belong to options for enhancing food production and agricultural sustainability (Foley et al. 2011). An optimized use of land and water resources is also one of the keys to the improvement of the current ecological and economic situation in Uzbekistan. The German-Uzbek project for 'economic and ecological restructuring of land and water use in the Khorezm region, Uzbekistan' (ZEF 2012) aimed at contributing to this goal. An improved water distribution within the irrigation system, which was also investigated within the framework of the Khorezm project (Schorcht et al. 2009, Conrad et al. 2007), is amongst the most important approaches for sustainable land use. Furthermore, better utilization of agricultural inputs, water and fertilizers, is another option. However, any mechanism to improve the situation depends on spatial information on the performance of the agricultural system. Decision makers and institutions specifically need accurate historical and current information on regional crop growth and yield (Hornidge et al. 2011).

Crop area and yield are the decisive parameters for an assessment of regional crop production. Knowledge on regional crop yields is necessary to assess overall productivity and identify areas with suboptimal crop growth. These areas of 'marginal land' could be the target of alternative, less resource-demanding, land uses that improve rural livelihoods. Furthermore, information on

crop yields is required for the assessment of regional yield gaps. The closing of these gaps is another chance of supporting and improving local and regional livelihoods. In most of Central Asia, however, there is no possibility to conduct the necessary analyses due to a lack of spatial and temporal datasets. The same is true for the Khorezm region. The main goal of this thesis is consequently the development of a suitable methodology for the analysis of regional crop growth, productivity and marginal land. The methodology should be able to assess crop performance on a regional scale for past growing seasons, help to understand yield variations on a field and regional basis, and show potential uses of the generated information in practice. Ideally, statements on crop performance and expected crop yields can already be deduced within-season, in order to achieve a higher planning security and prepare for possible shortcomings in expected crop yields. Such information can be crucial for decision-makers of higher administrative levels and international organizations. On the one hand it allows assessing the potential need for cereal imports to support food security in water scarce years. On the other hand it could be used for a rapid assessment of the annual cotton production, helping to better react to market fluctuations and assess expected revenues from cotton exports.

Remote sensing has proven to be an effective tool for such regional-scale analyses, especially in regions where ground truth data collection is difficult and data availability is scarce. There are numerous studies on the use of satellite data for crop yield modeling and prediction in many parts of the world (see chapter 3). Remote sensing is furthermore stated to be potentially useful for yield prediction in irrigated areas (Bastiaanssen et al. 2000). These developments are in line with the increasing importance of global agricultural monitoring. Efforts are currently undertaken to establish a global agricultural monitoring system of systems (Justice & Becker-Reshef 2007). There are also current operational crop yield monitoring systems at the country level. One of them is the European Monitoring Agriculture with Remote Sensing (MARS) project, coordinated by the Joint Research Center (JRC) of the EU (JRC 2012). The system focuses on Europe, but it is also used for monitoring and forecasting purposes in Africa, Russia, and Central Asia. Seasonal yield forecasts and performance indicators thus become available for Central Asian countries, including Uzbekistan. The main outputs of the system, which is currently in a pilot phase (published every two to three months), are the delineation of winter-wheat areas, decadal precipitation amounts, decadal temperature, decadal NDVI values, country-wide crop status and country-wide anticipated yields. This kind of information is useful for country-wide overviews and early warning, but it is not accurate enough for analyses at the sub-national or local scale due to some drawbacks like the use of coarse resolution satellite data for NDVI calculation (AVHRR 1.1 km data), a limitation of yield predictions to winter wheat, the country-wide aggregation of those predictions, and the lack of a validation of the results. Besides such operational systems there are also global models of vegetation productivity (e.g., Prince & Goward 1995) and crop yield (e.g., Liu 2009 but without the use of remote sensing data), yet the aforementioned drawbacks also apply to these models. Until now there are few

attempts for regional crop yield estimation in Central Asian irrigation systems.

It is obvious that there is a need for a different approach when it comes to crop yield monitoring of irrigation regions such as Khorezm. Furthermore, new and operational satellite systems and technologies promise higher spatial and temporal accuracies as well as applicability due to specific spectral characteristics, thus providing greater benefit for potential users of satellite-derived crop yield information. A corresponding approach will be presented in the next chapters. First, however, an overview of remote sensing for crop yield prediction will be given, and the approach taken in this study will be introduced.

1.2 Remote sensing of crop growth

Satellite data is ideal for regional analyses because of its large area coverage and comparably low or no costs. This advantage is especially useful for application in remote destinations where little or no consistent and reliable data is available, like the Khorezm region or the larger parts of Central Asia in general. Remote sensing has shown to be potentially useful for irrigated agriculture, as it allows deriving some decisive variables needed for water management: land use, irrigated area, crop type, crop yield, daily evapotranspiration (ET), seasonal ET, crop stresses and soil salinity. It can also provide historical data for as long as the sensor has been operational (Bastiaanssen et al. 2000). Following Bastiaanssen et al. (2000), crop yields derived from remote sensing can subsequently be used to assess water productivity, conduct a performance diagnosis, for strategic planning and for impact assessment. Detailed descriptions of remote sensing applications for agricultural purposes, including water management, are given by Pinter et al. (2003) and Hatfield et al. (2008). In general, there are three different ways to use remote sensing for crop yield prediction. According to Moulin et al. (1998) and Delécolle et al. (1992) they can be classified into (1) mechanistic, (2) empirical and (3) semi-empirical approaches. These approaches will be shortly described in the following paragraphs, and the chosen approach will be explained:

1. Mechanistic models integrate existing knowledge on biological systems into mathematical formulations (Delécolle et al. 1992). The subsequent modeling process can be defined as the 'dynamic simulation of crop growth by numerical integration of constituent processes with the aid of computers' (Sinclair & Seligman 1996, p.698). Crop models themselves are a simplified representation of an agricultural system (de Wit 1982). In the Khorezm region, the mechanistic crop model CropSyst (Stöckle et al. 2003) was for example used to simulate optimal growth of cotton crops at plot scale (Sommer et al. 2008). The result of this kind of modeling process is generally very precise and allows a more in-depth analysis of cropping systems (Moulin et al. 1998). Compared to other approaches, however, mechanistic models demand for a lot more input data. This amount of data is nonexistent

for the whole area of the Khorezm region and nearly impossible to collect on a regional and regular basis. Furthermore the actual spatialization of these models often works in combination with radiation transfer models (RTMs) that add another level of complexity and input data demand to the approach (Dorigo et al. 2007). Mechanistic crop models will therefore not be discussed in further detail, because they seem impracticable to use in the framework of this study and the ZEF/UNESCO Khorezm project.

2. Statistical or empirical models represent empirical relations between final crop yields, either derived *in situ* or taken from regional statistics, and one or more environmental factors like weather, soil, or remote sensing-based variables (Delécolle et al. 1992). Statistical approaches using remote sensing data to infer crop yields, or perform crop yield forecasting, have for example been presented for cotton (Dalezios et al. 2001), rice (Wang et al. 2010), and wheat (Becker-Reshef et al. 2010). While mechanistic crop models are mostly point-based, meaning that they are run at plot scale, empirical models are often applied on a regional scale. Despite their simplicity, empirical models have shown to be able to accurately predict regional crop yields in environmentally similar agro-regions (Becker-Reshef et al. 2010). However, there are different obstacles that prevent their use for this study. First, regression equations are only valid for a specific location and a specific period, which limits its transferability. Second, to apply these models at the regional scale a large amount of reliable, statistical yield data is required. This data is difficult to obtain in a lot of countries, including Uzbekistan. Consequently, this type of model was not considered here.

3. Finally, semi-empirical models are in-between mechanistic and empirical models. They mostly keep the deterministic daily time-step, but use simpler equations (Delécolle et al. 1992). The foundation of these models is the light use efficiency approach of Monteith (Monteith 1972, Monteith 1977). The approach is based on the fact that plant dry matter production depends on the absorption of solar radiation, which is expressed as the absorbed photosynthetic active radiation (APAR), and on the so-called light use efficiency (LUE), the efficiency with which plants can actually convert APAR into dry matter. Light use efficiency has been shown to react to water, temperature, and nutrient stresses amongst others (Field et al. 1995). Monteith's original approach was later refined to allow for the incorporation of remote sensing data (Kumar & Monteith 1981). The methodology was also adapted to estimate crop yields in agricultural areas (e.g., Lobell et al. 2003, Shi et al. 2007, Tao et al. 2005). This type of model seems most promising for the application to Central Asian irrigation regions because of its relative simplicity, low data demand and the ability to work in conjunction with remote sensing data. Overall accuracies, however, can be lower compared to the spatialization of mechanistic crop growth models (Maas 1988). Yet it has also been shown that the chosen model has to fit the research question. If, for example, the objective is simply to calculate

final crop yield, without studying the complex underlying physiological processes, simpler models are usually more appropriate than more complex ones (Spitters 1990).

Altogether there are few studies that investigate the use of LUE models for crop yield estimation until now. A primary study for the study region was carried out within the framework of the ZEF/UNESCO Khorezm project (Shi et al. 2007). The authors used the Monteith model as a basis and combined it with water and temperature stress terms as described by (Goetz et al. (1999)). The results were validated by comparing aggregated model outputs and official yield statistics. The difference between modelled and official yield was reported to be 10.2 % (Shi et al. 2007). According to the authors, future research should be directed towards enhanced possibilities of deriving decisive model input parameters from remote sensing data sources. However, there is currently no available method or model to investigate and monitor crop yield patterns throughout the Khorezm region. Consequently, the focus of this study will be on the development of such a methodology.

1.3 Research questions and objectives

The goal of this study is to detect the spatial variability of crop yields in the Khorezm region and to assess the productivity of the land at different scales as a support for economic assessments and spatial planning. Consequently, the questions that this study tries to answer concern the spatial and temporal patterns of crop yield in the Khorezm region:

- Where are areas of exceptionally high (hot spots) or low yields (cold spots)?
- How do crop yields evolve over time, and do hot and cold spots remain stationary?
- Are there consequently specific areas with low yields over multiple years, which is indicative of marginal land?
- Regarding new sensor developments, can these predictions be made for single fields? And if yes:
- Which specific fields are the most or least productive in Khorezm?

Answering these questions is crucial to secure rural livelihoods. Improvements in land and water management can only be implemented when regions of low productivity are known. Knowledge on the spatial distribution of these areas can help to identify reasons for suboptimal performance and to apply countermeasures directly, whether it is improvement in the irrigation system, supply of fertilizer etc. Yet in certain cases low productivity of fields may be permanent, and different paths have to be chosen. For example, if a field or area shows low crop yields over a longer period of time it may be indicative of marginal land. Knowledge of the distribution of marginal land allows identifying areas where different ameliorative measures are required, like alternative

land uses or planting of tree plantations (Khamzina et al. 2012). Finally, local stakeholders and authorities can greatly benefit from a working methodology for crop yield prediction in the study area, as it allows the timely estimation of regional crop production. Although statistical data is available at the district level, quicker and more objective information at a higher spatial scale is desirable to assess spatial variability of crop yields and detect and improve underperforming areas.

The fundamental assumption of this study is that a remote sensing-based LUE model is the right tool for gathering the necessary information to answer the questions on spatial and temporal patterns of crop yield and land productivity in the study area. This tool is consequently supposed to be useful in similar regions. The abovementioned questions can be answered by developing a satellite-based crop yield model that operates at two different scales:

- Medium spatial resolution (MODIS): Yield patterns of cotton and rice crops will be derived for the period 2003-2009. This information will enable answering questions concerning areas with above or below-average crop yield and their temporal development.
- High spatial resolution (RapidEye): Crop yield patterns will be modeled for the growing season 2009. This information is used to identify fields that have specifically high or low crop yields, which can serve to identify potential reasons for performance at the field scale. This dataset will furthermore be validated with actual yield data and therefore serve as a reference layer for the MODIS-based results.

There is currently no available methodology to carry out the described analysis. Consequently, the main objective of this thesis is to develop a multi-scale LUE model based on satellite imagery for regional crop yield mapping. The developed model can then be used to answer the core questions above. As there is no ready-to-use model available at the moment that meets the specific purposes of this study, the necessary model components have to be developed first. The methodological approach comprises the following technical objectives for model development:

- The generation of a RapidEye FPAR time series for the growing season 2009 based on *in situ* measurements.
- The use of this high resolution FPAR dataset to validate and calibrate MODIS imagery at the 250 m and 1000 m scale, and to determine the input most suited for the MODIS-based model.
- To derive an adequate estimator for regional crop water stress that can be used in the models.
- Integration of all components into a multi-scale LUE model that can incorporate RapidEye and MODIS data.

- To evaluate the accuracy of both the RapidEye and the MODIS scale using ground data and district statistics, and to compare model results on both scales.

Following model development and the analysis of the results, the next objective of this thesis is to quantify the regional distribution of marginal land in Khorezm, which can be used as an informational base to evaluate alternative land uses and to identify regions that need special consideration with regard to agricultural improvement. This information will be derived from a multicriteria analysis (MCA) that combines the multi-temporal MODIS crop yields and additional GIS data. Here, the specific goals are

- The localization of clusters of marginal land in Khorezm.
- Estimation of the accuracy of the results.
- Investigation of possible reasons for the distribution of marginal land.

A first study on cotton yield simulation in the Khorezm region using a LUE model was conducted by Shi et al. (2007). Shortcomings of the approach by Shi et al. (2007) included for example the selection of input data and model validation. When compared with the approach chosen by Shi et al. (2007), the envisaged improvements of the LUE model developed here are as follows:

- Application of the crop yield model for cotton and rice crops.
- The use of high resolution RapidEye data in addition to MODIS.
- Validation and calibration of the FPAR input data.
- Using an up-scaled FPAR dataset as the main input for the MODIS-based model (RapidEye to 250 m MODIS data) instead of choosing a downscaling approach (MODIS 1 km to MODIS 250 m).
- Development of an improved water stress factor.
- Application of the MODIS-based model for the period between 2003 and 2009.
- Validation of model results with data collected on the ground.

All research questions and objectives can be combined in a common framework that guides this thesis. This framework and the overall structure of the study at hand will be described in the next chapter.

1.4 Conceptual framework and structure

In the study at hand, time-series of remote sensing data from high and medium spatial resolution systems will be analysed to gain insights on regional crop growth. The combination of two spatial scales, one for the up-scaling of field measurements and both for model application, is expected to enhance the accuracy of crop yield prediction and provide useful information on temporal and spatial crop growth and yield patterns. The workflow to derive the information necessary for a thorough characterization of the agricultural system of Khorezm is presented in figure 1.3. The starting point of this thesis consists of FPAR *in situ* measurements that were conducted during the growing season 2009. This dataset was used to upscale FPAR to the RapidEye scale via correlation with vegetation indices (VIs). The resulting multitemporal RapidEye-based FPAR dataset was used for three main purposes: validation of the existing MODIS FPAR product (MOD15A2), calibration of MODIS 250 m NDVI data (transformation into FPAR), and as input to the LUE model. The main part of this thesis is the actual crop yield modeling. For this purpose, a LUE model was developed that can run with RapidEye and MODIS data as input. The RapidEye model calculated crop yields for cotton and rice at the field scale for the growing season 2009 and was validated with *in situ* yield data. The MODIS model resulted in multi-year crop yields of cotton and rice at the pixel scale (250 m) for the period 2003 to 2009. The last year was also used for comparison with the RapidEye-based results, to assess the plausibility of the MODIS model. In addition, information on field boundaries, meteorological and crop-specific parameters and crop maps at the respective satellite scale were necessary. The multi-year results from the MODIS model were further processed as the main input to a multicriteria analysis, which was complemented by secondary data. Thus, the spatial distribution of marginal land in the Khorezm region was mapped. This information, together with the crop yield information gained from both RapidEye and MODIS models, was finally used to make an objective statement on the spatial and temporal patterns of crop yields and marginal land in the Khorezm region, and thus obtain a characterization of this component of the agricultural system of an irrigation region in arid Central Asia.

The following chapter (chapter 2) will present the study area, the Khorezm district in western Uzbekistan. Afterwards, chapter 3 will introduce the theoretical background of this thesis, with special focus on satellite-based LUE modeling. This includes a short overview on the current state of research in the fields that are related to this study. The methodological sections begin with chapter 4, which describes field work in the study region, the up-scaling of FPAR ground measurements to the RapidEye scale, the validation of the MODIS FPAR product and finally the development of an empirical 250 m FPAR dataset based on MODIS NDVI data that will be used for the MODIS-based LUE model. Afterwards, chapter 5 will show the actual LUE modeling using RapidEye and MODIS data. The results from both scales will be compared for plausibility analysis. Chapter 6 subsequently describes the detection of marginal land in the

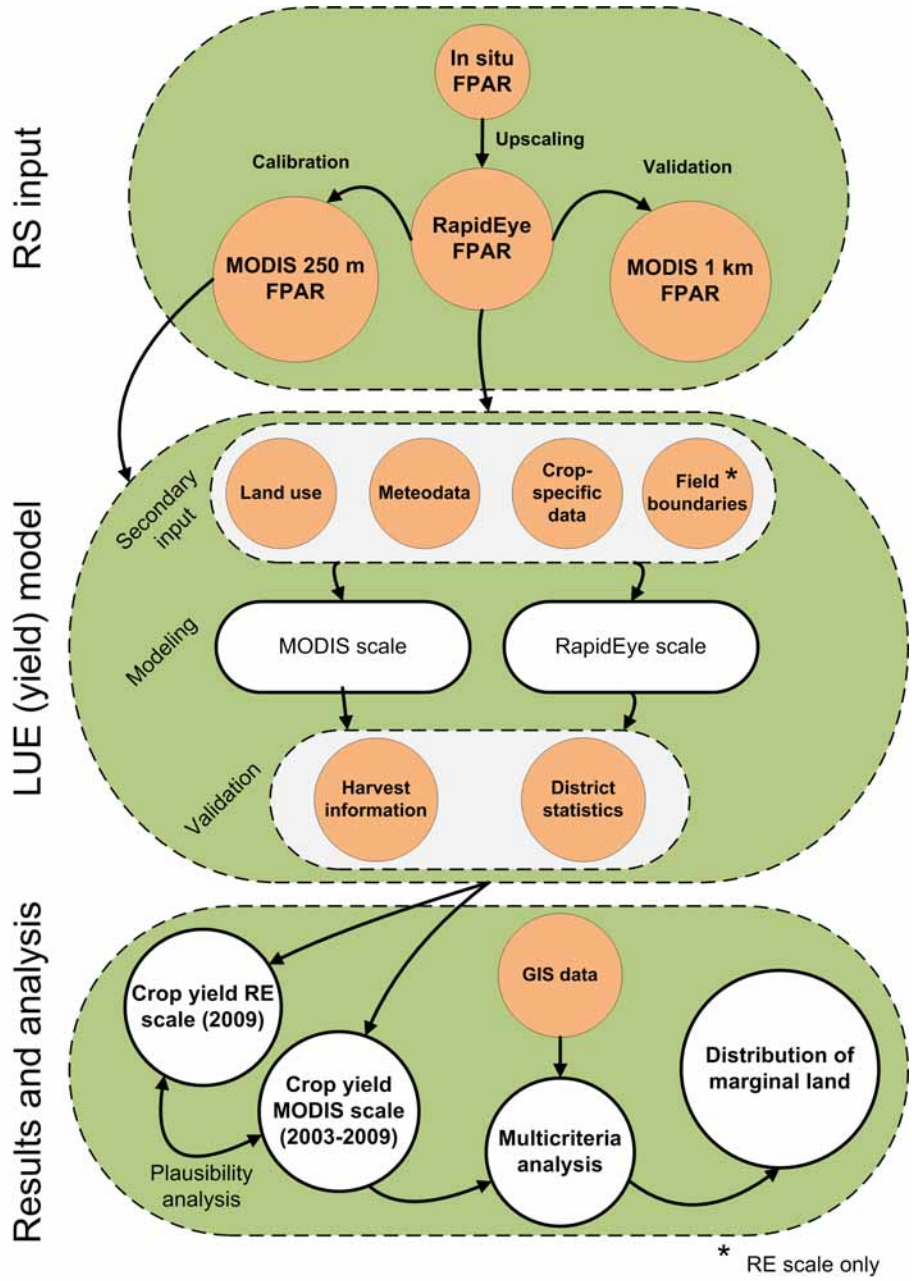

Figure 1.3: Flowchart demonstrating the main components of this study and their interdependencies.

study area, using seven-year crop yields derived from the MODIS-based LUE model as the main input. Finally, chapter 7 will present the conclusions concerning the results gained from chapters 4 to 6, and a final synthesis of this work will be presented as well as some recommendations on future research in this particular area.

2 Study area

2.1 Soviet influence, post-Soviet developments and the Aral Sea crisis

The largest part of western Central Asia belongs to the arid depression of the Aral Sea Basin (ASB). Figure 2.1 presents a general geographic overview of the region. The semi-arid and arid climatic conditions in the ASB are reflected in the widespread desert landscapes, marked by bare areas. Regional agricultural activity fundamentally depends on water for irrigation purposes. The green parts in figure 2.1 depict the irrigated areas of Central Asia. The Amu Darya Delta and especially the Khorezm region are highlighted, as it is the study region of this thesis. The pattern of the irrigated areas in the ASB indicates that they mostly follow the course of the major rivers and their deltas. Irrigated agriculture has been practiced in Central Asia for a long time, with the early beginnings dating back to around 8,000 years ago. Rapid expansion of regional irrigation activities started under Russian influence from 1918 onwards (O'Hara 2000), but large-scale land reclamation for agricultural production took place between 1950 and 1980 (Létolle & Mainguet 1996). The newly reclaimed land was mostly used for cotton production, which was concentrated in Uzbekistan, Turkmenistan and Tajikistan and was exported to the rest of the Soviet states (Létolle & Mainguet 1996). The following paragraphs will shortly summarize the developments in agriculture and related fields during the Soviet era (pre-independence), subsequently give a brief description of newer developments and problems that arose only after the independence of the Central Asian states (post-independence) and finally describe the main characteristics of the Aral Sea crisis.

The face of Central Asian agriculture was dramatically altered during the period of Soviet influence. Cotton was firmly established as the most important crop in the region, with Uzbekistan as the major cotton producer (Saiko & Zonn 2000). This was only possible through such measures as expansion of agricultural area via land reclamation, the expansion of existing irrigation infrastructure, the introduction of water management schemes, etc. The major part of these implementations started in the early 1950's. The irrigated area in 1950 amounted to approximately 5.4 million ha. By the end of the 80's the area reached around 9.4 million ha, a total increase of about 70 % as compared to the state in 1950 (Saiko & Zonn 2000). Large irrigation channels were built during this period. One example is the 1,400 km long Kara Kum Canal, which transports approximately 12.9 km^3 of water from the Amu Darya to 1 million ha

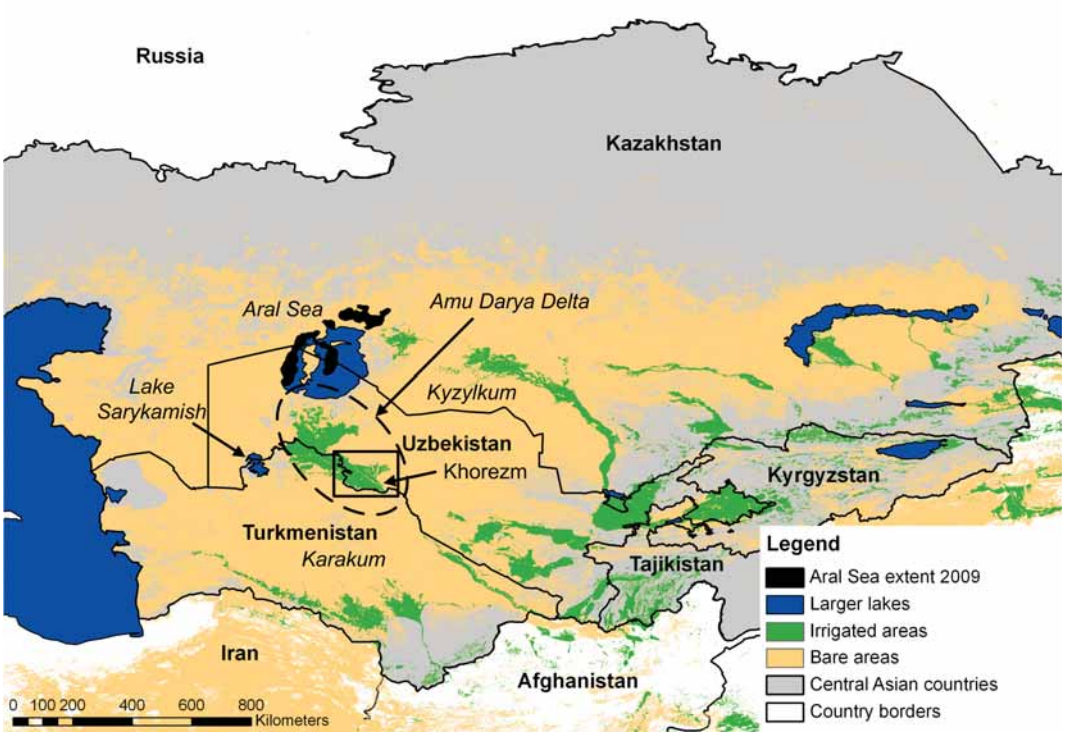

Figure 2.1: Overview of Central Asia. The Khorezm region is highlighted. The information on the spatial distribution of irrigated and bare areas was taken from GlobCover data (GlobCover 2008). Bare areas correspond to GlobCover class 200, irrigated areas represent an aggregation of the classes 11 (irrigated croplands), 12 (irrigated shrub or tree crops), and 13 (irrigated herbaceous crops).

of irrigated land in Turkmenistan (O'Hara 2000). This massive canal would have been worthless, if not for sophisticated water management schemes that divided the irrigation regions in so-called 'hydromodules'. The hydromodules determined the amount of water that was allocated to them each year (O'Hara 2000). The later abandonment of these water management schemes is stated to be one reason for additional problems the region faced after independence.

Until 1992 at the latest, the Central Asian states were part of the former Soviet Union (FSU). After the breakup of the FSU, the Central Asian states became independent and started following their own paths of development. The Uzbek state, for example, began to introduce wheat into the cropping cycle. These changes were mostly implemented at the expense of cotton area in order to achieve food security (Kienzler et al. 2011). Despite these changes, however, the largest part of the Soviet legacy of environmental and economic problems still remained. In fact, the problems were supplemented by newer ones that emerged due to the independence of the newly formed states. For example, disputes arose over water uses between upstream (Tajikistan, Kyrgyzstan) and downstream (Uzbekistan, Turkmenistan) countries of the Amu Darya. These disputes are based on the fact that, while river runoff is generated in the up-

stream mountainous regions, water consumption takes place in the downstream irrigated areas. While Tajikistan contributes 80 % to river flow, Uzbekistan is responsible for more than 50 % of water withdrawals (Micklin 2002). In water-scarce years (like the period 1999/2000) the tensions between states are especially obvious (Micklin 2002), and climate change is likely to intensify these conflicts in the long run (Bernauer & Siegfried 2012). After the breakup of the FSU, the irrigation and drainage network also began to collapse because of a lack of skilled workers and the financial means for canal maintenance. Nowadays the irrigation systems in the ASB are strongly deteriorated (see figure 2.8). However, these are just some of the examples of the current problems in the region.

The environmental and economic price for the large-scale expansion of irrigated agriculture in the ASB started to reveal itself in the 1980's, in the form of the Aral Sea crisis (Glantz et al. 1993). The Aral Sea disaster was not restricted to the lake itself, but affected the larger parts of the inner ASB and especially the delta regions of the Amu Dary and the Syr Darya. According to Spoor (1998), the crisis mostly concerned the actual vanishing of the lake, the salinization of the lake, the rivers and the irrigated land and water and soil pollution that affect human health in the region. The complex reasons and ecological and economic consequences of the Aral Sea disaster are for example thoroughly described in Létolle & Mainguet (1996). The agricultural sector in the region was especially affected by the general lack of sustainable land and water use in the region.

For example, even though the cotton exports of Uzbekistan outside the Soviet Union increased from 0.6 to 0.9 million tons between 1980 and 1996, average cotton yield decreased from 3.32 $t \times ha^{-1}$ to 2.34 $t \times ha^{-1}$ and cotton production decreased from 6.2 million tons to 3.2 million tons. Increasing exports could consequently only be realized by including more areas in the cropping systems. This is reflected in the water consumption for agricultural use, which increased from 34.6 $\times$ $10^9 m^3$ to 44.6 $\times$ $10^9 m^3$ during the same period. The loss of agricultural land due to degradation increased from 1.8 to 2.9 (with 1975 as the reference year equal to 1) (Saiko & Zonn 2000). The massive irrigation expansion led to a decline in the water inflow to the Aral Sea. Between 1910 and 1980, the river inflow into the Aral Sea steadily fell from 55 km^3 to 6 km^3, and for the period 2006 to 2010 averaged at about 4.1 km^3 (Micklin 2010). With the Aral Sea being a terminal lake in an arid region, the ceasing water flow led to the shrinkage of the Aral Sea. In 2009, the surface area of the lake was only 12.5 % of the area in 1960. At the same time, the average salinity rose from 10 $g \times l^{-1}$ to over 200 $g \times l^{-1}$ in some parts of the lake (Micklin 2010). The fast disappearance of the Aral Sea caused a variety of economic and ecological problems in the ASB, which are thoroughly described in the literature (e.g., Micklin 2007). Some examples of the most severe consequences of the Aral Sea disaster include (Micklin 2007, Micklin 2010):

- Vanishing of the fishes from the Aral Sea, caused by the increasing salinity levels. This

in turn caused the decline of the local fishing industry, enhanced by the growing difficulty to reach the lake. As a consequence, unemployment near the former lakeshore rose. The rising unemployment is even more severe as this area hardly supports any agricultural activity.

- The receding shoreline of the Aral Sea left behind a new desert, the Aral Kum. It is characterized by high salinity levels, with halophytic vegetation encroaching in the area. Salt and dust is blown from there to nearby areas, increasing the overall desertification and salinization in the ASB and affecting many ecosystems (see also Létolle & Mainguet 1996). One example is the widespread wetland area in the Amu Darya Delta, which poses as a habitat for many bird species.

- The desertification of the Aral Sea and the vast amounts of water diverted from the rivers were responsible for a dramatic loss of regional biodiversity dependent on the water. The once vast Tugai forests shrank to a fraction of their former size, from approximately 100,000 ha in 1950 to 20,000 to 30,000 ha in 1999 (Severskiy et al. 2005). These ecosystems depended on a regular inundation of the soil to wash out salts and replenish ground water, which stopped with large-scale irrigation (Giese 1998). Of the 70 species of mammals and 319 species of birds that lived in the region prior to 1960, only 32 and 160 remain today, respectively.

- The drying up of the Aral Sea had immediate consequences on human health, for example via the growing number of dust storms emanating from the former lake bed. Consequently, respiratory illnesses and cancer from inhalation of salt particles rose steadily, especially in Karakalpakstan, the region closest to the lake.

One of the irrigation systems central to the current situation in the ASB is the Khorezm region, located in western Uzbekistan. It exemplifies major parts of contemporary problems of land and water management in the inner ASB, especially the cotton production systems in the lowlands of Uzbekistan, and was the study region of the work carried out within the framework of this dissertation. The following sections will give a geographical overview and describe the agricultural practices in Khorezm.

2.2 Geographical overview of the Khorezm region

2.2.1 General information

The Khorezm region is located in the upper Amu Darya delta, one of the two major tributaries to the Aral Sea (figure 2.2). The region extends approximately from 42.1° to 41.1° N and from 60.0° to 61.5° E. To the northwest of Khorezm lies the autonomous republic of Karakalpakstan, which encompasses the area that directly borders the Aral Sea. Khorezm itself represents an Oblast (national district) of Uzbekistan, which is altogether made up of 13 Oblasts. Khorezm

in turn consists of 11 Rayons (regional districts), with the capital Urgench being centered in the region (see figure 2.2). Larger towns are also located throughout the districts. The general topography of the region is flat, with elevations approximately ranging from 70 to 110 m (compare figure 2.7). The lowlands of the Amu Darya delta are part of the larger Aral Sea Basin, which is defined by the regional geologic setting.

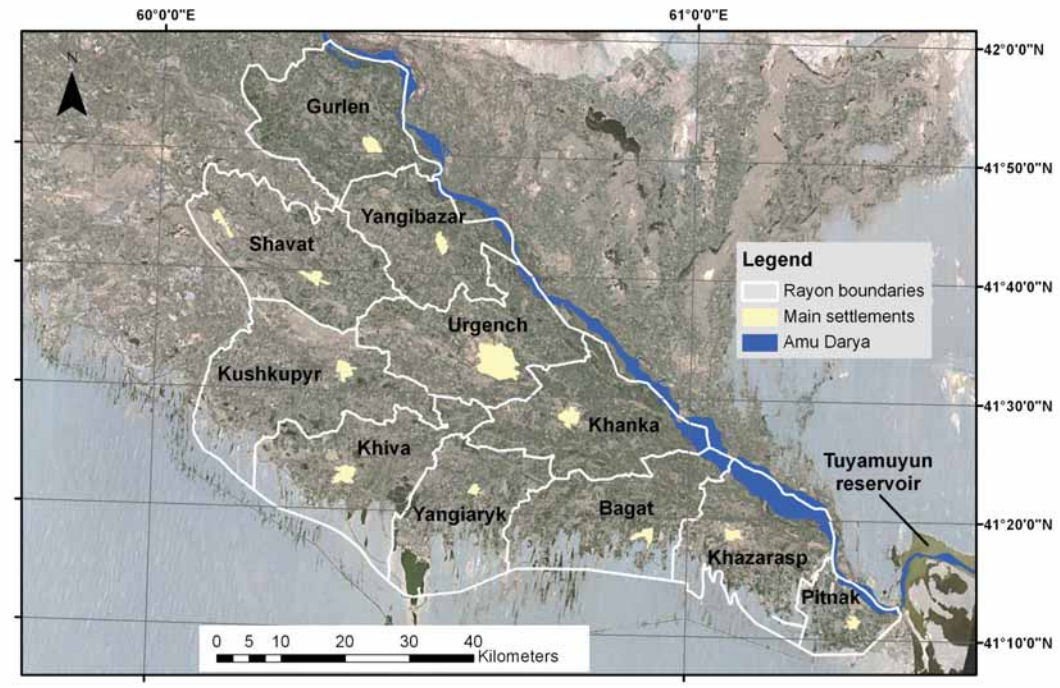

Figure 2.2: The study area, Khorezm, with its administrative districts (Rayons) and major settlements (Background: RapidEye mosaic).

2.2.2 Geology, geomorphology and soils

2.2.2.1 Geology

The Khorezm region and its surrounding areas are situated in the Turan lowlands and belong to the Turanian epi-paleozoic plate, a part of the Eurasian shield. The plate is composed of mesozoic and cenozoic sediments. The traces of a number of ancient massifs can be found within the Turanian plate, amongst them late Paleozoic volcanic belts and areas of hercynic origin (Koronovsky 2003). The depression of the Aral Sea originated from tectonic activities approximately 3 to 5 million years ago. The Aral Sea itself is one remnant of the Tethys ocean (Létolle & Mainguet 1996). Consequently, the major part of the Turanian plain is composed of marine sediments that were deposited during the Neogene-Pleistocene and the Mesozoic. These deposits can roughly be divided into different levels according to their vertical structure. One prominent dividing feature of these levels is the Ustyurt plateau, which begins

at the western shore of the Aral Sea. While the Ustyurt plateau represents marine sediments of the Mesozoic and the Tertiary, the lower level is made up of sandy deposits that form the large deserts in the region. Tectonic activities during the uplift of the mountains at the fringes of the Turanian plate (e.g., the Pamirs and the Karakorum) are responsible for a largely terrestrial sedimentation during the Paleocene and a transformation of the landforms. Quaternary sediments can mostly be found in the western part of the area. The uplift of the regional mountain ranges also supported the formation of river valleys like those of the Amu Darya and the Syr Darya rivers. Climatic conditions were rather constant during the Cenozoic, with dominant dry and continental conditions (Koronovsky 2003). Geologic conditions are the reason for Central Asia's wealth in natural resources like oil and gas reserves (Létolle & Mainguet 1996). For example, both Uzbekistan and Turkmenistan are heavy exporters of natural gas (Dorian et al. 1999).

2.2.2.2 Geomorphology

Khorezm is located between two major deserts, the Kyzyl Kum in the north and the Kara Kum in the south and west (figure 2.1). Both are sandy deserts, the dominating type in the region. Large parts of the Aral Kum, which represents the now exposed lake-bed of the Aral Sea, also belong to this type. Nowadays the sandy deserts of the region are dominated by aeolian processes (Lioubimtseva 2003). The Kara Kum covers the largest part of Turkmenistan and Uzbekistan southwest of the Aral Sea. The word 'kara' means 'black', the reason being the very dark, almost black color of the sands in this desert. The most prominent geomorphologic features in the Kara Kum are longitudinal dunes, which can reach a height of about 25-30 m, a length of 10-20 km, and a width of several kilometers (Lioubimtseva 2003). Barchans can be found in the Kara Kum (e.g., at the southern fringe of Khorezm), albeit much less frequent. Takyrs, flat areas consisting of clay surfaces (Breckle & Wucherer 2012), are also found throughout the dune fields in the Kara Kum. The Kyzyl Kum desert is situated between the Amu Darya and the Syr Darya Rivers as well as north of the Syr Darya. Only parts of the desert are characterized by sandy sediments. These sands have a different, more reddish, color and a large part of the sediments is fixed by vegetation (Lioubimtseva 2003). From a physical-geographical perspective, the Khorezm region itself is part of the Amu Darya delta and valley (Lioubimtseva 2003). This geomorphologic unit is dominated by alluvial sediments from the river. Former river beds can be found throughout the Khorezm region and the Amu Darya Delta, as the river has often changed its course on a geomorphologic timescale. Today, solonchaks and takyrs often developed at the bottom of these riverbeds (Lioubimtseva 2003). There are also findings that show that the antecessors of the Amu Darya have been alternating courses between the current riverbed that drains into the Aral Sea and alternative ones that drained for example into Lake Sarykamish or the Black Sea (compare Breckle & Geldyeva 2012). Agriculture in Khorezm takes place on former floodplains of the Amu Darya river, and the larger irrigation channels are partly ancient riverbeds of the Amu Darya.

2.2.2.3 Soils

The soils in the Khorezm region have developed on the alluvial sediment and the different micro-geomorphologic sites created in centuries of fluvial activity. On top of these palaeo-soils there is usually an anthropogenic horizon, developed under the influence of extensive irrigation during the last century (Akramkhanov et al. 2012). According to the FAO classification (figure 2.3, left), Khorezmian soils are mostly classified as arenosols (either gleyic/calcaric or aridic), calcaric cambisols, fluvisols near the river, or solonchaks in desert areas (FAO 2009). Soil texture ranges from silt loams, sandy loams, and loams to clay, which is however less frequent (Akramkhanov et al. 2012). High soil salinity is a general problem in the region. The natural conditions already support this phenomenon through flat terrain, high groundwater tables and soils that support capillary rise due to their rather heavy texture (Akramkhanov et al. 2012). According to Akramkhanov et al. (2012), the majority of subsoils in the Khorezm region are characterized by slight to medium salinity, while the largest part of the topsoil (above 60 cm) is highly saline. Soil salinity is also increased by the input of salts that emanate from the Aral Kum and are transported into the region via dust storms (Létolle & Mainguet 1996). The most important source of soil salinity, however, is the widespread irrigation system in the region, failing drainage of the soils, and resulting secondary soil salinization (Awan et al. 2011). High groundwater tables and soil salinization (figure 2.4) can also result from excessive water use. Groundwater salinity and tables as well as their environmental determinants and consequences have been thoroughly investigated and described for the region (Ibrakhimov et al. 2007, Ibrakhimov et al. 2011).

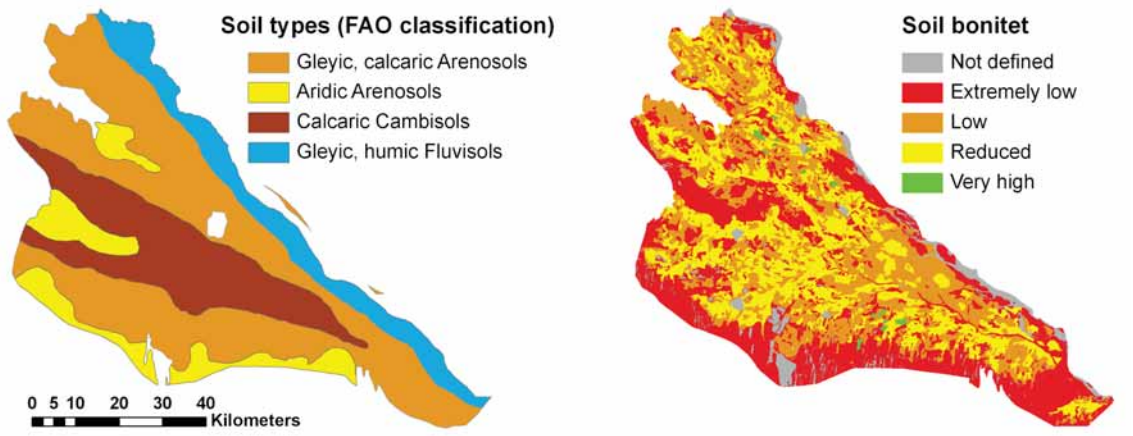

Figure 2.3: Maps showing the spatial distribution of soil types (left) and soil bonitet in 1996 (right) in the Khorezm region. Soil bonitet classification is further explained in the text.

An important and widely accepted characteristic for agriculture in the FSU is the so-called soil bonitet (figure 2.3, right). It is meant as a measure of the quality of the soil, determining the type

of crop best grown on the land and its expected yield. Several information layers are integrated to rank the quality of the soils between 0 and 100, indicating very bad up to excellent, fertile soils: bioclimatology, soil structure and skeletal characteristics, drainage and salinity level, level of erosion, and level of deflation. Soils are regarded as being marginal if they receive a rating lower than 40. According to the State Committee on Land Resources in Uzbekistan, this is the case for 23.8 %, or 55,760 ha, in Khorezm (GKZGK 2009).

Figure 2.4: Examples for soil salinization in Khorezm.

2.2.3 Climate, natural vegetation and water resources

The climate of the Khorezm region is dry and continental. Annual precipitation on average amounts to less than 100 mm (figure 2.5). Highest rainfall occurs in spring and winter. Yet precipitation is strongly exceeded by evapotranspiration (ET), which can reach up to 1,500 mm (Glazirin et al. 1999). The long-term mean potential evapotranspiration (ET_{pot}) from 1970 to 2007 was reported to be 1,378 mm per year (Conrad et al. 2012). The continental climate is also reflected in temperatures, with an average air temperate of approximately 26 ℃ in summer and 2 ℃ during the winter (Chub 2007). July is the month with the highest temperatures, with an average around 30 ℃ (figure 2.5). Maximum temperatures can reach up to 45 ℃ in July, minimum temperatures can fall to -29 ℃ in January. The average annual temperature is 13.1 ℃. The prevailing wind direction is north-northeast in July and northeast in January, with an average wind speed of 3-4 $m \times s^{-1}$ during both months (Chub 2007). The growing season of summer crops usually lasts from April to October. From a purely climatological perspective the growing season is characterized by a high aridity. Only the large-scale use of irrigation allows crops to grow.

Climate change will affect the Central Asian region and Khorezm. In the ASB, consequences of regional and global climate change can be distinguished. Regional climate change was shown

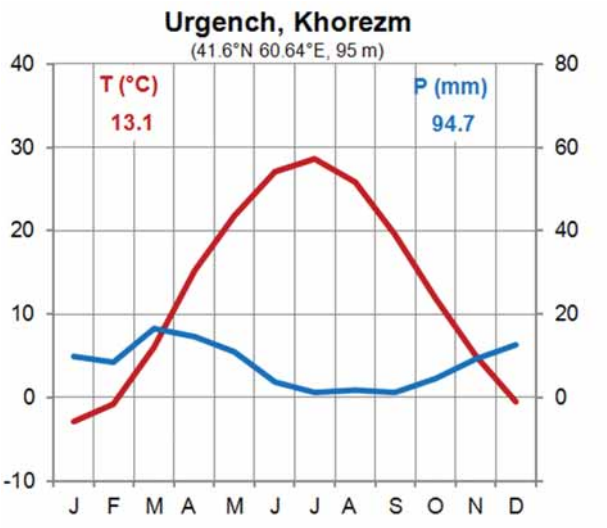

Figure 2.5: Walter-Lieth diagram of the study area showing the monthly distribution of mean annual temperature and precipitation for the period 1970-2007 (adapted from Conrad et al. 2012).

to be partly caused by irrigation activities in oases like Khorezm, which led to increased precipitation during the last 30-40 years (Lioubimtseva et al. 2005). Yet climate change in the ASB is mostly associated with the drying up of the Aral Sea. According to Middleton (2003), summer temperatures increase while winter temperatures decrease between 1.5 - 2.5 ℃ and the relative humidity decreased by about 2-3 %. Recent analyses, however, report a temperature increase in the Khorezm region in the last 20 to 40 years of around 0.5 to 1.5 ℃ (Conrad et al. 2012). The authors for example investigate the developments of growing degree days (GDD), the climatological planting date for cotton crops and ET_{pot}. They reach the conclusion that so far climate change does not adversely affect growing conditions in Khorezm. On the contrary, the fact that the observed temperature increase mostly happens in the winter months positively influences GDD for winter wheat and the planting dates for cotton, which could potentially be sown earlier in April (Conrad et al. 2012). ET_{pot} remained stable during the investigated period. Still the authors also state that it is difficult to distinguish between the effects of global and regional climate change. These positive changes will likely be balanced by large-scale climate change in the future, which is supposed to have an even greater influence in the region. Long-term projections from climate models show a general warming in the ASB and an increase in aridity (Lioubimtseva & Henebry 2009). Irrigation techniques will have to adapt to this new situation, since climate change will also affect its source, the glaciated mountains in the east and south of the region. Water stress in Central Asia is consequently likely to increase, mainly due to changes in the seasonality of river runoff. This means that there will be less water available for irrigation in the summer months (Siegfried et al. 2012), which will also affect livelihoods in the Khorezm region. A detailed description of the anticipated impacts of climate change in Uzbekistan, especially on agricultural water resources, can be found in Chub (2007).

The climatic conditions allow the growth of a variety of endemic desert plants that are adapted to the environmental conditions of the Turanian lowland. Due to a widespread occurrence of gypsic and calcic soil crusts in the region, there is an abundance of gypsum-tolerant plant species like *Tamarix* (Lioubimtseva 2003). *Haloxylon* (common name: Saxaul) and other halophytic desert vegetation often occur on solonchaks characterized by a high groundwater table, conditions that prevail in the vicinity of lakes, streams, or depressions (Lioubimtseva 2003). Takyrs in the Amu Darya and Syr Darya deltas feature a large variety of algae and lichen communities (Lioubimtseva 2003). Tugai forests dominate the annually inundated land of the large streams, while shrub vegetation, including different *Tamarix* species, dominates on non-inundated land. Tugai vegetation typically consists of different layers of vegetation. *Populus euphratica* dominates the tree layer (Khamzina et al. 2006) and reaches a height of up to 15 m (Lioubimtseva 2003). The lower layers often contain *Salix* and *Tamarix* species. Tugai forests are endemic to the region and nowadays highly threatened.

The general aridity during the growing seasons (figure 2.5) necessitates the use of river water for the irrigation of agricultural crops. Actual evapotranspiration (ET_{act}) often exceeds potential evapotranspiration during the summer months. For example, ET_{act} was modeled in a previous study using MODIS data (Conrad et al. 2007), and mean ET_{act} for cotton and rice fields was reported to be 768 and 798 mm for the growing season 2004, with maximum values of more than 1,200 mm. Nearly all water for irrigation purposes is abstracted from the Amu Darya river. The runoff of the Amu Darya originates in the Pamir Mountains. The total annual discharge within the river basin is approximately 74 km^3 (CAWATER-INFO 2012). While nearly 90 % of river runoff is formed on the territory of upstream countries (Tajikistan, Afghanistan, and Kyrgyzstan), the major consumer of river water is Uzbekistan. Of all water available on its territory, Uzbekistan uses 90 % for irrigation purposes (Hakimov et al. 2007). The water from the Amu Darya river is also mainly used for irrigation purposes in the Khorezm region, thus generating income for the rural population and producing crops and other agricultural products for export. It is therefore crucial for economic and social life in the region. Water availability changes from year to year. For example, the years 2000/2001 and 2008 have been years where water availability was very low in the Khorezm region (figure 2.6). According to Conrad (2006), the amount of water in the system in 2000/2001 was only half the long-term mean. As a consequence, crop yields were reduced up to one third and rice production was nearly non-existent (for the importance of rice production see below).

2.2.4 Economy and population

Total population of the Khorezm region in 2007 was about 1.5 million, which constitutes roughly five percent of the total population of Uzbekistan. Of the total Khorezmian population itself,

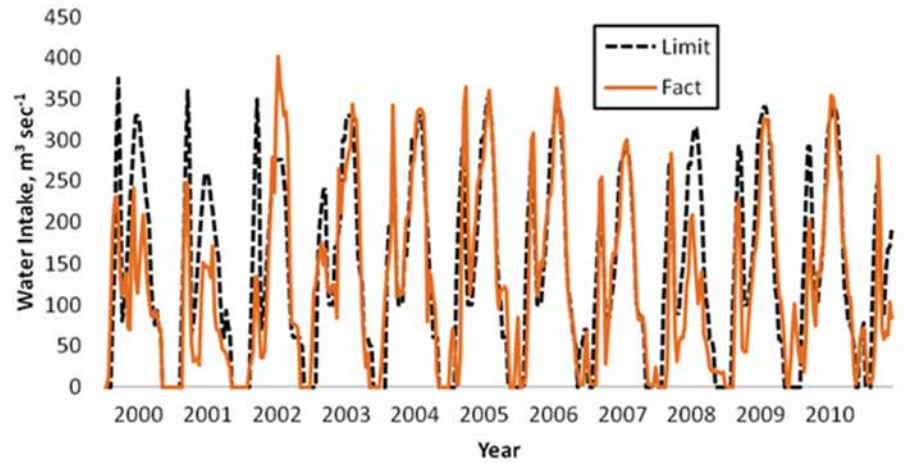

Figure 2.6: Water availability in Khorezm for the years 2001 to 2009. 'Limit' represents the amount of water planned for leaching and irrigation, 'fact' is the amount of water that the irrigation system actually received (source: CAWATER-INFO 2012).

about three quarters live in rural areas (Bekchanov et al. 2010). The livelihoods of a large part of the rural population of Khorezm depend on agriculture. According to Rudenko et al. (2012), the agricultural sector employs around 30 to 40 % of the regions inhabitants. Due to a steady population growth and little industrial development, the importance of agriculture is likely to increase in the future. This can increase the pressure on existing land resources even further. For the Khorezm region, the export of cotton constitutes about 98 % of the total monetary returns according to the local statistics division (OblStat) in Khorezm (Bekchanov et al. 2010). Water-scarce years like 2000/2001 lead to a reduced area that is dedicated to crops and consequently to reduced revenues for farmers. Such years have an even greater impact on rice farmers, because revenues are much higher but the permission to grow rice depends on general water availability (Veldwisch & Spoor 2008).

2.3 Agriculture in Khorezm

2.3.1 Irrigation system and organization

The water needed for irrigation purposes in the Khorezm region is diverted from the Amu Darya river at six water intake points (Conrad et al. 2007). These intake points feed the large magistral canals with water, which represent the backbone of the irrigation system. The irrigation and drainage system in Khorezm is constructed in a hierarchical way. The magistral canals distribute the water to canals of decreasing hierarchical order (primary, secondary and tertiary). The vast irrigation system (figure 2.7) altogether comprises 16,233 km of irrigation and 7,679 km of drainage channels (Conrad et al. 2007). Irrigation canals are used to transport water to the crop fields for irrigation; collectors are required for water drainage purposes.

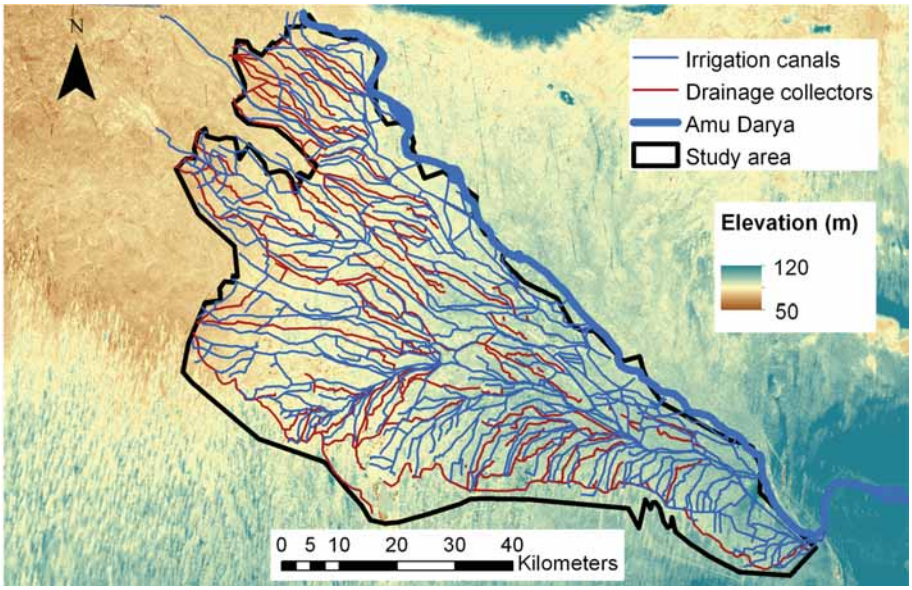

Figure 2.7: Characteristics of the irrigation and drainage network in Khorezm. The general relief of the area causes the water to flow from southeast to northwest. The main irrigation channels and drainage collectors follow that direction.

Some technical aspects of the irrigation system are exemplified in figure 2.8. One of the larger canals distributing the water from the intake points throughout the region is shown in figure 2.8 (upper left). This picture also shows that most of the larger canals and collectors in Khorezm are natural, which causes major water loses by percolation. The elevation of the canals is mostly lower than that of the agricultural fields. The water thus has to be pumped from the larger canals (figure 2.8, upper right) to canals of smaller hierarchical order (figure 2.8, lower left and lower right). Those canals finally distribute the water across the fields. The use of pumps to bring the water from the main channels to the field channels (secondary to tertiary) is often shared between farmers. Inadequate maintenance and control of pumps, as with the rest of the irrigation system, poses a major problem for water distribution in Khorezm (Wegerich 2004). In general, it was also shown that water distribution problems are mainly of an organizational origin (Wegerich 2004).

For example, initial farm restructurings in the Khorezm region led to the formation of a larger number of smaller farms, whose sizes ranged from 1 to 100 ha (Hirsch 2008). In terms of water management, these farms were organized in Water Users Associations (WUAs). Amongst other responsibilities, WUAs were supposed to maintain and manage the irrigation and drainage infrastructure (Veldwisch 2007). Based on former Kolkhoz boundaries, WUA establishment in Khorezm started in 2000 (Hirsch 2008). By 2005 all irrigated land was part of a WUA. Nowadays WUAs have been renamed to Water Consumers Associations (WCAs), an expression that will be used in the remainder of the text. From the beginning, WCAs have been

Figure 2.8: Some features of the irrigation system in Khorezm. The water is regionally distributed via irrigation canals of different sizes (upper left). Pumps are used to lift water to a higher level (upper right). From there it is distributed to farmers' fields via a huge network of smaller canals (lower left and right).

faced with financial problems, a lack of training of the members and unclear mandates (Hirsch 2008). Another problem is that the visibility of WCAs is low and farmers often do not know of their existence. Furthermore, there is often interference from higher-level state organizations (Hornidge et al. 2011). Due to the socio-economic situation, the location of a specific farm or WCA within the regional irrigation system and its hierarchy can determine its potential water availability. It was shown that access to irrigation water decreases with increasing distance to the water intake points from the Amu Darya river (Conrad et al. 2007). The distances of WCAs to the water intake points of the Khorezm region are shown in figure 2.9 (based on Conrad et al. 2007). The figure clearly illustrates that water has to travel the longest distances to reach the southern and western districts, located close to the desert borders, of the irrigation system.

2.3.2 Cropping practices, crops and other land use

The described irrigation and drainage system supports approximately 275,000 ha of irrigated land in the Khorezm region, which accounts for 50 % of its total area (Conrad et al. 2010). The major crops of the region are cotton, rice and wheat. Based on satellite estimates from 2004, the dominating crop is cotton (124,000 ha), followed by rice (73,000 ha), and wheat (54,899 ha)

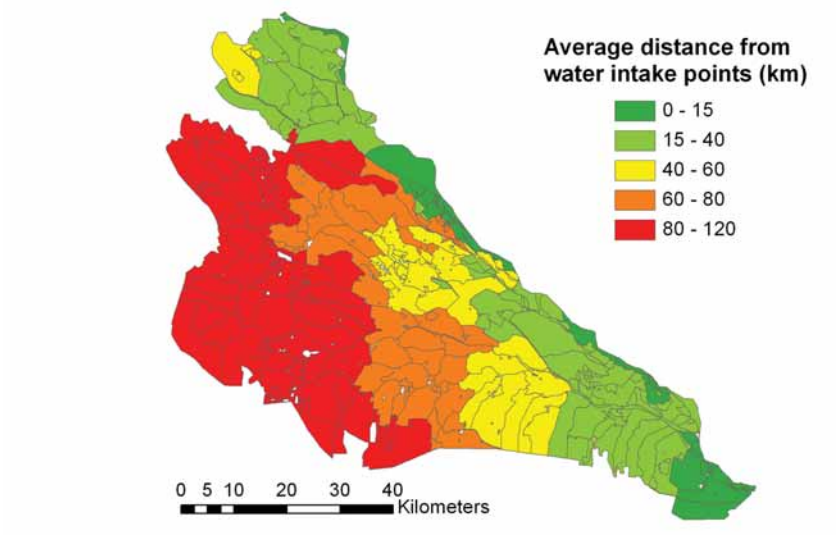

Figure 2.9: Average distances of WCAs from water intake points that divert irrigation water from the Amu Darya (adapted from Conrad et al. 2007).

(Conrad et al. 2007). The Khorezmian landscape is highly heterogeneous. Field sizes, on average, are less than 2 ha in size (Conrad et al. 2010). Agricultural parcels are furthermore often subdivided into smaller fields, to accommodate two or more crops. The agricultural sector itself is still dominated by a state-controlled quota system, which determines the area that has to be dedicated to cotton and wheat (Hornidge et al. 2011, Wehrheim & Martius 2008). The basis of the state-order is the soil bonitet map, which determines the crop yield that can be expected from each single parcel. Awan et al. (2011) report that the state order for cotton in Khorezm currently covers 50 % of the irrigated lands, while the state order for winter wheat covers 30 %. Overall concentration of plant nutrients like nitrogen, phosphate and potassium in the soil is low, which necessitates fertilization for agriculture. For the Khorezm region, nitrogen was determined to be the most limiting nutrient for the cultivation of cotton or winter wheat (Kienzler 2009). The state supplies subsidized agricultural inputs like fertilizer to the farmers, which in turn have to sell the goods that were produced in the framework of the state quota to fixed prices (Hornidge et al. 2011). The total area allocated to different crops has changed significantly during the last 20 years. For example, while the area allocated to cotton and rice nearly stayed the same, the area allocated to wheat has increased significantly. This increase in area was at the expense of fodder crops (Bekchanov et al. 2010). The areas of fruits and grape as well as vegetables and melons are more or less stable since independence (Bekchanov et al. 2010). There are mainly three types of agricultural production in Khorezm: state-ordered production, commercial production and household production (Veldwisch & Spoor 2008). As mentioned above, the state-ordered production concerns cotton and wheat, and is carried out by farmers on leased land with a size of 80 to 150 ha. Commercial production is freed from state order and focuses on rice as a commercial crop. Rice from Khorezm is exported throughout

Uzbekistan, which is why it was also titled the 'currency' of Khorezm. Local laborers furthermore often get paid directly in kilograms of rice (Veldwisch & Spoor 2008). Commercial production can also include fruits and vegetables, sunflower and fodder. Household, or dehqon (peasant), production finally concerns nearly every household in Khorezm and includes mostly fruits and vegetables (Hornidge et al. 2011). The following paragraphs will shortly introduce the main crops of Khorezm and their growing characteristics.

Winter wheat (*Triticum aestivum L.*) was mainly introduced in the cropping system of Uzbekistan and Khorezm after independence. It is a strategic crop that is supposed to help achieve food security (Kienzler et al. 2011). Accordingly, its area has increased steadily in the last two decades (Djumaniyazova et al. 2010). Winter wheat is sown in late autumn after the cotton and rice harvest, and is dormant in the winter. Crop growth continues around March and harvest is around May. Winter wheat is usually cultivated in rotation with a second summer crop, which is often (short duration) rice (see for example the classification results of Conrad et al. 2007 or Conrad et al. 2011). Further combinations are with vegetables or fodder maize, and sometimes the fields are left as fallow (Bekchanov et al. 2010). The growth characteristics of winter wheat can be seen in figure 2.10i-k. Cotton (*Gossypium hirsutum L.*) is a broadleaf crop that is grown in rows, with a typical row width of 60 or 90 cm (figure 2.10a). The irrigation is consequently done by furrow irrigation. Crop seeding begins in the middle of April, and maturity of the crop is reached around mid-September (Sommer et al. 2008). Plant biomass develops during the vegetative stage (figure 2.10b), and the crop can reach a height of up to 120 cm (Sommer et al. 2008). The harvestable part of the plant is the cotton fiber that develops inside the bolls. The development of the cotton bolls coincides with the time of maturity (figure 2.10c). The harvesting of the bolls is done by manual picking and usually starts shortly after maturity, in late September (figure 2.10d). The different cotton picks stretch over a longer period of time, and the contribution of the different picks to final crop yield is variable. For instance, the first, second, and third pick contributed 49 %, 35 %, and 16 % to the total yield in an experiment in 2005 reported by Sommer et al. (2008). Rice (*Oryza sativa L.*) is another important crop in the study region. Seeding starts in middle of June, and maturity is reached in the beginning of October (Devkota 2011). Biomass production of rice is very high between the beginning of August and mid-September. The plants can reach a canopy height of more than 90 cm (Ehammer et al. 2010, figure 2.10g). Harvesting of rice crops usually takes place in the middle or end of October. Rice cultivation in Khorezm is done in two different ways: direct sowing (figure 2.10e) and transplantation (figure 2.10f). In the first case rice is directly sown into flooded fields at the beginning of the season, in which case there was no winter wheat cultivated before. In the second case rice plants are initially cultivated in smaller fields, but at a much higher plant density. After wheat harvest, the seedlings are transplanted into former wheat beds. Rice is usually grown in smaller basins that are separated from each other (figure 2.10h).

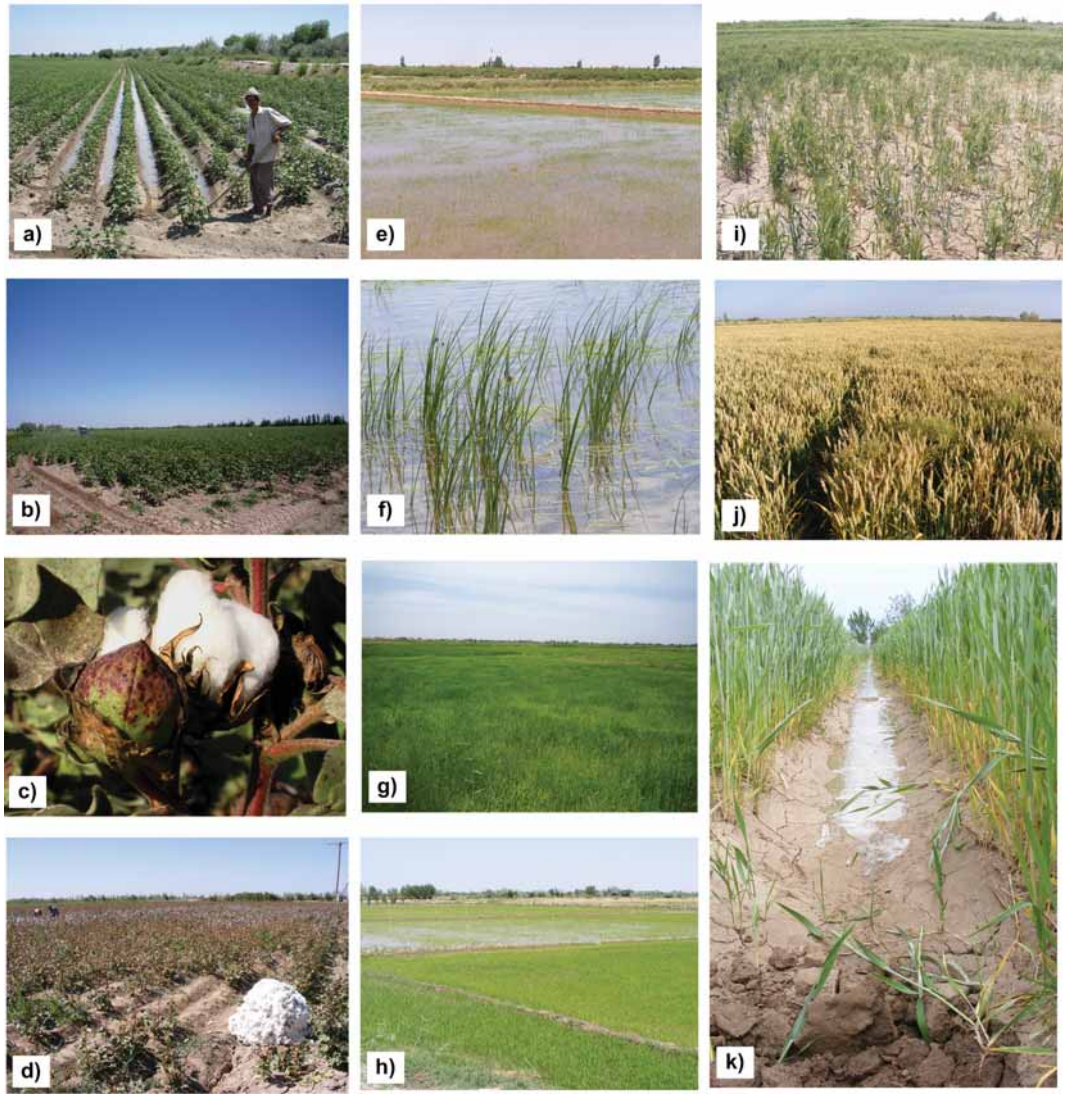

Figure 2.10: The main crops cultivated in the study region: cotton (first column), rice (second column) and winter wheat (third column). See text for further explanations.

Besides the three dominant crops, there is also a number of other land uses in the Khorezm region (figure 2.11). The remaining area is mostly cultivated with maize, sorghum, alfalfa, watermelons, sunflowers, agro-forestry, vegetables and fruits as well as tree plantations.

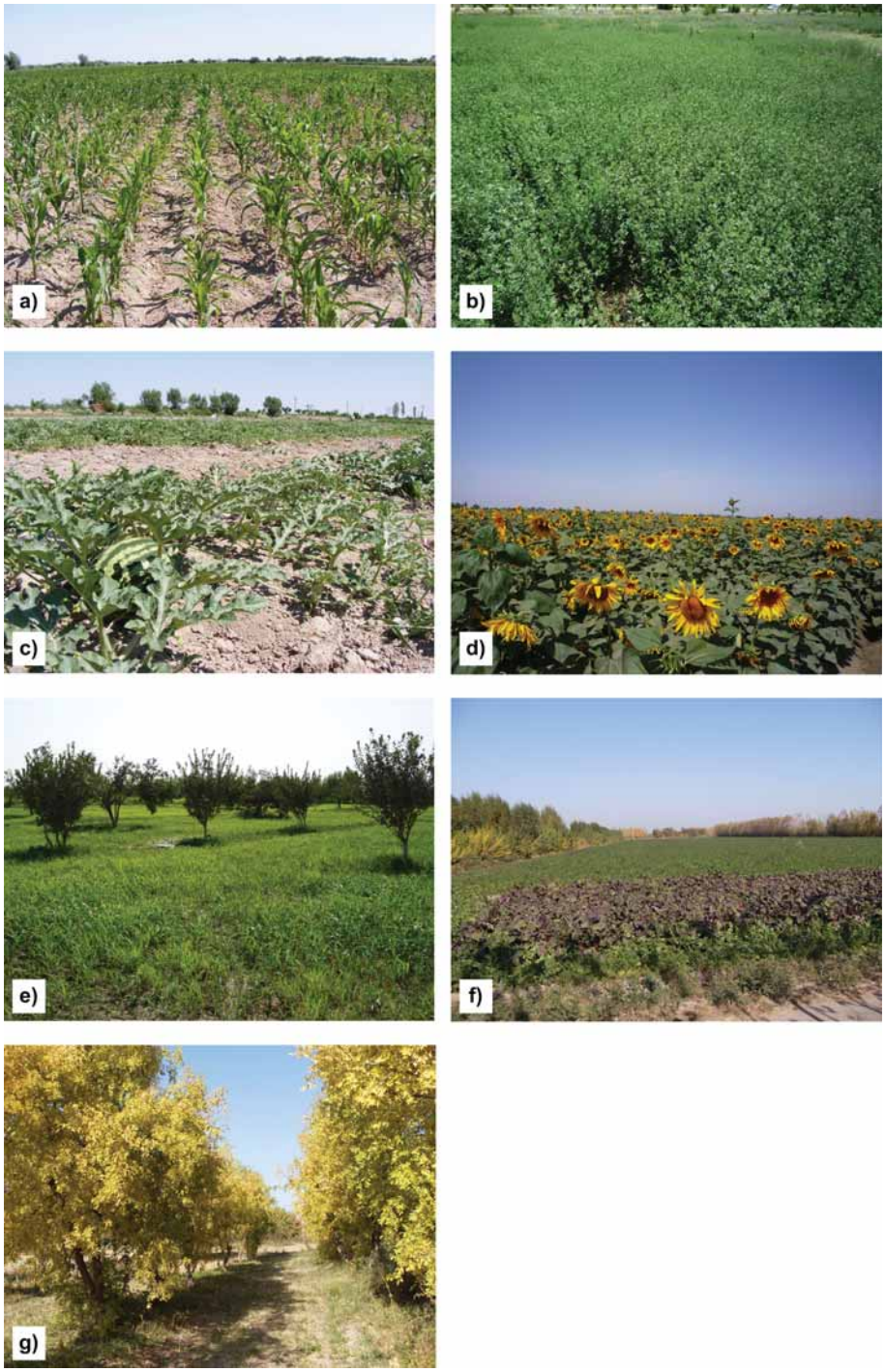

Figure 2.11: Minor land use in the Khorezm region, apart from the main crops, include maize (a), alfalfa (b), watermelons (c), sunflowers (d), agro-forestry (e; often fruit trees like mulberry), vegetables (f), and smaller forests (g).

3 Theoretical background and current state of research

The goal of this study is to estimate crop yields based on remote sensing data. The biological background to the formation of crop yield will be discussed in the following section (3.1). The chosen LUE approach is based on these concepts and will be discussed in more detail in the subsequent chapter. The historical development of the LUE concept will be described and a short literature review will be given, showing past developments and current trends (section 3.2). An overview on concepts to scale field data to high resolution imagery is presented in section 3.3. The theory of validating medium resolution imagery is covered in section 3.4. Definition of marginal land and the methodologies to map its distribution will be summarized in section 3.5. Finally, section 3.6 will integrate the major points and present a synthesis of the current gaps in knowledge.

3.1 Biological background

3.1.1 Photosynthesis

The two processes vital to crop yield formation are photosynthesis (PS) and net primary production (NPP). While the first acts at the leaf and plant scale, the second represents the integration over the whole canopy. Consequently, NPP can also be seen as plant photosynthesis (minus respiration) scaled to the canopy level. Photosynthesis is the basis for all terrestrial plant growth. During the process of PS, plants convert carbon dioxide from the air into organic compounds. These organic compounds are then used as the foundation for biomass accumulation. The photosynthetic process can be summarized according to formula 3.1 (Fageria et al. 2006):

$$6CO_2 + 12H_2O + photons \rightarrow C_6H_{12}O_6 + 6O_2 + 6H_2O \tag{3.1}$$

The process involves the conversion of CO_2 and water into sugar and oxygen via light energy. It takes place in the chloroplasts, which are mainly concentrated in the mesophyll structures inside the plant leaves (Jones & Vaughan 2010, see figure 3.1). Photosynthesis itself consists of three separate processes: the diffusion of CO_2 to the chloroplasts, the photochemical reactions and the dark reactions (Yoshida 1981). The latter are also known as the Calvin cycle. The processes of photosynthesis can also be formulated as (equation 3.2):

$$P_n = P_g - R_p - R_m \tag{3.2}$$

where P_n is net PS, P_g is gross PS, R_p is the rate of photorespiration and R_m is the mitochondrial (dark) respiration (for a comprehensive description of the dark respiration, see Hay & Porter 2006). Photorespiration occurs simultaneously with photosynthesis. Mitochondrial respiration is the process of energy release from the plants to their environment. This form of respiration can be separated into growth and maintenance respiration. While the first is involved in the growth of plant structures and biomass accumulation, the latter is important for maintaining crop physiological processes (Hay & Porter 2006).

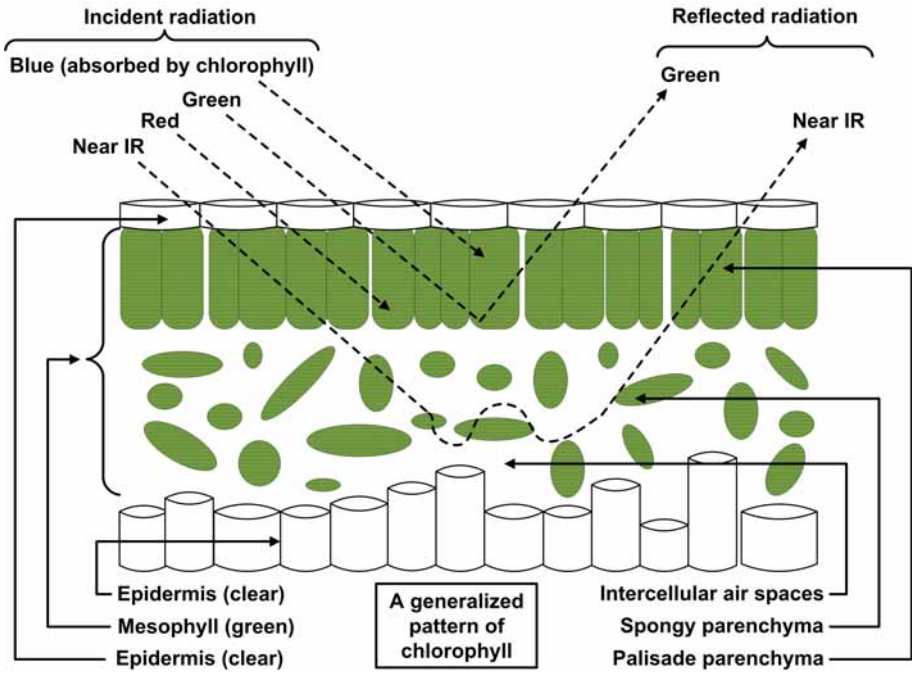

Figure 3.1: Light interactions in a schematic leaf cross section (adapted from Mavi & Tupper 2004).

3.1.2 Light interactions

Sunlight is the single most important factor for PS. Photons absorbed by the chloroplasts in plants carry the energy necessary to 'raise an electron within the thylakoid membranes to a higher energy state, thus initiating the photochemical events that split water to release the protons and electrons that drive the chemical reactions of the Calvin cycle' (Hay & Porter 2006, p. 75). Yet only specific wavelengths of the visible light are used for PS, which can be seen in the typical wavelength-specific spectral behavior of plant leaves (figure 3.1). The patterns in figure 3.2 additionally show that it is mainly the light between 350 and approximately 700 nm of the electromagnetic spectrum that is used for the photosynthetic process. Light in this spectral

region is also called photosynthetic active radiation (PAR), which was thoroughly investigated by McCree (1972a) and McCree (1972b). It is mainly blue and red light that is absorbed by plant chlorophyll. Reflectance and transmittance is higher in the green, explaining the natural color of plants. The transmissivity of a leaf thus mainly depends on its chlorophyll content, albeit it is only an intermediate state because sooner or later the transmitted light is reflected or absorbed by a canopy or the soil material (Tucker & Sellers 1986). In contrast to the red parts of the spectrum, light in the near infrared (NIR) is mostly reflected by green leaves. This characteristic is exploited by spectral vegetation indices in remote sensing (see section 3.2). The relation between reflection, absorption and transmission of a plant leaf across the visible, NIR and short wave infrared (SWIR) spectral regions is also shown in figure 3.3.

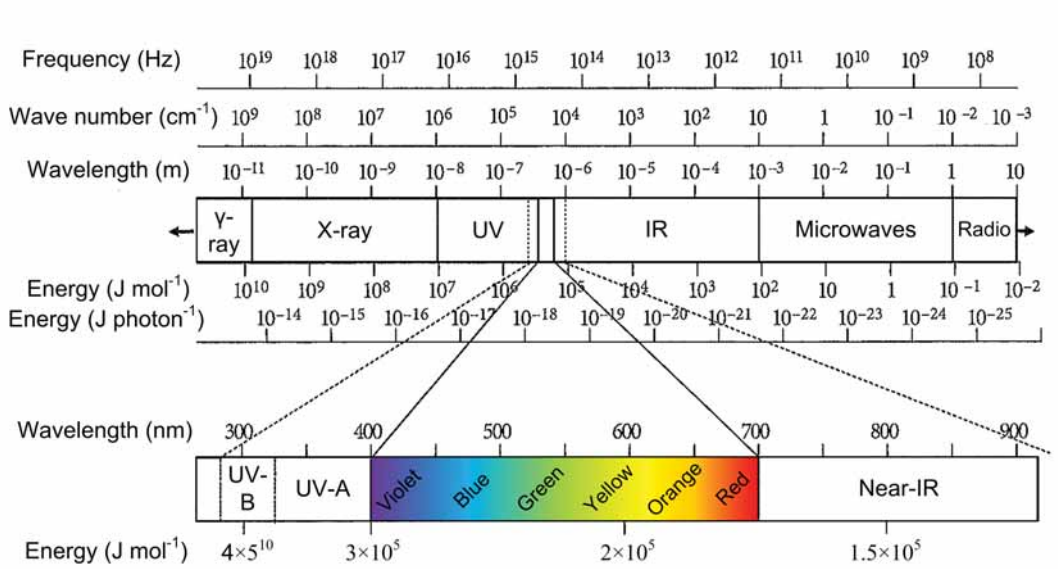

Figure 3.2: The electromagnetic spectrum (adapted from Jones & Vaughan 2010). The visible part of the spectrum is shown in colors.

3.1.3 Photosynthetic pathways

Plants are in constant interaction with their environment, for they have to exchange gases with the air. The interface structures for this exchange are the stomata, which are located in the epidermis of plant leaves. Plant stomata are microscopic openings, whose opening and closing is regulated by the plant according to a variety of environmental factors. The stomata exert a fundamental control on plant growth via the regulation of the amount of CO_2 that is led into the system. The maximal rate at which a plant under natural, optimal conditions is able to take up carbon dioxide is the species-specific photosynthetic capacity (Larcher 2003). For example, there is a large difference between the photosynthetic capacity of C_3, C_4 and Crassulacean Acid Metabolism (CAM) plants, with the photosynthetic efficiency increasing in this order. The difference between the C_3 and C_4 photosynthetic pathways is in the first stable product that is

created in the Calvin cycle. In the former case it is a sugar with three molecules, in the latter a sugar with four. This seemingly small difference has widespread consequences. For example, C_4 plants generally have a higher photosynthetic efficiency, a lower photorespiration, higher water utilization efficiency and higher response to light intensity as well as CO_2 and O_2 concentration in the air (Fageria et al. 2006). Consequently, C_4 plants are generally better adapted to arid environments. The plants treated in this study, cotton and rice, nevertheless belong to the group of C_3 plants.

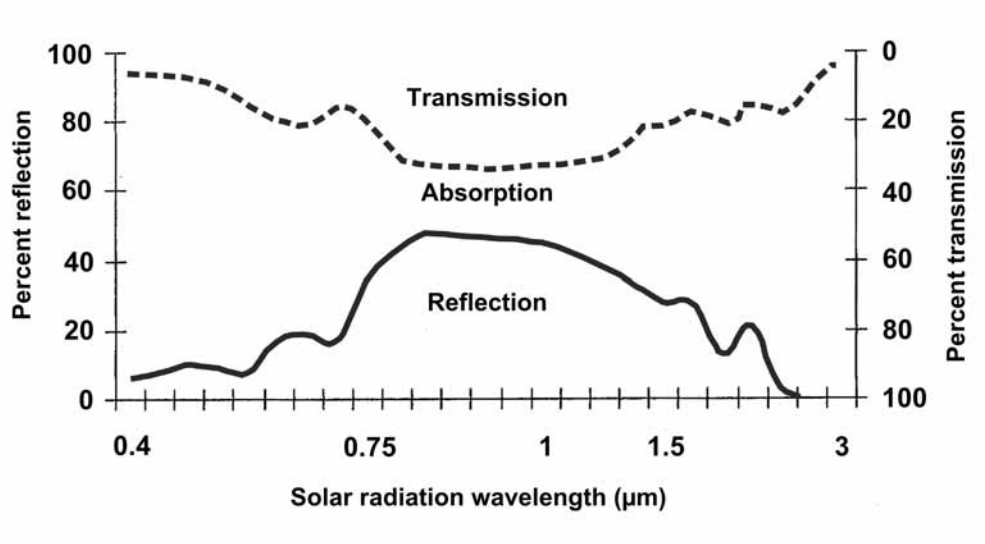

Figure 3.3: Transmission, absorption and reflection of light in a green leaf (adapted from Mavi & Tupper 2004).

3.1.4 Canopy processes

The process of photosynthesis ultimately leads to the growth of single plants. Processes at this scale can be described in great detail with laboratory measurements. For large scale assessments at the canopy scale, certain simplifications have to be made. There is a range of terms related to plant production that is important at the canopy scale (see for example Schulze et al. 2005), like the net ecosystem production (NEP) that can be defined as (equation 3.3):

$$NEP = GPP - R_a - R_h \tag{3.3}$$

In this equation, GPP is the gross primary production of a canopy or an ecosystem, R_a is the respiration of autotrophic plants and R_h is the respiration of heterotrophic (soil) organisms. If R_a is subtracted from GPP this results in the net primary production (NPP) according to equation 3.4:

$$NPP = GPP - R_a \tag{3.4}$$

The net primary production represents the annual carbon gain of (terrestrial) ecosystems through photosynthesis minus the plant-specific respiratory losses (Jones & Vaughan 2010). For a thorough review of these and other carbon-cycle concepts see Chapin et al. (2006).

3.1.5 Terms related to light absorption

Light is the most important resource for plant growth. At the canopy scale, light absorption can be described by different terms. As these terms are crucial for the LUE approach presented in the next section, they will be shortly explained in the following (for further information, see for example Gobron & Verstraete 2009a and Baret & Guyot 1991):

- Absorbed photosynthetically active radiation (APAR): PAR represents the total amount of photosynthetic active radiation that can theoretically be absorbed by plants. In reality, however, not all radiation is absorbed due to top-of-canopy reflection and transmittance and reflection by the soil. The remaining factor is the APAR.
- Intercepted photosynthetically active radiation (IPAR): the amount of light intercepted by the vegetation canopy.
- Fraction of photosynthetically active radiation (FPAR/FAPAR): APAR itself is difficult to measure, and is often approximated by the product of PAR and FPAR. The latter represents the fraction of photosynthetic active radiation absorbed by plants. Satellite-based vegetation indices are a direct estimator of FPAR.
- Fraction of intercepted photosynthetic active radiation (FIPAR): a simplification of FPAR, often used for ground measurements. FIPAR neglects the reflection at the top of the canopy and the transmittance and reflectance by the soil background. Despite these simplifications it has proven to be closely related to FPAR (e.g., Lobell et al. 2003).
- Green FAPAR/FPARgreen: similar to FPAR, but relates only to the green parts of the vegetation canopy. Stems and brown leaves are neglected.

APAR and IPAR are usually given in MJ, all other terms are dimensionless and scaled between 0 and 1.

3.1.6 Environmental interactions

Given non-limiting conditions of available light, rates of PS and NPP can increase until a saturation limit (Hay & Porter 2006). In reality, however, there are different factors that influence the actual rate of photosynthesis and respiration. These factors include, for example, temperature, water, nutrients, pests etc. The climate determines the general distribution of plants, and every plant has a defined range of climatic conditions in which it grows. The annual variation of temperatures in a given location (and partly the water availability) determine the photoperiod of a plant, which describes the season of active crop growth. The soil temperature also

determines when seeds emerge from dormancy (Hall 2001). On top of that, extremely low or high temperatures can always have negative effects on plant growth and crop production. High temperatures can for example inhibit germination and emergence (Hall 2001). The same is true for water availability, especially in semi-arid and arid areas where irrigation is the main requirement of plant growth (Steinmetz et al. 1990). Plant nutrients also play an important role. If the required nutrients are not readily available in the soil, plant growth may be hindered. That is why crops often need fertilization with nutrients like nitrogen (Kienzler et al. 2011). High soil salinity, on the other hand, has a negative effect on crop growth (Wiegand et al. 1996). Finally, the presences of pests or plant diseases can cause high yield losses.

The response of crops to different environmental factors is described in detail in Hall (2001). The described factors limit crop growth and yield. There are numerous studies showing that stress factors directly influence the efficiency with which a plant is able to convert sunlight into dry matter. This LUE is the fundamental concept to a type of model for crop growth analysis. The LUE approach was also chosen for this study because it is possible to apply to large areas by concurrent use of satellite data. The LUE approach will be described in the next sections.

3.2 Light use efficiency modeling

Running et al. (2000) introduced the framework and algorithms for the global terrestrial GPP and NPP products that are operationally available from MODIS satellite data. The algorithm of the MODIS NPP product is mainly based on Monteith's approach. According to Running et al. (2000), the basis of satellite-derived estimates of NPP consists of three components:

1. Monteith's original assumption that biomass production is directly related to APAR.
2. The link of APAR to satellite measurements via a close correlation between spectral vegetation indices and FPAR, and
3. The efficiency, and underlying causes of its variability, with which APAR is transformed into plant biomass. This efficiency is the LUE.

All three components constitute the LUE approach and will be discussed subsequently, followed by an overview of studies on LUE-based crop yield or biomass prediction.

3.2.1 Origins of the LUE approach

3.2.1.1 Light distribution and Beer's law

The foundation of the light use efficiency approach employed in this study goes back to the 1960s. In 1965, John Monteith developed a new model for light distribution in field crops (Monteith 1965). Its main assumption was that canopy photosynthesis depends on the distribution of light

within the crop canopy, which is nowadays widely accepted. Light distribution within a crop stand is controlled by the amount of leaf layers, approximated by the Leaf Area Index (LAI). The LAI is the 'total one-sided area of photosynthetic tissue per unit ground surface area' (Gobron & Verstraete 2009b, p.1). The influence of canopy structure on light extinction can be expressed by Beer's law (Equation 3.5; Monteith 1965, Campbell & Norman 1998):

$$I(LAI) = I(o)e^{-kL} \tag{3.5}$$

where $I(LAI)$ is the mean intensity of radiation on a horizontal plane at leaf area index L beneath the canopy, $I(o)$ is the light intensity at the top of the canopy, and k is a light extinction coefficient. The equation is valid for natural illumination and homogeneous media (Monteith 1965). The light extinction coefficient k is the ratio between the amount of radiation incident on a leaf or a canopy and the remaining radiation after transmission through the leaf or the canopy. FPAR can be derived via Beer's law by rewriting equation 3.5 into equation 3.6 (e.g., Turner et al. 2005):

$$FPAR = 1 - \left(e^{(LAI(-k))}\right) \tag{3.6}$$

Light extinction within the canopy, and thus the rate of photosynthesis, is controlled by leaf angles in the different canopy layers (Mavi & Tupper 2004). Another influencing factor that determines photosynthetic efficiency is the ratio between direct and diffuse solar radiation, as the efficiencies under diffuse light are usually higher (Turner et al. 2003, Aikman 1989).

3.2.1.2 Monteith's light use efficiency approach

Monteith (1969) expanded on his initial approach and gave a thorough description of all radiative processes in a crop stand. The ideas were further developed in later years. Monteith (1972) and Monteith (1977) integrated prior research in a canopy photosynthesis model that was used to study biomass accumulation and crop yield. The basic formula by Monteith has the form (equation 3.7):

$$P = APAR \times LUE \times \Delta t \tag{3.7}$$

where P is crop production (in $g \times m^{-2}$) and Δt is a temporal integrator throughout the growing season. APAR is given in MJ and LUE, the efficiency with which absorbed light is converted into biomass, in $gC \times MJ^{-1}$. It was shown earlier that APAR can be estimated via PAR and FPAR, resulting in equation 3.8:

$$P = FPAR \times PAR \times LUE \times \Delta t \tag{3.8}$$

where PAR is given in $MJ \times m^{-2}$ and FPAR is dimensionless. Monteith (1977) demonstrated that there is a linear relation between accumulated biomass in crop plants and the amount of

absorbed PAR (figure 3.4). The only difference was in the slope of the linear regression lines, an expression of the LUE varying between crop types.

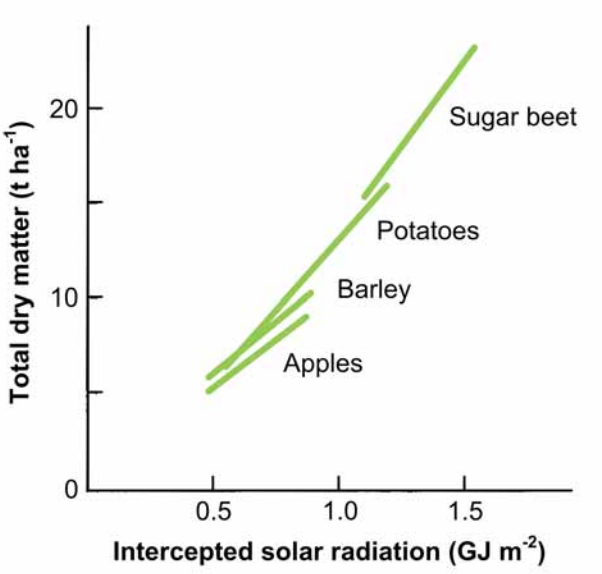

Figure 3.4: Intercepted solar radiation vs. total dry matter accumulation for different crop types (adapted from Hay & Porter 2006).

When used to calculate actual yield, the total crop production at the end of the season is usually multiplied with a harvest index (H_i), which represents the crop-specific ratio between aboveground biomass and the harvestable parts of the crop (Hay 1995). Accordingly, the H_i is scaled between 0 and 1.

3.2.1.3 Discussion on the validity of the LUE approach

The nature of the close relationship between cumulated intercepted solar radiation and crop growth was extensively discussed in the literature, as some authors believed it to be mathematically problematic and biologically overrated. This view was for example expressed by Demetriades-Shah et al. (1992). The main argument was that the comparison of crop growth and cumulated intercepted light is mathematically wrong, because ordered values always display positive and high correlations (Demetriades-Shah et al. 1992). They concluded that there will always be a high correlation between the two variables, even when some factor other than light is actually limiting crop growth. Furthermore, the authors criticized the concept of radiation use efficiency (RUE, synonymously used for LUE) because it incorporates all other soil and environmental factors that influence crop growth, some of which may have much more influence on crop growth than light interception. Reddy (1995) also criticized the concept of RUE and stated that it has no use in crop growth modeling because more general models, which are applicable in different environments, were needed. However, he agreed that the RUE term

had its use in comparing crop yield potential of different varieties under similar environmental conditions. The mathematical argument of Demetriades-Shah et al. (1992) was backed by Malet et al. (1997), who presented a mathematical theorem proving that the comparison of two cumulated variables will always result in high correlations. Hence they concluded that 'relating two cumulated variables should be avoided in plant growth and development models' (Malet et al. 1997, p. 141). However, they also added that the theorem only proved that cumulated variables show correlations that can be fundamentally different from the correlations derived from the comparison of the actual single measurements. They explicitly stated that this does not prove the underlying biological mechanisms of Monteith's approach to be wrong.

The original argument of Demetriades-Shah et al. (1992) was challenged by Kiniry (1994) and Arkebauer et al. (1994). Both authors showed that there is an overwhelming amount of scientific literature that proved the usefulness of RUE in the study of plant growth even if there are limiting factors on crop growth. These limiting factors can be incorporated into the RUE term because there are well-understood biological mechanisms explaining the influence of RUE on plant growth. According to Arkebauer et al. (1994) (p. 226), 'the interception of light and the use of that energy to accumulate plant mass is the fundamental description of plant growth'. Especially the variability of RUE, and the fact that this variability can be described with fluctuations in environmental conditions, is its main advantage for the description of crop growth. According to the advocates of the RUE approach, both facts were supposedly overlooked by Demetriades-Shah et al. (1992). The arguments against RUE were later repeated by Demetriades-Shah et al. (1994), but Monteith (1994) showed that their biological arguments were mainly insubstantial. He invalidated the argument that biomass and intercepted solar radiation are not dependent and independent variables, due to the fact that 'the amount of radiation intercepted by a crop stand at any instant is a function of its previous growth [...]' (Monteith 1994, p. 218). The reason is that standard regression methods apply as long as the errors of the respective temporal measurements of biomass and IPAR are not correlated.

The attractiveness of Monteith's approach stems from its combination of the growth-determining constraint of the PAR with the limiting ecological factor of the LAI, which determines the absorption of solar radiation via Beer's law. The approach also avoided a number of complexities related to carbon balance theory (Running et al. 2000). The decisive step in the development of remote sensing-based LUE models was the establishment of the link between spectral characteristics of plant canopies and plant growth.

3.2.2 The link to satellite spectral measurements and FPAR

3.2.2.1 Spectral measurements as indicators of crop yield

Plants absorb PAR and use it to convert CO_2 into biomass. Yet light in the PAR region is used differently by plants, at the leaf and at the canopy scale. Monteith (1969) found that when light penetrates deeper into a crop stand, red radiation increases and NIR radiation decreases (figure 3.1). As was shown plants absorb, transmit, and reflect light in different wavelengths to a certain degree (Suits 1972). This is relevant for an indirect estimation of canopy photosynthesis via remote sensing-based measurements. Early studies of plant spectral characteristics were mostly conducted on crops, and there were efforts to use spectral data for crop yield prediction (Idso et al. 1978). These studies were mostly limited to single satellite images being correlated with crop yield, and the results strongly depended on the acquisition date of the image, as the strength of the correlation itself depends on the crop stage (Hatfield et al. 1984).

Tucker (1979) utilized combinations of canopy reflectance in different wavebands, vegetation indices (VIs), for vegetation monitoring. The first VIs employed for such purposes were the simple ratio (SR, equation 3.9) and the Normalized Difference Vegetation Index (NDVI, equation 3.10):

$$SR = \frac{\rho NIR}{\rho RED} \tag{3.9}$$

$$NDVI = \frac{(\rho NIR - \rho RED)}{(\rho NIR + \rho RED)} \tag{3.10}$$

where ρNIR and ρRED are the reflectances in the NIR and the red spectral region, respectively. The NDVI was later theoretically proven to be linearly correlated to canopy photosynthesis rates and thus to be a predictor of canopy PAR absorption (Sellers 1985, Tucker & Sellers 1986). This characteristic of the NDVI stems from its integration of the ratio between reflected red and NIR light, as the absorption of red light is a direct indicator of photosynthesis. Amongst others, Hatfield et al. (1984) studied the potential of VIs to estimate the intercepted radiation in wheat canopies for integration in yield models. The author also found a linear relationship between the NDVI and FIPAR.

Pinter et al. (1981) suggested that the summation of the NDVI over the critical growing stages of a crop delivers much better crop yield predictions as compared to estimates from single images, because the integral of the index is associated with photosynthesis rates. Similar ideas were implemented by Tucker et al. (1981) for the calculation of dry matter accumulation in winter wheat. They found that SR and NDVI, accumulated over the growing season, correlated strongly with crop production. A concise and short overview on the developments regarding crop yield modeling using VIs at that time is given by Hatfield (1983).

3.2.2.2 Large-scale applications

The potential of satellite-derived NDVI for regional and global productivity assessment was further investigated by Box et al. (1989), who confirmed previous findings of VIs being more closely related to rate (productivity, FPAR) than state (LAI, biomass) variables. Tucker et al. (1985) investigated total herbaceous biomass production in the Sahel zone by calculating the seasonal sum of the NDVI derived from AVHRR data, and found good correlations with biomass at the end of the season. The author effectively established the link to Monteith's approach by stating that the feasibility of his study was based on the linear relation between VIs and FPAR and the 'relationship of this integral to primary production and yield [...]' (Tucker et al. 1985, p. 236). A similar study was conducted by Goward et al. (1985), who utilized the NDVI integration approach to study seasonal vegetation patterns of North America. From a methodological viewpoint, Prince (1991) discussed the implications of applying a local point-based model for different sorts of vegetation types at the global scale. According to the author, the main hurdle was the vegetation-specific LUE, which was so far only derived for crop types on a local scale. The question was whether and how LUE could be derived at a scale appropriate for large-area applications. Prince (1991) further stressed that LUE may very well be dynamic and, especially in semi-arid environments, controlled by temperature and water stress.

3.2.3 Light use efficiency: measurements and causes for variation

3.2.3.1 LUE dynamics

The PAR conversion efficiency of different vegetation types was initially assumed to be constant throughout the growing season. Different crop types indeed have similar light use efficiencies over a whole season, especially if well fertilized and with sufficient soil moisture. Later studies proved that LUE varies during the growing season due to environmental stress (Hilker et al. 2008). This also holds true for different crop types (Lobell et al. 2002), and has for example been shown for irrigated rice crops (Campbell et al. 2001). In such cases a variable LUE needs to be calculated. A study on short grass ecosystems, for example, found that the estimation of annual NPP was inaccurate when a fixed LUE value was applied instead of a dynamic one (Nouvellon et al. 2000). The variability is caused by plant respiration and suboptimal climate conditions (Running et al. 2000), where the most limiting climate factor determines LUE. According to Hilker et al. (2008), other influencing factors are temporal variations in solar irradiance, chlorophyll content and leaf-sun geometry. The proportion of direct and diffuse sunlight further plays an important role for LUE estimation (Turner et al. 2003). Diffuse radiation penetrates more efficiently into plant stands. Consequently, LUE and plant production tend to be higher under diffuse illumination (McCallum et al. 2009). Yet more important is the crop-specific reaction to climatic conditions that differ from optimum levels. The impact of environmental limits on NPP through the LUE of different vegetation types was investigated by Runyon et al. (1994). Environmental limits were quantified by constraints of

temperature, soil moisture and vapor pressure deficit (VPD). The authors found that, depending on vegetation type, corresponding FIPAR ranged from less than 25 % to 92 %. Capturing this variability is essential for large-scale NPP and crop yield monitoring. Crop growth is commonly modeled by reducing a crop-specific maximum light use efficiency value (LUE_{max}) to the actual light use efficiency (LUE_{act}) via the necessary stress terms (equation 3.11; Hilker et al. 2008, McCallum et al. 2009):

$$LUE_{act} = LUE_{max} \times T \times W \tag{3.11}$$

Here, T is a temperature stress factor and W is a water stress factor. These are the crucial limits to all plant growth, albeit water availability supposedly is more important (Garbulsky et al. 2010). Nevertheless, at the local scale, other factors may also play a role in the determination of crop growth (e.g. nitrogen stress due to insufficient fertilization).

3.2.3.2 Estimation of spatial and temporal variation of crop-specific LUE

The type of stress that is necessary to incorporate in an estimation of LUE depends on crop type and region. Not only natural conditions influence crop LUE, but also the remote sensing data itself. It should, for example, be taken into account that LUE values in remote sensing-based models are usually lower than values taken from field-based studies (Bradford et al. 2005). This is due to the nature of the imaging process, where measurements are averaged for each pixel. Scale effects play a significant role in the regional estimation of LUE, not only because of averaging effects. The spatial variability of LUE also depends on species composition per pixel and variability within individual species. Bradford et al. (2005) found that LUE varies between C_3 and C_4 crops, with LUE of C_4 crops being higher than that of C_3 crops. This observation was supported by Turner et al. (2002), who stated that C_4 crops have the highest LUE values, followed by non-nitrogen fixing C_3 plants and nitrogen-fixing C_3 plants. According to Bradford et al. (2005), the environmental down-regulation is less important than the differences between photosynthetic pathways at annual time scales. Environmental regulation of LUE is mainly important for shorter time periods. The sub-pixel mixture of different crop types and natural vegetation should be taken into account before applying a LUE algorithm (Bradford et al. 2005). The problem of spatial heterogeneity was also stressed by Turner et al. (2002), who investigated 'effects of spatial variability in light use efficiency on satellite-based NPP monitoring'. The authors suggest the use of a higher resolution land use or land cover classification as a possibility to circumvent the mixed-pixel problem. General scale effects with special regard to FPAR will be discussed below.

3.2.3.3 Recent developments in LUE research

The latest research suggests that not just LUE_{act}, as affected by environmental conditions, but also LUE_{max} can vary between vegetation types and seasons (Wang et al. 2010). Different

authors therefore asked to reconsider current LUE approaches that assign fixed LUE_{max} values to specific vegetation types. LUE_{max} is now more and more viewed as a variable, which can vary from pixel to pixel, than a fixed value. Similar to LUE_{act}, it strongly depends on sub-pixel heterogeneity. Wang et al. (2010) presented a methodology to dynamically assess LUE_{max} via EVI and minimum canopy albedo calculated from MODIS data. Earlier, Sims et al. (2006) already showed that EVI alone could be used to derive an estimation of LUE_{max}.

Possible alternative approaches for estimating LUE_{act} are also considered. One such approach is the direct estimation of LUE by means of the Photochemical Reflectance Index (PRI; Garbulsky et al. 2008). The PRI can be calculated from MODIS bands 11 (526-536 nm) and 12 (546-556 nm). The PRI directly correlates with the efficiency of photosynthesis (Gamon et al. 1992) and may be superior in remote sensing-based LUE studies, especially in biomes with low seasonal change in vegetation structure and a high carbon uptake variability (e.g., Mediterranean forests; see Garbulsky et al. 2008).

Finally, there are also efforts to reduce the amount of variables involved in LUE models (mainly climate) and develop production models that solely rely on remote sensing data. In a modeling study focusing on North American ecosystems, Sims et al. (2006) showed that the enhanced vegetation index (EVI) alone was superior to the MODIS GPP product (MOD17; Running et al. 2004) for estimating GPP. They argue that an assessment of LUE using independent (climate) data may be unnecessary in some cases. Their results, however, varied between ecosystems. The authors stated that EVI is likely less suited for GPP estimation in arid and semi-arid regions. They also discuss the possibility of using EVI as a direct estimator of LUE, as opposed to the PRI. The argument is that the baseline LUE, as derived from the PRI, often varies and that the EVI might be better suited for this purpose. EVI-based LUE models have recently also shown to be superior to, for example, the MODIS GPP product in a model comparison at a forest site (Wu et al. 2010). The combination of EVI and PRI for the estimation of LUE for varying sky conditions was investigated by Nakaji et al. (2007), who found promising results for this combination in a Japanese forest. These results follow the argumentation of Sims et al. (2006), who also advocated the combination of EVI and PRI for the estimation of LUE. However, investigations for all of these new developments are still ongoing and their use has yet to be proven in a large variety of eco and agro-system types.

3.2.4 Remote sensing-based crop yield estimation based on the LUE approach: current state of research

In this section, the more recent studies on crop yield estimation with the LUE approach will be presented. The short review will discuss studies based on medium (first part) and high resolution (second part) imagery. The focus will be on the decisive parameters of the LUE approach, their derivation, the satellite data used in the process, the scope of applicability and

respective accuracy. Special attention will be on the implementation of environmental controls for LUE estimation. The main goal of the review is to identify existing gaps in knowledge and the most promising approach for crop yield modeling in the Khorezm region. An overview of the relevant studies discussed in this section is also given in table A.1 (Appendix A.2).

3.2.4.1 LUE studies based on medium resolution imagery

Table A.1 also illustrates that all studies based on medium resolution imagery use MODIS or AVHRR data, with spatial resolutions ranging from 250 m to 8 km. Temporal resolution varied between 8 and 18 days. Some authors also implemented irregular time steps for their model. Yet in general these parameters vary only slightly between the different studies mentioned in table A.1. An important factor in each study is the derivation of FPAR. As shown in the table, most studies utilize the SR or NDVI for this purpose. Vegetation indices are used to calculate FPAR via linear regression models. The necessary equations are taken from literature. None of the studies calculated transformation equations specifically for their study region. On the contrary, the equations have often been developed in other regions and for other crop or vegetation types. This complicates uncertainty assessments. The largest differences concern the implementation of LUE and crop stresses. In general one can distinguish between studies that implement LUE down-regulation and those who do not. LUE down-regulation means that a maximum LUE value, which is valid if environmental conditions are not limiting, is dynamically minimized relative to the increase in crop stress. The most important crop stresses accounted for in the literature are temperature and water stress. Some authors also incorporate growth constraints due to leaf phenology (Yan et al. 2009). Turner et al. (2003), for example, found that LUE of corn crops declined towards the end of the season, and that this decline was probably caused by a simultaneous decrease in foliar nitrogen content. All these factors potentially decrease crop LUE and thus crop yield. First, studies that do not use LUE down-regulation are presented.

3.2.4.2 Without LUE down-regulation

Amongst them is the work of Moriondo et al. (2007), who presented a coarse resolution approach based on NOAA AVHRR data for quasi-operational wheat monitoring in two provinces of Italy. The found RMSE was 0.44 $t \times ha^{-1}$ and 0.47 $t \times ha^{-1}$ (with average measured yields of 2.86 $t \times ha^{-1}$ and 2.62 $t \times ha^{-1}$). They used a fixed LUE value of 1.0 $g \times MJ^{-1}$ for the whole growing season. Instead of incorporating crop stress in LUE, the authors implemented a dynamic calculation of the harvest index based on seasonal NDVI data. Depending on NDVI values at specific growth stages the overall harvest index is diminished, which leads to overall reduced yield amounts. Their study showed that this approach was feasible, but it depended on the utilization of a mechanistic crop model to simulate the phenological stages of the wheat. In that regard the authors also use a kind of down-regulation, which however cannot easily be compared to LUE because it is based on different physiological assumptions. Using the method-

ology of Moriondo et al. (2007) as a basis, Maselli et al. (2011) subsequently developed a modified version for wheat yield estimation in Tuscany, Italy. They used 16 day, 250 m MODIS data for their approach and also included crop phenology. This information was subsequently employed to estimate a dynamic H_i that is determined by the range and mean of NDVI values depending on crop stage. The study showed mixed results, with over and underestimation of provincial crop production (the product of crop area and crop yield) depending on the year. The main problem was identified to be the lack of an adequate incorporation of environmental variability through the LUE term. A model run that experimentally incorporated an adapted LUE value resulted in increased model accuracy.

A simple model without LUE down-regulation was presented by Báez-González et al. (2002), who used 1.1 km AVHRR NDVI in combination with ground-measurements of PAR to estimate corn yield in irrigated and non-irrigated fields in Mexico. The accuracy was 0.05 $t \times ha^{-1}$ (irrigated fields) and 0.32 $t \times ha^{-1}$ (non-irrigated fields), respectively. The authors concluded that clouds and management influenced the model results. However, this may have partly been due to the fact that no LUE was used in the model. Furthermore, the approach heavily depended on ground measurements to estimate crop developmental stages, which governed partitioning processes in the model.

3.2.4.3 With LUE downregulation - single stress

A model for grassland biomes (including millet and sorghum fields) was presented by Seaquist et al. (2003), who used 8 km AVHRR PAL data to estimate GPP of Sahelian vegetation. Climatological data from station networks was integrated to calculate potential and actual evapotranspiration, which in turn functioned as a water down-regulator. The model was later adapted to continental climates via temperature regulators by Brogaard et al. (2005), who calculated grassland primary production of Inner Mongolia from 1982 to 1999. It was shown that the model could depict the variability of GPP better than a model based solely on NDVI or a more complex plant-soil nutrient-cycling model. The results underline that it is important to customize the approach to the environmental conditions of the region of interest.

3.2.4.4 With LUE downregulation - multiple stresses

An important step in the development of satellite-based LUE modeling was the development of the MODIS GPP and NPP algorithm (MOD17). Running et al. (2000) described the fundamentals of the MOD17 algorithm, which was later further elaborated by Zhao et al. (2005). MODIS GPP data is produced operationally and at the global scale. The official accuracy of the MOD17 GPP and NPP product is stated to be within 10.4 % and 9 % of average published results, respectively (NASA 2012). It was found that the MODIS algorithm tends to overestimate GPP at low productivity sites and underestimate GPP at high productivity sites,

which can most likely be attributed to the FPAR product that is used as input and problems of accurately determining LUE (Turner et al. 2006). Zhao et al. (2005) listed three other sources for uncertainty in the MOD17 product: the underlying land cover classification, input climate data and the LAI product (MOD15A2). The MOD17 product was for example used to estimate wheat yield in semi-arid areas of the U.S. (Reeves et al. 2005), but the results showed that the product is unsuitable for crop yield assessment at smaller scales. The authors achieved acceptable accuracy only at the state-level. The reasons for this behavior were the coarse resolution of MODIS data itself and the climate data used in the algorithm, geometrical problems of the MODIS data, algorithm parameters, inability of the land cover map to distinguish different crop types, inability of the algorithm to determine start and end of the season, and the lack of spatial cultivar information to assign appropriate values, for example, to the harvest index. The authors suggested that the use of regional crop masks, local meteorological data and an enhancement of the physiological parameters in the GPP algorithm would significantly improve its performance. Consequently, the use of global products for crop yield assessment at the regional scale is likely to produce substandard results. This was for example shown by Fensholt et al. (2006), who evaluated the collection 4 and 4.5 of the MODIS GPP product for estimating primary production of Sahelian vegetation. The 'cropland' class of the MODIS biome scheme was one of the investigated classes. They found that the MOD17 algorithm predicted field-based biomass values with reasonable accuracy, but there was still a large amount of uncertainties involved. As a potential alternative, they used PAR derived from Meteosat, the MODIS FPAR product (MOD15), and the Shortwave Infrared Water Stress Index (SIWSI) (Fensholt & Sandholt 2003) to derive vegetation water stress. A regression against ground measurements revealed that this data combination was better able to capture variations of biomass at the local and regional scale. The authors subsequently recommended altering the MOD17 algorithm for semi-arid biomes. Zhang et al. (2008) further showed that MOD17 underestimated GPP at a winter wheat-maize site on the Tibetan Plateau. They identified two main problems for this underestimation: First, the incorrect assumption of crop LUE_{max} by the MODIS algorithm. The results improved significantly after LUE_{max} was adapted via field measurements. Second, the fact that cropland is inappropriately represented in the MODIS biome scheme (especially double cropping). The authors suggest that both aspects should be incorporated in future versions of the MODIS algorithm in order to ensure regional applicability. Meanwhile, customized models seem to be better suited for regional-scale assessments. For example, Lobell et al. (2002) investigated the productivity of North American agriculture for the period 1982 to 1998 with elements of the CASA model (see below), using regional statistics to calibrate LUE. The model results had a high correlation with production data of the major North American crops (e.g., corn, soybean and wheat). The authors stated that the choice of using a water stress term decisively influences model results, especially for irrigated agriculture. Bastiaanssen & Ali (2003) presented a model to predict irrigated crop yields in Pakistan based on Monteith's model, aspects of CASA and the surface energy balance for land (SEBAL;

Bastiaanssen et al. 1998). The study relied on 1.1 km, bi-monthly AVHRR data and was supported by ground-based meteorological stations. The innovative part was the use of the evaporative fraction (EF), derived from SEBAL, as a proxy for crop water stress. The resulting RMSEs were: 26 % (wheat), 32 % (sugarcane), 37 % (rice), and 49 % (cotton). The authors concluded that future studies should focus on the combination of high and low resolution images, which can decisively enhance model accuracy. This was also found by Tao et al. (2005), who compared the Carnegie Ames Stanford Approach (CASA; Potter et al. 1993, Field et al. 1995) and the Global Production Efficiency Model 2 (GLO-PEM2; Prince & Goward 1995) for the simulation of maize production in China. CASA is a global model that combines gridded data of NDVI, radiation, climate, vegetation characterization, soil type and texture as well as soil carbon and nitrogen contents to estimate annual NPP. LUE is dynamically limited using variables for temperature and water stress. The first accounts for low temperatures and deviations from the optimal temperature, the second for vegetation water stress that is parameterized via the ratio of actual (ET_{act}) to potential (ET_{pot}) evapotranspiration. GLO-PEM2 is based on data from the AVHRR sensor, from which it derives NDVI and temperature, soil moisture and vapor pressure deficit as constraints for light use efficiency. Validating model results with data from 122 agricultural experimental stations, Tao et al. (2005) found both models to perform equally well in spatial terms, but underestimating actual crop yields. The accuracy depended on the use of water down-regulation and the distribution of irrigated agriculture. Owing to the spatial resolution of the used AVHRR data, the authors stated that pixel heterogeneity was a major problem.

A study focusing on winter wheat-maize double cropping systems was conducted by Yan et al. (2009), who used the VPM model (Xiao et al. 2004) to simulate inter-annual variations of GPP using MODIS 500 m EVI data and climate parameters derived from local weather stations. The model included different kinds of stresses. Temperature stress was derived from minimum, maximum, and optimum temperatures and water stress was included via the Land Surface Wetness Index (LSWI) (Xiao et al. 2004). Furthermore, a phenological scalar was introduced, which reduced crop growth in the senescent stage. The authors found a good agreement between modeled and tower-observed GPP ($R^2 = 0.798$). Their study showed that the inclusion of crop-specific parameters is an important step for accurate modeling, which is not yet incorporated in global datasets like MOD17. MODIS NDVI data at the 250 m scale was also used in a LUE model by Patel et al. (2006), who simulated regional wheat yield in India. To derive accurate estimates of wheat crop distribution, the authors used two scenes of higher resolution AWIFS data for crop identification. FPAR was derived from MODIS NDVI in order to drive the model in conjunction with meteorological data from ground stations. The authors stated that wheat yield could be estimated satisfactorily at the regional scale, with a bias between 0.064 and 0.206. The LUE efficiency was varied according to crop development stage, where water stress was incorporated based on field observations. Finally, Shi et al. (2007) presented

an approach to derive cotton yields for the Khorezm region based on MODIS and ground-based meteorological data. Their study was the starting point for this work and the subsequent chapters. The authors used a customized LUE model that was partly based on the logic of the MOD17 algorithm, in that it used minimum temperature and vapor pressure deficit (VPD) to constrain potential crop growth via LUE_{act}. A MODIS 250 m FPAR dataset was generated via dynamic downscaling of the MODIS 1 km FPAR product via its correlation with the MODIS 250 m NDVI product. The results were validated with local statistical data. They showed that the difference between modeled and reported cotton yield was around 11 %, but, depending on district, the model underestimated cotton yield up to 22 %.

3.2.4.5 LUE studies based on high resolution imagery

In addition to medium resolution satellite data, 30 m Landsat imagery was also used as input to LUE modeling. Lobell et al. (2003) conducted a study with seven Landsat images, in conjunction with field measured FAPAR profiles, to estimate regional crop yield (maize, wheat and soybean) in the Yaqui valley of Mexico. The found accuracies varied between 3 and 30 %, depending on estimates of planting date. LUE was assumed to be constant and stress to be absent, limiting potential transferability to other cropland areas. The approach presented by Lobell et al. (2003) was also tested with other satellite data (Lobell & Asner 2003) and later used for more advanced analyses of yield growth opportunities in India (Lobell et al. 2010). A sophisticated study with few satellite images was presented by Liu et al. (2010). They used hyperspectral CASI in combination with Landsat imagery and ground-based meteorological data. Because satellite data acquisitions were insufficient for accurate modeling of FPAR over the growing season, the authors used a dynamic canopy model to simulate the FPAR signal over the growing season. This signal was then updated with actual satellite acquisitions. A novelty of the approach was the deduction of water stress via the NIR-SWIR trapezoid method presented by Ghulam et al. (2008). A comparison between actual corn dry yield and the LUE model resulted in an R^2 of 0.72 (RMSE = 0.72 $t \times ha^{-1}$) for two years with differing crop growth conditions. Pan et al. (2009) investigated the application of a LUE model for crop yield estimation in the semi-arid plateau region in China. They used a single Landsat image, acquired at the peak of the growing season, in combination with ground-measured FPAR for this purpose. In addition, they tested whether the use of high spatial resolution Quickbird imagery for crop discrimination resulted in significant improvements in the modeling process. This was actually the case, as Landsat imagery proved to be inappropriate for small scale crop detection. The use of a single Landsat image, similar to Lobell et al. (2003), also resulted in good model results, as a correlation of model results with area-averaged farmer-reported yields yielded an R^2 of 0.86.

3.3 Scaling field data to the satellite level

3.3.1 Spatial resolution and the choice of scale

The information that can be derived from RS measurements depends on different models concerning the scene for which measurements are made, the sensor used for the measurements and the atmosphere that influences RS data collection (Strahler et al. 1986). Especially the scene model influences data collection, which represents the spatial structure of the landscape that is being sensed. Landscape spatial structure can be characterized by the size of the dominating landscape features. The mean object size of the dominating features, for example settlements in urban areas or trees in a forest environment, strongly influences the utility of different RS systems. In general, one can distinguish between two cases. In the first case, the ground resolution of a sensor is smaller than the objects of interest. In the second case, the ground resolution is larger than the object of interest. Spatial resolution thus influences the derivation of biophysical parameters like FPAR or the spatial aggregation of vegetation indices like the NDVI. If, in the case of an agricultural landscape, the pixel resolution is smaller than the average field size, a single field will be covered by multiple image pixels. In this study, this is the case for RapidEye data. If the pixel resolution is larger than the average field size, multiple fields will be covered by a single pixel. This is the case for MODIS data. Here the problem of mixed pixels that cover multiple crop types arises. Ideally, the image resolution should always match the spatial structure of the ground scene. In reality, however, there is a constraint imposed by the availability of existing RS systems. A comparison of different sensor types for a subset of the agricultural system of Khorezm exemplifies this (figure 3.5). One can see, for example, that RapidEye and other higher resolution sensors are generally better suited to capture agricultural fields in the Khorezm region. Depending on the research question, however, one can be restricted to medium or coarse resolution satellite imagery, which is the case in this study. The modeling approach implemented here requires a high temporal resolution of image data. In addition, crop yield patterns are to be studied for multiple years and for a larger region. These requirements are currently only met by medium resolution RS data like MODIS. As will be shown, RapidEye can be used for the same purpose, but with a much higher spatial resolution and precision. However, RapidEye imagery is only available since 2009; information for earlier years can only be studied with medium resolution imagery.

3.3.2 Scaling FPAR

In cases where processes are studied at larger scales, scaling becomes necessary. Scaling represents the process of transferring biophysical parameters or models from one scale to another (Friedl 1997). There are numerous studies on methods of up-scaling FPAR and associated challenges. As shown earlier, NDVI and FPAR display a strong linear relationship. This relationship depends on a suite of factors related to canopy characteristics, soil background (Baret & Guyot 1991), timing and arrangement of the measurements and atmospheric conditions.

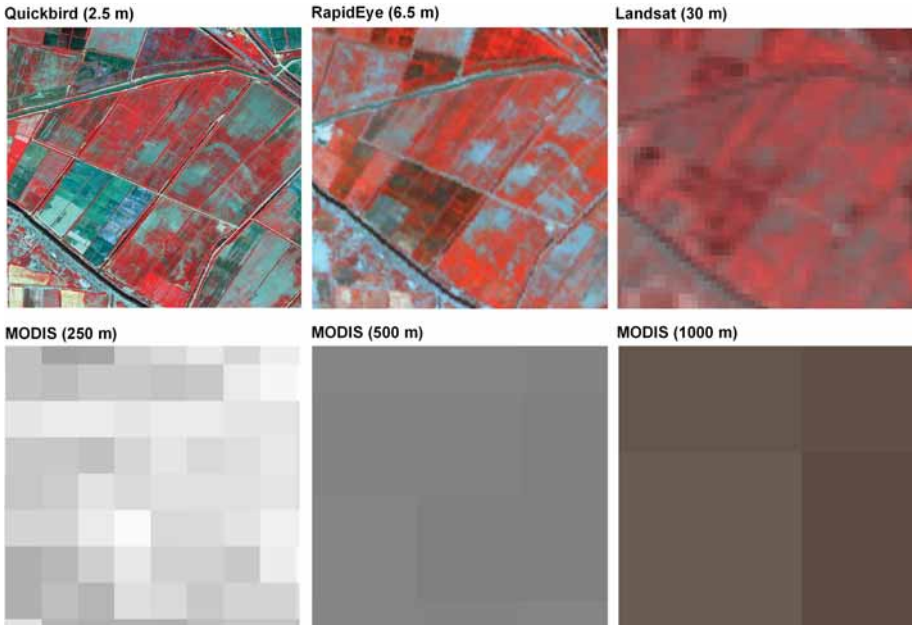

Figure 3.5: A comparison of different sensor systems shows the influence of spatial scale on the ability to derive information from the objects of interest. All subsets show the same extent.

For example, solar and viewing angles were proven to influence the relationship between daily averaged and instantaneous measurements of FAPAR (Myneni & Williams 1994, Goward & Huemmrich 1992). Yet one of the most important determinants of the relationship between NDVI and FPAR is the scale at which it is investigated. This also plays an important role if field data is to be scaled to high and medium resolution satellite imagery. The advantage of up-scaling FPAR via spectral indices like the NDVI is that previous studies have proven their relationship to be independent of, or only slightly modified by, landscape spatial heterogeneity (Asrar et al. 1992, Friedl et al. 1995). These findings also apply to spatially heterogeneous row crops, and are therefore of special importance to this thesis. Yet although NDVI-FPAR relations seem to be independent of spatial heterogeneity, it was shown that they are affected by soil color (Goward & Huemmrich 1992). Averaging effects also influence up-scaling of biophysical parameters. Spatial averaging of NDVI or FPAR introduces little uncertainty into their linear relationship (Friedl et al. 1995), but the NDVI itself is not scale invariant (Friedl et al. 1995). This means that NDVI from low spatial resolution data underestimates the actual spatial mean value of the high spatial resolution NDVI (Friedl et al. 1995). These relationships have to be kept in mind for further analyses.

The relationships between NDVI and FPAR, and the factors that determine them, are mostly based on *in situ* studies (Epiphanio & Huete 1995) or radiative transfer modeling (Roujean & Breon 1995). Few studies investigated the relationship between FPAR and vegetation indices by comparing field data with satellite measurements. Existing studies for example showed that

the linear relation between ground-based FPAR and satellite-based (AVHRR) NDVI strongly depends on atmospheric conditions, and that large differences can occur between atmospherically corrected images and those that were not atmospherically corrected (Hanan et al. 1995, Ruimy et al. 1994). Newer research on the estimation of FPAR from remote sensing measurements mostly concerns improved statistical analyses and the use of enhanced vegetation indices. The first development is based on the observation that traditional ordinary least squares (OLS) regression can be inadequate. Consequently, there are studies that deal with improved linear regression models for adequate derivation of FPAR (Leblanc & Fernandes 2005). The second development is based on the introduction of many enhanced VIs that are supposed to be superior to the traditional NDVI. For example, Vina & Gitelson (2005) used the Green NDVI, the Wide Dynamic Range Vegetation Index (WDRVI; Gitelson 2004), and the Red Edge NDVI to infer green FAPAR from spectral measurements. The authors state that Red Edge NDVI most accurately estimated $FAPAR_{green}$. Their results suggest that these indices can be used as a supplement to the NDVI, as they do not saturate at high biomass regions (Vina & Gitelson 2005). Different vegetation indices, calculated from high resolution RapidEye data, and their relation to ground-based FPAR of cotton and rice crops was investigated by Ehammer et al. (2010). Their results suggest that vegetation indices that incorporate the soil background can also perform better than traditional indices. Finally, Cohen et al. (2003) combined both approaches. The authors used a range of VIs that were combined into a single index for regression analysis.

3.4 Validation of medium resolution satellite data

3.4.1 Background

Remote sensing products have to be validated in order to assess their accuracy and enhance their applicability (Yang et al. 2006). Validation is defined as the assessment of product accuracy by means of independent data (Justice et al. 2000), which is represented by *in situ* measurements or high-resolution aerial or satellite imagery. To this end, independent data is compared to the satellite product of interest. Studies showed that a direct comparison between ground and medium resolution satellite data is inaccurate due to the large differences in scale (Hufkens et al. 2008), which is illustrated in figure 3.6. The widely recognized methodology for the validation of medium resolution satellite data involves the aforementioned high resolution imagery. In a first step the field data is scaled to the high resolution imagery. This up-scaling procedure can be conducted either via the use of an inverted RTM or transfer functions. The latter range from simple empirical regressions to more sophisticated approaches like neural networks. Once scaled to the high resolution, a subset of the original field data is usually used to validate the scaling procedure (Dorigo et al. 2007). This is a decisive step, as the high resolution map of the biophysical product of interest is regarded to be of a higher accuracy than the medium resolution product it is compared to (Morisette et al. 2002). It is important to quantify the

bias of this first step. If the compiled high resolution product is biased, the whole exercise of validation becomes superfluous. Once the quality of the high resolution product is assessed, it must be matched to the medium spatial resolution for further analyses. The matching is achieved by spatial aggregation of the high resolution data, usually by calculating the mean value of the biophysical parameter. There are different issues related to the aggregation and comparison that have to be taken into account. For example, the coordinate systems of both satellite datasets must be equal and they should be co-registered (Morisette et al. 2006). The accuracy of the comparison gained by co-registering both datasets depends on the native spatial accuracy of the data. MODIS measurements, for example, are designed to achieve sup-pixel accuracy (Wolfe et al. 1998). After the high resolution imagery is aggregated and matched to the medium resolution, the data can be either used to calibrate or validate medium resolution data and products (Baccini et al. 2007). A major part of the global satellite product validation effort can actually be traced back to the launch of the MODIS sensor and other operational medium and coarse resolution systems like VEGETATION (www.vgt.vito.be/) and MERIS (earth.esa.int/web/guest/missions/esa-operational-eo-missions/envisat/instruments/meris/).

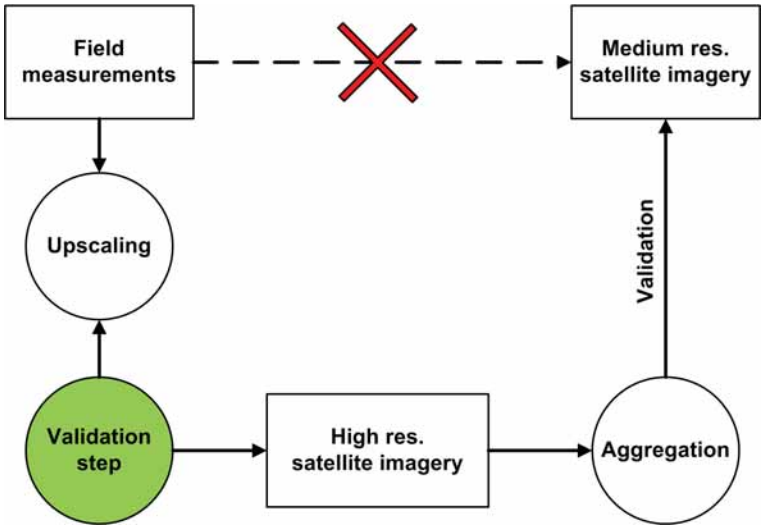

Figure 3.6: Typical scheme for the validation of medium and coarse resolution biophysical products from satellite data. A direct comparison of field and medium resolution satellite data is intuitive, but wrong. See text for further explanations. The graphic was adapted from Hufkens et al. (2008).

3.4.2 Methods for the validation of medium resolution RS products

With the advent of these satellite systems and the products derived from their spectral measurements, objective and coordinated validation efforts became a necessity. One of the largest validation efforts started with the launch of the MODIS sensor. A detailed framework for the validation of MODIS land products was established (Morisette et al. 2002). The MOD-

LAND validation approach was designed to use data from existing field programs, science data networks and international research efforts (Morisette et al. 2002). The field campaigns of the BigFoot program were specifically designed to provide data for the validation of MODIS land cover, LAI, FPAR and NPP products (Tian et al. 2003). Nowadays there are similar global validation efforts that have developed standards concerning validation of medium resolution products. One example is the VALidation of European Remote sensing Instruments (VALERI) project, which does not focus on a single sensor but rather on the comparison of multiple systems and the algorithms to derive the corresponding biophysical products (Weiss et al. 2001). The focus of validation protocols is mostly on the field data collection and the subsequent up-scaling procedures. These protocols have largely been developed for the validation of global LAI products (Morisette et al. 2006). Field sampling procedures usually employ a two-stage sampling design (Morisette et al. 2006). *In situ* measurements are conducted within so-called Elementary Sampling Units (ESU), which are typically 20 m by 20 m in size. The distribution of the ESUs within a landscape is stratified depending on land cover distribution. The heterogeneity of the study area also determines the number of ESUs that are necessary for an accurate characterization of the spatial variation of the biophysical parameter of interest. Field measurements are conducted in those ESUs, the type of sampling depending on land cover type and instrument (Morisette et al. 2006). Up-scaling is usually achieved by correlating the field data with the vegetation index value of the corresponding pixel. Newer studies showed that it is preferable to use objects instead of pixels for this step (Wang et al. 2004, Yang et al. 2006). This means that landscape stratification is applied to the high resolution data first. The implementation of this step helps to reduce errors due to inaccurate GPS readings, lack of sufficient field data for correlation analyses or spatial mis-matches between the high and medium resolution satellite datasets (Tian et al. 2003). Within-field variability can also be reduced by this procedure. Landscape stratification can for example be conducted by segmentation methods (Wang et al. 2004). Field measurements are then compared to the mean spectral signal of the landscape object. For this study, efforts were made to stick to the described standards as closely as possible. The methodology for field data collection is described in more detail in chapter 4.2.1.1.

3.4.3 Studies on FPAR validation

Many of the described developments concerning satellite product validation are based on efforts to assess the accuracy of global datasets like the MODIS LAI product. Yet while the MODIS LAI product has been validated extensively, until now there has been little research specifically focusing on the MODIS FPAR product using *in situ* and high resolution satellite data (Gobron & Verstraete 2009a). Amongst the few existing studies, Steinberg et al. (2006) validated the collection 4 MODIS FPAR product in a boreal landscape in Alaska using *in situ* and high resolution IKONOS and Landsat ETM+ images. They found MODIS overestimating FPAR values of both, *in situ* and high resolution satellite data, around 20 %. Li et al. (2010) evaluated

the MODIS FPAR product (no collection version was mentioned) for temperate grasslands in China using *in situ* and high resolution satellite data of the Beijing-1 satellite, and found MODIS FPAR to underestimate high resolution FPAR. Fensholt et al. (2004) assessed relationships between NDVI, LAI and FPAR (collection 4) in a semi-arid environment in Senegal and found different overestimations of FPAR varying between 8 and 20 %. Similar results were found by Huemmrich et al. (2005), who investigated the collection 3 MODIS LAI/FPAR product for 2001/2002 in western Zambia. They reported MODIS FPAR exceeding *in situ* measurements by around 20 %. This overestimation seems to be especially true for arid and semi-arid regions because of the heterogeneity of their vegetation cover. Finally, Chen et al. (2010) compared the collection 5 MODIS FPAR product with FPAR derived from Landsat-5 TM data. The study area was the semi-arid rangeland of Idaho. In contrast to the previously mentioned overestimations, the MODIS FPAR data was in good accordance with FPAR derived from Landsat. Steinberg et al. (2006) assumed that some of the issues found in collection 3 and 4 of the MODIS LAI/FPAR product may have been solved for collection 5, and Chen et al. (2010) attributed the good agreement of their data and MODIS FPAR to these changes. Some issues concerning the overestimation of the FPAR product over sparse vegetation are actually supposed to be resolved in collection 5 (USGS 2012). Until now there are no studies on the validation of MODIS FPAR for an agricultural landscape. Results from similar biomes (e.g., grasslands) may indicate expected results for croplands, but there are still large vegetation-specific differences. The temporal and spatial variability of cropland is much larger due to varying field sizes and crop phenology, which supposedly influences the quality of MODIS retrievals.

3.5 Marginal land and remote sensing

3.5.1 Background

Agricultural activities usually take place on suitable land that can be managed with an adequate amount of input. In the arid and semi-arid regions of the world, necessities often require crop cultivation on areas that are environmentally marginal. This marginality can for example be due to a high risk of soil erosion or high variability of rainfall patterns. Cassel-Gintz et al. (1997) developed a global marginality index based on net primary productivity, the aridity coefficient (the ratio of actual to potential evaotranspiration, c.f. Prentice et al. 1992), variability of the seasonal precipitation patterns, the potential irrigation capacity, soil fertility and the slope of the land. They found that most agricultural areas in arid Central Asia can be classified as marginal in terms of the prevailing natural conditions. Cropping in these areas is only possible through irrigation, fertilizer and pesticide inputs. Freshwater applications are also needed to cope with soil salinization, which lowers the suitability of land for agricultural production.

3.5.2 Definition of marginal land

The physical environment is an important consideration when defining marginal land. Yet such as done in humid regions of Western Europe, the land marginality for agriculture can be further viewed with respect to the economic value that is gained from a certain piece of land (e.g., via crop yields). According to Smit et al. (1991) (p. 335), the marginality of land 'relates fundamentally to the economic viability of land uses'. Smit et al. (1991) (p. 336) define marginal land as 'land parcels or types for which there are few viable uses, or for which uses are either only just viable or not always viable'. Thus, the holistic definition of land marginality considers both environmental and economic factors (Deal 2006). This definition corresponds to that of local farmers in the Khorezm region, who perceive marginal land as 'unproductive' (Dürbeck 2010), i.e., unable to support long-term cultivation of major crops such as cotton, wheat, rice, or maize. According to both interviews with farmers and consultations with scientific experts, land constantly producing low yields is seen as an indicator of marginality (Dürbeck 2010), which is in line with the scientific perception (Deal 2006). This unproductive land is the result of multiple factors, including poor soil quality due to salinity, unsound management practices and a lack or untimely supply of irrigation water.

3.5.3 Methods for delineating marginal land

The Food and Agricultural Organization (FAO) of the United Nations (UN) established a general framework for land evaluation. It has been used extensively for a variety of purposes, including the finding of suitable areas for agriculture (Martin & Saha 2009). New developments concerning climate change, desertification, and the role of biodiversity have led to an effort to update the original land evaluation framework (FAO 2007). The procedures applied within the framework are manifold and include consultation with stakeholders, land resource surveys, and spatial modeling and analysis (FAO 2007). The latter includes the use of GIS (Geographical Information Systems), and has often been applied in conjunction with a land suitability assessment. It allows to explicitly evaluate spatial problems concerning site search and site selection (Malczewski 2004). For further information see chapter 6.

3.5.4 Literature and this study

Besides GIS, remote sensing has furthermore offered the opportunity to include up-to-date information in such analyses. However, this has been mostly restricted to remote sensing-derived land-use or land-cover maps (e.g., Bandyopadhyay et al. 2009). Few studies have used higher-level information from remote sensing in the framework of a GIS-based land suitability assessment, and none have been targeted towards the identification of marginal land. This is a particular challenge given the wide number of factors determining it, as described earlier.

3.6 Synthesis and knowledge gaps

In general there has been little research on LUE modeling for agricultural purposes, especially in irrigated areas of Central Asia. This gap in LUE modeling exists despite the simplicity of the approach and the potential to use it in conjunction with satellite imagery. Of the presented LUE studies, only a few were further carried out at the regional scale. One reason for this is the need for an accurate crop classification. It is not always possible to carry out this task, which may be the reason why there are still few multi-year applications of LUE models. Thus, cropping systems are rarely investigated over time. While there are few studies on LUE modeling at medium resolution, there are even fewer studies that employ high resolution imagery for this purpose. Implementing the LUE approach with high resolution data poses additional problems that have to be coped with. The LUE approach requires multiple image acquisitions, distributed throughout the growing season, for accurate calculations. Another challenge is the correct implementation of stress factors to estimate LUE. This is especially difficult for irrigated agriculture, where water stress plays a dominant role. Furthermore it was shown that FPAR is the decisive input parameter for the approach. Its accuracy also determines the accuracy of the resulting yield calculations. Many of the presented studies simply use existing regression equations based on radiative transfer models, or equations that were established in different regions or for different crops, to transform vegetation index values into FPAR. The accuracy of the resulting FPAR dataset is unknown in these cases. If existing FPAR datasets are used, often no data validation is performed. This can also have a decisive influence on the model calculations, because it has been shown that quantification of product accuracy is crucial. The last section demonstrated the challenges in defining marginal land and shortly introduced methods for its delineation. Finally, it showed that there are very few studies on the spatial identification of marginal land, and none that utilizes remote sensing data for this purpose despite its potential benefits. This study answers some of the questions addressed in this section and proposes a methodology for satellite-based LUE modeling at high and medium resolutions. Furthermore, it shows potential applications of the results. The following chapters will address each topic separately.

4 Derivation of multi-scale FPAR data by empirical up-scaling of *in situ* measurements to RapidEye and MODIS scales*

4.1 Introduction

FPAR is the main remotely sensed input parameter for the LUE model. As described in chapter 3, a thorough assessment of biophysical products is a preliminary for further application. This is especially true since errors in FPAR will propagate to the final yield assessment. This chapter describes the compilation of regional FPAR products at the RapidEye and MODIS scale. The chapter consists of two parts. The first part describes the scaling of *in situ* FPAR measurements to the high resolution RapidEye imagery via statistical techniques. Thus, spatially explicit FPAR maps at the field scale are generated. The second part covers the optimization of regional FPAR products at the 250 m MODIS scale, which is necessary for multi-year crop yield assessments. Following the existing literature, two approaches were considered. One often implemented approach is the dynamic down-scaling of existing biophysical products via regression with higher resolution vegetation indices like the NDVI (Shi et al. 2007, Steinberg & Goetz 2009). This approach will be tested via the validation of the collection 5 MODIS FPAR product in the Khorezm region. The developed RapidEye FPAR product served as a benchmark for this evaluation. Another approach is the direct up-scaling of RapidEye FPAR to the MODIS scale via regression with vegetation indices. Different MODIS vegetation indices and products were tested to determine the most suitable for up-scaling RapidEye FPAR. Ultimately, this chapter will try to answer the question which approach is more feasible for regional, multi-year crop yield monitoring based on MODIS data. The general workflow of this chapter is also graphically summarized in figure 4.1.

*Parts of this chapter are based on Fritsch et al. (2012) and Fritsch et al. (2011), as well as field work described in Ehammer et al. (2010) and Ehammer (2011)

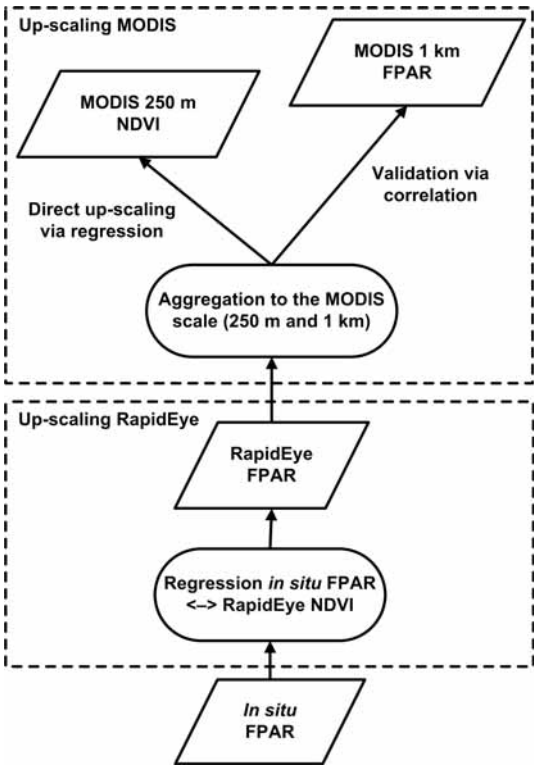

Figure 4.1: Graphical description of the contents of this chapter. The workflow comprises the up-scaling of FPAR to the RapidEye and MODIS scale. At the MODIS scale, a direct up-scaling via regression between RapidEye FPAR and MODIS NDVI and a validation of the RapidEye and MODIS FPAR datasets were compared.

4.2 Up-scaling *in situ* FPAR via RapidEye spectral measurements

4.2.1 Data and methods

4.2.1.1 Field measurements

The general principles of up-scaling field measurements for calibration and validation of high and medium resolution imagery were already summarized in chapter 3. This chapter describes the methodology that was actually implemented. *In situ* measurements of FPAR were conducted during the growing season 2009. The sampling design of field measurements is critical for the derivation of accurate high resolution reference maps, especially in heterogeneous semi-arid biomes (Hufkens et al. 2008) and agricultural landscapes (Tan et al. 2005). The sampling scheme chosen for *in situ* data collection was in line with existing recommendations on the validation of moderate resolution biophysical products (Morisette et al. 2006). Ground measurements were carried out northwest of the regional capital Urgench, arranged in a grid of 3 km $\times$ 3 km (figure 4.2).

This location was chosen because the crops at the site were representative of the cropping system

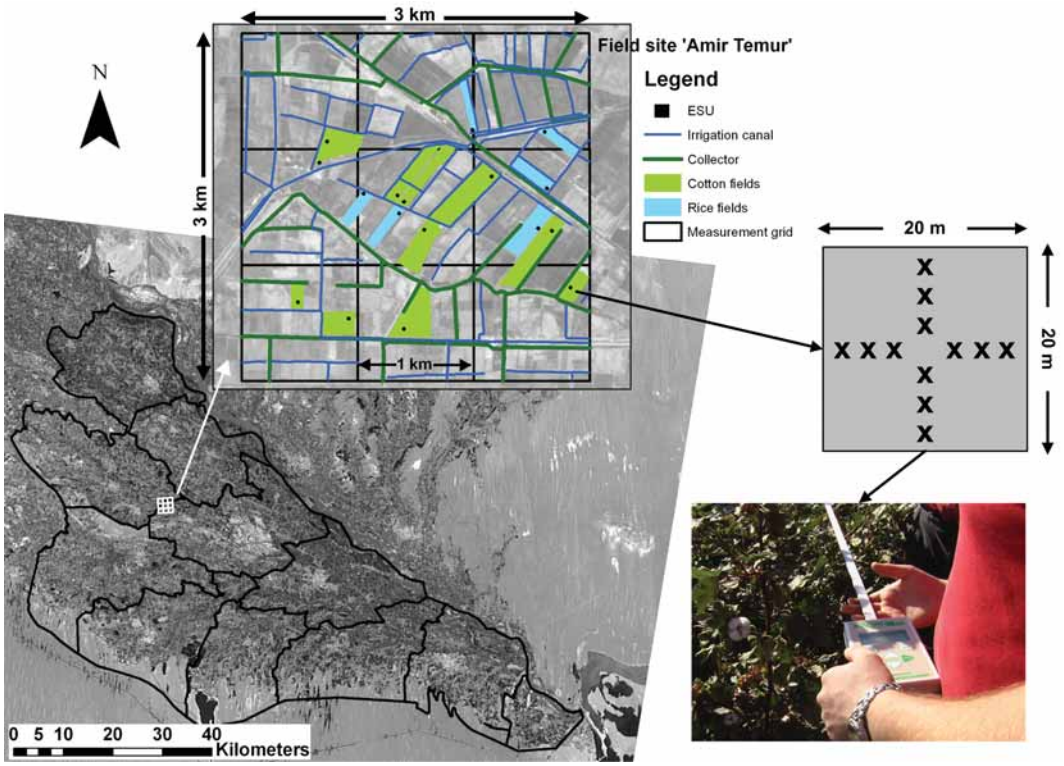

Figure 4.2: Field site and sampling design of the FPAR measurements conducted in 2009.

in Khorezm, fields were easily accessible and there was no impervious surface in the vicinity. Figure 4.3 shows the exact dates of measurements. For comparison, it also shows the acquisition dates of the RapidEye images that will be further discussed in the next section. All cotton fields were sampled five times between the end of June and the end of August, rice fields were sampled four times during this period and wheat fields were sampled two times between middle of May and beginning of June. Wheat fields were sampled to include all major crops in the up-scaling procedure. Further details on the field measurements and the up-scaling procedure can be found in Ehammer et al. (2010) and Ehammer (2011). In the following, those aspects that are essential to the derivation of FPAR are described.

Altogether, ten cotton fields, six rice fields and eight wheat fields were sampled every second week. Depending on the field size, between one and two Elementary Sampling Units (ESUs) with a size of 20 m $\times$ 20 m were sampled in each field. The locations of the ESUs were randomly chosen within each field, but it was assured that they were located in significant distance (approximately two RapidEye pixels) to roads and channels to avoid border effects. In each ESU, measurements were conducted at 12 spots, arranged in a cross. The corner coordinates of each ESU were measured using a Garmin GPS 12 device. Four individual FPAR measurements were made that covered an area of about 1 m^2. An AccuPAR LP-80 ceptometer (Decagon Devices, Inc.) was used for the measurements. The ceptometer is equipped with an 80 cm long

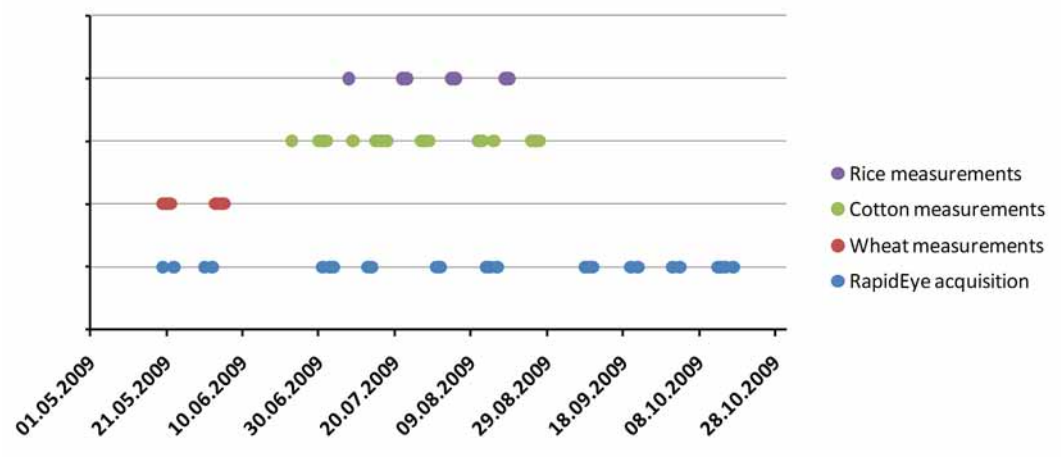

Figure 4.3: Dates of ground measurements of wheat, cotton and rice as well as RapidEye acquisition dates.

sensor bar, which holds 80 sensors that are sensitive to light in the PAR wavelengths. The device calculates FPAR via the relationship between readings of above and below-canopy PAR (in $\mu mol \times m^{-2}s^{-1}$), which were recorded at each spot. The fractional interception of light in a plant canopy, FPAR, can be calculated by equation 4.1:

$$FPAR = 1 - t - r + tr_s \tag{4.1}$$

With t being the light transmitted by the canopy, r the part of the photosynthetic active light that is reflected by the plant canopy and r_s is the light that is reflected from the soil surface (Decagon Devices Inc. 2010). The transmittance in a canopy, t, is represented by the measurements made below the canopy, near the ground. The measurements above the canopy represent the available photosynthetic active radiation (=1). For calculations with the AccuPAR, the last two terms of equation 4.1 are ignored, so that the actual fraction of intercepted photosynthetic active radiation (FIPAR) is calculated according to equation 4.2:

$$FIPAR = 1 - t \tag{4.2}$$

The actual readings for this type of measurement are taken with an upward-facing device. As shown in chapter 3.1.5, FIPAR can differ slightly from FPAR. However, light in the PAR waveband is mostly absorbed. Consequently, the error caused by this simplification is usually smaller than 0.05 in the PAR region (Decagon Devices Inc. 2010). The reflected part of PAR was thus neglected in the following analyses and FIPAR was assumed to be similar to FPAR. All measurements were conducted around solar noon, between 10 a.m. and 2 p.m., which is also recommended in the AccuPAR manual (Decagon Devices Inc. 2010). The maximum tilt an-

gle of the RapidEye acquisitions was approximately 20 degrees, but most scenes were recorded at angles less than 10 degrees. The characteristics of the measurements are in line with authors like Goward & Huemmrich (1992), who stated that 'caution should be exercised in employing far off-nadir, early morning or winter measurements to characterize the seasonal dynamics of vegetation APAR' (p. 137).

Furthermore, to avoid over or underestimation of FPAR, the recommendations of Tewolde et al. (2005) for the measurement of cotton row crops were followed. Mid-day measurements served to avoid row shading at very high sun angles, which is especially important under direct illumination that was most often the case in Khorezm. The placement of the sensor bar was another important factor during measurements, which depended on the row width of the crops. A row width of 90 cm, for example, allowed placing the sensor bar directly from one row centre to the next. In the case of a row width of 60 cm, however, straight alignment from one row to the next would cause the sensor bar to sample parts of the adjacent row. For very high or low sun angles this would cause the sensor bar to be partly in the shade, and thus to overestimate true FPAR values. In this case, the sensor bar was aligned diagonal between the centres of two rows. For measurements in wheat and rice fields, no row width had to be accounted for.

4.2.1.2 RapidEye data and pre-processing

The RapidEye satellite constellation was launched in 2008 and consists of five identical satellites able to acquire multispectral images on a near-daily basis (RapidEye 2011). On-ground swath width is 77 km (Tyc et al. 2005). Each satellite carries a multispectral sensor with bands in the blue (440-510 nm), green (520-590 nm), red (630-685 nm), red edge (690-730 nm), and near infrared (NIR, 760-850 nm) range of the solar spectrum (Tyc et al. 2005). The level 1B (L1B) data used in this study has a ground resolution of 6.5 m. Basic pre-processing was already applied to L1B data, including radiometric and sensor corrections as well as on-board spacecraft attitude and ephemeris corrections (RapidEye 2011). The RapidEye system was tasked to collect image data for the Khorezm region throughout the growing season 2009. Altogether 25 images were acquired, representing ten time steps (figures 4.3 and 4.4). Image acquisition failed only in April and the first half of May due to high cloud cover. Parts of the study area could furthermore not be covered by image acquisitions. This was obvious at time step 1 (May 20 and May 23, see figure 4.4), which was characterized by a data gap caused by incomplete regional coverage. The missing data concerned altogether 1,460 cotton and 554 rice fields (calculated using the field-based crop map described in the next section). Furthermore, the eastern part of the Khorezm region was also not covered from time step 5 through 8 and again at time step 10. This affected between 336 and 1,333 cotton, as well as between 3 and 187 rice fields. Because of the resulting number of missing scenes and the fact that the peak growing season was amongst the period not captured by image acquisitions, the eastern area was excluded from the subsequent crop yield modeling. Minor gaps also occurred at time step 6 in the north-western part

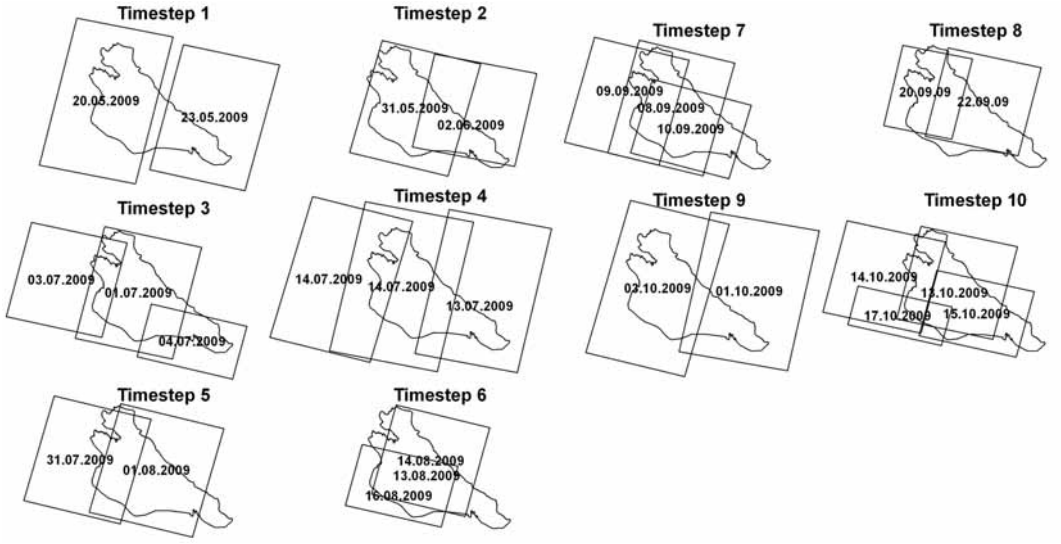

Figure 4.4: Illustration of RapidEye image coverage during the growing season 2009.

and at time step 8 in the southern part of the region.

The following processing steps were applied to all images: atmospheric correction, geometric correction, cloud masking and calculation of vegetation indices. Atmospheric correction of all scenes was done with the ATCOR 2/3 software (version 7.1) for flat terrain (Richter 2009). Dry rural atmospheres and visibilities between 10 and 50 km were chosen for the correction. Geometric correction was conducted by matching all RapidEye scenes to two pan-sharpened SPOT 5 scenes (spatial resolution: 2.5 m) that were acquired in 2006 and rectified with ground control points from a differential GPS. Each RE scene was geo-corrected with 30 to 35 manually set ground control points. The resulting geometric error was less than one RapidEye pixel. Additional details concerning atmospheric and geometric correction of the satellite data are described by Conrad et al. (submitted) and Conrad et al. (2010). Clouds partly affected satellite image acquisitions early in the season (May 23 and June 2), with a cloud cover of 12 and 8 %, respectively. Clouds were extracted from the cloud masks delivered with the L1B product, and those areas were masked from further processing. Finally, NDVI and EVI were calculated from all surface reflectance RE data.

4.2.1.3 Crop classification

The field-based crop map described in this section was the basis for the RapidEye-based crop yield model and it was used in the process of validating the MODIS FPAR product. The map was based on the time series of RapidEye image data described above. A short description of the classification methodology will be given in the following. Further methodological details can be found in Conrad et al. (submitted).

Table 4.1: Ground truth statistics for the RapidEye-based crop map (adapted from Conrad et al. submitted).

	Number of samples		
Landuse class	Field sampling	Quickbird	Total
Cotton	23	58	81
Rice	23	25	48
Wheat	4	19	23
Wheat-rice	1	83	84
Wheat-sorghum/maize	26	0	24
Sorghum/maize	18	0	18
Trees/crops	28	52	80
Fallow/unused	1	60	61

Ground truth information on the different crops in the study region was sampled during the growing season 2009. The sampled crops and crop rotations were: cotton, wheat, wheat-rice, wheat-maize/wheat-sorghum, rice, maize, sorghum, alfalfa, trees and crops, trees, sunflowers, watermelons and fallow or unused (compare figure 4.5). However, only cotton, rice, and wheat (for up-scaling) were required for this study. Land use sampling consisted of two steps. The first step was to collect crop information directly in the field. To this end, randomly distributed fields in the larger vicinity of the capital Urgench were visited, and the required information (location of field, crop type, crop height, crop rotation, GPS coordinates) was noted. Yet only a limited amount of training data could be gathered during the season 2009 in the Khorezm region. To acquire sufficient information for an accurate classification, additional data was extracted from very high resolution Quickbird (QB) data (pan-sharpened to 2.5 m ground resolution) by visual interpretation in a second step. Altogether seven QB scenes from two locations (see figure 4.5) were used in this process. The field boundaries were intersected with the multi-temporal QB data, and random fields were chosen in both locations. These fields were then visually assessed and, together with their corresponding seasonal development, the crop type was inferred. During this process, only crop types that could be identified with great certainty were chosen as training samples. This was possible because some crops feature unique spatial patterns, which are visible in the QB images (e.g., cotton rows). The distribution of the combined ground truth data from steps one and two is displayed in figure 4.5. The final number of samples varied between crop types (table 4.1). Altogether, 421 samples were employed for training and validation of the classification methodology. The reference data was split in two halves for training and validation.

A random forest classifier was used for crop mapping. Random forests are a combination of several classification trees, which are calculated based on randomly drawn subsets of the input

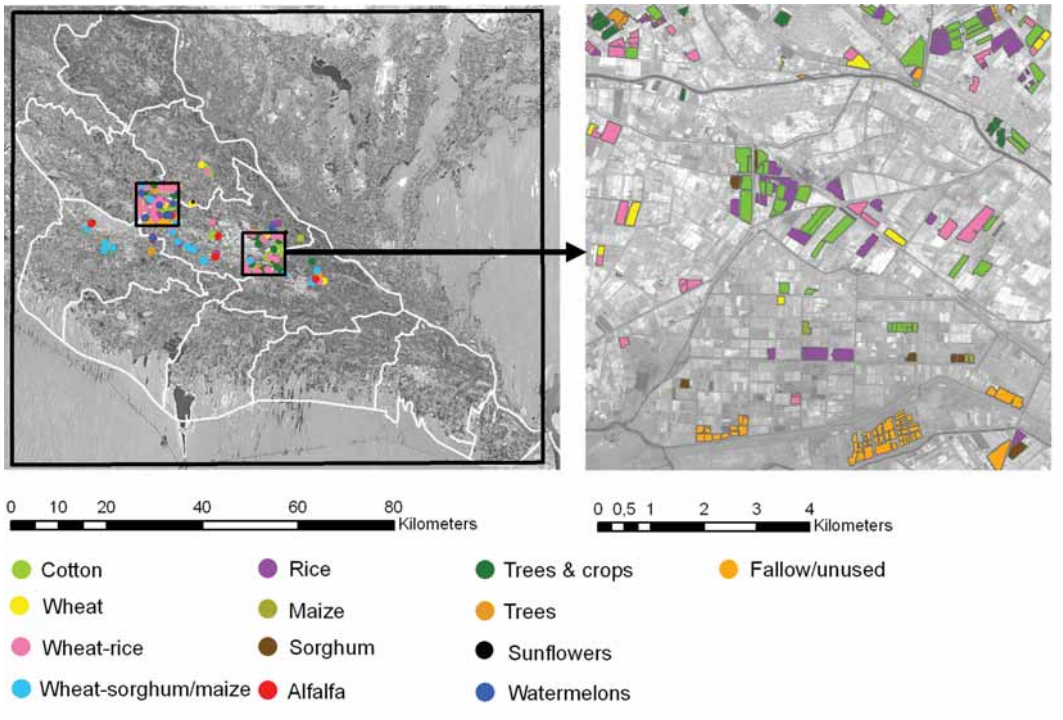

Figure 4.5: Location of the ground truth information (adapted from Conrad et al. submitted). The black rectangular shapes (left) represent the location of the Quickbird scenes (2.5 m ground resolution) used for visual extraction of training samples. The right-hand side shows a close-up of one of the scenes with the respective fields randomly chosen as training data.

data (Breiman 2001). Classification trees represent decision trees that sort datasets through splits, each consisting of one input feature and threshold value optimally separating training samples into two groups (Breiman et al. 1984). The general concept of random forests is to build multiple classification trees leading to multiple possible classification decisions. The final classification is derived by a majority vote. For the derivation of the crop map, an ensemble of 511 classification trees was used (Conrad et al. submitted). Features employed for classification were the mean and standard deviation of RapidEye bands one to five, the NDVI, and the EVI. All features were calculated per field. The necessary field boundaries were based on the segmentation of high resolution SPOT 5 data from 2006 and the subsequent classification into field and non-field objects (Conrad et al. 2010). Consequently, the final crop map was also field-based. For some classes there was insufficient ground data for classification (e.g., alfalfa, sunflowers), whilst others were combined into one class because they were difficult to separate (e.g., maize and sorghum; see table 4.1). The classes distinguished in the final map were: cotton, fallow, maize/sorghum, rice, trees, wheat-fallow, wheat-rice and wheat-sorghum/maize. Based on the field samples, the overall accuracy of the map was calculated to be 85 % (Conrad et al. submitted). The producer's and user's accuracy for cotton, rice, wheat, wheat-rice and wheat-maize/sorghum are presented in table 4.2, respectively (Conrad et al. submitted). Cotton

and rice were the essential crops for this study, and the accuracies were high in both cases. The accuracies for the wheat classes were acceptable (users' accuracies between 0.67 and 1.00). Yet since these classes were merely required for comparison with the MODIS land cover map and not directly for modeling, generally lower accuracies were neglected. The compiled crop map was afterwards used for the generation of a regional high resolution RapidEye-based FPAR product.

4.2.1.4 Statistical up-scaling of *in situ* FPAR to the RapidEye scale

The goal of this step was to compile two RapidEye-based FPAR datasets, one with an average FPAR value for each cotton and rice field and one with a value for each pixel in a RapidEye image. The first dataset was afterwards used for crop yield modeling, the latter served for the up-scaling of FPAR to the MODIS scale. In both cases, statistical up-scaling from *in situ* to RapidEye data was conducted by analyzing the correlation between means of the field measurements and NDVI values calculated for segments of RapidEye data. Two segment sizes were chosen, one that represented the boundary of an individual field and one that represented homogeneous patches with similar spectral characteristics within a field.

The field boundaries required in the first case were derived by manual digitization. The sub-field object scale was derived by image segmentation of the original RapidEye image data (Ehammer et al. 2010). Spectral information from RapidEye data was used in the process of generating the smallest possible, spectrally similar image objects (Ehammer et al. 2010). RapidEye NDVI data was aggregated on both scales by averaging, and it was subsequently compared to the field data for each field and image object. To this end, all field data points were averaged per image objects (whole fields and homogeneous segments of fields), and the final value was correlated with the satellite-based NDVI value of the corresponding object. All data points were pooled for the comparison, resulting in one regression equation per crop for the season. These steps are detailed in Ehammer et al. (2010) and Ehammer (2011). In the following, only the most important steps and those that were previously not described will be highlighted. The regression equations for cotton and rice at the field scale presented in Ehammer et al. (2010) were applied to averaged NDVI values (pooled data for all time steps), which led to the generation of multi-temporal, field-based FPAR maps. The correlation coefficient was reported to be 0.88 for cotton and 0.95 for rice.

In contrast to the field scale, the compilation of pixel-based FPAR maps was based on smaller image objects. The spectral information of single pixels and their objects differed slightly, with standard deviations for NDVI at the object scale of 0.044 (cotton), 0.058 (rice) and 0.049 (wheat). The mean NDVI of these image objects was afterwards correlated with the associated *in situ* FPAR data of cotton, rice and wheat. The resulting regression equations were applied to the RapidEye NDVI data (individual pixels), accounting for the crop type of each pixel.

Table 4.2: Confusion matrix indicating the producer's and user's accuracies of the classification (adapted from CONRAD ET AL. submitted).

	Cotton	Fallow-unused	Sorghum-maize	Rice	Trees-crops	Wheat	Wheat-rice	Wheat-sorghum,maize	Producer's accuracy
Cotton	41								1
Fallow-unused		28			2				0.93
Sorghum-maize	4		2	1	2				0.22
Rice	2		1	19	1		1		0.79
Trees-crops					35		5		0.88
Wheat						11			1.00
Wheat-rice							38	4	0.90
Wheat-sorghum, maize					2		3	8	0.23
User's accuracy	0.87	1.00	0.67	0.95	0.83	1.00	0.79	0.67	

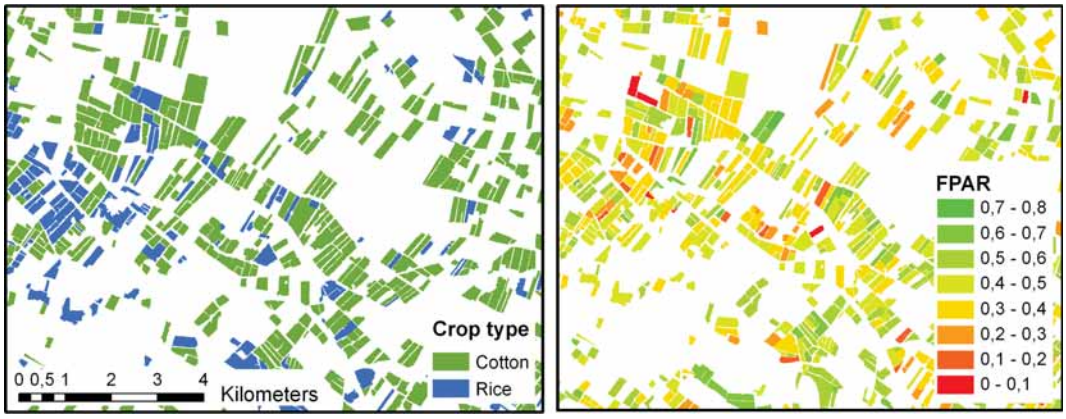

Figure 4.6: Subset of the study region showing the field-based crop map (left) and the corresponding crop-specific FPAR map (right; based on images from September 20 and September 22).

Thus, FPAR maps were generated from RapidEye data at the pixel scale. Although all pixels belonged to a specific land use class, not all crop types and land uses were sampled during fieldwork. Specific regression equations based on field measurements were only used for the main crop types in the study region (cotton, rice and wheat-rice rotations). For other crops and land uses regression equations of the pooled data for all crops were used, because the overall difference between regression equations was small. Fields classified as having a mixture between trees and crops were omitted from further analysis. To assess the regression models, the coefficient of determination (R^2) was calculated.

4.2.2 Results and discussion

Using the crop-specific regression equations for the field scale, regional FPAR maps were calculated for each single time step. The detailed results will not be shown here, as they have been extensively presented and discussed in Ehammer et al. (2010) and Ehammer (2011). The crop map described in section 4.2.1.3 was included in the regionalization to be able to apply the crop-specific equations. An example for the regional FPAR product at the field scale is presented in figure 4.6. The seasonal development of FPAR for cotton and rice per field will be further discussed with relation to the RapidEye-based yield model in chapter 5.3.

At the small object scale, field measurements of FPAR and NDVI derived from RapidEye were generally well correlated (figure 4.7). The coefficient of determination ranged from 0.64 (wheat-rice) to 0.83 (rice). While the relationships are linear for all crops, the correlation strength showed crop-specific differences. For cotton in particular, correlations between FPAR and NDVI were lower compared to rice. This was probably due to the general difference in growth habit between the two crops. Cotton canopies are more heterogeneous than rice canopies because of their woody components influencing the vegetation structure. In contrast, rice displays a

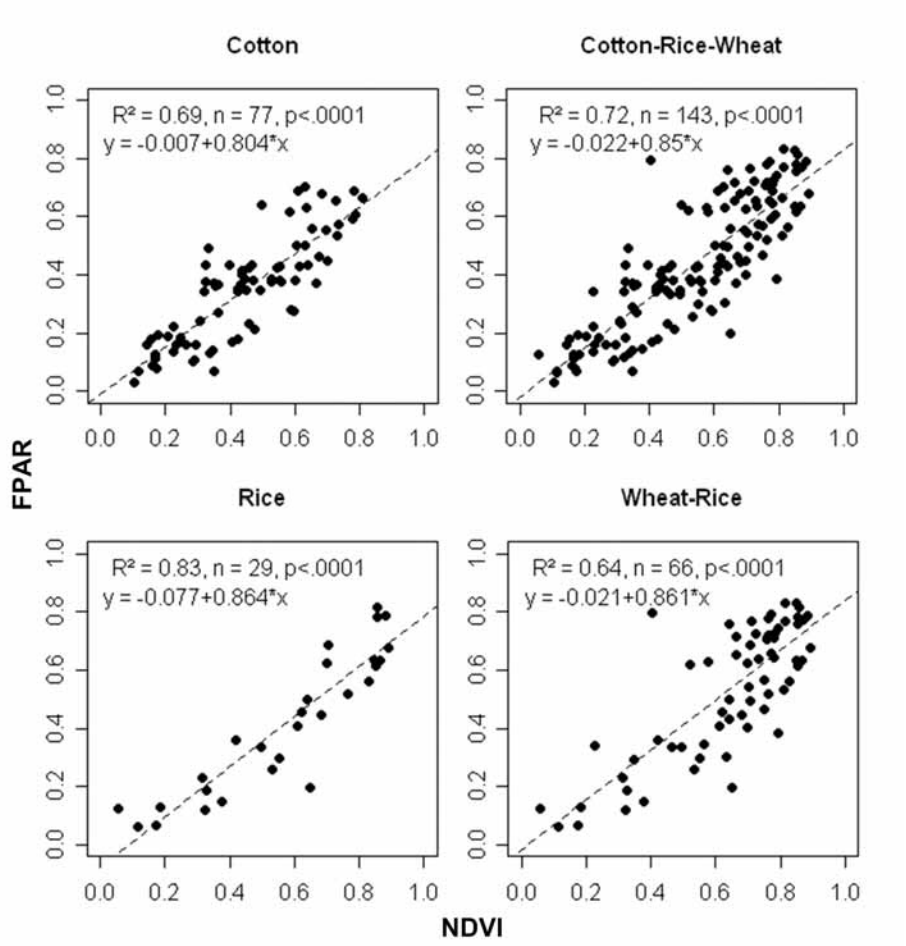

Figure 4.7: Scatterplots showing the crop-specific correlations between NDVI (RapidEye) and FPAR (field measurements) together with the coefficient of determination (R^2), the total number of observations (n), p values, and the resulting linear regression model (adapted from Fritsch et al. 2012).

homogeneous canopy and is grown in basins. Cotton is grown in rows and has frequently larger patches of bare soil within one field. A mixture of soil and crops decreased the correlation between field measurements and satellite VIs, as these conditions were also reflected in the NDVI values of the single segments. A similar picture can be inferred from the standard error of the data, which ranged from 0.1 (cotton and rice) to 0.12 (cotton-rice-wheat) and 0.14 (wheat-rice). Based on the dominance of cotton and rice crops during the investigated period, the overall standard error for the region was assumed to be around 0.1. No significant bias was discernible in the data, meaning that the high resolution FPAR maps had no tendency to under or overestimate field data. This was a decisive prerequisite for independent calibration and validation of the MODIS 250 m NDVI and the 1 km FPAR product.

The developed regression equations were used to transform pixel-based NDVI values into FPAR

in conjunction with the crop map. An average regression was applied to crops unmeasured in the field. The similarity of the regression equations for cotton and rice, two crops that differ largely in terms of canopy and background characteristics, proved this approach to be justified. It was also shown that, for example, cotton and maize or sorghum show a very similar seasonal development of the NDVI (Conrad et al. submitted). Earlier studies furthermore stated that the linear relation between NDVI and FPAR varies little with plant characteristics or illumination conditions (Asrar et al. 1992). Soil background color, however, influences the relationship (Fensholt et al. 2004), but its variations can be neglected in the study region due to widespread homogeneous soil conditions (see chapter 2). The crops sampled for this study represented different degrees of vegetation cover fractions (cotton as a row crop, wheat and rice with very dense canopies). Soil wetness can also influence the correlation between FPAR and NDVI by altering soil color and light distribution in crop canopies. But measurements were also conducted on fields that were partly or fully irrigated. Hence, it was assumed that the largest part of the regional crop growth variability was captured by the field measurements. This was backed by the fact that most of the growing season was covered by the field measurements.

The high resolution FPAR maps clearly show the seasonal development of the crops in the irrigation system (figure 4.8). The maximum value of FPAR was 0.83 at the peak of the season. Rice crops typically showed a larger peak FPAR value than cotton, with a difference of approximately 0.1 FPAR units. The green areas in figure 4.8 are mostly wheat fields. Some of these wheat fields are already harvested on August 1, indicated by a change from green to red colors. These fields generally show higher FPAR values later in the season, indicating cultivation of a summer crop on the same field. Infrastructure like roads, channels or urban areas clearly stand out through low FPAR values throughout the season. The same is true for fallow fields. Cotton and rice fields are characterized by peak FPAR values at August 13 and September 8. The RapidEye-based maps were subsequently aggregated to the MODIS resolutions (250 m and 1 km grids) by averaging and compared to the corresponding MODIS pixel value.

4.3 Optimization of regional FPAR information at the 250 m MODIS scale

4.3.1 Validation of the MODIS FPAR product

4.3.1.1 Data and methods

4.3.1.1.1 MODIS data and pre-processing

For validation of the MODIS FPAR product, the collection 5 MODIS LAI/FPAR (MOD15A2) and the collection 4 MODIS land cover (MOD12Q1) products were used. Based on these products, the MODIS Adaptive Processing System (MODAPS) calculates FPAR (Zhao & Running

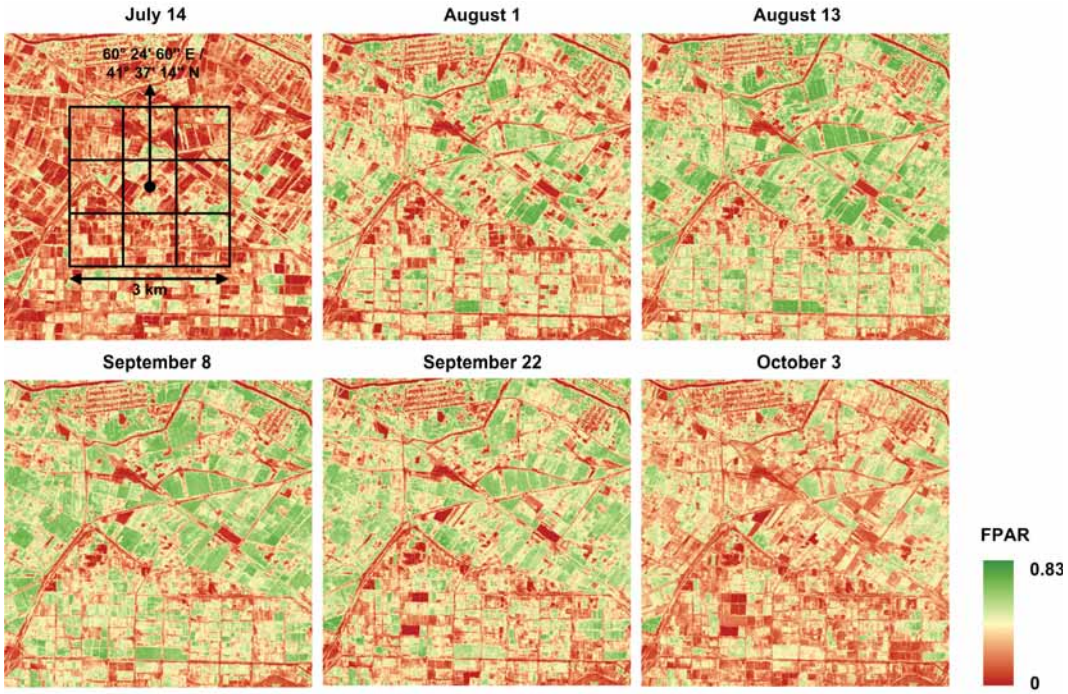

Figure 4.8: Subset of the final pixel-based dataset that shows the seasonal development of FPAR (adapted from Fritsch et al. 2012). The grid in the upper left corner (July 14) represents the site where field measurements were acquired (Ehammer et al. 2010).

2010). The MOD15A2 product is an 8-day composite, derived from the inversion of a radiative transfer model. Spectral measurements from the red and near-infrared sensor bands are compared by a cost function to modeled spectra for different canopy and soil types. All solutions within the range of uncertainty are considered acceptable and the mean weighted FPAR for all retrievals is used as output (Myneni et al. 2003). The land cover classification limits possible solutions of the inversion process according to specific biome types, determining which values from the underlying look-up table (LUT) are used for the three-dimensional inversion algorithm. The range of possible solutions is thus reduced and unrealistic parameter combinations are excluded. If the main algorithm fails (e.g., due to cloud cover during data acquisition) a backup algorithm is used that is based on empirical relationships between FPAR and NDVI. MOD15A2 composite data used for this study was chosen to correspond to the acquisition dates of the RapidEye images (table 4.3). All MODIS data is distributed with quality assessment science data sets (QA-SDS) that allow the general evaluation of the data and the application of user-defined quality criteria. Issues addressed by the QA-SDS are for example the state of the detectors, atmospheric conditions, the algorithm used and aerosol levels (Myneni et al. 2003).

MODIS land cover determines the basic structural characteristics of the land surface used as input parameters for the FPAR retrieval process. Misclassification of land cover can therefore cause errors in the FPAR product (Tian et al. 2000). The MOD12Q1 product is gener-

Table 4.3: MODIS composites and RapidEye image acquisitions used for validation of the MODIS FPAR product (adapted from Fritsch et al. 2012).

MODIS composite number	MODIS composite period	RapidEye acquisitions
185	04.07.-12.07.	14.07.
201	20.07.-28.07.	01.08.
217	05.08.-13.08.	13.08.
241	29.08.-06.09.	08.09.
257	14.09.-22.09.	22.09.
265	22.09.-30.09.	03.10.

ated via a decision tree approach using training data from sites representative of global biomes (Friedl et al. 2002). Five classification schemes are included, type 3 being the one used for $LAI/FPAR$ retrieval. The MOD12Q1 product used for comparison was from 2001, which is employed in the LAI/FPAR algorithm (Zhao & Running 2010). The RapidEye based crop map was compared with the MODIS land cover product in the course of validating the MODIS FPAR product. Thus, the legends of both maps were matched by rearranging the detailed RapidEye information to the relevant MODIS classes, which were broadleaf crops and grasses/cereal crops. Theoretically, the first should include crops like cotton, maize and sorghum, the latter wheat and rice. Hence, cotton and maize/sorghum were combined to broadleaf crops. Wheat, rice and all wheat rotations were reclassified as grasses/cereal crops. All other land use classes of the MODIS and RapidEye maps were assigned to the class 'other land use'. For a direct comparison, the RapidEye map was aggregated to the MODIS resolution by a majority filter. A confusion matrix was calculated to assess the accuracy of the MODIS product.

For this study, the impact of spatial heterogeneity on the accuracy of the MODIS FPAR product was assessed. Therefore, the sub-pixel coverage of MODIS pixels with agricultural land use classes was first calculated using the RapidEye-based crop map. Field boundaries were intersected with a 1 km MODIS grid and the relative area of agricultural fields and classes (from the RapidEye crop map) per MODIS pixel was calculated (this step is further described in chapter 4.3.2). They were generally split in homogeneous and heterogeneous pixels. There was a lack of pixels with a general agricultural cover between 90 and 100 % for further analysis. A trade-off had to be solved between homogeneity and number of pixels for a sound analysis. MODIS pixels with a relative area of greater or equal 80 % offered a sufficient number of samples and were considered as 'homogeneous' pixels. Accordingly, pixels with less than 80 % cover were considered as being heterogeneous. The information on these two groups was finally included in the process of validating the collection 5 MODIS FPAR product, assuming it plays a decisive role for its overall performance.

4.3.1.1.2 MODIS product validation

Validation of MODIS FPAR was conducted for six specific periods during the vegetative phase, as described in the last section. Scatterplots of FPAR from MODIS and RapidEye were generated in order to visually assess potential differences. Pearson's correlation coefficient (r) was calculated for each comparison. For quantitative validation, different error measures were calculated, including bias (equation 4.3), Root Mean Square Error (RMSE; equation 4.4) and precision (equation 4.5) (see Tan et al. 2005 and Wallach 2006 for a more thorough description).

$$Bias = \frac{1}{N}\sum_{i=1}^{N} D_i \tag{4.3}$$

Concerning bias, D_i represents the differences between measured (RapidEye) and modeled (MODIS) values (Wallach 2006). N is the total number of observations. The bias is the mean of the summed differences between RapidEye and MODIS observations (Wallach 2006). It is positive if MODIS under-predicts and negative if it over-predicts.

$$RMSE = \left[\frac{1}{N}\sum_{i=1}^{N}(X_i - T_i)^2\right]^{\frac{1}{2}} \tag{4.4}$$

The RMSE represents the error between measured (RapidEye, X_i) and modeled values (MODIS, T_i) after calculating their squares and the root of the result. The RMSE can also be labeled as the uncertainty of the data, as RapidEye data represents estimates of the true values. The RMSE has the advantage that it does not compensate between over and under-prediction (like the bias) and that it has the same unit as the original data (Wallach 2006). Finally, the precision is the standard deviation of the satellite sensor measurements X_i (for both RapidEye and MODIS) with regard to the average of those measurements μ. It indicates the amount of variation inherent in the data (Tan et al. 2005).

$$Precision = \left[\frac{1}{N-1}\sum_{i=1}^{N}(X_i - \mu)^2\right]^{\frac{1}{2}} \tag{4.5}$$

4.3.1.2 Results and discussion

4.3.1.2.1 Validation of the collection 5 MODIS FPAR product

Product validation was done separately for homogeneous and heterogeneous pixels, in order to assess the differences between both groups. The total number of pixels used for comparison varied due to differing coverages of the study region by RapidEye data (figure 4.9). The results are described and discussed in the following paragraphs.

Validation of MODIS pixels with more than 80 % agricultural land use

Figure 4.9 (a)-(f) shows the comparison between MODIS and RapidEye FPAR for six dates in 2009. The linear correlation coefficients (Pearson), the total number of samples used for the analyses and the 1:1 lines are shown. The scatterplots of the different periods demonstrate a fair relation between RapidEye and MODIS data, but comprise some obvious outliers. Correlation coefficients are low, but increase considerably in the second half of the investigated period (September and October). Higher correlations with the progression of the season can be explained by a decreasing amount of soil background, which was also observed by Steinberg et al. (2006), who found that MODIS FPAR was more accurate for areas with denser canopies compared to sparsely vegetated surfaces. Combining all periods into one dataset significantly increases the correlation coefficient to 0.7.

As the season progresses, the data points deviate more from the 1:1 line. There is a general overestimation of FPAR by the MODIS product. This finding is in line with the results of Fensholt et al. (2004), Huemmrich et al. (2005) and Steinberg et al. (2006). The observed overestimation is also confirmed by the calculated error measures (table 4.4). Besides one exception (RE: August 1), there is a negative bias, which varies between -0.01 and -0.124. The RMSE provided similar results, ranging from 0.072 to 0.138 (mean: 0.115). These numbers suggest that the MODIS product overestimates RapidEye-based values between 7.2 and 13.8 %. Both MODIS and RapidEye FPAR have a comparable variation in the data in terms of precision, with the MODIS precision being slightly higher.

Validation of MODIS pixels with less than 80 % agricultural land use

A comparison of MODIS pixels with less than 80 % agricultural land use is presented in figure 4.9 (g)-(l). The correlation coefficients show an indistinct seasonal pattern, with higher values in the middle and end of the investigated period. The overall level of correlation is higher than for homogeneous pixels, but this is only true for single periods and can be due to insufficient data points. The combination of all periods leads to similar correlations ($r = 0.69$).

The overestimation of FPAR from heterogeneous MODIS data is also reflected in the measures of error. Bias and RMSE are higher for MODIS pixels with larger heterogeneity in most cases. Exceptions occur on August 1 and October 3 (bias), as well as on July 14, August 1 and September 9 (RMSE). The mean RMSE is 0.114, which is comparable to the mean RMSE for homogeneous pixels (0.115). This similarity is caused by a higher RMSE for homogeneous pixels obtained during the first two investigated periods, which raises the overall RMSE. From the given data one can conclude that overestimation is between 6.2 and 15.3 %. The precision of heterogeneous pixels is comparable to that of homogeneous pixels. In general, the measures of error vary less between homogeneous and heterogeneous pixels than the corresponding correlation coefficients.

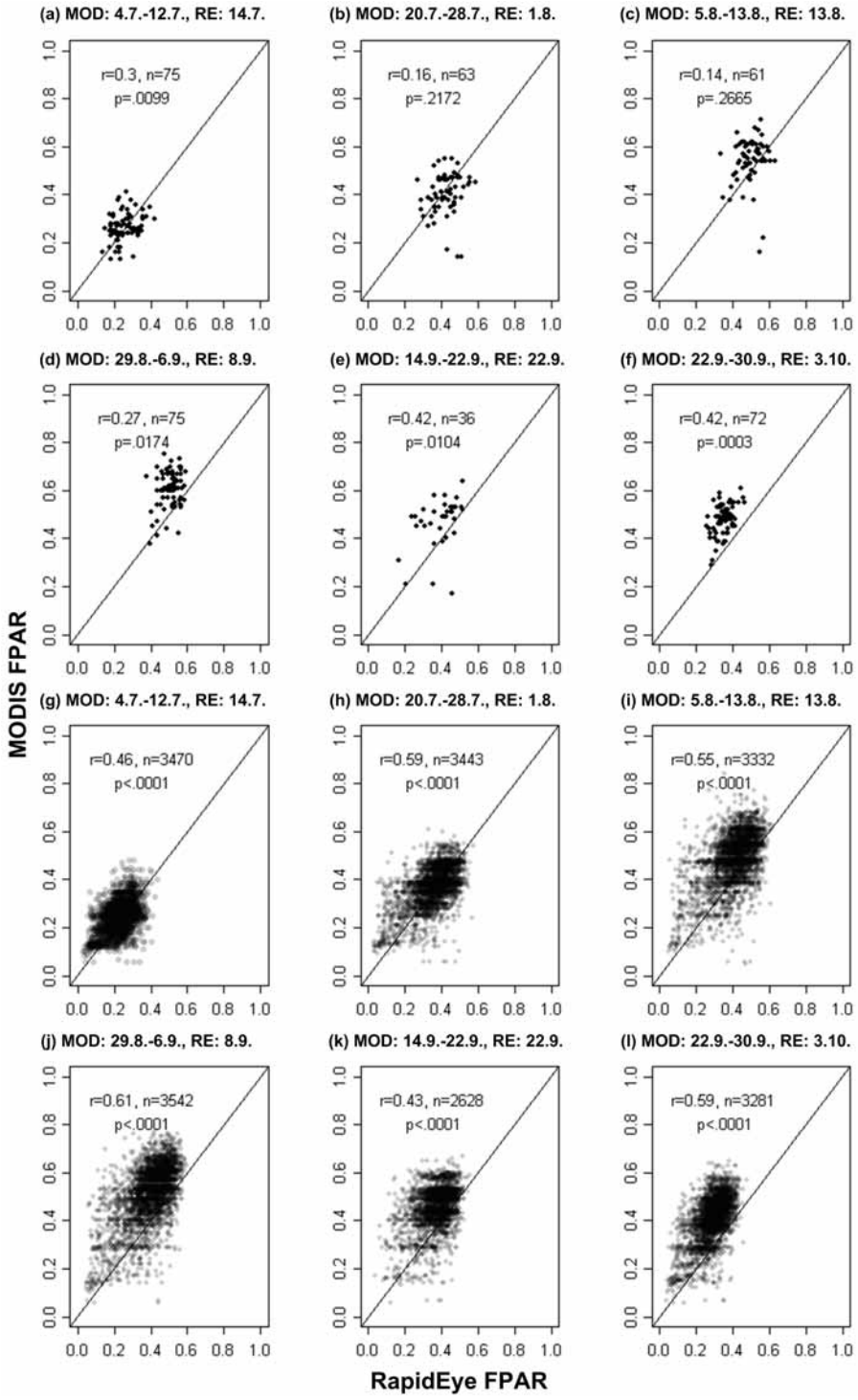

Figure 4.9: A comparison of FPAR data from RapidEye (x-axis) and MODIS (y-axis) imagery. The letters (a)-(f) denote comparisons for pixels with >80 % crop cover, the letters (g)-(l) the ones for pixels with <80 % cover. The Pearson correlation coefficients, p values, total number of observations, and 1:1 lines are also shown (adapted from Fritsch et al. 2012).

Table 4.4: Measures of error calculated from MODIS and RapidEye FPAR values for MODIS pixels with greater or equal than 80 % (letters a-f) and with less than 80 % (letters g-l) agricultural cover (adapted from Fritsch et al. 2012).

			Precision	
Comparison	Bias	RMSE	MOD	RE
(a) MOD: 4.7.-12.7., RE: 14.7.	-0.010	0.072	0.246	0.246
(b) MOD: 20.7.-28.7., RE: 1.8.	0.022	0.104	0.296	0.262
(c) MOD: 5.8.-13.8., RE: 13.8.	-0.042	0.115	0.311	0.250
(d) MOD: 29.8.-6.9., RE: 8.9.	-0.105	0.131	0.279	0.222
(e) MOD: 14.9.-22.9., RE: 22.9.	-0.075	0.128	0.322	0.300
(f) MOD: 22.9.-30.9., RE: 3.10.	-0.124	0.138	0.249	0.217
(g) MOD: 4.7.-12.7., RE: 14.7.	-0.018	0.062	0.237	0.241
(h) MOD: 20.7.-28.7., RE: 1.8.	-0.014	0.081	0.285	0.305
(i) MOD: 5.8.-13.8., RE: 13.8.	-0.075	0.124	0.330	0.315
(j) MOD: 29.8.-6.9., RE: 8.9.	-0.116	0.153	0.347	0.321
(k) MOD: 14.9.-22.9., RE: 22.9.	-0.085	0.123	0.296	0.283
(l) MOD: 22.9.-30.9., RE: 3.10.	-0.116	0.139	0.304	0.266

The larger variability in the correlation between the MODIS and RapidEye data is caused by a larger scatter for heterogeneous pixels, which can presumably be attributed to greater spatial heterogeneity and background influence with less agricultural cover. In this case, background consists of land cover classes such as settlements, water, bare soil, bushes, etc. What does this mean with respect to the study area? Figure 4.10 presents a histogram of the relative area of agricultural fields per MODIS pixel, illustrating that the majority of pixels have significantly lower agricultural cover and are heterogeneous. This greatly influences the accuracy and applicability of the MODIS FPAR product due to a large variability of the sub-pixel land cover composition.

The observed overestimation of FPAR by the MODIS product is especially pronounced starting from late August. The performance of the FPAR algorithm is influenced by sub-pixel heterogeneity and the amount of soil background (Myneni et al. 2002). Problems of the underlying biome classification (Steinberg et al. 2006, Yang et al. 2007) or the use of the empirical back-up algorithm due to low data quality of the MODIS products (Steinberg & Goetz 2009) were also often identified as reasons for deviations between MODIS and high resolution satellite or *in situ* data. However, analysis of MODIS quality data showed that more than 90 % of the investigated pixel values were retrieved by the primary algorithm, cloud-free and assigned the highest possible overall quality. The remaining pixels nearly all belonged to irrelevant land cover classes (urban, desert and water), which is why near-perfect conditions in terms of data quality

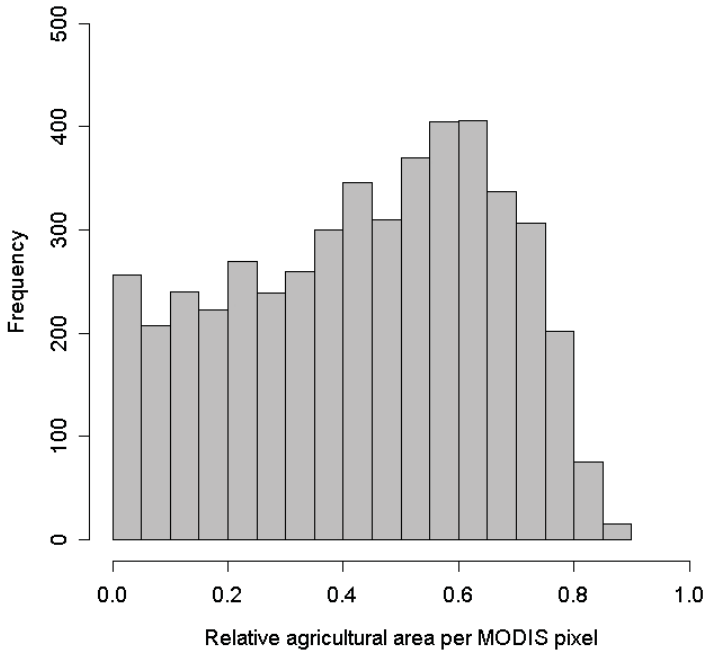

Figure 4.10: Histogram depicting the relative amount of agricultural fields per MODIS pixels for the study region (adapted from FRITSCH ET AL. 2012).

could be concluded. Subsequent analysis therefore concentrated on MODIS land cover data and sub-pixel heterogeneity, which will be described in the following section.

4.3.1.2.2 Evaluation of the MODIS land cover product, scale influences and other sources of error

A visual comparison of the RapidEye and MODIS land use and land cover maps is presented in figure 4.11, and table 4.5 shows the associated area statistics. A quantitative comparison reveals that the area of broadleaf crops is quite similar in both maps, yet the ratio between broadleaf and cereal crops strongly deviates in the MODIS map (table 4.5). RapidEye-based results show that broadleaf crops (cotton and maize/sorghum) and cereal crops (wheat, rice) are similar in terms of areal extent, both having a share of around 39 %. In contrast to this balance in the RapidEye map, grasses/cereal crops dominate in the MODIS map (53.83 %) and are highly overestimated. Based on visual interpretation, the urban class was underestimated because there are many smaller villages in the region that have not been identified. They have been misclassified as grasses/cereal crops or shrubs. The total agricultural area from RapidEye is approximately 2,331 km^2. In comparison, broadleaf crops and grasses/cereal crops from MODIS add up to 3,475 km^2. This overestimation can be attributed to the pixel size of MODIS and to the found misclassifications.

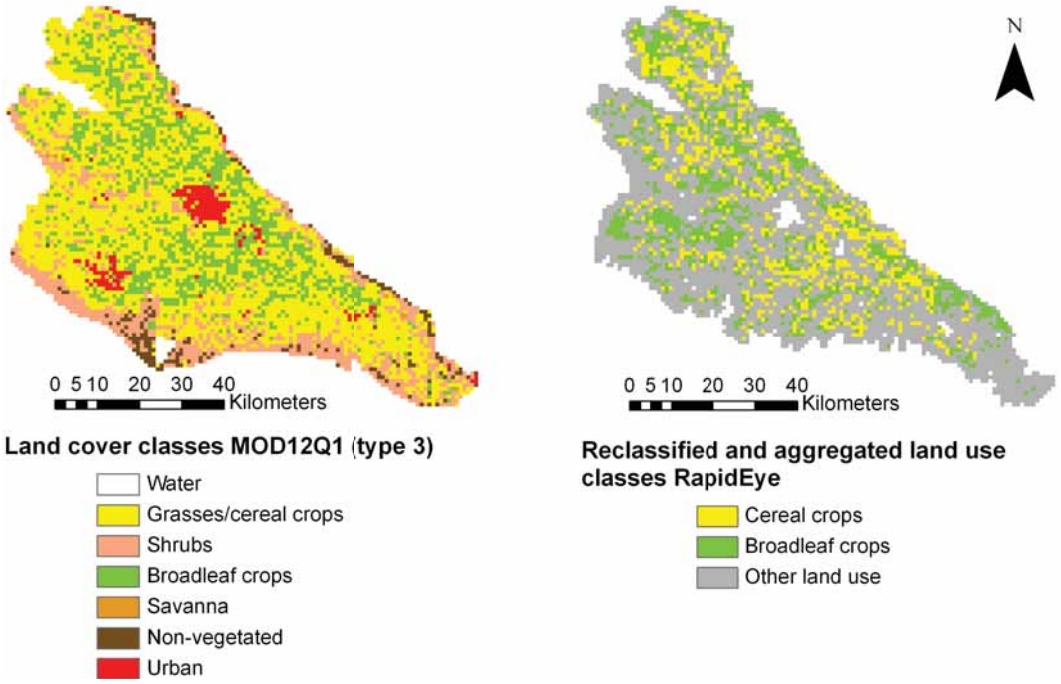

Figure 4.11: A comparison of the MOD12Q1 land cover product (2001) and the reclassified and aggregated RapidEye-based land use classification (2009) (adapted from Fritsch et al. 2012).

MODIS class-based and overall classification accuracy was calculated after the RapidEye crop map was aggregated to the MODIS scale. For grasses/cereal crops, the producer's accuracy is 57.3 % and the user's accuracy 19 %. For broadleaf crops, the producer's accuracy is 28.2 % and the user's accuracy is 23.6 %. The overall accuracy amounts to 29.9 %. Altogether, the MODIS land cover map hardly contains correct locations of the dominant crops in the study region. The reason is most likely the temporal mismatch between both maps (8 years), as agriculture in the region is highly dynamic and crop rotations change from year to year.

Negative effects of biome misclassification on product accuracy were found by Tan et al. (2005). Myneni et al. (2002) showed that misclassifying broadleaf crops as grasses/cereal crops can cause a difference of around 12 % in retrieved LAI values (this number would assumingly be lower for FPAR retrievals, due to its general insensitivity to plant structural parameters). Nevertheless, Yang et al. (2007) pointed out that the error of the MODIS LAI product was unlikely to be caused by misclassification alone, because misclassification between similar biomes (cereal and broadleaf crops, in their case) only causes minor errors. A thorough and area-wide validation for Khorezm was difficult due to the spatial heterogeneity of the region (most pixels are characterized by a mixture of different crop types). To determine the impact of misclassification on FPAR accuracy, correctly classified and misclassified pixels of broadleaf and cereal crops were

Table 4.5: A comparison of land cover and land use-specific areal statistics from MODIS and RapidEye maps (adapted from Fritsch et al. 2012).

MOD12Q1 (2001)		RapidEye (2009)	
Class	Area (km^2)	Class	Area (km^2)
Grasses/Cereal crops	2,463.53	Grasses/Cereal crops	904.72
Broadleaf crops	1,011.82	Broadleaf crops	899.41

compared (figure 4.12).

Misclassification does not significantly affect the overestimation of MODIS FPAR in this case, which is in line with Yang et al. (2007). In figure 4.12, this overestimation is present whether the pixels have been correctly or incorrectly classified as broadleaf or cereal crops, respectively. Differences are negligible, which is also reflected in the correlation coefficients. The RMSE was 0.101 (broadleaf-broadleaf), 0.115 (broadleaf-cereal), 0.115 (cereal-cereal) and 0.108 (cereal-broadleaf). Therefore, scale issues are most likely the main source of error for the MODIS FPAR product.

To verify this, RapidEye and MODIS FPAR for pixels correctly classified as broadleaf and cereal crops were compared, stratified based on the relative area of broadleaf and cereal crops (figure 4.13). The results demonstrate that a relative crop area of less than 60 % has an insignificant effect on the overestimation. The overestimation only slightly decreases for correctly classified pixels with a crop area of more than 60 %, yet the RMSE of this group is still the same amount of all other observed values (RMSE = 0.116).

The RMSE further drops to 0.094 if the pixel was correctly classified and the crop cover was larger than 80 %. Only two pixels in all six MODIS images belonged to this category ($n = 12$), which is why this number can merely be seen as an indicator. The remaining overestimation cannot be thoroughly explained by the conducted analyses. According to Wang et al. (2001), the uncertainty associated with the MODIS FPAR input channels can cause an offset of around 0.1, which may explain a part of the findings. Further research is needed to evaluate this. Yet due to the fact that there is still a considerable quantity of background even in the most homogeneous pixels used in this study, the magnitude of error is likely to be caused by this background influence, which is further described in Myneni et al. (2002). This corresponds to the assumption that the magnitude of error is inversely related to the quantity of the dominant crop type in a MODIS pixel (Tian et al. 2003). It means that the smaller the field size and the higher the spatial mixture of different crops, the higher the resulting error. With respect to the study area and its neighboring regions, the spatial structure consequently has a negative impact on the applicability of the MODIS FPAR product, whose spatial resolution is inadequate

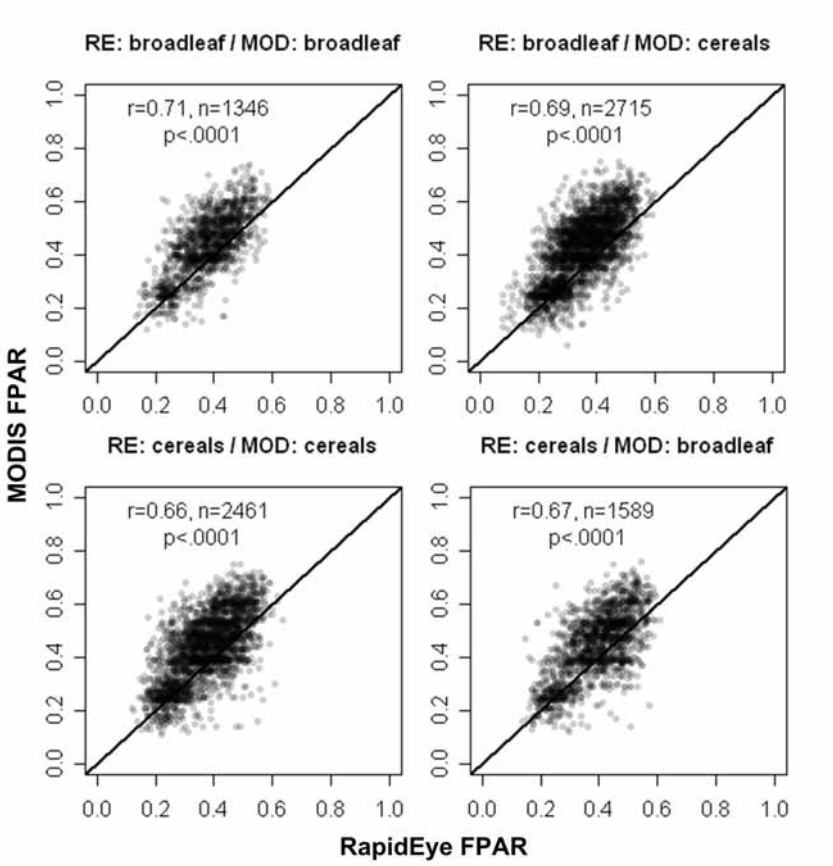

Figure 4.12: Comparison between RapidEye (x-axis) and MODIS (y-axis) FPAR in relation to misclassification between broadleaf and cereal crops. RE is the aggregated class from the RapidEye crop map and used as the reference, MOD is the class label of the MODIS land cover map (adapted from Fritsch et al. 2012).

for crop-specific analyses in these small-scale irrigation systems.

It can be assumed that the spatial heterogeneity of a MODIS pixel is much smaller at 250 m resolution than at 1 km. This was investigated in the next step. The ultimate goal was to derive an accurate FPAR product at 250 m spatial resolution, compiled via regression with the high resolution RapidEye FPAR maps.

4.3.2 Direct up-scaling of FPAR based on 250 m MODIS NDVI data

4.3.2.1 Data and methods

4.3.2.1.1 MODIS data and pre-processing

In contrast to the last chapter, where the validation of the MODIS 1 km FPAR product was detailed, this chapter describes the generation of a 250 m FPAR product through direct up-scaling of the RapidEye FPAR to the MODIS scale. A qualitative comparison of both datasets

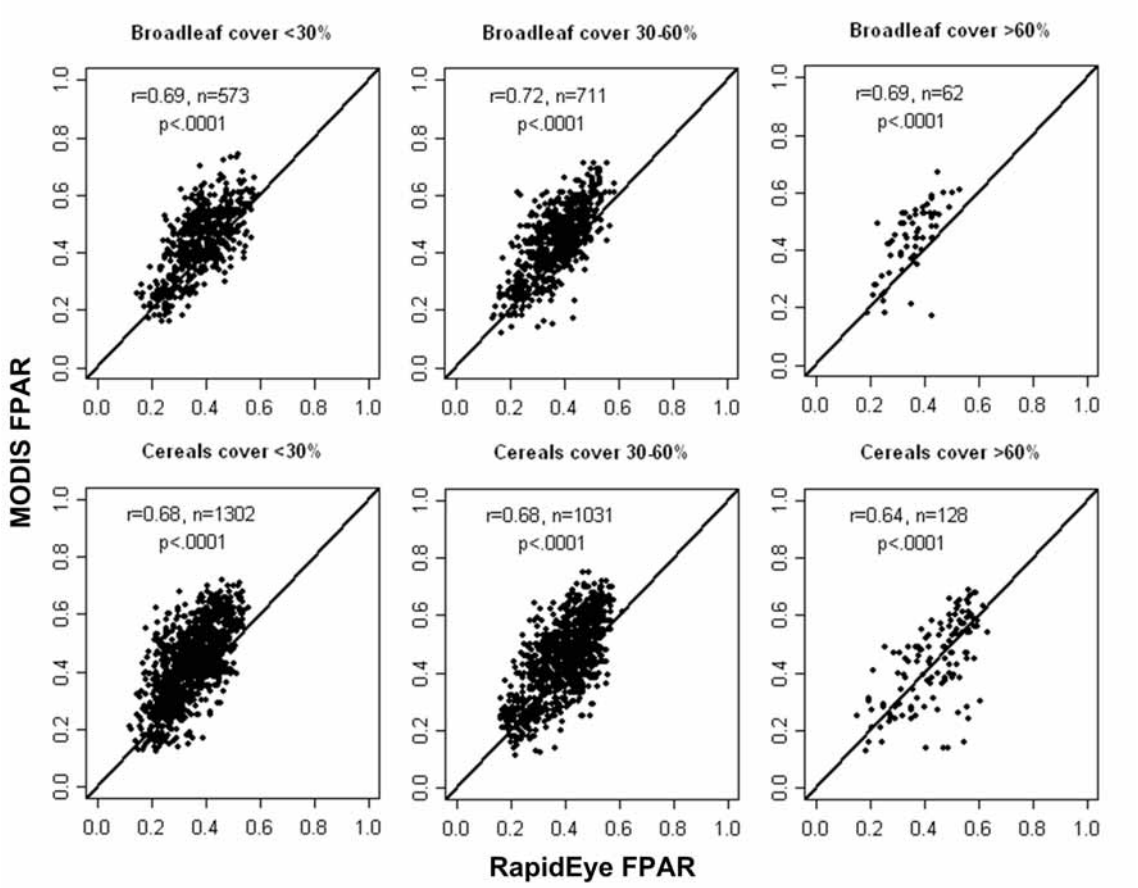

Figure 4.13: Comparison between RapidEye (x-axis) and MODIS (y-axis) FPAR for pixels correctly classified as broadleaf (upper part) and cereal crops (lower part), and in relation to the relative area of the respective group at the MODIS scale (adapted from Fritsch et al. 2012).

will allow to determine the optimal way of generating a consistent FPAR dataset for crop yield monitoring. The up-scaling procedure consisted of correlating MODIS data with the high resolution RapidEye FPAR maps. The resulting regression equations were subsequently applied to all MODIS images.

For the sake of simplicity, and to allow comparisons with similar studies, the NDVI derived from MODIS was chosen as vegetation index for correlation with the high resolution FPAR maps. Yet it was unclear which MODIS reflectance product would be optimally suited to the purpose. The first possibility was the use of daily surface reflectances (MOD09GQ) to calculate NDVI values. This dataset fits the daily time-step of the crop yield model. It is also well suited to effectively compare single acquisition days to the RapidEye imagery. One problem with this approach is that daily MODIS can be subject to difficulties in the imaging process, like atmospheric influences or low view angles. The second possibility is thus to use composited data that

Table 4.6: MODIS 250 m datasets used in this study (all collection 5) (adapted from Fritsch et al. 2011).

Product name	Parameter	Temporal resolution	Reference
MOD09GQ	Surface reflectance (used to calculate NDVI)	Daily	Vermote et al. (2011)
MOD09Q1	Surface reflectance (used to calculate NDVI)	8-day	Vermote et al. (2011)
MOD13Q1	NDVI, EVI	16-day	Solano et al. (2010)

minimizes these influences and promises better data quality, even though it aggregates image data for multiple days. For this purpose, 8-day or 16-day composites can be utilized. The first offers the advantage of having a higher temporal resolution, which might be advantageous for fast-growing crops, the second is known to be the most robust dataset with the least amount of error in it. To determine the optimal method for regional up-scaling of FPAR, all datasets were tested (table 4.6).

All datasets were reprojected into the UTM projection (WGS 84, zone 41 N) using the MODIS Reprojection Tool (MRT, USGS 2012). The QA-SDS of the image scenes were extracted for further analysis. The NDVI was subsequently calculated from daily and 8-day surface reflectances. Both the 8-day and the 16-day MODIS products are maximum value composites. The MODIS compositing process is further described by Wolfe et al. (1998). The 16-day composite vegetation index product includes the NDVI, the EVI, and associated quality information (Solano et al. 2010). In contrast to the NDVI, the EVI is supposed to compensate for atmospheric and background influences and is not affected by the typical saturation of the NDVI in high biomass regions (Huete et al. 2002).

4.3.2.1.2 Data analysis

Data analysis consisted of the comparison between MODIS vegetation indices and the high resolution RapidEye-based FPAR maps as well as investigation of the sub-pixel heterogeneity of MODIS 250 m data. The statistical relationships between RapidEye FPAR and MODIS NDVI/EVI products were evaluated by aggregating RapidEye FPAR maps at the 250 m scale via averaging. Both datasets were graphically compared with scatterplots, and the coefficient of determination (R^2) was used as a quantitative measure for the assessment of the relationships between FPAR and NDVI/EVI. MODIS sub-pixel heterogeneity was calculated using the RapidEye-based crop map. The map was intersected with a 250 m MODIS grid and the relative areas of all crop classes for each pixel were extracted. The information was then used to as-

sess the regional heterogeneity of the 250 m pixel size and to select homogeneous pixels for the exploration of crop-specific correlations between MODIS VIs and high resolution FPAR data. The latter step was implemented to test for differences between crop types.

4.3.2.2 Results and discussion

4.3.2.2.1 Statistical relationships between MODIS VIs and RapidEye FPAR

NDVI calculated from daily surface reflectances (MOD09GQ)

NDVI data calculated from daily surface reflectance showed mediocre correlations, with R^2 ranging from 0.37 to 0.67 (figure 4.14). There was a large variation in the data, especially for the comparison on September 22. Analysis of the quality information showed that low correlations occurred despite the fact that all data used in this analysis was produced with ideal quality for all bands. Further investigation indicated that the observation coverage of single MODIS pixels (the obscov parameter) had a strong influence on the results. The obscov parameter represents the area of MODIS grid cells that is covered by the actual sensor observation (Wolfe et al. 1998). Daily data can suffer from a low obscov. For the dates in figure 4.14, the maximum coverage of a grid cell by an observation was 62 % (October 3). Mean observation coverage for all pixels was 11.55 % (July 14), 10 % (August 1), 19.5 % (August 13), 35.27 % (September 8), 25.57 % (September 22), and 37.8 % (October 3), respectively. The results suggested that the lower the obscov parameter was for each pixel, the lower the correlation between MODIS NDVI and RapidEye FPAR.

NDVI calculated from 8-day surface reflectances (MOD09Q1)

The comparison between RapidEye-based FPAR and MODIS NDVI, calculated from 8-day surface reflectances, shows patterns similar to daily data (figure 4.15). In general there is less variation in the data and R^2 values are higher, except for October 3. Better correlations can be attributed to the use of composited data, as the MODIS (maximum value) compositing process discards low quality observations (Wolfe et al. 1998). Pooled observations also showed high correlation with RapidEye-based FPAR, with an R^2 of 0.69 (figure 4.16). The differences between regression lines for single composite periods and the pooled data are marginal.

A problem of the (8-day) compositing procedure is the fact that the exact date of the maximum value that is used for the composite is difficult to identify. This date can actually be at the very beginning or the end of the 8-day period. Consequently, a comparison between RapidEye and MODIS data can lead to situations where a RapidEye acquisition would actually be closer to an earlier or later MODIS composite period than the one chosen for the comparison. The impact of the choice of MODIS composite periods for the comparison was therefore also investigated. In the case of MOD09Q1 data, R^2 was highest when composite periods were chosen that directly

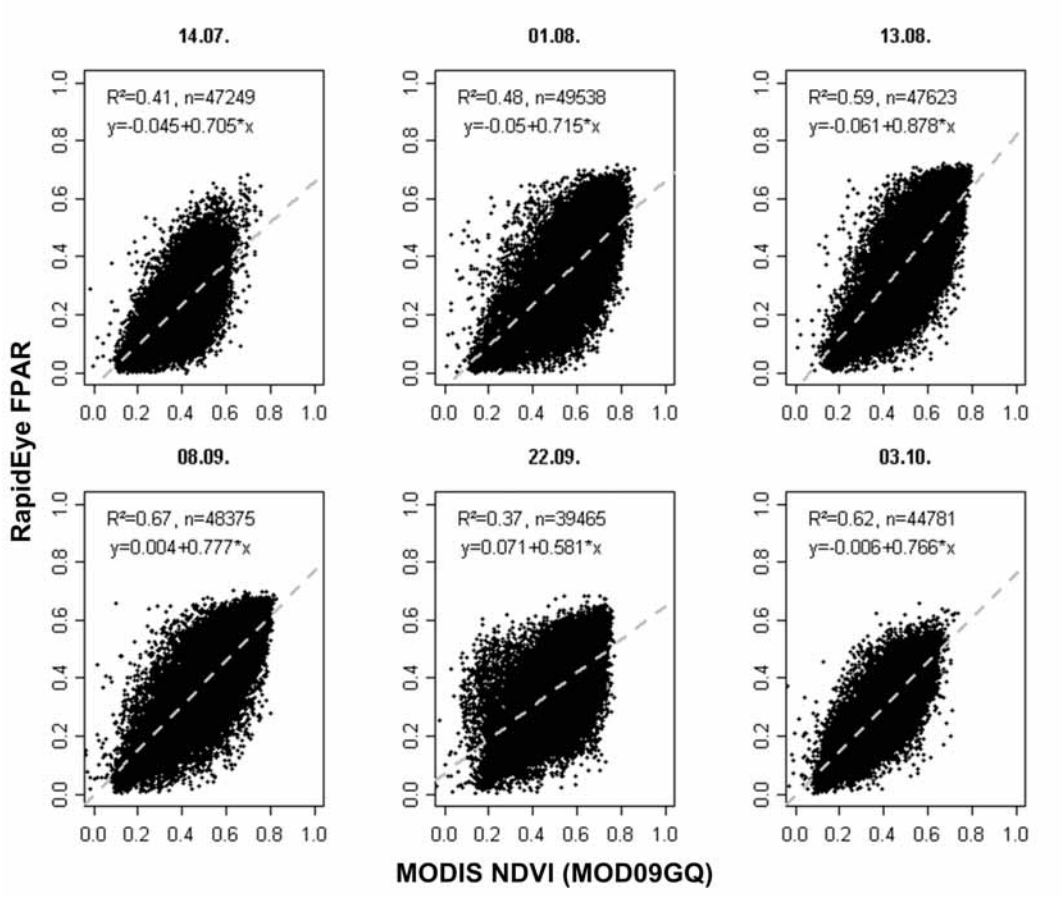

Figure 4.14: Scatterplots comparing RapidEye FPAR and MODIS NDVI calculated from daily surface reflectances (adapted from Fritsch et al. 2011). All p-values <0.0001.

included the RapidEye acquisition dates. Correlations with previous and subsequent composites were lower in all cases, showing that the analysis was not influenced by the choice of inadequate composite periods.

NDVI and EVI from 16-day composites (MOD13Q1)

Figure 4.17 presents the comparison between RapidEye FPAR and 16-day MODIS NDVI/EVI for all data points. Both indices show relatively high correlations, with slightly higher R^2 values for the NDVI. A similar picture is drawn by a comparison of the single time steps (data not shown here). The EVI thus was not superior to NDVI, as reported in other studies (Chen et al. 2006). This can be attributed to the fact that biomass was not high enough to cause the NDVI to saturate, which is also reflected in the FPAR data, where maximum values were around 0.7. Considering the pooled datasets, the coefficient of determination of the 16-day NDVI and EVI (0.66 and 0.62) is higher than for daily data (0.62), but lower than for 8-day NDVI (0.69). The MOD13Q1 product further covers a period of 16 days, which can be too long to capture

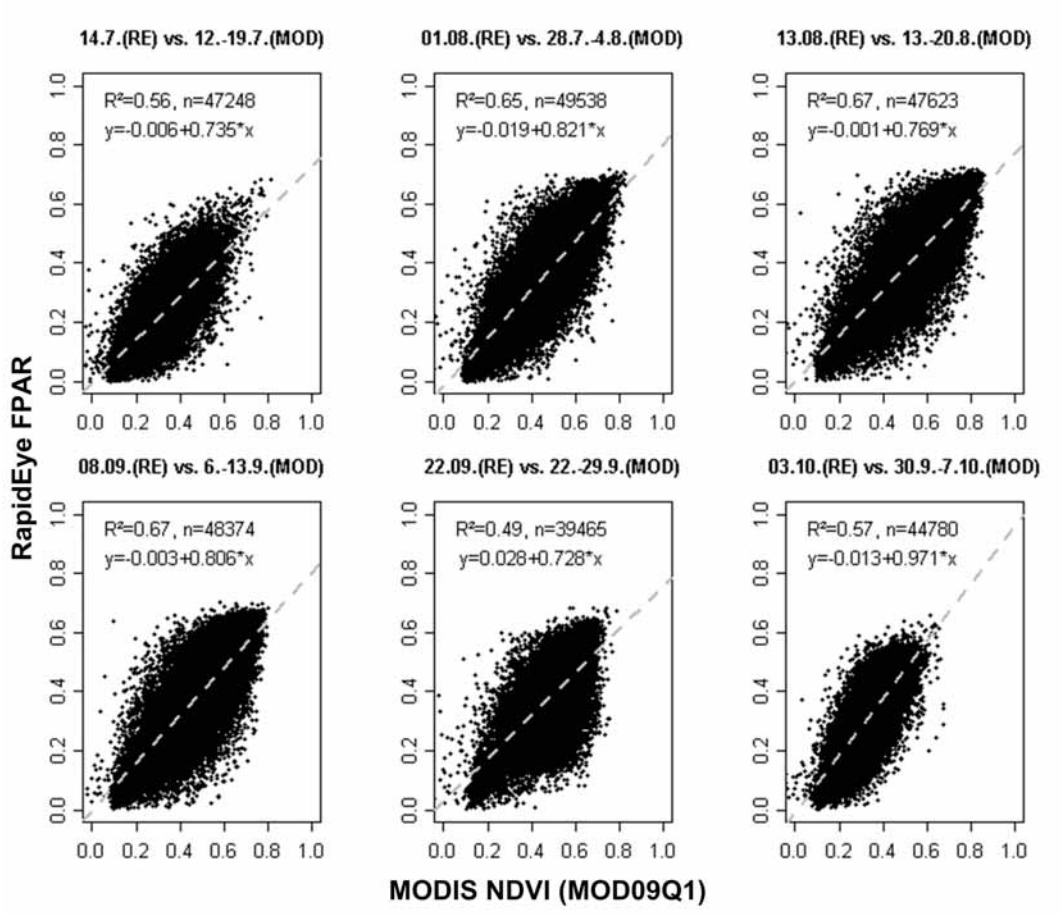

Figure 4.15: Scatterplots for RapidEye FPAR and MODIS NDVI calculated from 8-day surface reflectances (adapted from Fritsch et al. 2011). All p-values <0.0001.

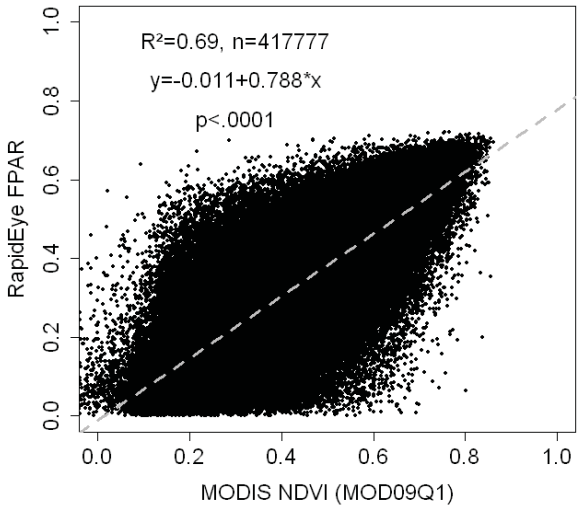

Figure 4.16: Comparison of the pooled 8-day MODIS NDVI with RapidEye-based FPAR.

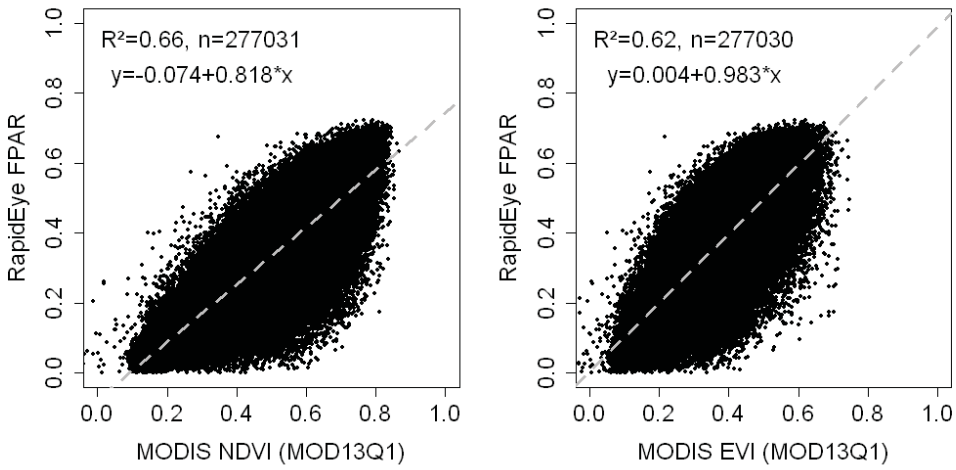

Figure 4.17: Relationships between RapidEye FPAR and MODIS NDVI (left) and EVI (right) from the 16-day MOD13Q1 product. All datasets were combined for the comparison (adapted from Fritsch et al. 2011). All p-values <0.0001.

the decisive stages in the phenological development of crops (Chen et al. 2006). This is further complicated by the compositing process itself, which causes neighboring pixel values to be collected at different times during the period. The actual dates can be close together or up to 30 days apart in certain cases.

In a final step, MODIS NDVI and EVI were evaluated with regard to pixel homogeneity. For this purpose, MODIS pixels with cotton, rice and wheat coverage of larger or equal 90 % were first selected. Data from all time steps was also combined in this case, and the pixels were afterwards compared to RapidEye FPAR (figure 4.18).

Again, the NDVI shows slightly higher R^2 values than EVI. Linear regression models vary only slightly between crop types, but more between NDVI and EVI. It can be assumed that crop types play a minor role for the relationship between the vegetation indices and FPAR, despite differing considerably in their structural characteristics. The observation that NDVI-FPAR relationships are independent of variations in canopy heterogeneity was also made previously (Fensholt et al. 2004). The EVI is more closely related to FPAR, with regression lines being close to the 1:1 line. This backs existing studies that use EVI as a direct estimator of ecosystem productivity (Sjöström et al. 2011). MODIS pixels with a crop cover of less than 10 % were also investigated, with similar results. However, the overall level of correlation was lower, with R^2 ranging between 0.43 and 0.54 for NDVI, and between 0.37 and 0.49 for EVI. The fact that crop-specific regression models differed insignificantly at the MODIS scale allowed the aggregation of all pixels for regression analysis. This step enables the application of the

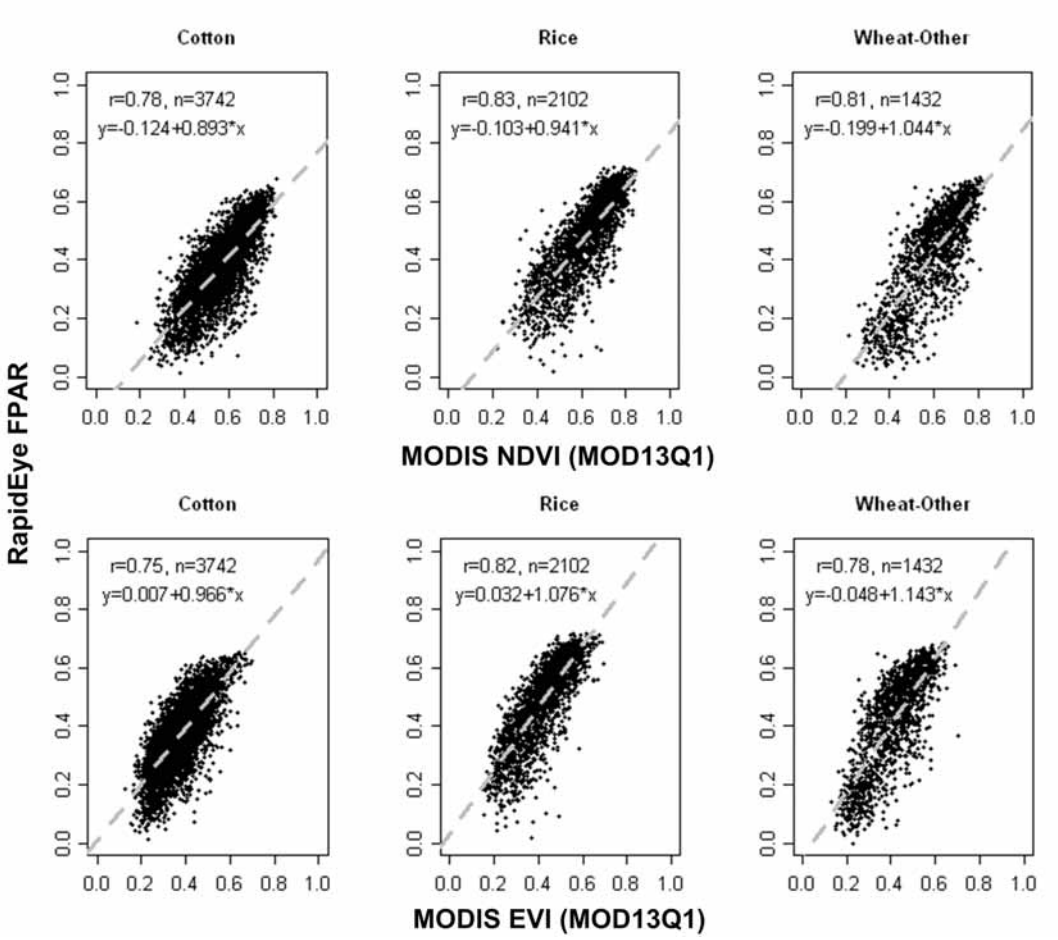

Figure 4.18: Relationships between MODIS NDVI/EVI and RapidEye FPAR for MODIS pixels with a cotton, rice and wheat cover higher than 90 %. All datasets were combined for the comparison (adapted from Fritsch et al. 2011). All p-values <0.0001.

equations to years where high resolution FPAR or land use data is unavailable.

4.3.2.2.2 MODIS sub-pixel heterogeneity

Table 4.7 shows the composition of MODIS pixels for different crop classes, subdivided by cover categories. Altogether, 67,141 pixels were used for the analysis. It was assumed that a MODIS pixel with a cover of more than 90 % can be regarded as homogeneous. At the 250 m scale, there were sufficient pixels for all classes in this category to perform statistical analyses, yet they made up only a small amount of the total. There was a clear difference between crop classes. Cotton had the largest area coverage, followed by rice and wheat. Accordingly, cotton had the highest number of pixels with more than 90 % crop cover. All other area fractions were equally distributed, with cotton also having slightly higher values compared to rice and wheat. The table clearly shows that, at the 250 m scale, the largest part of MODIS pixels is still covered by less than 30 % agriculture. The reason is the landscape structure of the region: agricultural

fields are separated by irrigation and drainage channels of varying sizes, there are often areas of bare soil between fields, and numerous small rural settlements are scattered throughout the region. In a next step, crop classes were reclassified in order to check whether homogeneity significantly increases when structurally similar groups (broadleaf and cereal crops) are created: cotton, maize, and sorghum were merged into the class broadleaf crops all wheat rotations and rice were merged into the class cereal crops. The percentages slightly changed afterwards, with cereal crops showing similar patterns as broadleaf crops. The number of pixels with more than 90 % cover was even higher. Yet the number of very heterogeneous MODIS pixels with less than 30 % cover still dominated in all cases. This number could only be lowered to approximately 40 % by adding up all crop areas. In doing so, however, the possibility of crop-specific analyses, like crop yield modeling, would be lost. The analysis suggested that the 250 m scale was better suited for this study, but that there are still scale and heterogeneity effects that have to be taken into account.

4.3.2.2.3 Comparison between regional FPAR maps based on MODIS VIs

For a regional evaluation of the results, the linear regression models were used to transform vegetation index values into FPAR. Figure 4.19 shows a comparison between all resulting maps for one period (September 8). As indicated by the regression analyses, no striking differences are visible in the maps. Mean FPAR for all maps varies only between 0.38 and 0.41. The single noteworthy difference is the maximum FPAR for EVI (0.74), which is considerably higher than for all NDVI maps (0.59-0.62). The upper right map in figure 4.19 shows the combined standard deviation of all images. The mean standard deviation exemplifies that differences between products are minimal, although there are also higher values visible in the image. Yet these values mostly correspond to pixels that cover large areas of water (irrigation and drainage channels) or bare soil. A visual comparison with the 1 km MODIS FPAR product (lower right in figure 4.19) reveals that the 250 m FPAR maps are much better suited to capture the spatial patterns in the region. This is further exemplified by a comparison of two subsets in figure 4.20.

The comparison between the different MODIS vegetation indices and the MODIS FPAR product revealed that the NDVI calculated from 8-day surface reflectances at a resolution of 250 m showed the highest correlations with the RapidEye-based FPAR dataset. The 8-day composite period supposedly also has advantages on studying crop growth in Khorezm compared to the 16-day period. The daily NDVI product was discarded because of data issues related to the obscov parameter. The 8-day NDVI product was hence deemed best suited for application in regional crop yield modeling. Consequently, NDVI time series were compiled for all investigated years, and the regression equation from section 4.3.2.2.1 was used for transformation into FPAR time series data (see chapter 5.4).

Table 4.7: The percentage of crop-specific area within MODIS pixels at the 250 m scale, subdivided into different cover categories (adapted from Fritsch et al. 2011).

Crop	>90 %	80-90 %	70-80 %	60-70 %	50-60 %	40-50 %	30-40 %	<30 %
Cotton	1.23	2.81	3.34	3.61	3.93	4.54	4.94	75.60
Rice	0.67	0.96	1.04	1.18	1.38	1.70	2.09	90.97
Wheat	0.44	0.50	0.69	0.97	1.31	1.59	2.06	92.43
Broadleaf crops	1.79	3.82	4.33	4.48	4.71	5.26	5.55	70.07
Cereal crops	2.51	3.82	4.03	4.23	4.62	4.85	5.47	70.47
All crops	6.25	12.16	11.73	9.21	7.22	6.18	5.42	41.82

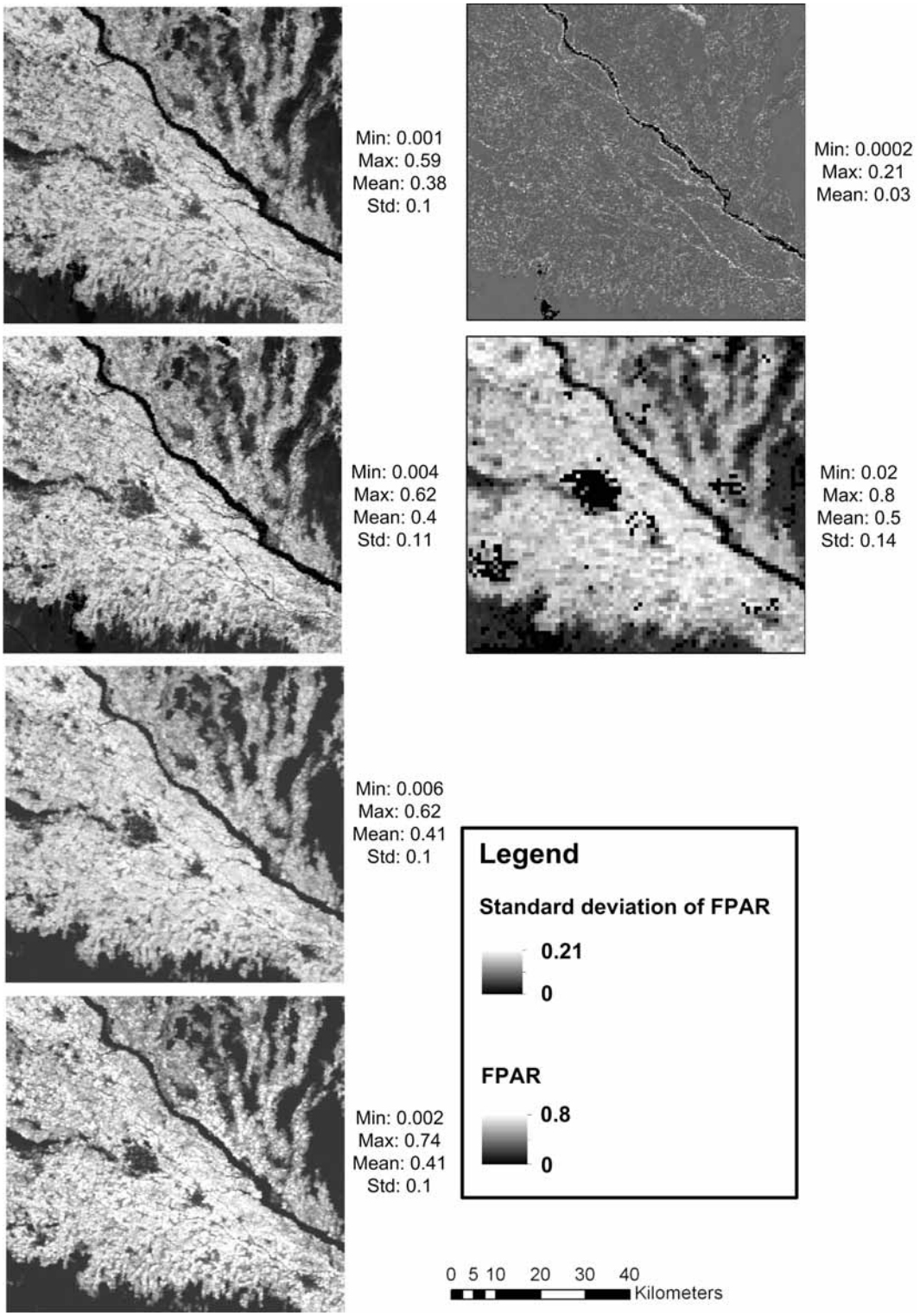

Figure 4.19: Comparison of FPAR maps derived via linear regression from different MODIS 250 m products. The images represent (from upper left to lower right): daily NDVI (September 8), 8-day NDVI (September 6 - September 13), 16-day NDVI (August 29 - September 13), 16-day EVI, the standard deviation for all data sets, and the 8-day 1 km MODIS FPAR product for comparison (adapted from Fritsch et al. 2011).

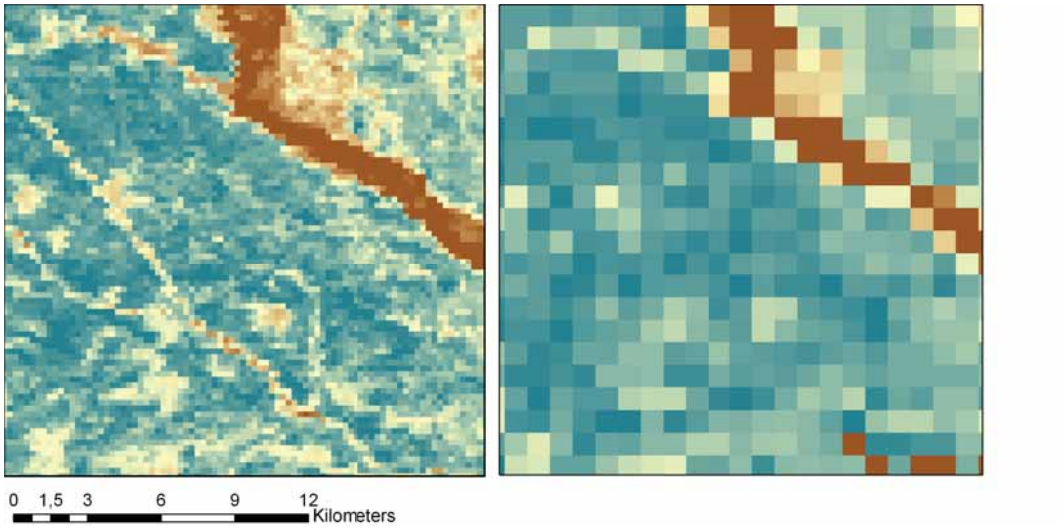

Figure 4.20: A subset of the Khorezm region (northwest of Urgench) comparing the 8-day FPAR product at 250 m spatial resolution (left) and the 1 km MODIS FPAR product (right).

5 Remote sensing-based crop yield modeling

5.1 Introduction

Numerous models of vegetation productivity on different scales have been developed and applied for climate change research, ecology, and policy support (Cramer et al. 1999, Cramer & Field 1999). The LUE approach to productivity modeling can be easily applied and has few input data requirements. The LUE approach states that unstressed plant growth is linearly related to the amount of light absorbed by the plant canopy, which in turn is quantified through the APAR. FPAR is strongly correlated with satellite-based vegetation indices like the NDVI (Myneni & Williams 1994), thus making the approach appealing for remote sensing. So far there are numerous global and regional satellite-based LUE models (McCallum et al. 2009).

In chapter 3 it was shown that actual application of the approach for crop yield modeling has remained limited to some geographic areas, despite its potential for accurate estimation of regional crop yields. Crop yield modeling studies that employed the LUE approach were mostly based on medium resolution sensors like MODIS (Shi et al. 2007, Maselli et al. 2011, Patel et al. 2006) and AVHRR (Tao et al. 2005, Bastiaanssen & Ali 2003). These studies made use of the high temporal frequency of image acquisitions and large swath widths as a prerequisite for capturing the seasonal development of canopy FPAR and its application over large areas. In addition, data from satellite sensors like MODIS are now available for more than a decade. This coverage makes the data useful for investigating regional changes over several years. Still, few authors have investigated an agricultural area for multiple years (for example, Maselli et al. 2011). A disadvantage of medium resolution data is that it complicates application for smaller fields due to its large pixel sizes. For this kind of task, high resolution remote sensing data is better suited. Yet the effective use of the LUE approach at the field scale is primarily hindered by the trade-off between high spatial and temporal resolution of satellite sensors. There have been studies on LUE models driven by high-resolution satellite data like Landsat, but they rely on single or few images only (Lobell et al. 2003, Pan et al. 2009), or on multi-sensor techniques (Liu et al. 2010). The first approach assumes a certain seasonal FPAR profile, which can lead to uncertainties in the results due to deviations from this profile caused by environmental conditions or different field practices. The second approach has an inherent need of sensor cross-calibration. Both approaches have shown to be able to deliver results with high accuracies, but they can complicate the process. Furthermore, the temporal resolution

of Landsat is suboptimal, especially when single images are additionally subject to cloud cover. In general, LUE-based yield mapping would greatly benefit from satellite data that combines high spatial and temporal resolution with an adequate swath width. The RapidEye constellation is one of the first systems to offer a high spatial resolution (6.5 m) combined with a temporal resolution of one (off-nadir) to approximately five days for nadir acquisitions (RapidEye 2011). It potentially opens up new possibilities of satellite-based LUE modeling via a precise tracking of growing season canopy FPAR.

The following sections describe the development of a satellite-based model for regional crop yield estimation in the Khorezm region. Section 5.2 introduces the general, scale-independent framework for crop yield modeling, which comprises components and parameters that can be used by the RapidEye as well as the MODIS scale. Model evaluation is described in section 5.2.5. Section 5.3 subsequently presents the high resolution RapidEye-based application for field-based estimation of crop yields for the year 2009. Afterwards, section 5.4 treats crop yield estimation at the MODIS scale for the years 2003-2009. The year 2009 represents a year where both models overlap. It will be used to demonstrate the relationships between crop yields at both the RapidEye and MODIS scales as well as evaluate scale influences similar to FPAR in chapter 4.3.1. This comparison will be presented in section 5.5.

5.2 Scale-independent framework for crop yield modeling

5.2.1 Basic yield model and its components

Crop yields were estimated using the general LUE approach in combination with the concept of a stress-induced reduction in daily LUE. A similar approach was previously implemented to simulate cotton yields for the Khorezm region based on MODIS data (Shi et al. 2007). The general workflow is summarized in figure 5.1. Crop yield was calculated following equation 5.1:

$$Y = \left(\sum_{SoS}^{EoS} (FPAR \times LUE_{act} \times PAR) \right) \times H_i \tag{5.1}$$

where Y is final crop yield (in $g \times m^{-2}$), SoS and EoS are start and end of season, LUE_{act} is the actual light use efficiency (in $gC \times MJ^{-1}$), PAR is the photosynthetic active radiation (in $W \times m^{-2}$), and H_{i} is the unitless harvest index (Hay 1995) that is scaled between 0 and 1. For comparison purposes, final crop yield is recalculated to $t \times ha^{-1}$. Daily plant growth thus depends on the amount of photosynthetically active radiation absorbed by crops ($APAR = FPAR \times PAR$) and the efficiency with which crops convert light energy to biomass (LUE). The product inside the brackets represents daily accumulation of aboveground biomass (AGBM), which is summed up over the growing season. Crop yield is then derived by applying H_{i} to the final AGBM at the end of the season. H_{i} represents the fraction of total aboveground

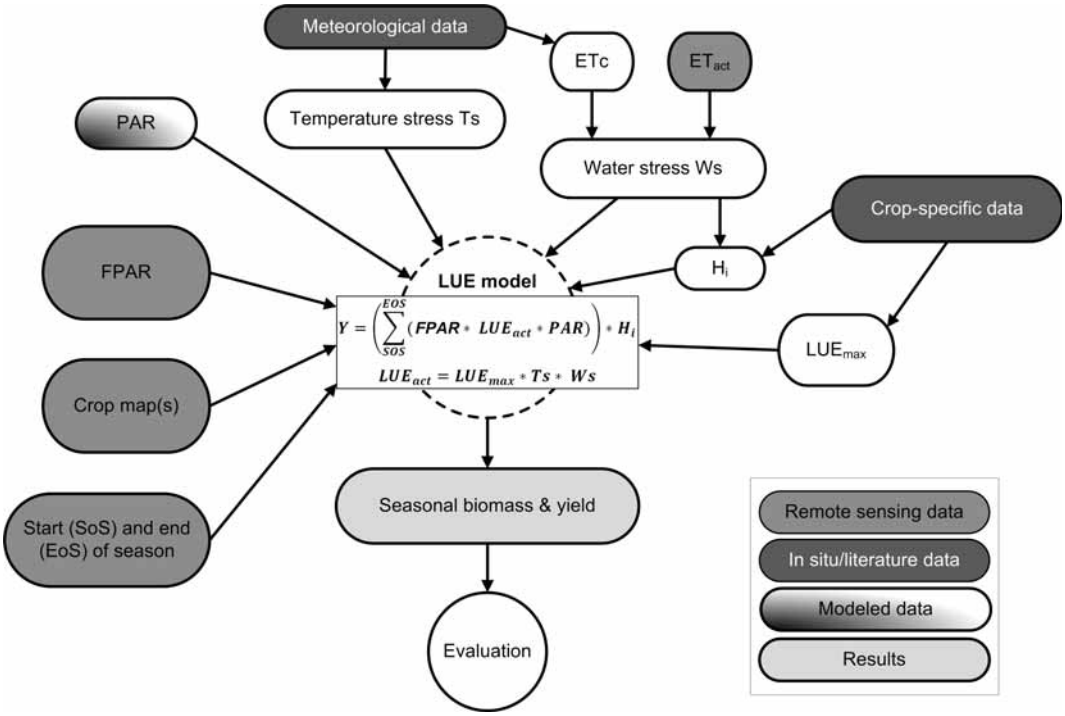

Figure 5.1: Framework for crop yield modeling at the RapidEye and MODIS scale. The input to the LUE model consists of remote sensing, meteorological and crop-specific data.

biomass to the economic yield of the plant (Hay 1995). Values of 0.36 (Shi et al. 2007) and 0.44 were taken as initial H_i values for cotton and rice, respectively. Both were afterwards dynamically down-regulated according to seasonal water stress (see below). The H_i of rice was close to values for conventional flood irrigation reported by Devkota (2011) and within the range of values reported by Bastiaanssen & Ali (2003).

LUE varies between vegetation types. Cotton and rice are both C_3 crops, which is reflected in the similarity of their LUE_max values (Turner et al. 2002). Monteith's original approach assumed ideal growth conditions. In reality, and especially in arid regions, this is rarely the case. Thus, LUE has to be rewritten to incorporate plant stresses (equation 5.2; compare also chapter 3):

$$LUE_{act} = LUE_{max} \times T_s \times W_s \tag{5.2}$$

where LUE_act represents the daily actual light-use efficiency, LUE_max is the maximum crop-specific light-use efficiency, T_s represents temperature and W_s water-induced stresses (both scaled between 0 and 1). FPAR originated from the high resolution RapidEye-based maps, whose preparation is described in chapter 4.2, and from the medium resolution MODIS-based dataset described in chapter 4.3.2. As the main input, the MODIS 250 m FPAR dataset was generated by calibration with the high resolution RapidEye data, as described in section 4.3.2.2.1.

$LUE_{\max}$ was taken from literature and assigned to fields and pixels based on the land use maps presented in sections 4.2.1.3 and 5.4.1.2.

Values for H_{i}, as reported in the literature, are often values for an unstressed harvest index. In reality, H_{i} decreases with increasing crop stress. The effect of sub-optimal irrigation on cotton yield was for example demonstrated by Constable & Hearn (1981). Hence H_{i} has to be reduced if stress occurs. Another reason for the reduction of maximum H_{i} is that field-derived H_{i} values, which often stem from experimental measurements, are not directly transferable to the satellite scale as the latter often represents area-averaged values. Thus, the harvest index for cotton and rice in this study was calculated by combining the crop-specific maximum H_{i} with an adjustment factor that represented the average water stress during the main growing period (equation 5.3):

$$H_{iact} = H_{imax} \times T_{savg} \tag{5.3}$$

H_{iact} is the actual harvest index that is assigned to each field and pixel in the study area, H_{imax} is the original unstressed harvest index and T_{savg} is the average water stress factor for the main growing period. A similar approach for H_{i} reduction is for example implemented in the CropSyst model (Stöckle et al. 2003).

5.2.2 PAR modeling

Daily PAR was assumed to be 48 % of the incoming global radiation (McCree 1981). Hourly values of global radiation (in $MJ \times m^{-2}h^{-1}$) were calculated as the sum of the incoming beam irradiance and the diffuse sky irradiance. The data was afterwards summed up to daily values. The reference object for both parameters is a horizontal plane. Further quantities that are necessary for the calculation are the day of year and the equation of time, the time of solar noon, the zenith angle of the sun and the atmospheric transmittance τ. It controls the type of incoming radiation (direct or diffuse). The calculation of all quantities is described in detail in Campbell & Norman (1998) and in Appendix A.1.

5.2.3 Estimation of LUE

Chapter 3 described how the actual light use efficiency of a crop depends on environmental stress during the season. Temperature and water were identified to be the most important limiting factors. Consequently, environmental down-regulators for temperature and water stresses were incorporated to derive daily LUE_{act} for cotton and rice from $LUE_{\max}$. Initial values for $LUE_{\max}$ were set to 2 $gC \times MJ^{-1}$ for cotton (Sommer et al. 2008) and 2.2 $gC \times MJ^{-1}$ for rice (Kiniry et al. 1989). While the $LUE_{\max}$ value for cotton was used in the simulation of potential yield in Khorezm with a mechanistic crop growth model, Kiniry et al. (1989) calculated the value for rice as the mean of several rice experiments. The latter source was

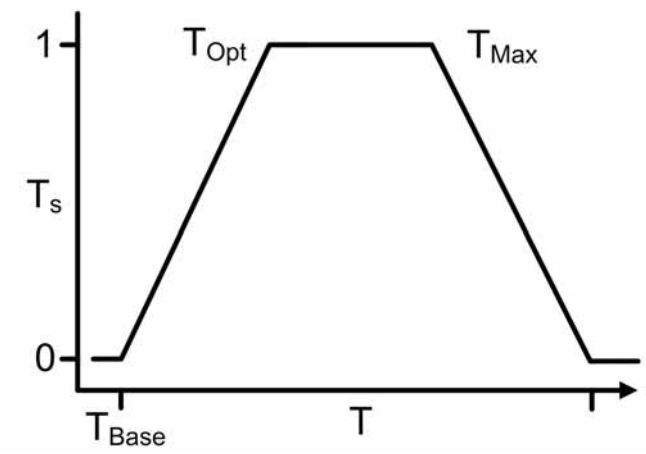

Figure 5.2: Parameterization of the temperature stress (T_s) factor via a linear ramp function. The cardinal points are the base temperature (T_{base}), the optimal temperature (T_{opt}), the maximum temperature (T_{max}) and the temperature beyond which growth stops (not labeled in figure).

chosen due to a lack of published local LUE_{max} values. The crop stress scalars T_s and W_s were calculated from T_{avg} and the ratio between actual evapotranspiration (ET_{act}) and crop evapotranspiration (ET_c). Average daily air temperature was transformed into T_s via a linear ramp function that incorporated the decisive temperatures for each crop (figure 5.2). These cardinal temperatures were taken from Sommer et al. (2008) and the ORYZA2000 model (Bouman et al. 2001). T_{base} is the temperature below which no crop growth occurs (8 ℃ for cotton and rice). Above that, crop growth linearly increases with temperature until it reaches T_{opt} (20 ℃ cotton, 25 ℃ rice). Temperatures beyond T_{opt} have no further benefit for plant growth. Temperatures rising above T_{max} (30 ℃ cotton, 35 ℃ rice) start to reduce crop growth, which decreases T_s until temperatures are too high for any growth at all (40 ℃ cotton, 42 ℃ rice).

In arid and semi-arid regions, environmental stress mostly occurs due to water limitations. If sufficient rainfall is absent or negligible, irrigation is required to provide the necessary soil moisture for growth processes. Yet even though some authors neglect crop water stress in the presence of irrigation (e.g., Lobell et al. 2003), this is an assumption that is hardly justifiable in the study region because of the well-known and widespread problems of irrigation water availability and distribution. Different approaches have been chosen to parameterize crop water stress, ranging from the use of climate data (Shi et al. 2007) or vegetation indices in the SWIR band (Yan et al. 2009) to the incorporation of soil moisture indicators (Lobell et al. 2002). For irrigated agriculture, spatially explicit deduction of the crop water status via crop evapotranspiration measures has proven favorable (Bastiaanssen & Ali 2003, Seaquist et al. 2003). Thus the water stress scalar in this study was calculated via the ratio of the actual evapotranspiration (ET_{act}) to the reference crop evapotranspiration (ET_c). The calculation was done per MODIS pixel as (equation 5.4, see Tao et al. 2005):

$$W_s = 0.5 + 0.5\frac{ET_{act}}{ET_c} \tag{5.4}$$

A similar approach was also implemented in related studies on satellite-based LUE models (Seaquist et al. 2003, Brogaard et al. 2005).

ET_{act} was derived from the SEBAL model (Bastiaanssen et al. 1998), which was specifically formulated with respect to irrigated agricultural crops. The SEBAL model calculates the latent heat flux λE as the residual of the total energy balance (equation 5.5):

$$R_n = G_0 + H + \lambda E \tag{5.5}$$

where R_{n} is the net radiation, G_0 the ground heat flux and H is the sensible heat flux. G_0 is derived via an empirical relationship between R_{n} and G_0 as well as information on surface temperature. In the original SEBAL model, H is estimated by employing a scene-specific search for cold (wet, $H = 0$) and hot (dry, $\lambda E = 0$) pixels (Bastiaanssen et al. 1998). These pixels are subsequently used to estimate the gradient of vertical air temperature (dT). H is then calculated as (equation 5.6):

$$H = \rho_{air} c_p \frac{dT}{r_{ah}} \tag{5.6}$$

Here, r_{ah} is the aerodynamic resistance of heat transport, ρ_{air} is the air density and c_{p} the specific heat of the air (Bastiaanssen et al. 1998). METRIC is another ET model that is based on SEBAL (Allen et al. 2007). In contrast to the latter, it uses the reference ET (ET_{ref}) for internal calibration instead of the evaporative fraction (Allen et al. 2007). For the study at hand, a version of the SEBAL model was used that is based on the modified estimation of H from the METRIC model. The selection of cold and hot pixels was further modified by using an automated selection process involving NDVI and a land cover classification. The ET_{act} data used in this study is based on Knöfel (2013), and will be detailed there. Further details of these methods can also be found in Conrad (2006) and Conrad et al. (2007).

Crop potential evapotranspiration (ET_{c}) was calculated according to Allen et al. (1998). The general formula (equation 5.7) reads as:

$$ET_c = ET_0 \times K_c \tag{5.7}$$

where ET_{c} is the crop evapotranspiration ($mm \times d^{-1}$), K_{c} is the dimensionless crop coefficient and ET_0 represents the reference evapotranspiration ($mm \times d^{-1}$) from a homogeneous grass surface (Allen et al. 1998). In the following, the procedures for obtaining ET_0, K_{c} and ET_{c} will be explained. ET_0 was calculated by implementing the Penman-Monteith equation as described in Allen et al. (1998). The formula for daily ET_0 is (equation 5.8):

$$ET_0 = \frac{0.408\Delta\,(R_n - G) + \gamma \frac{900}{T+273} u_2\,(e_s - e_a)}{\Delta + \gamma\,(1 + 0.34u_2)} \tag{5.8}$$

where R_n is the net radiation at the surface of the crop ($MJ \times m^{-2} day^{-1}$), G is the soil heat flux density ($MJ \times m^{-2} day^{-1}$), T the air temperature at 2 m height (°C), u_2 the wind speed at 2 m height ($m \times s^{-1}$), e_s is the saturation vapor pressure (kPA), e_a is the actual vapor pressure (kPa), $e_\mathrm{s} - e_\mathrm{a}$ the vapor pressure deficit (kPa), Δ is the slope vapor pressure curve ($kPa \times\ ^\circ C^{-1}$) and γ is the psychrometric constant ($kPa \times\ ^\circ C^{-1}$). Δ describes the slope of the curve representing the relation between saturation vapor pressure and air temperature, and γ gives the relation between the partial pressure of water in the air to its temperature. All equations and calculation steps can be found in Allen et al. (1998). To estimate extraterrestrial radiation (which is required to calculate R_n) or vapor pressure, the height above sea level (m) is required. For this purpose, a SRTM digital elevation model (Rabus et al. 2003) was used to extract the correct altitude for each MODIS pixel. As ET_0 was to be related to ET_act, MODIS 1 km pixels were used as the reference for calculation. Consequently, parameters required for the calculation of ET_0 that varied spatially were calculated for each pixel. Besides the altitude, these included the latitude and longitude. All meteorological parameters needed for estimating ET_0 at each pixel location were calculated as the mean of the two nearest meteorological stations.

ET_0 represents potential crop growth under non-limiting conditions, meaning that soil water limitations, soil salinity, crop density, pests and diseases as well as weed infestation or low soil quality are all assumed to have no negative effect on crop growth (Allen et al. 1998). ET_c is similar in this fashion, but incorporates additional crop-specific conditions. Where most of the regional climatic conditions influence ET_0, ET_c is mostly regulated by crop-specific characteristics like crop height, canopy albedo, canopy resistance and evaporation from the soil (Allen et al. 1998). The conversion between ET_0 and ET_c is done via K_c, which accounts for the fact that the maximum amount of ET from a crop surface changes mainly with growth stage. For example, ET_c from a crop surface will be up to 20 % higher than ET_0 ($K_\mathrm{c} = 1$). Other influencing factors include the crop type, climate of the growing season and soil evaporation. The concept of the crop coefficient K_c is represented in figure 5.3.

As shown in figure 5.3, K_c varies with four distinctly defined crop growth stages: the initial stage, the crop development stage and the mid and late-season stage. The initial stage covers the period between the sowing date and the time the crop reaches 10 % ground cover. After that the development stage begins, which covers the period until the mid-season phase. Per definition the mid-season stage starts at effective full cover, which mostly coincides with flowering. For row crops such as cotton, effective full cover can also be defined as the time when the canopy reaches full closure. The late-season stage starts at maturity and lasts until full senescence. However, it often stops earlier due to harvest (Allen et al. 1998). In summary,

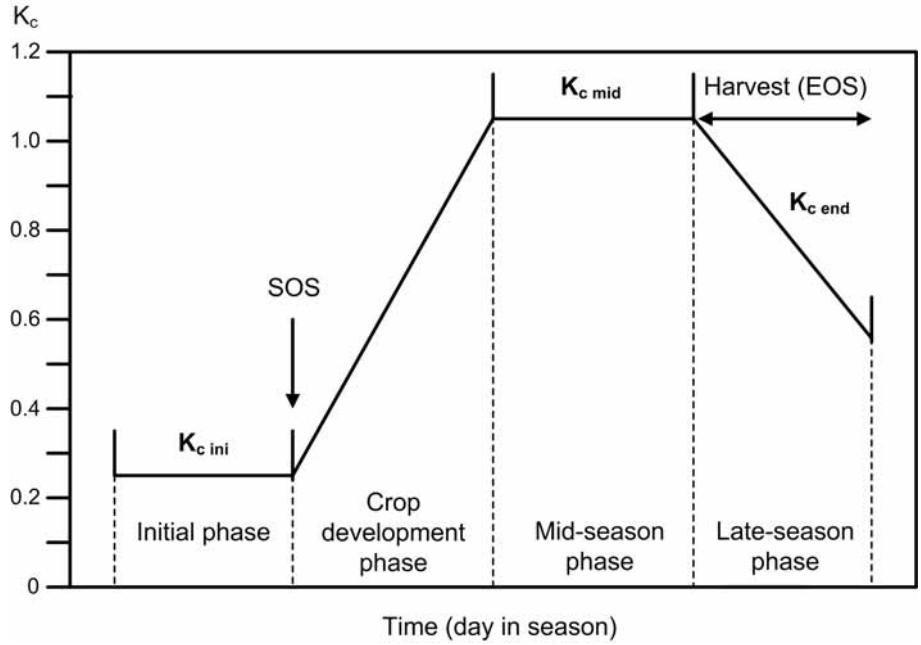

Figure 5.3: Illustration of the variation of the K_c coefficient during the season (adapted from Allen et al. 1998). See text for further explanations.

Table 5.1: K_c values and duration (in days) for the initial, development, mid and late-season stage for cotton and rice (Conrad 2006).

	Duration of stage				K_c		
Crop	Initial stage	Crop development	Mid-season	Late-season	Initial stage	Mid-season	Late-season
Cotton	60	50	60	55	0.35	1.20	0.70
Rice	50	25	30	30	0.80	1.15	0.60

the data needed for calculating ET_c (equation 5.7) consists of ET_0, K_c and the length of the respective crop stages. The values for K_c and the length of crop stages are shown in table 5.1. The numbers are reported in Conrad (2006), representing official data from the Central Asian Research Institute of Irrigation (SANIIRI).

Accurate calculation of ET_c via K_c requires knowledge on sowing and harvest dates. This information was available from the CRI for the year 2009, and was used for the RapidEye-based model. However, for the largest part of Khorezm and for the remaining years 2003 to 2008 it was lacking. Consequently, a different simulation strategy was chosen for the crop yield model. As described earlier, the development phase starts at a crop ground cover of 10 %. Previous

studies showed that the TIMESAT software (Eklundh & Jönsson 2010) can be used to identify crop phenological parameters (Boschetti et al. 2009). The start of season, as calculated with TIMESAT (see section 5.2.4), has shown to correspond roughly to the green-up of crops. Although this point in time may deviate from the one where 10 % ground cover is reached, the logic behind both approaches is similar. In this study, it was thus assumed that SoS corresponds to the start of the development stage of K_c. As a consequence, daily ET_c was calculated for each 250 m MODIS pixel from 2003 to 2009 using the spatial distribution of the SoS, ET_0, annual crop maps, the values for K_c and the duration of the crop stages reported in table 5.1. The rising K_c value during the crop development phase was simulated in two steps. First, the starting value was set to the K_c value that represents the initial phase of the crop. In a second step, the K_c values for the crop development phase were linearly interpolated between the value for the initial phase and the value for the mid-season, accounting for the length of the development phase. A similar step was implemented for the late-season phase. Harvest was assumed to take place at the end of the late-season phase. Yet if its length exceeded the end of the season (EoS), which was also calculated with TIMESAT, this date was used as harvest date.

Finally, daily water stress for each pixel was calculated as the ratio between the actual and the crop evapotranspiration according to equation 5.4. Figure 5.4 shows an example of such a comparison. In the beginning of the season, ET_{act} is much higher than ET_c, which can be caused by a flooding of the fields prior to crop emergence. Until the beginning of May, a low K_c prevents ET_c from increasing. This changes with the start of the crop development phase (point (1) in figure 5.4), and ET_c steadily rises until the beginning of June. Around this time ET_c starts to exceed ET_{act}. This is an indication of water stress, meaning that the crop in this stage could theoretically evaporate more water than is actually the case. The reasons can be manifold, but the bottom line is that there is not enough water available for non-limited crop growth. The water stress factor changes correspondingly in this phase. In the example presented in figure 5.4, ET_{act} again exceeds ET_c at the end of August. This continues until the end of the season, but ET_c already drops to zero around mid-September when K_c, according to the length of the different crop stages presented in table 5.1, drops to zero due to harvesting of the crop. In any case, this period is not characterized by water stress.

5.2.4 Estimation of the Start of Season (SoS) and End of Season (EoS)

Ecological models often depend on information regarding vegetation phenology (e.g., Smith et al. 2010). For example, certain plant processes only start at specific crop growth stages. Phenological information can also be used for remote sensing-based crop yield estimation (Boschetti et al. 2011). In this study, the dates for the SoS and the EoS at the RapidEye scale were taken from field observations made during the cropping season 2009. These dates were used to model crop yield for the whole study area. The SoS and the EoS were also incorporated for the

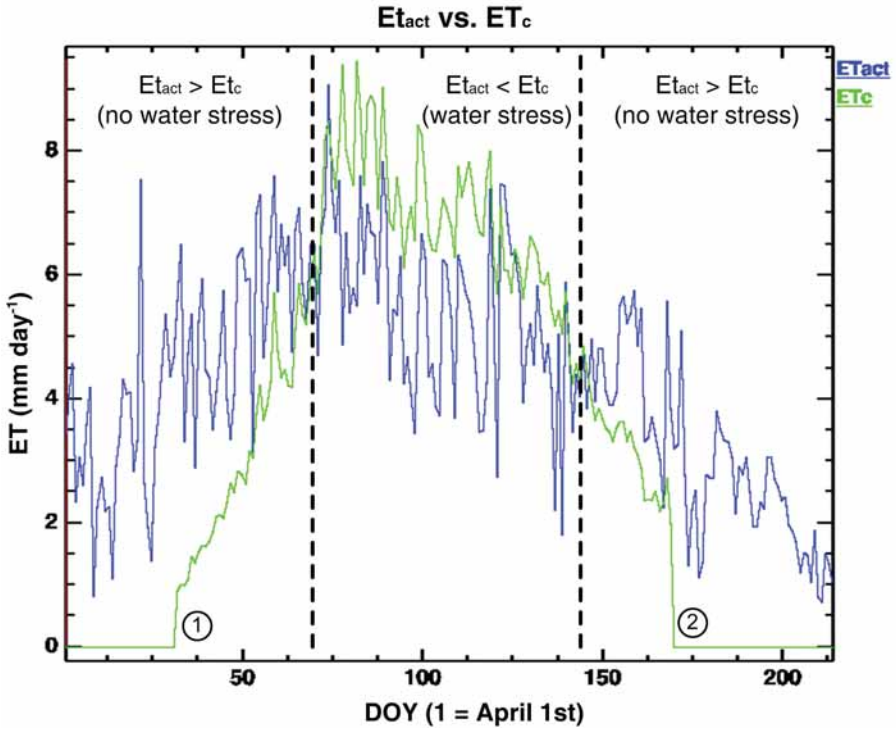

Figure 5.4: Graphical display of the calculation of water stress via the ratio between ET_{act} and ET_{c}; (1) corresponds to the start of the development phase of the crop; (2) is the harvest date.

yield model at the MODIS scale. However, the fact that the model was applied to multiple years without proper *in situ* information required a more objective approach towards the choice for those dates. Pixel-based values for the start and end of season were derived with the TIMESAT software, version 3.0 (Eklundh & Jönsson 2010). It was specifically designed for the analysis of satellite time-series data (like AVHRR or MODIS) and the derivation of phenological information. The software first fits a smoothed curve to the upper envelope of the original time-series. Afterwards, different phenological parameters can be derived from the smoothed curve (figure 5.5).

Three different smoothing algorithms can be used for curve fitting: Gaussian, logistic and a Savitzky-Golay filter. The latter was chosen here. TIMESAT allows the user to select a variety of settings that control curve fitting and seasonal parameters. The parameters used in this study are summarized in table 5.2. The following description is taken from Eklundh & Jönsson (2010). The Savitzky-Golay window size is the number of time steps that are used in the smoothing process. The number of envelope iterations (between one and three) describes whether or not the smoothed curve is fitted to the upper envelope of the time series. In the case described here, no such fitting was implemented. The spike method is used to filter outliers in the time series. The chosen median filter (MF) removes values that differ from the median

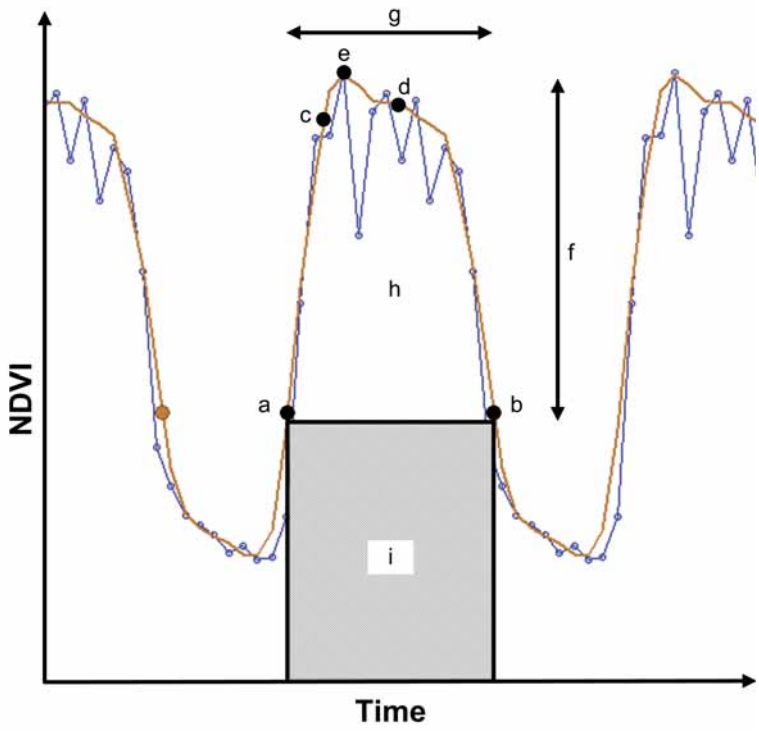

Figure 5.5: TIMESAT approach to time series smoothing and derivation of phenological parameters. The blue line represents the original time series, the brown line is the time series after smoothing with TIMESAT. The following parameters can be derived: start (a) and end (b) of season, 80 %-levels of the NDVI curve (c and d), the point with the highest NDVI value (e), the seasonal amplitude (f), the seasonal length (g) and the small (h) and large (i) integrals of the NDVI curve (Eklundh & Jönsson 2010).

within a given window. The threshold for the difference to the median is defined by the standard deviation (Spike SD in table 5.2). Next, the seasons per year control whether one or two seasons per year are detected. The parameter ranges from 0 (one season) to 1 (two seasons), a value of 0.5 was chosen for all years. For the modeling procedure, the most important parameters were the ones that control the dates of the start and end of season. The amplitude season start and the amplitude season end are threshold values between 0 and 1 that define where *SoS* and *EoS* are being set. The amplitude is given by the distance between the minimum and peak values of the curve fitted to the original time series (see also Jönsson & Eklundh 2002 and figure 5.5).

Seasonal parameters derived from TIMESAT have for example proven useful for monitoring rice phenology (Boschetti et al. 2009). However, there is no clear and objective method for choosing the right settings. As the start and end of season were amongst the decisive variables in the MODIS crop yield model, determining the right values was crucial. As a consequence, the TIMESAT settings were evaluated individually for each year (table 5.2). As can be seen in table 5.2, there were only minor differences in the settings between the years. This indicates that crop

Table 5.2: TIMESAT settings selected to derive *SoS* and *EoS* from 2003 to 2009. See text for further explanations.

Year	SG window size	No. of env. iterat.	Spike method	Spike SD	Seas. per year	Amplitude season start	Amplitude season end
2003	4	1	MF	2	0.5	0.25	0.8
2004	4	1	MF	2	0.5	0.25	0.8
2005	4	1	MF	2	0.5	0.25	0.8
2006	6	1	MF	2	0.5	0.35	0.8
2007	6	1	MF	2	0.5	0.30	0.8
2008	6	1	MF	2	0.5	0.30	0.8
2009	4	1	MF	2	0.5	0.25	0.8

phenology can be derived consistently from year to year. Published data on sowing and harvest dates in the study area were used to cross-check the results. Even though this information was not enough for quantitative analyses, it allowed for an estimation of the accuracy of the results and their impact on the crop yield model.

5.2.5 Model evaluation

For the purpose of evaluating the model at the RapidEye scale, field data for cotton and rice from the CRI was used. Cotton yield was sampled for sub-fields within the borders of larger fields (figure 5.6b). Rice yield data was sampled for smaller experimental plots (inset in figure 5.6b) as part of a research project aiming at the evaluation of conservation agriculture in the study region (Devkota 2011). To characterize the performance of the model, bias (equation 4.3) and RMSE (equation 4.4) were calculated. Furthermore, the impact of the different environmental down-regulations (EDR) like T_s and W_s on model accuracy was investigated and a simple sensitivity analysis of the model parameters H_i and LUE_{max} was conducted.

The outcomes of the MODIS model were evaluated by comparison with official yield statistics from OblStat (OBLSTAT 2010). Official data was only available at Rayon level. Consequently, the average modeled crop yield for each Rayon was calculated for this purpose. The bias, RMSE, percentage error (PE; the error as a percentage of the official value) and the Pearson correlation coefficient served as quality indicators for this comparison (see chapter 5.4). In addition to the comparison with official statistics, the results of the MODIS model were compared to those of the RapidEye model. To this end, MODIS pixels with varying crop cover were first selected by combining the MODIS data with the RapidEye-based crop map of 2009. Afterwards, the results at both scales were compared. This way the impact of spatial heterogeneity on model results at different scales could be evaluated.

5.3 Field-based crop yield modeling using high resolution RapidEye data

5.3.1 Data and methods

The characteristics of the RapidEye data used in this study were already described in section 4.2.1.2, which also described pre-processing of the data and the derivation of high resolution FPAR maps. These FPAR maps, for all available RapidEye time steps, were the main input to the crop yield model described in this chapter.

5.3.1.1 Meteorological data collection and processing

Daily average temperature (T_{avg}) from six stations (figure 5.6a) was taken as input for the model. Short time data gaps (up to ten days) were filled by linear interpolation. In contrast, larger gaps were filled by using data from the nearest adjacent station, thus creating continuous time series of the parameters. To be able to use the data in the model, it was converted to raster data first. For this purpose, Thiessen polygons were created with the location of the meteorological stations as the basis. The daily data from the meteorological stations was then assigned to its corresponding polygon. Finally, daily raster layers representing regional temperature data were created from the polygons. The presented simple approach was preferred to more sophisticated interpolation methods such as Kriging, because these need more data points for accurate results. This was also backed by the fact that there was only a minor regional temperature gradient.

5.3.1.2 Calculating seasonal FPAR profiles

The seasonal crop-specific FPAR was calculated for each field in the region. NDVI values were averaged per field, which were derived by intersecting RapidEye images with field boundaries (Conrad et al. 2010). The crop map was used to select cotton and rice fields. Linear transfer equations for cotton and rice (Ehammer et al. 2010), developed at the field scale, were subsequently used to calculate FPAR from NDVI. Temporal linear interpolation was applied to the data, to match the daily time step of the model. Not all fields were covered by the same images (see figure 4.4). Linear interpolation was conducted with the available acquisition dates as the anchor points, which could vary from field to field. For this purpose the 'Zoo' package (Zeileis & Grothendieck 2005) for analysis of irregular time-series, available for the R software for statistical analysis (R Core Team 2012) was used. If a field was only partly covered by an image, the image was excluded from the calculation. For the purpose of interpolation, the first and last day was set to 1 April and 31 October, respectively. Zero FPAR was assigned to both dates, assuming no crop growth at these dates.

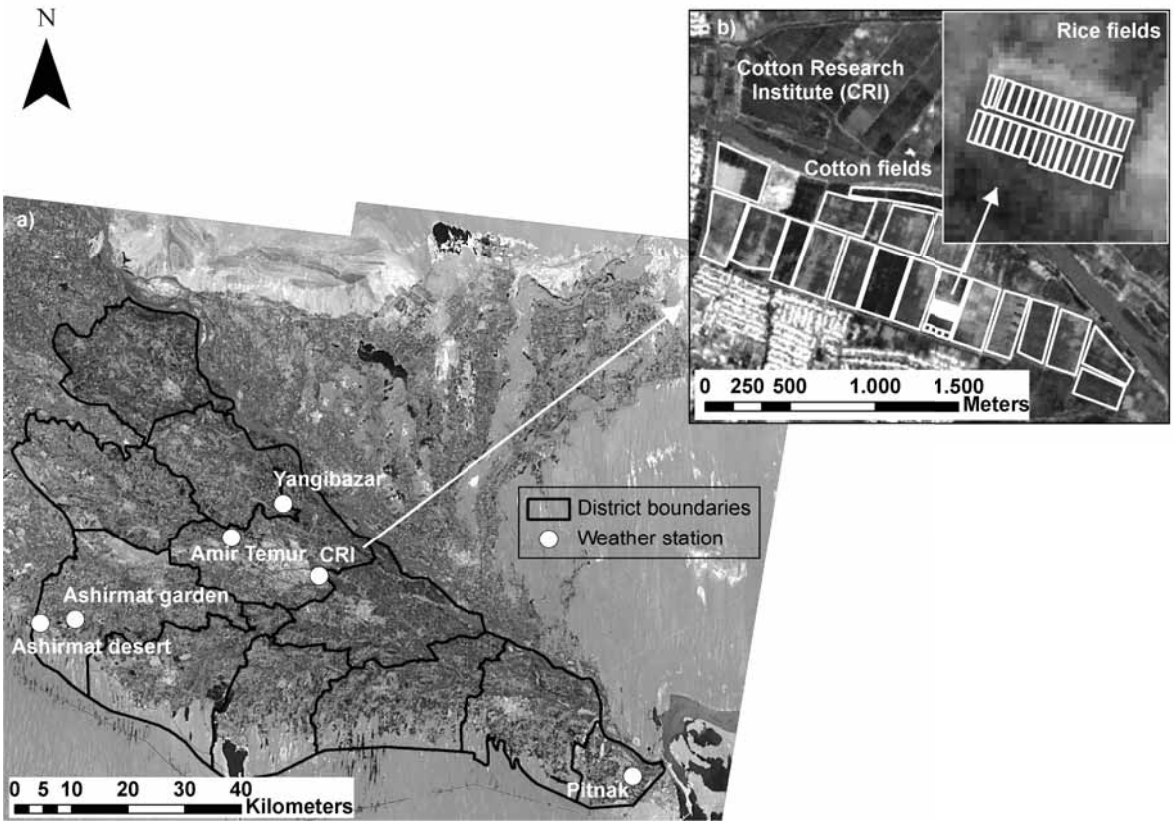

Figure 5.6: The location of meteorological stations within the Khorezm district (a). Field data for model evaluation was collected for related research at the Cotton Research Institute (b). The inset in (b) shows the location of the experimental rice fields.

5.3.2 Results and discussion

5.3.2.1 Model inputs and parameters

The mean daily interpolated time series of FPAR at field scale for cotton and rice during the growing season 2009 is shown in figure 5.7. The dates chosen for the start and end of season are also indicated. Cotton (figure 5.7a) generally reached lower maximum FPAR values as compared to rice (figure 5.7b) of approximately 10 %. Rice crops displayed a distinct increase in growth around the beginning of July, which is characterized by a steep slope. Rice reached maximum FPAR in the middle of August, cotton in the beginning of September. The variation in the data, as shown by the standard deviation in figure 5.7, was similar. Rice had a slightly larger standard deviation throughout the season, especially in the beginning of the season around 21 May and the first week of July.

In this study, FPAR was used as the main driving variable of the model. The results show that canopy phenology was adequately captured by the RapidEye acquisitions, as the FPAR curves show the typical crop-specific behavior. This is also confirmed by comparisons with ground mea-

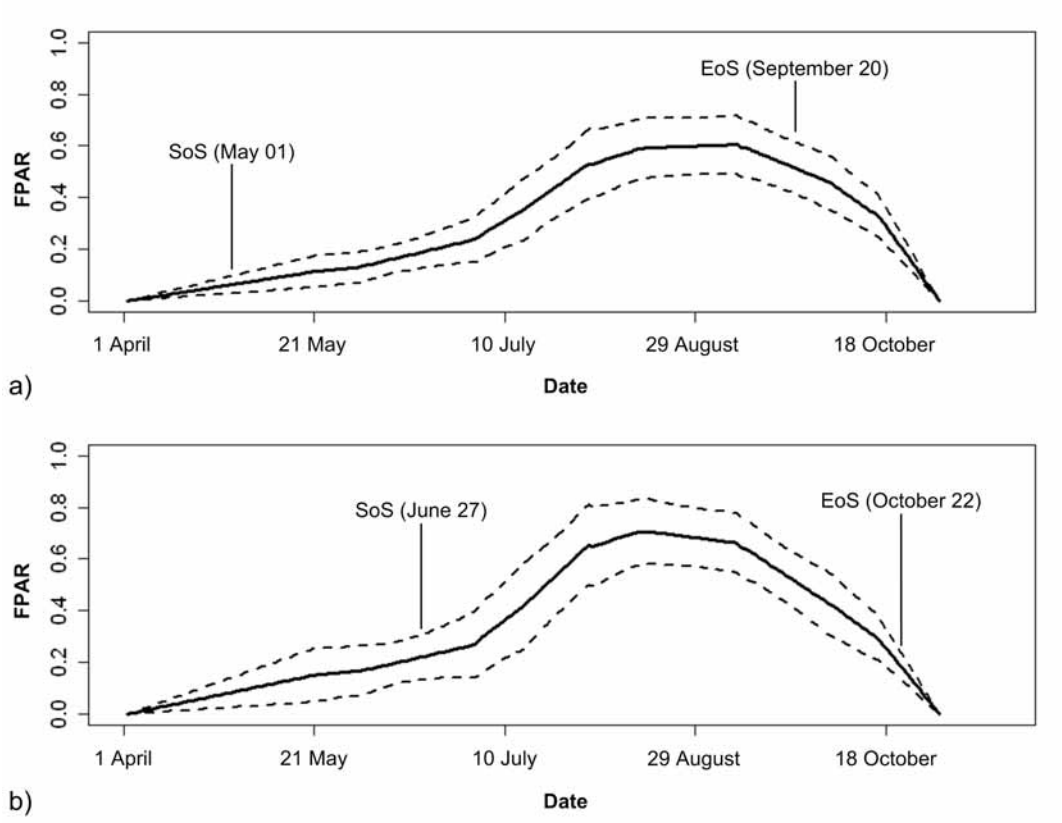

Figure 5.7: FPAR development for cotton (a) and rice (b) during the growing season 2009. Solid lines represent the interpolated mean, dashed lines the standard deviations. *SoS* and *EoS* represent the start and the end of the season, respectively.

surements (Ehammer et al. 2010) and studies based on MODIS satellite imagery (Conrad et al. 2011).

Besides the calculation of seasonal $FPAR$ profiles, estimation of PAR and LUE_{act} were decisive for the successful implementation of the model. PAR will be further discussed in section 5.4.2.3. The estimation of LUE_{act} was controlled by water (W_{s}) and temperature (T_{s}) stress terms. Seasonal trajectories of W_{s} and LUE_{act} will also be discussed later (section 5.4.2), as the parameter is based on MODIS data. Temperature stress will be discussed in this section, as it is based on ground data. T_{s} showed different magnitudes for cotton and rice due to its parameterization, but the temporal patterns were similar (figure 5.8a and b). There was also little variation between stations. The coefficient of variation (CV) for the growing season ranged from 34 % (Station Pitnak) to 40 % (Station Yangibazar) for cotton and from 42 % to 48 % for rice, respectively. The mean daily CV between all stations amounted to 8.7 % for cotton and to 9.3 % for rice. Temperature-stress free days occurred between the beginning of May and late August (rice) and September (cotton). Temperature-induced crop stress occurred mostly in the beginning and end of the season and was due to lower temperatures. While T_{avg} steadily rose

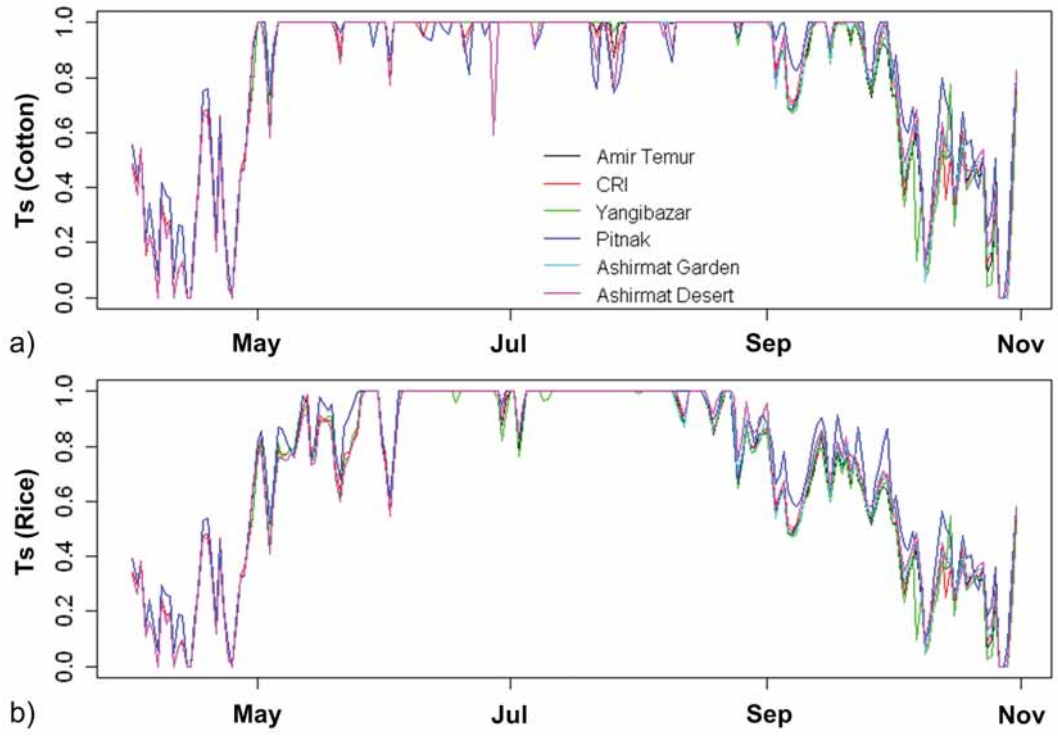

Figure 5.8: Seasonal course of the temperature stress index T_s, which was calculated separately for cotton (a) and rice (b).

until May (with a few days of less than 8 °C), it was favorable for the largest part between May and September. Reduced growth during this period was due to temperatures slightly above T_{max}.

5.3.2.2 Model accuracy and uncertainties

Modeled cotton and rice yield was compared with harvest information from the CRI. Table 5.3 shows the corresponding values for the bias and RMSE. For cotton, the lowest RMSEs resulted from combined water and temperature stress terms (29.1 %). The model underestimated actual crop yields in this case. Using no stress or T_s only resulted in a large overestimation of measured yield (63.35 % and 55 %, respectively). The largest error occurred when no stress term was implemented. The second largest error resulted from the usage of T_s only. The implementation of W_s only resulted in the second lowest RMSE for cotton (29.48 %), which was slightly higher than when both T_s and W_s were used. The errors for rice painted a different picture as compared to cotton. In the case of rice, the use of W_s only actually resulted in the lowest RMSE values (30.43 %), underestimating actual crop yields to some degree. This was followed by the case of T_s only, with an RMSE of 30.75 %. In this case, reference yields were somewhat overestimated. A combination of T_s and W_s resulted only in the third lowest RMSE of 39.75 %, again underestimating actual yields. Finally, the incorporation of no stress terms

at all led to both the largest overestimation and the highest RMSE (45.65 %). Overall, the difference in RMSE between T_s only and W_s only was significantly larger for cotton than for rice. Altogether, cotton shows the lowest RMSE when both temperature and water stress are accounted for. In comparison, rice has lower RMSEs in the case of T_s or W_s only, as compared to the combined use of both terms. In these 'best case' scenarios, the absolute amount of error is higher for rice than for cotton.

The results for cotton show that if water stress only is taken into account, the resulting RMSE is slightly higher than the one obtained by using both T_s and W_s. In the case of rice, the RMSE is even lower. In both cases, the bias is furthermore lower when only W_s is used. The results show that temperature stress was minimal during the growing season 2009 and that this parameter had only little effect on model accuracy. The use of W_s only as well as T_s and W_s terms combined results in a positive bias, indicating that the model underestimates actual crop yields. The reason for this behavior is difficult to identify. One explanation is that the first 1.5 months of the season were not covered by satellite measurements in the area where the CRI is located (compare figure 4.3). If decisive periods in canopy development are not captured by image acquisition, maximum canopy FPAR could have been lower than actual values. This might have led to an underestimation of final yield in this area. In general, however, a comparison with published *in situ* values (Ehammer et al. 2010) shows that maximum FPAR is similar.

Validation of the model indicated that the accuracy was reasonable and merited its application at the regional scale. The RMSE for cotton and rice yield was within the range of comparable studies. For example, Lobell et al. (2003) found an error between approximately 3 and 30 % for maize, wheat, and soybean rotations in the Yaqui valley, Mexico, using Landsat imagery. Using medium resolution AVHRR data for crop yield estimation in Pakistan, Bastiaanssen & Ali (2003) calculated a relative RMSE of 26 % for wheat, 32 % for sugarcane, 37 % for rice, and 49 % for cotton. These errors were considerably higher than the ones reported here. Moriondo et al. (2007) also used AVHRR data for estimating regional wheat yield in two Italian provinces and found altogether lower RMSEs of 15.4 % and 17.9 %. However, the major difference between these studies and the study at hand is that crop yields were calculated at the field scale instead of the Landsat or aggregated regional scale. This is a major advantage of the RapidEye data, and the found errors show that it can easily compete with similar approaches.

Different values for the crop-specific parameters $LUE_{\max}$ and H_i (T_s was neglected due to its small influence) may have led to different accuracies. A sensitivity analysis was consequently conducted to investigate the effect of changing parameter values on the overall RMSE (figure 5.9). $LUE_{\max}$ and H_i were varied from -40 to 40 %, by steps of 10 %. Only one parameter at a time was varied. The results for cotton (figure 5.9) show that the decrease as well as the increase of one parameter would mostly have led to larger RMSEs. Only if H_i for cotton was

Table 5.3: Bias and RMSE for cotton (n = 38) and rice plots (n = 18) as a function of different combinations of stress indices. EDR = Environmental Down-Regulation, T_s = Temperature stress, W_s = Water stress.

Crop	Use of EDR	Bias	RMSE (% of mean)
Cotton	Ts + Ws	0.22	0.73 (29.10)
Cotton	No stress	-1.46	1.59 (63.35)
Cotton	Ts only	-1.14	1.38 (55.00)
Cotton	Ws only	0.19	0.74 (29.48)
Rice	Ts + Ws	0.83	1.28 (39.75)
Rice	No stress	-1.08	1.47 (45.65)
Rice	Ts only	-0.09	0.99 (30.75)
Rice	Ws only	0.11	0.98 (30.43)

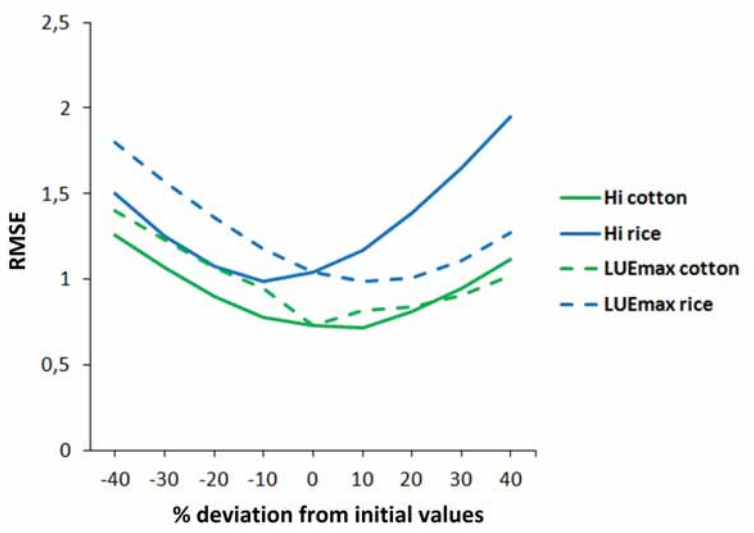

Figure 5.9: Sensitivity analysis for the model parameters $LUE_{\max}$ and H_i for cotton and rice.

increased by 10 %, the overall RMSE was slightly lower than the one obtained from the initial values. The RMSE for rice was lowest either when H_i was reduced by 10 % or when $LUE_{\max}$ was increased by 10 %. Both initial values led to slightly higher RMSEs.

The remaining error is likely to be caused by uncertainties that comprise errors of the field measurements, the empirical up-scaling of NDVI to FPAR, yield data collection, and model formulation. The latter can for example result in errors by not accounting for additional crop stresses like nitrogen stress, caused by insufficient fertilization, or pest infestation. Although the errors found in this study were assumingly caused by missing RapidEye data, these conditions could occur in other regions or different years.

Table 5.4: Regional crop yield statistics in 2009 based on the LUE model at the RapidEye scale.

Crop	Number of fields	Minimum yield ($t \times ha^{-1}$)	Maximum yield ($t \times ha^{-1}$)	Mean yield ($t \times ha^{-1}$)	Standard deviation of yield ($t \times ha^{-1}$)
Cotton	15,299	0.040	3.87	1.81	0.69
Rice	5,668	0.008	6.31	3.61	1.05

5.3.2.3 Spatial and temporal patterns of crop yield and biomass in 2009

Model validation showed its ability to predict cotton and rice yield with acceptable accuracy. In a next step regional yields at field scale were calculated using temperature and water stress down-regulation for cotton as well as water down-regulation only for rice crops. The resulting regional statistics are shown in table 5.4. The spatial distribution of yields showed characteristic patterns (figure 5.10). High cotton yields were found in the central and northern parts of the region (figure 5.10, upper part) lower yields were clearly distributed at the fringes of the district, close to the desert. The easternmost areas were the exception, being characterized by low cotton yield despite their vicinity to the river. The lower part of figure 5.10 presents the spatial distribution of rice yield. Rice fields were located in the northern districts and close to the Amu Darya river, but there was also a concentration in the south-eastern part. The highest yields could also be found in the northern districts.

The regional distribution of crop yields in the Khorezm region indicates that it roughly follows the general access to water. Water is abstracted from the river and fed into the irrigation system at altogether six water intake points (Conrad et al. 2007). In theory, the farer away from these intake points an area is located the less water remains for the irrigation of agricultural fields. This fact can explain the higher concentration of rice fields close to the river, and the generally lower yields in the southern and western areas (Ruecker et al. 2012).

The seasonal accumulation of AGBM (figure 5.11) partly reflected the FPAR trajectories presented in figure 5.7. AGBM of rice started to grow in June and increased fast in July, August and September. The standard deviation of AGBM for all rice fields increased until the end of the season. Cotton AGBM substantially increased only in the middle of July and most growth occurred from July to early September. The standard deviation of cotton was higher for the second half of the growing season. This was especially obvious at the end of the season, where the standard deviation of both cotton and rice was around 3-4 $t \times ha^{-1}$. The mean standard deviation was 1.36 $t \times ha^{-1}$ for cotton and 1.55 $t \times ha^{-1}$ for rice.

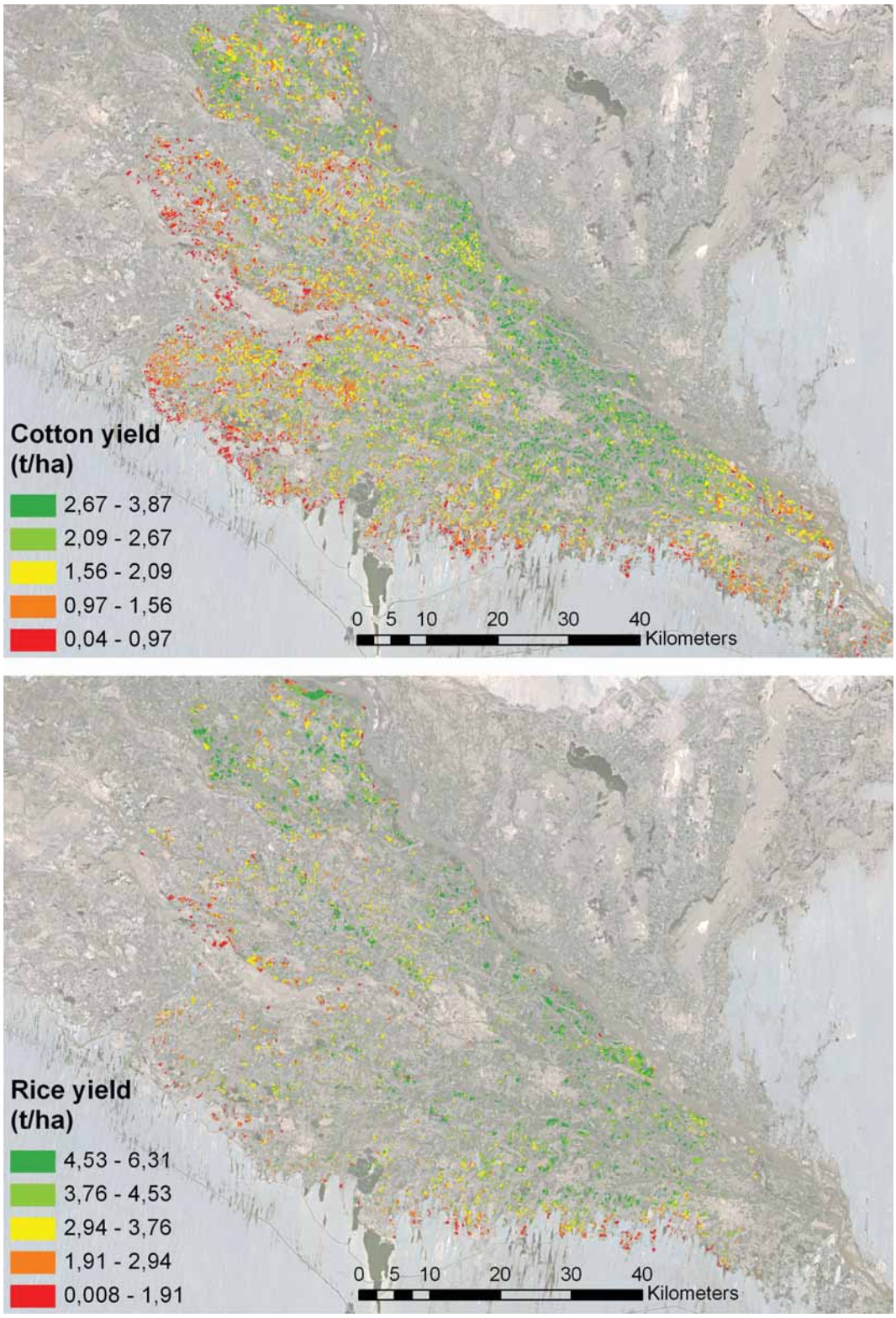

Figure 5.10: Spatial distribution of cotton (upper part) and rice yield (lower part) in $t \times ha^{-1}$ (background: RapidEye mosaic).

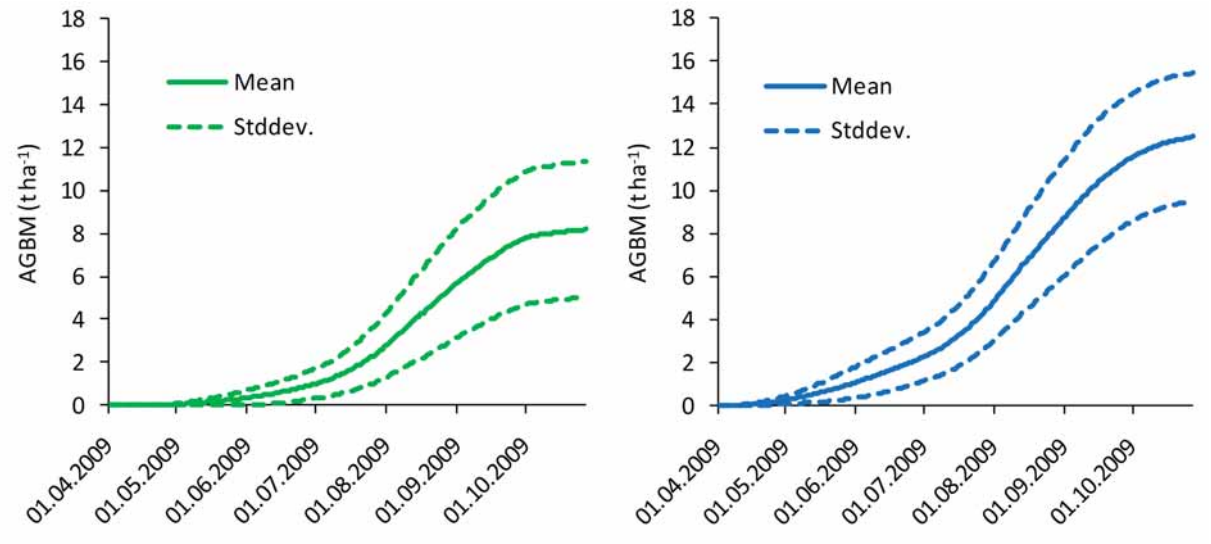

Figure 5.11: Mean and standard deviations for the accumulated AGBM for cotton and rice at field scale for the whole study area.

5.4 Pixel-based crop yield monitoring using medium resolution MODIS data

5.4.1 Data and methods

The following section describes the methodology to calculate regional biomass and crop yield based on MODIS data. The most important pre-processing step is the preparation of MODIS time-series, which is described in section 5.4.1.1. The approach to calculate yields is crop-specific and thus requires an annual crop map for the study region. The corresponding crop classification procedure is explained in section 5.4.1.2. Meteorological and crop-specific data used for the MODIS model are presented in section 5.4.1.3, and the analysis of the results is outlined in section 5.4.1.4.

5.4.1.1 MODIS data and pre-processing

The 8-day MODIS surface reflectance product (MOD09Q1), described in section 4.3.2.2.1, forms the basis of the medium resolution crop yield calculation procedure. As described, the NDVI calculated from the MOD09Q1 product showed the highest correlations with the high resolution RapidEye FPAR maps. Furthermore, the temporal resolution of the product allows adequately capturing crop phenology in the study region. The general workflow for MODIS data pre-processing is shown in figure 5.12. Annual MODIS data from 2003 to 2009 was used for the calculations. In a first step, the data was downloaded from the MODIS data archive using the NASA Reverb ECHO Tool (reverb.echo.nasa.gov/reverb/). The original HDF (Hierarchical Data Format) data has a sinusoidal projection (Seong et al. 2002). All data were re-projected

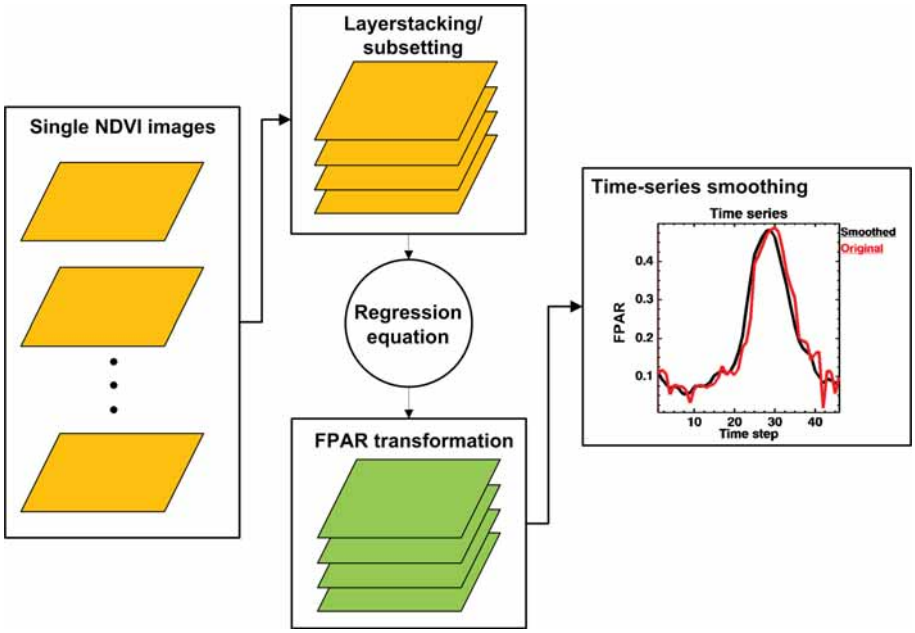

Figure 5.12: An overview of MODIS data pre-processing.

to the UTM Zone 41 North (Datum WGS 84) projection and converted to GeoTIFF (Geographic Tagged Image File Format) files using the MODIS Reprojection Tool. After the data was downloaded, re-projected, and converted to GeoTIFF, the NDVI was calculated for each of the 46 single images per year, for all years. Subsequently, annual NDVI layerstacks were constructed from the single images and each stack was subsetted to restrict further analyses to the extent of the Khorezm region. The transformation equation developed in section 4.3.2.2.1, using all MODIS and RapidEye images for the year 2009, was used to calculate FPAR from NDVI values (equation 5.9):

$$FPAR = -0.0112 + 0.788 \times NDVI \tag{5.9}$$

Although the overall quality of the MODIS data was high (see section 4.3.1.2), for example due to low cloud cover during the growing season, the resulting FPAR time series showed positive or negative outliers in some cases (figure 5.12). Annual time series were therefore smoothed prior to further use. For this purpose, a temporal central moving-average filter with a window of three was applied to the time series.

5.4.1.2 Land use information

Regional crop yield modeling, and the identification of areas with high or low yields, required the location of the different crop types, which necessitated the use of crop maps for the present study. The crop maps used in this study were taken from Conrad et al. (2011), who compiled

maps for the years 2004 - 2007. Building on this reference dataset, the remaining years, 2003, 2008 and 2009, were classified (Conrad et al. in review). The final crop maps for all years are displayed in figure 5.13. The satellite data employed for this purpose were also 8-day MODIS NDVI composites, calculated from the MOD09Q1 product. Quality assessment was applied to the MODIS time series, and data affected by clouds or data production issues were temporally linearly interpolated. To achieve high geometric accuracy, MODIS imagery was further aligned with geo-referenced high resolution ASTER data that was available for the Khorezm region (Conrad et al. 2011). The ASTER datasets were used to classify field-based land use in the Khorezm region in a related study (Conrad et al. 2010). The ASTER-based crop maps were used as training and validation samples for the MODIS-based classification. To this end, MODIS time series and ASTER crop maps were intersected and pixels that met crop-specific homogeneity criteria were selected as samples (Conrad et al. 2011).

The classification itself was done with Classification and Regression Trees (CART), described by Breiman et al. (1984). Building on CART, Conrad et al. (2011) implemented a modification of the original methodology in their study. Instead of using the original NDVI time series as input to the classification tree, the time series were temporally segmented with varying degrees of segment sizes. Temporal metrics were subsequently calculated for all segments. These metrics consisted of the mean, standard deviation, minimum, maximum, and range of the NDVI data. The results gained from this analysis showed that certain combinations of temporal segmentation can achieve results that are between 6-7 % more accurate than accuracies that result from the use of the original NDVI dataset.

The overall accuracies of the crop maps were stated to be around 84 % (Conrad et al. 2011). However, this statement is only valid for the maps between 2004 and 2007. The reference samples were used for the remaining years under the assumption that the temporal crop profiles, collected for four years in the study area, accurately represent possible variation of these profiles. This assumption is backed by the fact that the crop types themselves do not change in Khorezm, only their spatial distribution and rotation. This leads to characteristic and crop-specific phenological signals, which can be classified. Yet an independent estimate of map accuracy could not be reported. The crop maps were subsequently used to create masks for the dominant crop types in the study region, which were then assimilated into the crop yield model.

5.4.1.3 Meteorological and crop-specific data

In comparison to the RE modeling, only data from the meteorological station in Urgench was used to run the LUE model at the MODIS scale. This change was implemented for two reasons. First, the chosen station covered the complete modeling period, in contrast to most other stations. Second, it was shown that temperature stress only has a minor influence on the accuracy of the crop yield model. The temperature variation throughout the region was furthermore

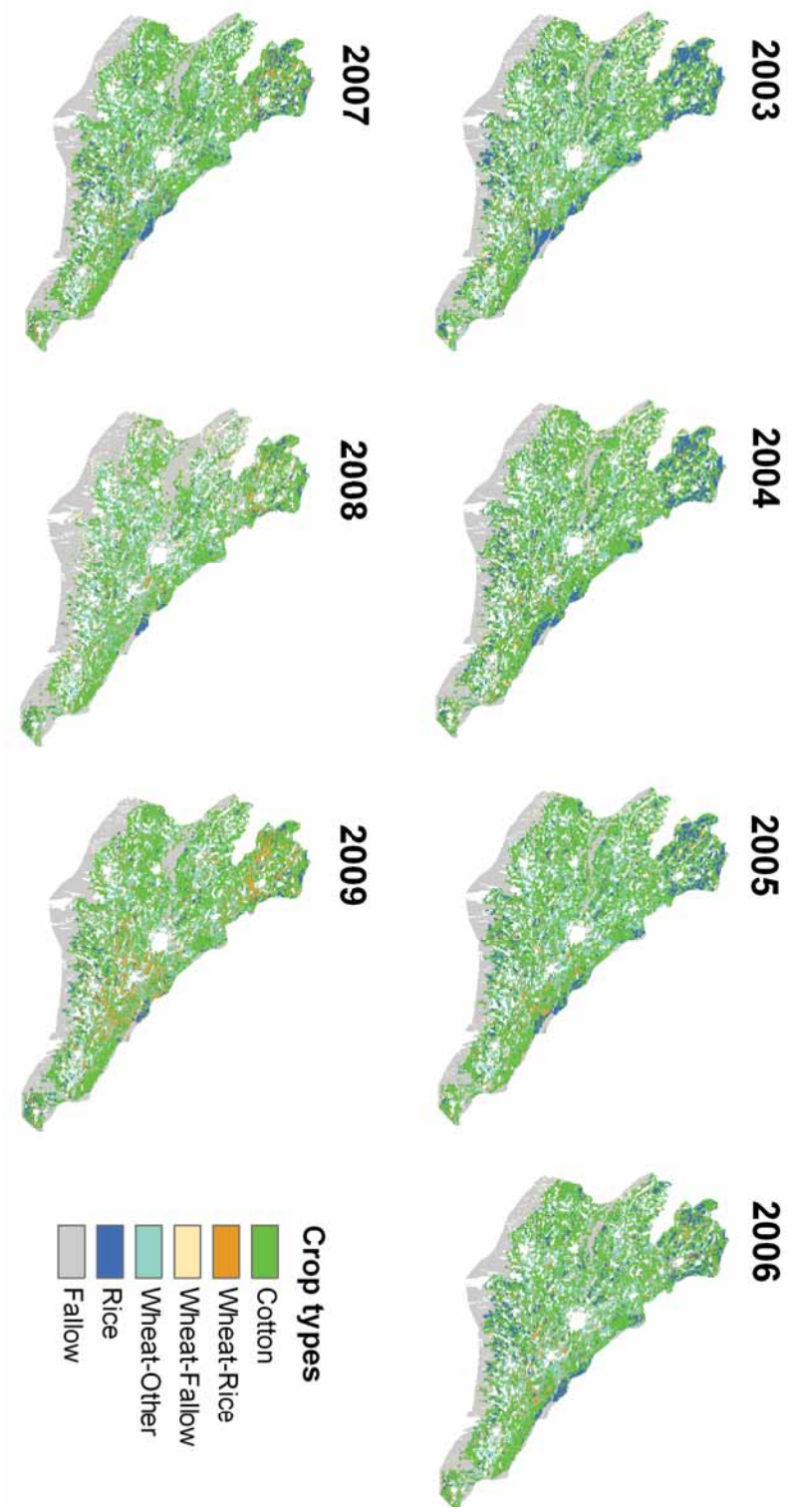

Figure 5.13: Crop type maps for the Khorezm region (2003 to 2009) (based on data taken from Conrad et al. in review).

negligible, which justified this simplification. Finally, the two crop-specific parameters, $LUE_{\max}$ and H_{i}, were adopted from the RapidEye scale. Yet instead of using the original values, the adjusted values resulting from the sensitivity analysis were used.

5.4.1.4 Spatial analysis of crop yield patterns

One of the main questions of this work was the identification of areas with significantly higher or lower crop yields. Consequently, spatial patterns of the yield maps were investigated by calculating hot spots and cold spots of crop yield. The Getis-Ord Gi^* statistic, as implemented in ArcGIS (ESRI), was employed for this purpose. The Gi^* statistic is further described in Getis & Ord (1992) and Ord & Getis (1995). In order to be a cluster of high (hot spot) or low values (cold spot), the values of a feature have to be surrounded by high or low values, respectively. The Getis-Ord Gi^* is a local statistic that measures the degree of clustering for a study area. Local statistics do not calculate statistical parameters for a complete area. Instead, they use the location as well as the variable value to calculate statistical parameters for single features (in the case described here: pixels). The hot spot analysis tool in ArcGIS uses the Gi^* parameter to investigate where significantly higher or lower values of a variable cluster spatially (ESRI 2012). Gi^* is calculated as follows (equation 5.10, taken from ESRI 2012):

$$G_i^* = \frac{\sum_{j=1}^{n} w_{i,j}x_j - \overline{X}\sum_{j=1}^{n} w_{i,j}}{S\sqrt{\frac{\left[n\sum_{j=1}^{n} w_{i,j}^2 - \left(\sum_{j=1}^{n} w_{i,j}\right)^2\right]}{n-1}}} \tag{5.10}$$

In this equation, x_{j} is the attribute value for feature j, $w_{\mathrm{i,j}}$ is the spatial weight between feature i and j and n is the total number of features (pixels) used in the analysis (ESRI 2012). $\overline{X}$ is the mean of all attribute values (equation 5.11):

$$\overline{X} = \frac{\sum_{j=1}^{n} x_j}{n} \tag{5.11}$$

Finally, S is the standard deviation of the attribute values and is written as (equation 5.12):

$$S = \sqrt{\frac{\sum_{j=1}^{n} x_j^2}{n} - \left(\overline{X}\right)^2} \tag{5.12}$$

Three parameters control the output of the calculations: the conceptualization of spatial relationships, the method used for distance calculations and a threshold distance. The conceptualization determines how the spatial relationships between features are treated (ESRI 2012). For this study, the fixed distance band method was used. This method analyzes all features within a critical distance range and assigns a value of 1 to these features. All features outside the fixed distance are not accounted for and receive a weight of 0. As distance calculation method (between features or pixels), the Euclidean distance was chosen. The threshold distance for the hot spot analysis tool depends on the spatial autocorrelation of the features (and their variable

values) in the study area. To choose the correct distance for the hot spot analysis, the global Moran's I statistic for determining the spatial autocorrelation was used. Moran's I is calculated according to equation 5.13:

$$I = \frac{n}{S_0} \times \frac{\sum_{i=1}^{n} \sum_{j=1}^{n} w_{i,j} z_i z_j}{\sum_{i=1}^{n} z_i^2} \tag{5.13}$$

where z_i and z_j represent the deviation of an attribute for feature i and j from their mean (e.g., x_i - $\overline{X}$) and S_o is the aggregate of all spatial weights (equation 5.14):

$$S_0 = \sum_{i=1}^{n} \sum_{j=1}^{n} w_{i,j} \tag{5.14}$$

For more detailed information on the calculation of Moran's I see ESRI (2012) and Getis & Ord (1992). Amongst other parameters, the application of the Global Moran's I tool in ArcGIS results in a z-score for a specific, fixed distance. A z-score, along with the associated p-values, can be used to determine whether or not to reject the null hypothesis. In the case of Global Moran's I, the null hypothesis is that the location of features in a study area, along with their parameter values, are a result of random processes. A high z-score indicates that the null hypothesis can be rejected, and the found pattern is not random. With regard to the hot spot analysis implemented in this study, the goal is to find the distance with the highest z-score. This indicates that, at the found distance, there is spatial interaction between features and their values in a dataset. To find the correct distance, the Global Moran's I tool was run multiple times, until an appropriate distance was found. The found threshold distance was subsequently used for a hot spot analysis of all years for cotton and rice crops.

5.4.2 Results and discussion

5.4.2.1 Derivation of *SoS* and *EoS* from MODIS time-series

The software TIMESAT was used to estimate annual, pixel-based values for the start and the end of the season, which were necessary to constrain the model runs to the actual growing season. The mean Khorezm-wide dates for *SoS* and *EoS* of cotton and rice are shown in table 5.5. Mean cotton *SoS* ranges from April to June, with most years having a mean value in May. There is a smaller range for the *EoS*, with means in September. Rice *SoS* is in June for all years and shows only slight variations. The same is true for rice *EoS* values, which, similar to cotton, all occur in September. To avoid false values, which could have a negative impact on the modeling process, *SoS* and *EoS* had to be in a specified temporal window. This window was viewed as representing plausible values for *SoS* and *EoS* for cotton and rice, and was chosen according to local agronomic conditions. For *SoS*, it ranged from May 1 to June 15 and from May 15 to July 15 for cotton and rice, respectively. For *EoS*, a window from September 7 to October 15 was defined for both cotton and rice. In case the dates extracted by TIMESAT failed to fall within those windows, a generic standard value was assumed (*SoS*

Table 5.5: Khorezm-wide mean annual values of *SoS* and *EoS* for cotton and rice. 'Percent valid' describes the percentage of crop-specific pixels that fall within a plausible period for *SoS* and *EoS*.

Year	*SoS*(cotton)	*EoS*(cotton)	Percent valid (*SoS*/*EoS*)	*SoS*(rice)	*EoS*(rice)	Percent valid (*SoS*/*EoS*)
2003	May 11	Sep 24	40 / 95	Jun 16	Sep 17	83 / 92
2004	May 29	Sep 19	35 / 92	Jun 21	Sep 14	93 / 85
2005	May 04	Sep 18	37 / 92	Jun 05	Sep 11	80 / 75
2006	May 31	Sep 24	32 / 94	Jun 23	Sep 15	92 / 88
2007	Jun 02	Sep 16	38 / 93	Jun 25	Sep 13	93 / 88
2008	Apr 25	Sep 28	24 / 92	Jun 17	Sep 24	76 / 99
2009	May 31	Sep 21	32 / 95	Jun 27	Sep 17	86 / 92

cotton: May 1, *SoS* rice: June 1, *EoS* cotton/rice: October 15). The percentage of valid pixels varied strongly between crop types (table 5.5). It was very low for cotton *SoS*, ranging from 24 % to 40 %. In contrast, rice showed much higher percentages (76 % to 93 %). A likely reason is the quality of the temporal NDVI profiles of cotton crops used by TIMESAT. For example, different management-related and environmental factors influence crop fields in the beginning of the season. Ploughing, weeds on fields and irrigation can influence NDVI profiles that often showed much more variability and noise as compared to rice profiles. Future analyses should focus on an enhanced derivation of seasonal parameters from those NDVI profiles, for example by using different settings or smoothing methods. Estimates of the *EoS* gave different results (table 5.5). Both cotton and rice were characterized by high percentages of valid pixels. The percentage for cotton was always greater than 90 %. Percentages for rice varied between 75 % and 99 %. Estimations of the *EoS* were more reliable than those of the *SoS*. One reason might be that, at the end of the season, there is much less variation in the NDVI profiles. Finally, there is very little overall variation in seasonal parameters between years.

For accuracy assessment of the estimates, they were compared to literature values taken from studies conducted in Khorezm (table 5.6 and 5.7). The exact location of all experimental sites reported in the literature was known, and MODIS-based *SoS* and *EoS* represented the mean of the pixels surrounding those sites. Quantitative assessment was not possible due to a lack of sufficient data, but the available data should suffice to determine the general quality of the estimates. Table 5.6 lists the dates of crop emergence and compares it to the *SoS* estimates from MODIS, because both parameters describe the point in time when crops start their vegetative growth. In general, *SoS* corresponds well to crop emergence. The differences for cotton range from three to eight days. For the evaluation of rice estimates there were also two years available. In 2008 the difference was seven days, and in 2009 the emergence date of rice was exactly cap-

Table 5.6: Comparison between dates of crop emergence (literature values) and the corresponding pixel-based values for *SoS* from MODIS data.

Reference	Year	Crop	Date literature (stage)	Mean *SoS*
Forkutsa (2006)	2003	Cotton	May 8 (emergence)	May 11
Sommer et al. (2008)	2005	Cotton	May 12 (emergence)	May 04
Devkota (2011)	2008	Rice	June 24 (emergence)	June 17
Devkota (2011)	2009	Rice	June 27 (emergence)	June 27

Table 5.7: Comparison between harvest dates (literature values) and the corresponding pixel-based values for *EoS* from MODIS data.

Reference	Year	Crop	Date literature	Mean *EoS*
Forkutsa (2006)	2003	Cotton	September 24 (1^{st} pick)	September 24
Kienzler (2009)	2004	Cotton	September 23 (1^{st} pick)	September 19
Sommer et al. (2008)	2005	Cotton	September 13/14 (1^{st} pick)	September 18
Devkota (2011)	2008	Rice	October 08	September 24
Devkota (2011)	2009	Rice	October 22	September 17

tured. In the case of harvest dates, there were large differences between cotton and rice (table 5.7). The differences between the *EoS* and the first pick of cotton ranged from zero to four days.

While the date of the first cotton pick is very well captured by TIMESAT parameters, other picks are consequently left out of the calculation process. This means that the model stops the calculation process too soon and potentially underestimates actual crop yields. A similar behavior was observed for rice. The differences between harvest and *EoS* dates were 14 and thirty-five days, which is an especially large difference. In contrast to larger cotton fields at the CRI, the experimental plots where the rice data was gathered were very small and not evenly covered by a single MODIS pixel. Analysis of the NDVI curves at the MODIS scale revealed that there was a great mixture with other crop types, even crop rotations. These mixed profiles were likely to be one cause for TIMESAT estimating wrong dates. The mean Khorezm-wide dates presented in table 5.5 back this observation by also showing generally earlier dates for *EoS*. Rice yield may also have been underestimated as a consequence. However, Devkota (2011) showed that biomass accumulation during the last 20 to 30 days is negligible for conventional cropping with continuous flood irrigation. As continuously irrigated rice is the normal case in the Khorezm region, one can assume that there will only be a minor effect of *EoS* estimates on modeled rice yield. In conclusion, the end of the season is captured more accurately for cotton crops, although the model seems to be stopping too early in both cases.

5.4.2.2 Crop stress and LUE_{act}

The actual light use efficiency at the MODIS scale was calculated in a different manner than that at the RapidEye scale. LUE_{act} was also derived by constraining LUE_{max} via temperature and W_s terms. Yet the results at the RapidEye scale showed that high temperatures have only a minimal effect on the calculated results. Consequently, the crop growth restrictions due to high temperatures were neglected at the MODIS scale. This generally simplified the approach. Another simplification for multi-year crop modeling was that all crop types were assigned the same (minimum) temperature restrictions. Temperature stress at the MODIS scale was considered to linearly decrease between -8 and 8 ℃. Daily minimum temperatures above 8 ℃ were assumed to pose no constraint to crop production. Water stress was calculated for each crop, similar to the RapidEye-scale model, as the ratio of ET_{act} to ET_{c}.

Parameters accounting for temperature and W_s determine the actual light-use efficiency of the crops, which in turn controls annual biomass accumulation and yield formation. As it was shown that W_s has the decisive influence on crop yields, the temperature stress term will mostly be neglected in the following discussion. The mean seasonal W_s scalar for cotton crops is shown in figure 5.14. In general, the patterns look similar from year to year. The stressed period is approximately from the beginning of May to mid-September. One of the main observations is that the minimum of the W_s factor (and consequently the maximum W_s) repeatedly occurs between the middle of June and the middle of July. This period largely corresponds to the main irrigation period in Khorezm (Forkutsa et al. 2009). The fact that W_s is highest during this period means that an insufficient amount of water was available for irrigation or that irrigation was delayed. Yet W_s is never high enough to completely inhibit crop growth. In fact, the mean W_s factor for cotton rarely drops below 0.6. A visual interpretation of the curves in figure 5.14 suggests that there are insignificant differences between the years. Only 2008 and 2009 stand out. In 2008, due to significantly decreased water availability, persistent W_s stretches out over a longer time span. The mean W_s factor is also slightly lower compared to other years. The opposite is true for 2009, where the lowest mean W_s of all years occurs. The variation is also lower for 2009, with a standard deviation of 0.06 compared to 0.08-0.11 for other years. Minimum values show a slightly different variation from year to year. Table 5.8 (upper part) shows descriptive statistics for the W_s parameter for cotton. As seen in table 5.8, minimum W_s factors are similar from year to year. The only exception is 2003, where the minimum W_s factor slightly drops to 0.57.

The results for rice differ somewhat from those of cotton (figure 5.15 and table 5.8, lower part). The stress period for rice is equally long, with an exception in 2003. In contrast to cotton, a period of maximum W_s is difficult to identify. The statistics (table 5.8, lower part) illustrate that overall stress levels of rice crops are generally lower. Mean values for the W_s scalars are higher than 0.91 in all years, and the minimum values are also mostly higher compared to cotton. This

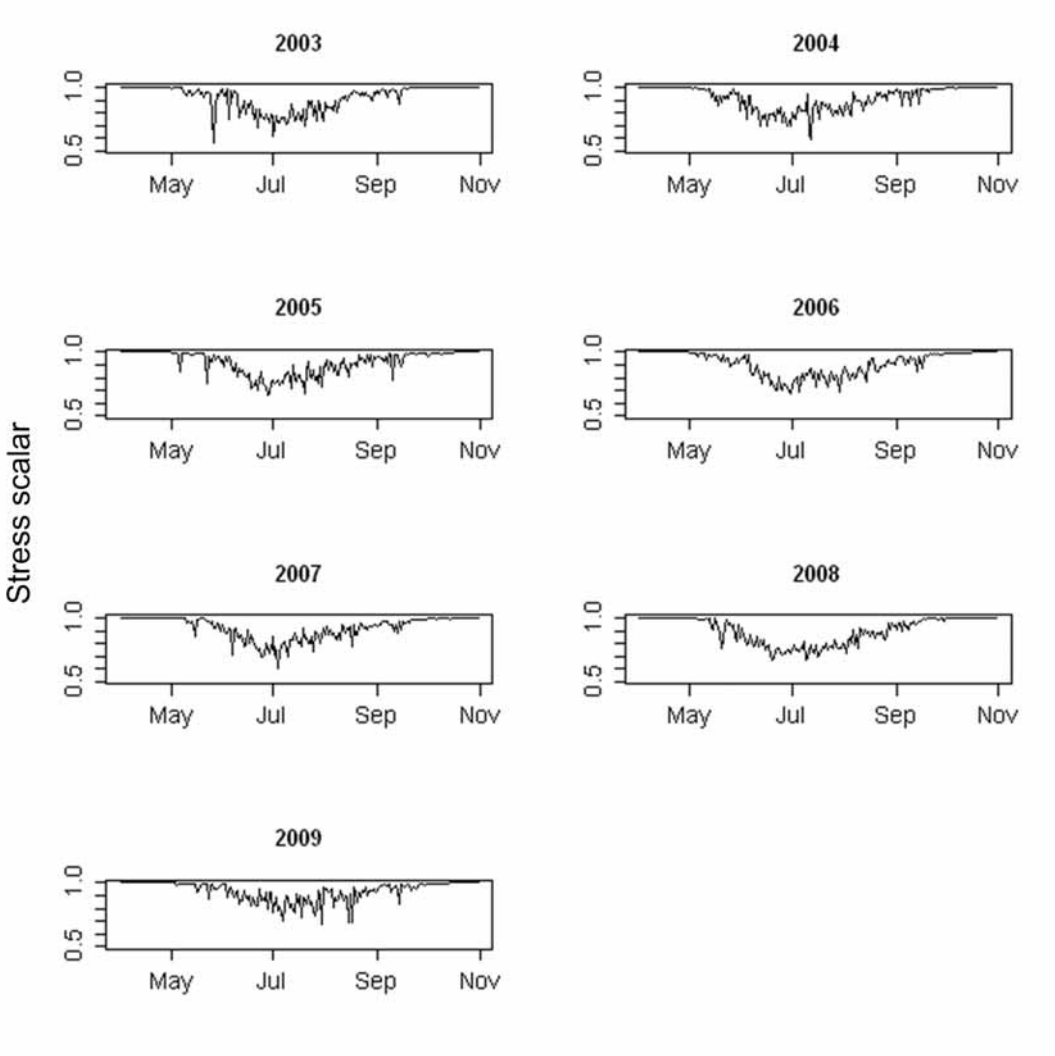

Figure 5.14: Water stress scalar for cotton crops from 2003 to 2009. A value of 1 means no stress, a stress factor of 0 completely inhibits crop growth. The calculation period is from April 1 to October 31. Note that the y-axis is scaled from 0.5 to 1.

result was to be expected, since rice is usually permanently flooded. However, the numbers show that this is not always the case and W_s can also affect rice crops. Compared to other studies in irrigated areas (Lobell et al. 2003), this underlines that W_s cannot be neglected here. Water stress in rice crops points to suboptimal irrigation timing or a lack of water availability as the reason for the W_s conditions.

Figure 5.16 displays the temporal evolution of the mean W_s factors for cotton and rice, taken from table 5.8. It visualizes the differences and shows that maximum W_s was experienced in 2008 by both crops. In 2009, on the other hand, the lowest W_s during the investigated seven-year period occurred for cotton. In comparison, minimum values for rice were observed in 2003. In other years the W_s factors are rather stable.

Table 5.8: Descriptive statistics for the water stress factor W_s for cotton and rice crops from 2003 to 2009.

Cotton	Min	Max	Mean	Std
2003	0.57	1	0.92	0.10
2004	0.60	1	0.92	0.08
2005	0.66	1	0.92	0.09
2006	0.69	1	0.92	0.08
2007	0.62	1	0.93	0.08
2008	0.65	1	0.89	0.11
2009	0.73	1	0.94	0.06
Rice	**Min**	**Max**	**Mean**	**Std**
2003	0.76	1	0.97	0.05
2004	0.61	1	0.95	0.06
2005	0.72	1	0.95	0.07
2006	0.73	1	0.94	0.06
2007	0.67	1	0.95	0.06
2008	0.72	1	0.91	0.09
2009	0.73	1	0.96	0.05

The descriptive statistics for LUE_{act} are displayed in table 5.9 for cotton (upper part) and rice (lower part). A similar picture as for W_s can be inferred for LUE_{act}. Rice generally has higher values for LUE_{act}, which is mostly visible in the total mean values (cotton: 1.59, rice: 1.64). Bastiaanssen & Ali (2003) reported a range of literature values for LUE of cotton and rice. According to the list of Bastiaanssen & Ali (2003), the only available source for cotton LUE reports a value of 1.44. Compared to this study, the found LUE_{act} for cotton was slightly higher than the one reported in Bastiaanssen & Ali (2003). Rice LUE ranges from 1.43 to 2.7, depending on rice variety. None of the varieties, however, are similar to those investigated here. The mean values for rice LUE_{act} are within the range of the reported values, albeit at the lower end. Altogether, the found results seem plausible, yet a direct comparison with reported values is difficult due to different environmental conditions, cultivar types, etc.

The overall differences between mean values of LUE_{act} are comparable to those of W_s, but LUE_{act} evolves differently (figure 5.17). Altogether there is more variation in LUE_{act} between the years. In 2007, 2008 and 2009 the same patterns as for W_s can be observed. The year 2008 represents the year with the lowest average LUE_{act}, and the the year 2009 the year with the highest values. The remaining years show a steady increase until 2006 (with the exception of 2004). After 2006, LUE_{act} decreases until its lowest values in 2008. The differences between the curves in figure 5.16 and figure 5.17 are likely to be caused by the temperature stress term

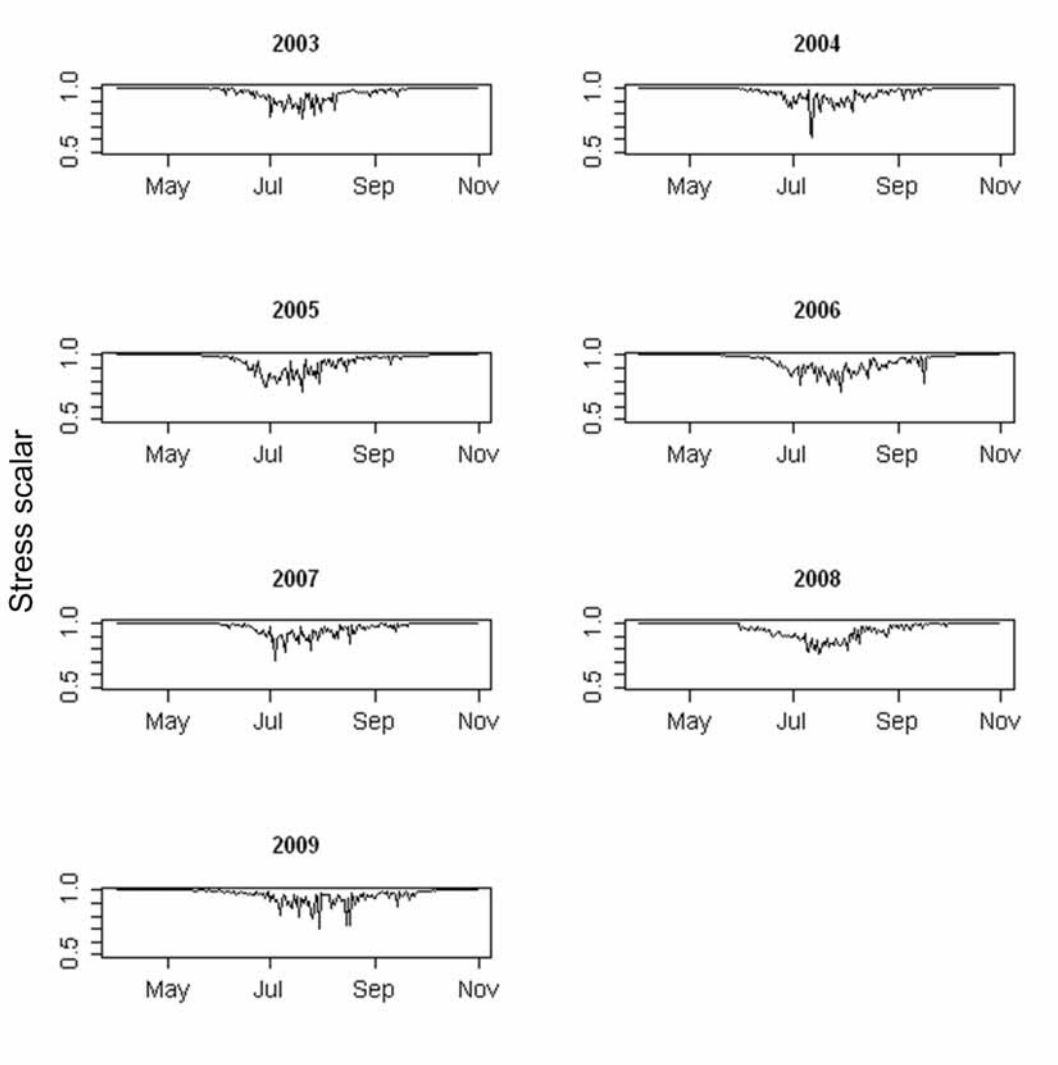

Figure 5.15: Water stress scalar for rice crops from 2003 to 2009. A value of 1 means no stress, at a value of 0 crop growth is completely inhibited. The calculation period is from April 1 to October 31. Note that the y-axis is scaled from 0.5 to 1.

of the model. The parameter supposedly had a larger negative influence on LUE_{act} in 2003 and 2004, which resulted in lower LUE_{act} in those years. However, overall differences between the years are still small for W_{s} and LUE_{act}.

5.4.2.3 Estimation of PAR

To accurately assess model results, and the impact of the different model components on them, a comparison between measured and modeled global radiation was carried out. Data from the meteorological station in Yangibazar was used for this purpose (for station locations see figure 5.6), as this was the only station that recorded data throughout the whole period of investi-

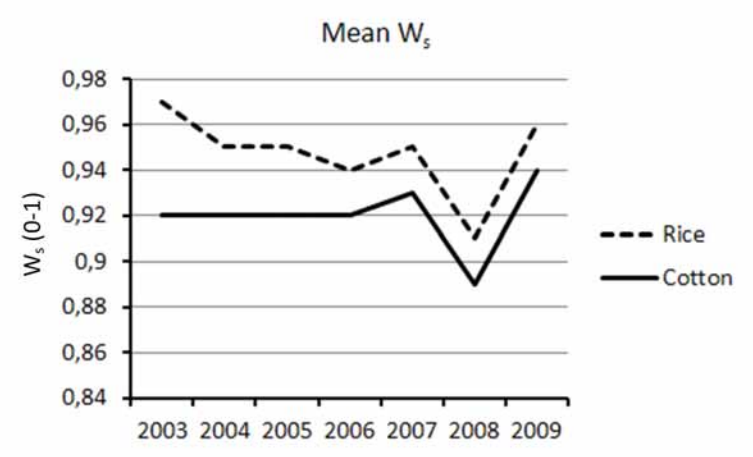

Figure 5.16: Mean W_s scalar for cotton and rice from 2003 to 2009. The higher the value, the lower the water stress.

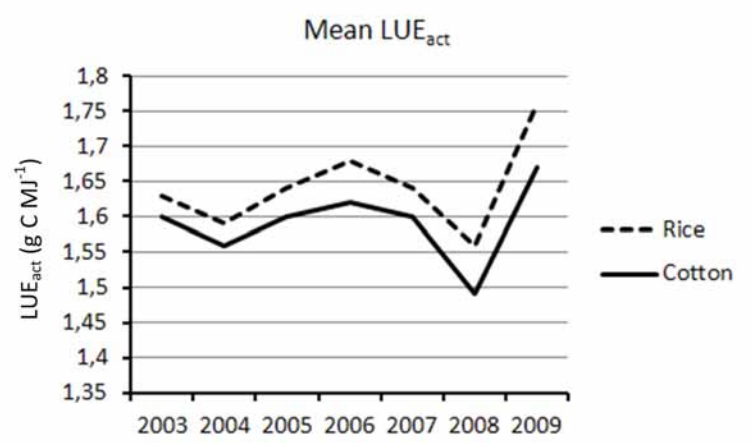

Figure 5.17: Mean LUE_{act} for cotton and rice crops from 2003 to 2009.

gation. The data from the meteorological station in Yangibazar was first aggregated to daily values by calculating the daily mean global radiation. Afterwards the measured global radiation was converted to MJ. The comparison was conducted only for the decisive parts of the growing season, from April 01 to October 31. Minor data gaps were left out of the comparison. For quantitative assessments, the bias and the RMSE were calculated from time series of both measured and modeled data.

A visual comparison of both datasets can be seen in figure 5.18. The figure shows that the model fits the measured data relatively good. In general, however, the model overestimates measured data. This overestimation is especially pronounced between 2003 and 2006. From 2007 to 2009, modeled data even underestimates measured data during the peak of the season. The overestimation is likely caused by cloudy conditions in the study region; the sudden drops in global

Table 5.9: Descriptive statistics for the LUE_{act} of cotton and rice crops from 2003 to 2009.

Cotton	Min	Max	Mean	Std
2003	0.16	2	1.60	0.37
2004	0.37	2	1.56	0.38
2005	0.56	2	1.60	0.40
2006	0.63	2	1.62	0.38
2007	0.37	2	1.60	0.38
2008	0.54	2	1.49	0.45
2009	0.72	2	1.67	0.31
Rice	**Min**	**Max**	**Mean**	**Std**
2003	0.13	2	1.63	0.34
2004	0.45	2	1.59	0.35
2005	0.58	2	1.64	0.35
2006	0.76	2	1.68	0.32
2007	0.46	2	1.64	0.34
2008	0.61	2	1.56	0.38
2009	0.88	2	1.76	0.28

Table 5.10: Bias and RMSE for the comparison between measured and modeled global radiation between 2003 and 2009.

Year	Bias	RMSE (% of mean)
2003	-2.84	5.61 (26.95)
2004	-1.94	4.77 (22.04)
2005	-1.72	3.59 (16.40)
2006	-2.13	4.07 (18.90)
2007	-1.16	3.90 (17.36)
2008	-0.31	4.21 (18.06)
2009	-2.14	4.46 (20.40)

radiation point to this source. A quantitative comparison between measured and modeled data is given in table 5.10. The bias is negative in all cases, meaning that modeled data always overestimates the measured data. The lowest bias occurs in 2008, when over and underestimation are nearly balanced. The RMSE also shows only little variation, from 3.59 to 5.61. Altogether this corresponds to an error between 16.4 and 26.95 %.

The conducted comparison shows that, while modeled data fits the measured values quite well, clouds in the region were underestimated. Future versions of the crop yield model should incorporate a more advanced representation of global radiation and PAR, maybe by derivation from actual satellite measurements. In any case, cloud conditions need to be accounted for to

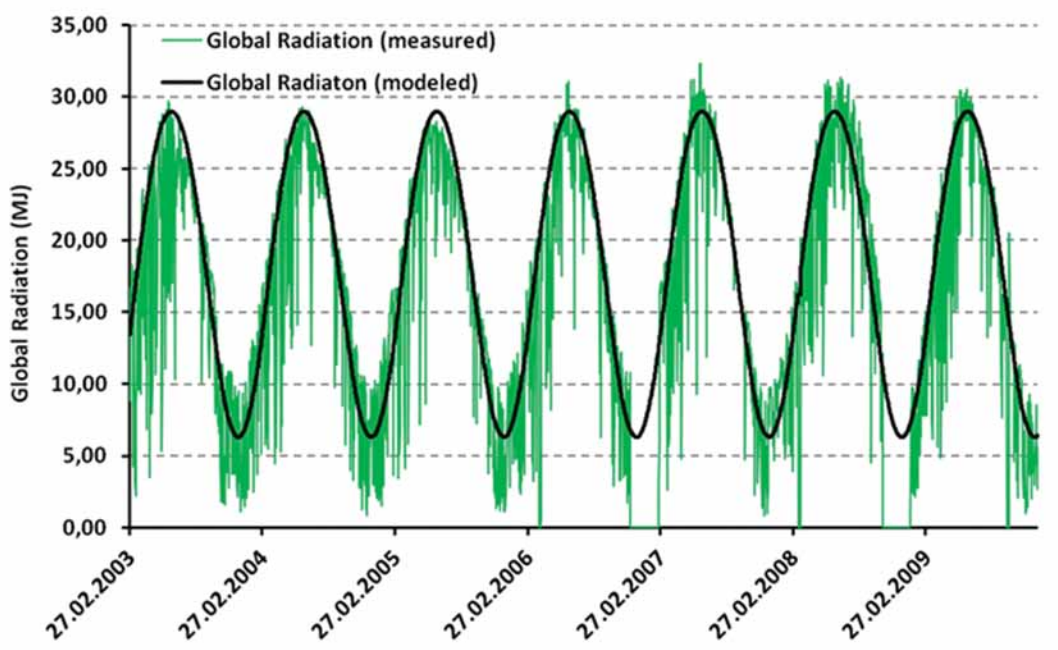

Figure 5.18: Comparison between measured and modeled global radiation (in MJ) between 2003 and 2009. For visual purposes, annual data is shown.

accurately calculate global radiation and PAR.

5.4.2.4 Spatial and temporal cotton and rice yield monitoring from 2003 to 2009

The MODIS-based crop yield model was used to estimate cotton and rice yields for the Khorezm region for the years 2003 to 2009. The associated crop yield patterns are shown in figure 5.19 (cotton) and figure 5.20 (rice). Table 5.11 presents the descriptive statistics derived from those maps. The statistics show that, at the Oblast level, there are only small differences for crop yields between years. The minimum and maximum yield, the mean yield and the standard deviation of crop yields have a very small inter-annual range. Only in 2008, when water availability for the whole region was low, the mean yield of both crops (and the maximum yield for rice) is lower compared to the other years.

The maps in figure 5.19 and figure 5.20 prove that crop yields are highly variable throughout the region. Yet while small-scale patterns can change from year to year, the general multi-annual pattern seems to be constant. In general, crop yields decrease from northeast to southwest. In other words, the farer away from the river and the closer to the desert in the south, the lower the crop yields. Obviously, this does not mean that high crop yields cannot be achieved in the southern districts. The Rayons Khiva, Yangiarik and Bogot also feature areas with high cotton and rice yields.

Table 5.11: Descriptive statistics for cotton and rice yield (in $t \times ha^{-1}$) from 2003 to 2009.

Cotton	Min	Max	Mean	Std
2003	0.01	6.2	3.0	0.7
2004	0.01	5.9	2.9	0.7
2005	0.05	5.7	3.1	0.8
2006	0.02	5.7	2.9	0.8
2007	0.08	5.6	3.1	0.8
2008	0.04	5.8	2.7	0.7
2009	0.08	5.5	3.1	0.8
Rice	Min	Max	Mean	Std
2003	0.02	6.1	3.7	1.0
2004	0.03	6.5	3.7	0.9
2005	0.01	6.4	3.9	0.9
2006	0.10	6.3	3.6	0.9
2007	0.20	6.6	3.8	0.8
2008	0.40	5.3	3.2	0.7
2009	0.02	6.4	3.4	0.9

Pitnak is mostly characterized by lower crop yields in most years, despite the fact that it directly borders the Amu Darya. The identified general pattern of crop yields is somewhat altered in 2008, when much larger areas were characterized by lower crop yields. In addition, figure 5.20 shows that very few areas were actually dedicated to rice in 2008. The corresponding yield was also relatively low.

To quantify the visually identified crop yield patterns in more detail, a Global Moran's I as well as a Gi^* hot spot analysis was conducted as described in chapter 5.4.1.4. The results of the Global Moran's I analysis for cotton crops can be seen in figure 5.21. The figure shows the z-scores for a range of distances. According to ESRI (2012), a distance for the hot spot analysis should be chosen at which a significant interaction between features and their values exist. The Moran's I analysis can be used to identify this distance. The higher the z-score, the more suiting the distance is for the hot spot analysis. It can be seen in figure 5.21 that z-scores initially increase with the distance. From a distance of around 13,000 m onwards, the z-scores start to increase only marginally. Eventually a distance of 17,000 m was deemed appropriate and further used in the Gi^* hot spot analysis.

The results of the hot spot analysis show that there are significant hot spots and cold spots of cotton and rice yield in the study region for the years 2003 to 2009 (the results for cotton yield are shown in figure 5.22). Figure 5.22 displays the z-scores associated with the Gi^* statistic calculated for cotton yield in Khorezm. The z-score is basically the standard deviation of a

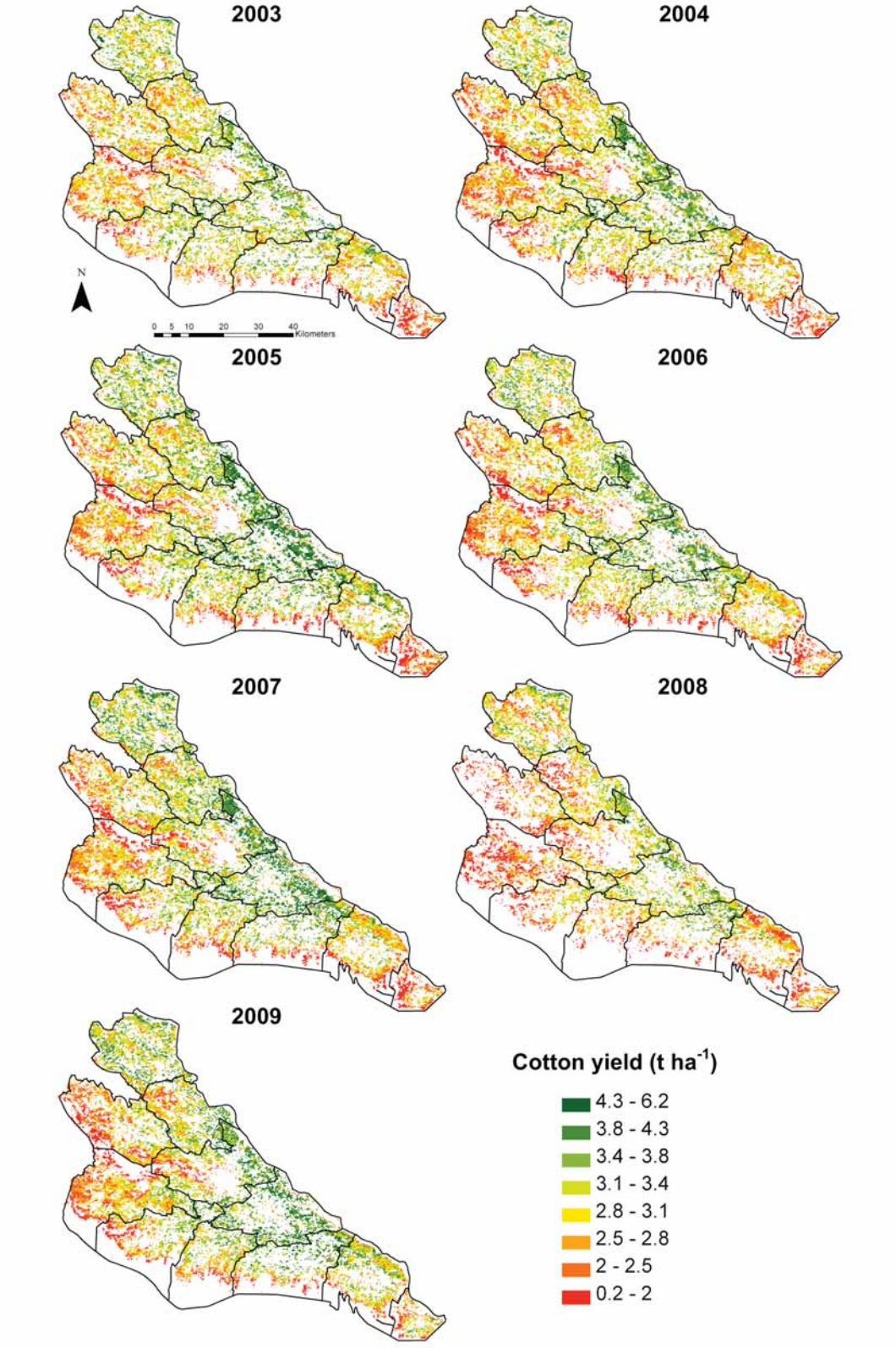

Figure 5.19: Cotton yield patterns from 2003 to 2009.

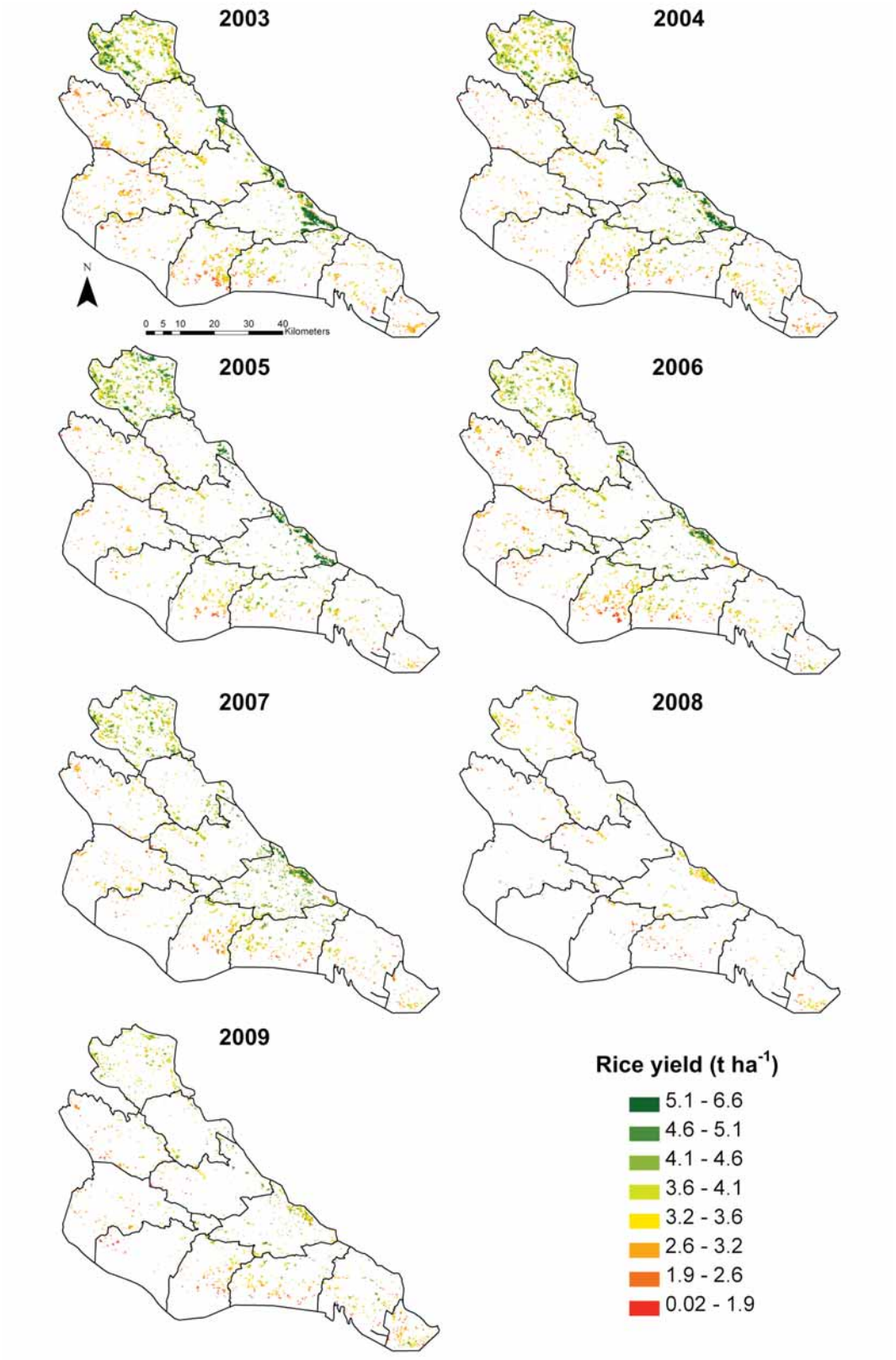

Figure 5.20: Rice yield patterns from 2003 to 2009.

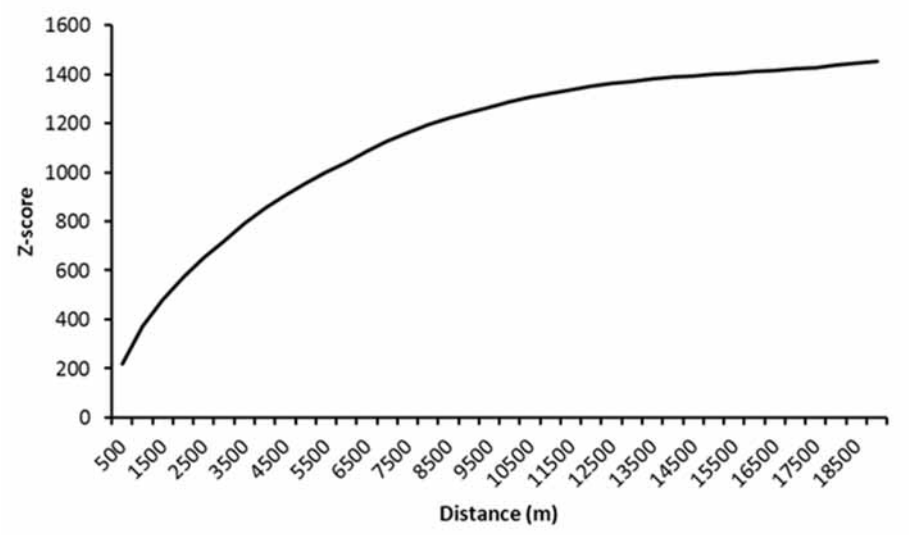

Figure 5.21: Z-scores from the Global Moran's I analysis for a range of distances (cotton yield).

normal distribution (ESRI 2012). Z-scores are complementary to p-values, which represent the probability of a spatial pattern, or the values associated to spatial entities, being the result of a random process. With regard to figure 5.22, a z-score greater 2.58 or smaller -2.58 corresponds to a p-value of 0.01. This means that the red and blue patterns in figure 5.22 correspond to hot and cold spots that are significant at the 99 % confidence level. The patterns confirm that clusters of high cotton yield tend to concentrate close to the river and in the center of the region, while clusters of low yield can mainly be found in the southwestern parts and in the east (Pitnak). The same patterns were found for rice (see appendix A.3), albeit they are less obvious due to the low number of rice pixels for each year.

5.4.2.5 Model evaluation and uncertainties

The results of the MODIS-based crop yield model were mainly evaluated by comparison with official statistics from 2004 to 2009, which were made available through OblStat (OBLSTAT 2010). As a first step, model results were aggregated at the Oblast level by simple averaging and subsequently compared to the official data. The correlation between model results and official statistics for cotton and rice crops for the period 2004 to 2009 can be seen in figure 5.23 and figure 5.24. Cotton shows a relatively good correlation (r = 0.69). More variation in cotton yield is visible in the model results as compared to official statistics. Rice only has a moderate correlation (r = 0.50). Figure 5.24 demonstrates that this low correlation coefficient is likely caused by the strong deviation of the model from official statistics in 2006. In general the model for cotton and rice follows the trend of the official data rather well. For cotton this is mostly true for the period 2007 to 2009. There is a general overestimation of official cotton yield by the model and a general underestimation of official rice yield. The exception is rice yield for the

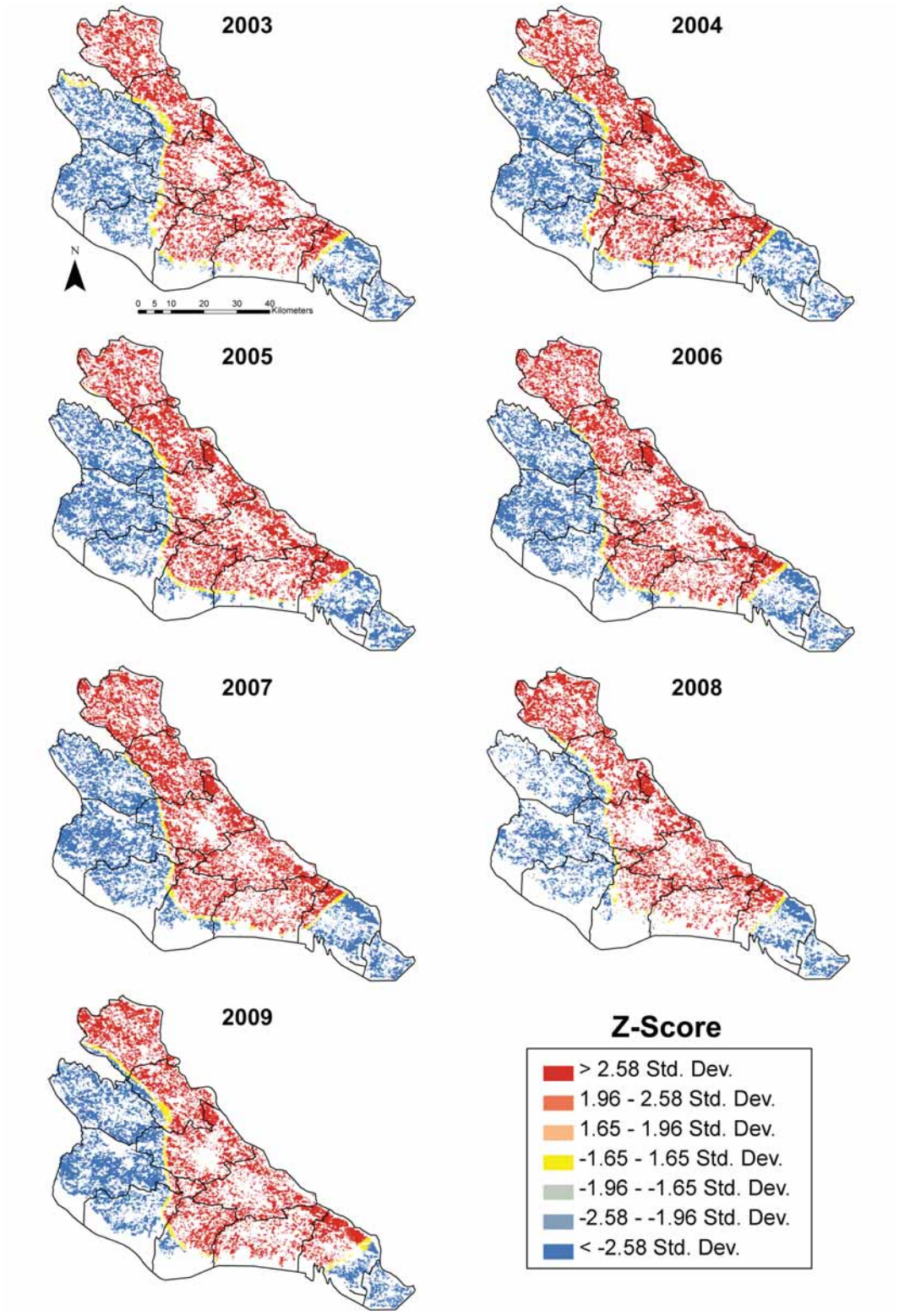

Figure 5.22: Results of the Getis-Ord Gi^* hot spot analysis for the years 2003 to 2009 for cotton yield.

years 2004 and 2005, where model results are very close to official figures. These interpretations are supported by the measures of error that are presented in table 5.12. The bias for cotton ranges from -0.28 to -0.6, and is negative in all cases. In contrast, the bias for rice ranges between 0.01 and 0.87, and is positive in all cases. The RMSE ranges from 0.40 to 0.67 for cotton and from 0.68 to 1.13 for rice. Consequently the PE ranges from 10.5 % to 23.8 % for cotton and from 2.48 % to -19.40 % for rice.

In the next step, the model was evaluated at the Rayon level. Maps of the correlation coefficient between model and official data at this level are shown in figure 5.25. Overall the correlation coefficients are highly variable from Rayon to Rayon. For cotton, the correlation coefficient ranges from -0.47 to 0.91. For rice, the range is from -0.83 to 0.93. The figure also shows an interesting pattern of high and low correlations for both crops. The three Rayons with the highest values for cotton (Kushkupir, Khiva and Yangiarik) are also the ones that have a medium to strong negative correlation for rice crops. Vice versa, the Rayons with a medium to high correlation for rice (Gurlen, Yangibazar, Urgench and Khonka) only have a medium or even negative correlation for cotton. Only one Rayon (Shovot) shows a high correlation for both crops. The reasons for these opposing correlations are difficult to identify. One reason may be inherent in the official crop statistics used for model evaluation, whose accuracy cannot be determined. Another reason could be the fact that there is very little rice area in the Rayons with a low or negative correlation. Yet how this fact potentially influences model results remains to be investigated. The variability of r is further illustrated by figure 5.26, which shows examples of Rayons with high or low correlation coefficients, respectively. The figure also illustrates that the model not always underestimates official statistics. This assumption is backed by the measures of error at Rayon level presented in table 5.13. While model estimations for cotton result in a continuous negative bias (overestimation), only seven out of ten Rayons show a positive bias for rice (underestimation). For three Rayons (Urganch, Khonka and Khiva), the model actually overestimates official rice yields.

The RMSE is highly variable at the Rayon level, and ranges from 0.15 to 0.96 for cotton, and from 0.26 to 1.51 for rice. The percentage error was also calculated for all Rayons and all years for cotton (figure 5.27) and rice (figure 5.28). In principle, the PE shows similar patterns as the correlation coefficients in figure 5.25. For cotton, the south-western districts are characterized by the lowest errors (usually below 10 %). The districts close to the river have the highest PEs, with a maximum of 43 % in 2005. The patterns for rice are less obvious. Altogether the southern districts, including Shovot, are determined by large negative errors. The negative deviation of the model from official statistics can be as high as -46 % in 2008. In contrast, the highest positive PE for rice is 51 % and also occurs in 2008.

A comparison with published values confirms that the found accuracy of the crop yield model

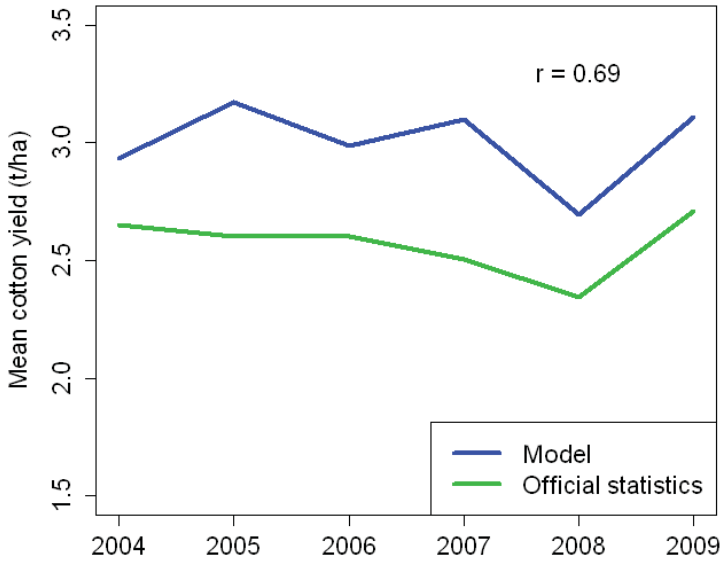

Figure 5.23: Comparison of mean cotton yield derived from model results and official statistics at Oblast level. Note that, due to the small number of observations, the correlation is not significant.

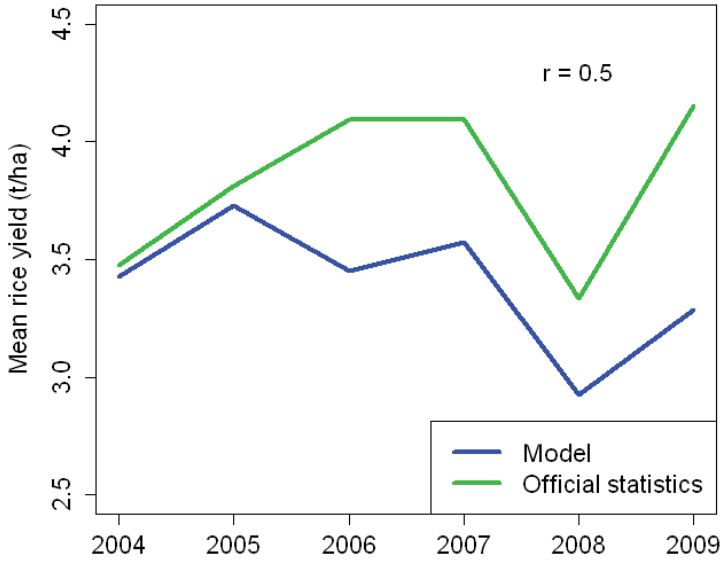

Figure 5.24: Comparison of mean rice yield derived from model results and official statistics at Oblast level. Note that, due to the small number of observations, the correlation is not significant.

Table 5.12: Measures of error for the comparison between model results and official statistics at the Oblast level: Bias, RMSE and mean percentage error (PE, in %).

Cotton	Bias	RMSE	Mean PE (%)
2004	-0.28	0.40	10.5
2005	-0.57	0.66	22.0
2006	-0.39	0.51	14.9
2007	-0.60	0.67	23.8
2008	-0.35	0.40	15.6
2009	-0.40	0.49	14.4
Rice	**Bias**	**RMSE**	**Mean PE (%)**
2004	0.04	0.75	2.5
2005	0.01	0.68	-0.4
2006	0.64	0.98	-14.1
2007	0.52	0.95	-10.4
2008	0.41	1.01	-7.4
2009	0.87	1.13	-19.4

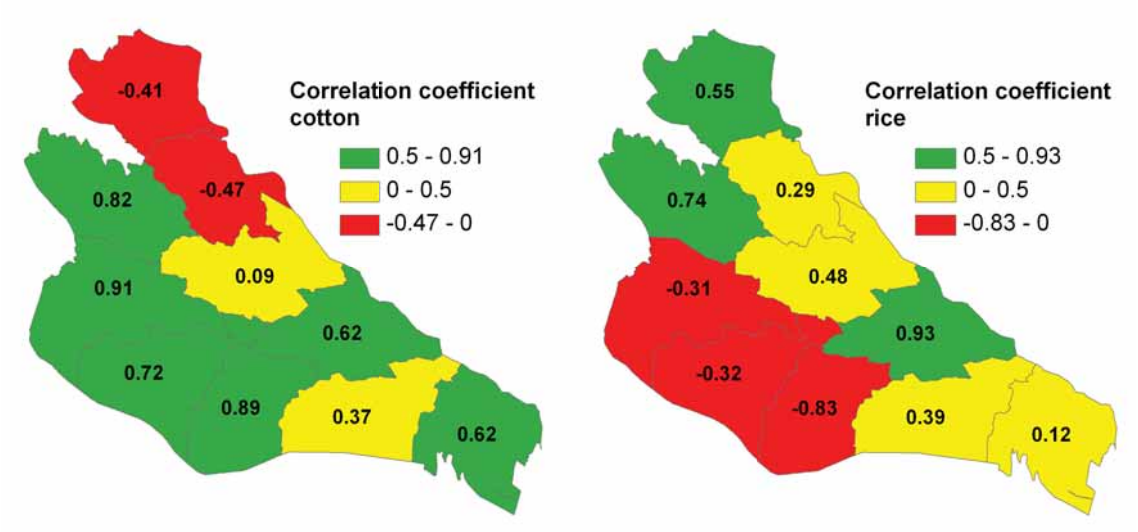

Figure 5.25: Correlation (Pearson) between model results and official statistics at Rayon level for cotton (left) and rice (right).

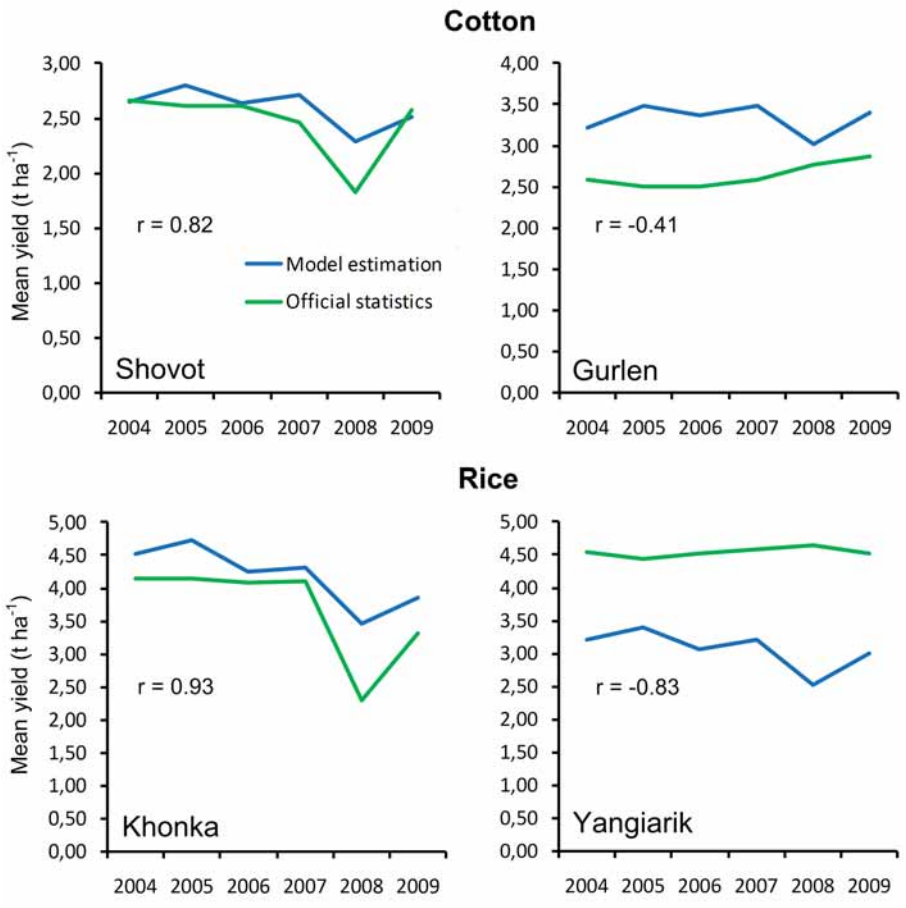

Figure 5.26: Comparison of mean cotton (above) and rice (below) yields from the crop yield model with official statistics for selected Rayons in Khorezm (see also table 5.13).

Table 5.13: Measures of error and the correlation coefficient (see also figure 5.25) for cotton and rice yields at Rayon level. **: significant at the .05 % level, *: significant at the .1 % level (two-tailed test).

	Cotton				Rice			
Rayon	Bias	RMSE	r	PE	Bias	RMSE	r	PE
Bogot	-0.41	0.43	0.37	21.86	1.22	1.34	0.39	-42.19
Gurlen	-0.70	0.74	-0.41	18.50	0.03	0.45	0.55	-16.62
Kushkupir	-0.13	0.15	0.91**	4.35	0.07	0.50	-0.31	-20.27
Urganch	-0.70	0.72	0.09	20.57	-0.11	0.26	0.48	-7.65
Khazarasp	-0.38	0.42	0.62	19.13	1.14	1.48	0.12	-24.35
Khonka	-0.94	0.96	0.62	33.10	-0.51	0.61	0.93**	16.25
Khiva	-0.13	0.16	0.72	5.88	-0.03	0.71	-0.32	-25.07
Shovot	-0.14	0.23	0.82**	-2.40	0.81	0.88	0.74*	-29.54
Yangiarik	-0.36	0.39	0.89**	12.20	1.47	1.51	-0.83**	-33.55
Yangibazar	-0.42	0.51	-0.47	10.53	0.18	0.35	0.29	-11.23

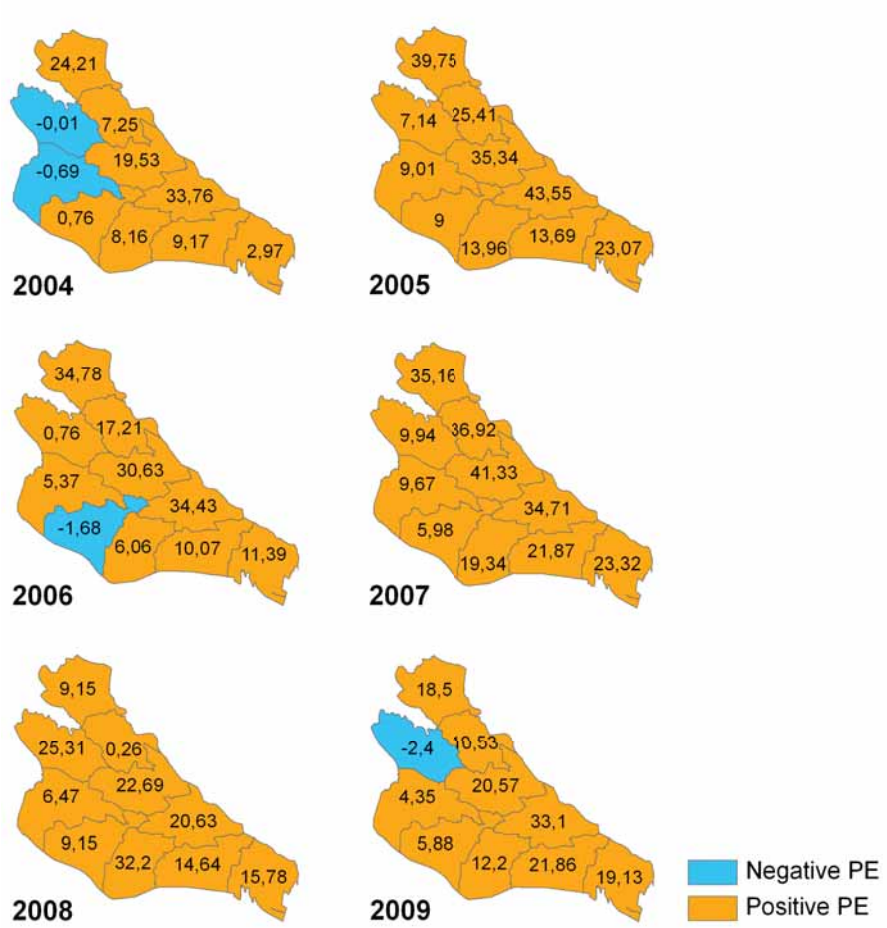

Figure 5.27: Maps of the percentage error (PE) for cotton yield from 2004 to 2009 at Rayon level.

is well within the range of related research. The RMSE of cotton in this study ranged from 0.4 $t \times ha^{-1}$ to 0.67 $t \times ha^{-1}$ at the Oblast level, with a mean RMSE of 0.52 $t \times ha^{-1}$. The PE for cotton in this study ranged from -2.4 % up to 43.6 % for all Rayons and all years, with an average difference of 10.5 % to 23.8 % from 2004 to 2009. In comparison, Shi et al. (2007) reported percentage errors ranging from -22.8 % to 14 % for the year 2002. Average differences between estimated and officially reported cotton yield amounted to 10.6 %. The average Khorezm-wide error calculated by Shi et al. (2007) is comparable to the lower boundary of the errors found in this study, yet there are larger differences between Rayons. While the model of Shi et al. (2007) resulted in relatively large underestimations of reported cotton yields, this study found mostly overestimations of the reported values. The reason is likely to be the different parameterization of both models. Shi et al. (2007) also used temperature and water stress terms to reduce potential biomass growth. The water stress term, however, was derived from a meteorological station in the form of the vapor pressure deficit. As can be seen in Shi et al. (2007), this results in a water stress scalar that is, on average, much lower than the

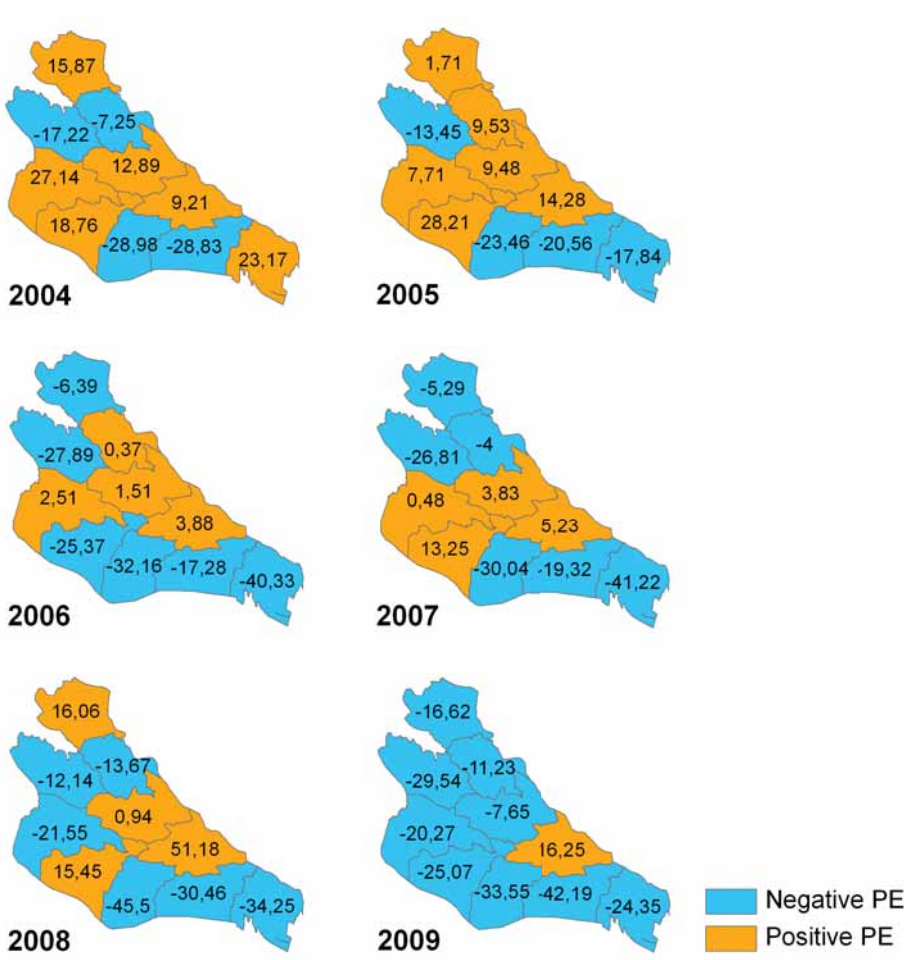

Figure 5.28: Maps of the percentage error (PE) for rice yield from 2004 to 2009 at Rayon level.

stress scalars calculated here (meaning altogether higher water stress). Because one single stress scalar is assumed to be representative for the whole region, this may have caused the found underestimations. Another approach that is comparable to the one presented here is the study of Bastiaanssen & Ali (2003), who calculated an RMSE of 0.55 $t \times ha^{-1}$ for cotton crops in the Indus Basin of Pakistan. Cotton yield in their study area was relatively low, with an average yield of 1.29 $t \times ha^{-1}$. Consequently, the relative RMSE was 49 %. They attributed this high error rate to the fact that cotton fields were mostly small, which resulted in a high percentage of mixed pixels that were used in their yield model based on AVHRR imagery. Another reason was the misclassification of cotton and rice, caused by the similarity of both crops. Furthermore, the relationships between final cotton biomass and actual yield are more complex as compared to other crops, due to the continuous boll production (Sommer et al. 2008). This fact may also have contributed to the error in cotton yield estimation of this study. Rice yield was estimated by Bastiaanssen & Ali (2003) with an RMSE of 0.62 $t \times ha^{-1}$, which corresponds to an error rate of 37 %. The RMSE of the rice crop yield model introduced in this study ranged from

0.68 to 1.13 $t \times ha^{-1}$ at the Oblast level. The mean RMSE was 0.92 $t \times ha^{-1}$. While the lower limit of the RMSE was comparable to the one of Bastiaanssen & Ali (2003), the average was slightly higher. The average PE, however, was lower in this study (-8.2 %). Again, the reason was the relatively low mean values of rice yield in the study of Bastiaanssen & Ali (2003). The amount of error in rice yield estimation found in this study is also comparable to the error described by Boschetti et al. (2011). In the three Italian provinces investigated by the authors, the RMSE ranged from 0.86 $t \times ha^{-1}$ to 0.96 $t \times ha^{-1}$. The mean RMSE calculated in this study is within this range. In contrast to the underestimation of rice yield by the model found in this study, however, Boschetti et al. (2011) reported a general overestimation by their model. This overestimation was attributed to boundary effects and the fact that stress factors were not incorporated in the model.

Minimum yields are close to zero. These numbers seem unlikely, as even marginal cotton or rice fields can still have a yield as high as 1 to 1.5 $t \times ha^{-1}$ (compare minimum yields reported in Shi et al. 2007). The very low minimum yields found by the model can be caused by misclassification of the underlying crop map. For example, it can happen that bare fields are wrongly classified as cotton fields because the field is partially covered by grass in the beginning of the season. If this is the case, final crop yield on these fields will be close to zero at the end of the season as there is no actual crop growth taking place. The same thing can happen to rice fields, for example if a small lake or fish pond is wrongly classified as a rice field. The maximum cotton yields found in this study were relatively large. Analysis of the input data showed that these high values are primarily also likely to be caused by crop misclassification. While the input pixel to the model was classified as cotton, analysis of the corresponding FPAR curve often showed that the underlying crop was in fact a rotation of winter wheat with a summer crop. Consequently, depending on the start of the season, the resulting crop yields were overestimated.

5.5 Relationships between model estimates on RapidEye and MODIS scale

This section presents the results of a comparison between model results at the RapidEye and the MODIS scale. The comparison was conducted to serve two purposes: to allow for a more detailed evaluation of the model at the MODIS scale and to be able to make a statement on model performance for the case of incomplete pixel coverages by crop types. Evaluation of the MODIS model via the results at the RapidEye scale was done under the assumption that the latter was more accurate. Comparison of the MODIS and RapidEye scale for different degrees of crop cover is important for potential application of the model in different areas. As MODIS pixels are rather coarse, the question of the accuracy of the model for areas with smaller field sizes arises.

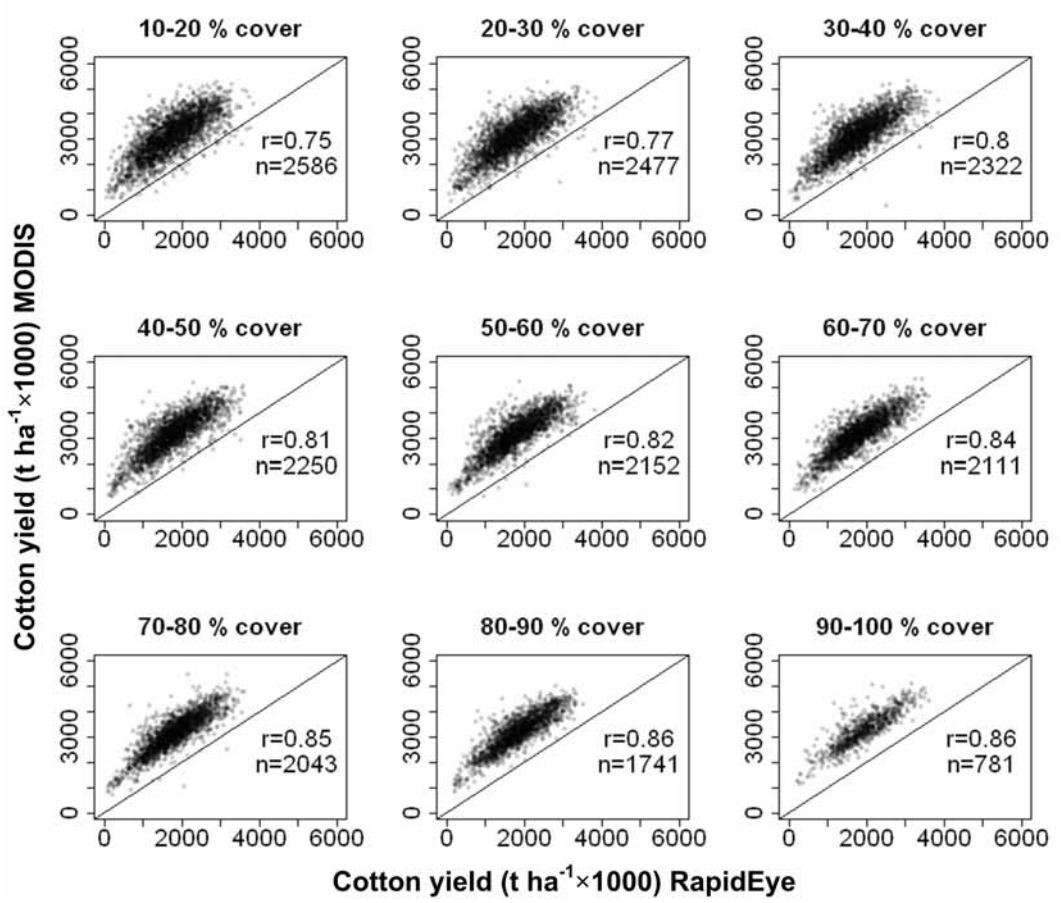

Figure 5.29: Comparison of cotton yield estimated with MODIS (y-axis) and RapidEye (x-axis) data for different degrees of cotton cover.

Figure 5.29 and figure 5.30 visualize the relationships between crop yields derived from MODIS and RapidEye data. Figure 5.29 shows the relationships for cotton, figure 5.30 presents the data for rice. Both figures show a generally very close relation between MODIS and RapidEye crop yields. Correlation coefficients are high, ranging from 0.75 to 0.86 for cotton and from 0.64 to 0.79 for rice. Figure 5.29 clearly shows that MODIS overestimates RapidEye-based cotton yield. This finding is in line with the comparison between MODIS yields and official statistics. This conclusion is also backed by the measures of error in table 5.14. There is a negative bias for cotton in all cases. The average RMSE amounts to 1.4 $t \times ha^{-1}$. The relationships between MODIS and RapidEye for rice also show a good correlation between both datasets (figure 5.30), although the overall correlation is slightly lower as compared to cotton. However, as already indicated in figure 5.30, the bias and RMSE are lower in the case of rice (table 5.14). The bias shows that the MODIS model underestimates RapidEye-based rice yields, with an average bias of 0.52. The average RMSE for rice amounts to 0.82 $t \times ha^{-1}$. Again, there is a similar tendency in the comparison with RapidEye model estimates as in the comparison with official statistics.

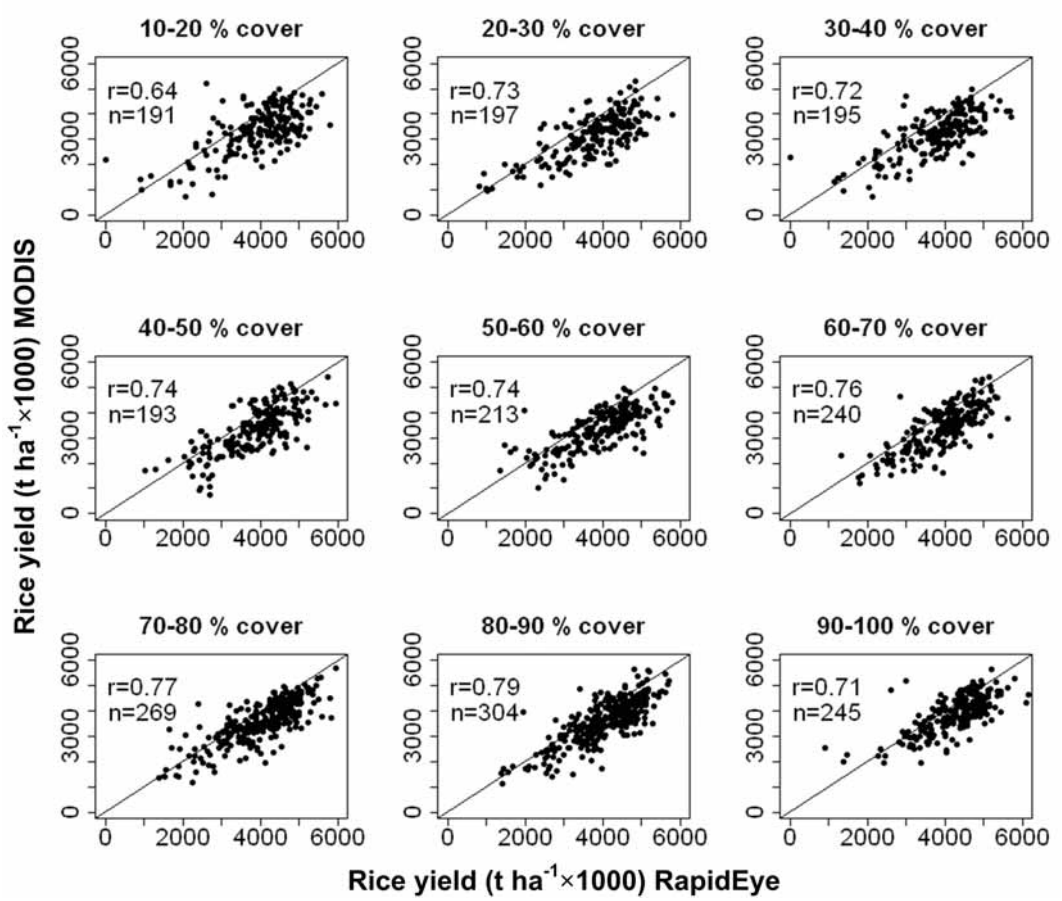

Figure 5.30: Comparison of rice yield estimated with MODIS (y-axis) and RapidEye (x-axis) data for different degrees of rice cover.

The correlation of both model scales was also investigated with regard to the percent crop cover of MODIS pixels, which is also shown in figures 5.29 and 5.30. Both figures show the correlation with regard to the specific crop cover of cotton and rice at the MODIS scale, respectively. The remaining area can consist of all other crop and land cover types. The scatterplots clearly show that the correlation between both model estimates at both scales is independent from the crop cover of MODIS pixels. There is, however, a tendency to higher correlations with increasing crop cover.

Table 5.14: Bias and RMSE for the comparisons between crop yields from MODIS and RapidEye-based models for different degrees of crop cover.

	Bias		RMSE	
Percent cover	Cotton	Rice	Cotton	Rice
10-20	-1.35	0.60	1.46	1.00
20-30	-1.34	0.63	1.44	0.91
30-40	-1.35	0.55	1.42	0.87
40-50	-1.34	0.52	1.42	0.83
50-60	-1.32	0.58	1.39	0.85
60-70	-1.32	0.54	1.38	0.78
70-80	-1.31	0.47	1.36	0.74
80-90	-1.32	0.45	1.37	0.70
90-100	-1.32	0.37	1.37	0.68

6 Marginal land mapping*

6.1 Introduction

Most agricultural areas in arid Central Asia can be classified as marginal in terms of prevailing natural conditions (Cassel-Gintz et al. 1997), and allow cropping practices only under irrigation, fertilizer, and pesticide inputs. Freshwater applications are also needed to cope with soil salinization, which lowers the suitability of land for agricultural production. Agriculture in Khorezm therefore often operates at the margin of feasibility, for example because of high groundwater salinity and tables (Ibrakhimov et al. 2011) or the low water availability (Bekchanov et al. 2010). The risk of yield uncertainties is high due to the region's location in the downstream part of the Amu Darya River, where the water availability is influenced by many external, climate-related and political factors (Manschadi et al. 2010).

The challenge being addressed here is identification of marginal land, i.e. the cropland areas in Khorezm that could benefit from remedial measures or alternative land uses. The identification of marginal land is a prerequisite for implementing alternatives. According to both interviews with farmers and consultations with scientific experts, land constantly producing low yields is seen as an indicator of marginality (Dürbeck 2010), which is in line with the scientific perception (Deal 2006). This unproductive land is the result of multiple factors, including poor soil quality due to salinity, unsound management practices and a lack or untimely supply of irrigation water.

Few studies have used higher-level information from remote sensing in the framework of a GIS-based land suitability assessment, and none have been targeted towards the identification of marginal land. This is a particular challenge given the wide number of factors determining it, as described earlier. Therefore, a framework for a land suitability assessment method based on remote sensing and GIS data for the detection of marginal land in Khorezm is proposed in the following, with a focus on the analysis of the resulting spatial distribution of marginal lands in the region.

*This chapter is based on Dürbeck (2010)

6.2 Data and methods

A Multi Criteria Analysis (MCA) based on GIS and remote sensing data was chosen for detecting marginal lands. This technique belongs to the suite of tools for land suitability assessment (Malczewski 2004). The land suitability assessment is generally defined as 'an appraisal and grouping, or the process of appraisal and grouping, of specific types of land in terms of their absolute or relative suitability for a specific kind of use' (FAO 2007, p. 65) and thus can be used for detecting marginal land that has a low suitability for annual cropping.

6.2.1 Methodology overview

The main principle of a MCA is the evaluation of multiple variables within a weighing scheme that can vary in complexity. In terms of land suitability assessments, the variables can be understood as indicators of the suitability for a specific land use (Malczewski 2004). The weighted overlay concept, as implemented in the weighted overlay tool in ArcGIS (ESRI 2012), was therefore used for the MCA (figure 6.1). In technical terms, the concept of weighted overlay is to combine multiple (raster) datasets that use a common evaluation scale and weigh them according to their importance (equation 6.1):

$$S = \sum_{i=1}^{n} (w_i \times v_i) \tag{6.1}$$

where S is the (land use) suitability, i is the layer number, w_{i} is the weight of layer i (between 0.1 - 1.0), and v_{i} is the coded suitability value of layer i (here between 1 and 5). The weights (w_{i}) show the importance/relevance of a respective data layer (variable) as indicator for marginal land. To achieve a common evaluation scale, the data need to be classified in suitability categories (v_{i}) with, for instance, high values indicating a high probability of occurrence of marginal land. All weighted data layers are added up, and thus the final marginality of land is derived for each land unit (in the case of raster data: pixels). The resulting land-use suitability map depicts the distribution of areas of different marginality. According to Malczewski (1999), an important prerequisite of a successful MCA is to base all processing steps on the preference of the decision makers and on expert knowledge. This applies to the selection of the data, its evaluation, classification, and subsequent weighing. The detailed steps undertaken after expert interviews for land-use suitability evaluation based on marginality are described hereafter (for further information see also Dürbeck 2010).

6.2.2 Input data selection and preparation

The selection of data for the identification of marginal land is decisive for the MCA, and often mirrors a compromise between data demand and data availability. A variety of approaches was used to concretize the MCA following the expert interviews in Khorezm (Dürbeck 2010), which indicated a combination of management-related and environmental factors. The available GIS

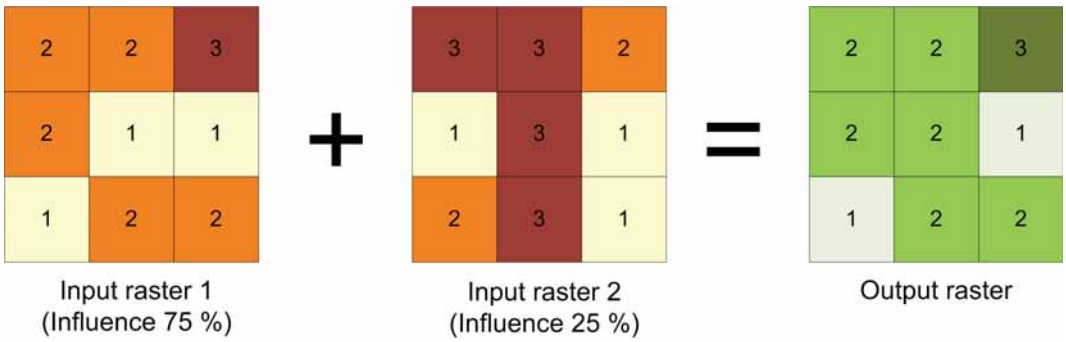

Figure 6.1: Representation of the weighted overlay process in ArcGIS (ESRI 2012, modified).

data sets useful for the marginal land detection allowed elaboration of a comparatively coarse mapping scale only. Complementary information was derived from the MODIS results with a resolution of 250 m pixel size. The coarse MODIS resolution impeded the precise assessment of single fields. Only parts of single fields and a mixture of different crop types and background is captured by the satellite pixels. In a first step, the resulting map is therefore only an indication of marginal land at each pixel.

The common classification of cropland productivity in Uzbekistan is the bonitet, which is the base for the governmental state order for lands of different productive potential. However, according to the opinion of experts, the existing soil bonitet data have to be treated carefully because they are not fully reproducible and often outdated. The information was used in the present study as a general indication of land suitability, but due to its limitations only a small weight was assigned to it.

Remote sensing-based geo-information could significantly improve the quality and amount of the input data, because it is the only reliable data source available at the regional scale. For the period 2000-2009, remote sensing-based annual land-use maps based on Conrad et al. (in review) were selected. These maps comprise the spatial distribution of the following land-use classes: cotton, wheat-rice, wheat-fallow, wheat-other, rice and fallow/unused. Because the focus was on the identification of marginal lands within irrigated areas, those areas classified as unused for cropping throughout the past ten years were masked out.

The frequency of the occurrence of fallow/unused land during the period 2000-2009 served as an indicator of unproductive (i.e., marginal) land. As cotton is the dominant crop in the region, information on (average) cotton yield derived from the 7-year data set (2003-2009) was used as another input for the MCA. The derived crop yields were reclassified and used as the main layer for the MCA (section 6.2.3 and table 6.1).

The expert interviews suggested also including environmental factors in the MCA, such as soil or

groundwater conditions as well as irrigation infrastructure. The capillary rise from the shallow, saline groundwater table enhanced by high rates of evapotranspiration is known to result in soil salinization. Whilst reliable details on soil information for the entire region were missing, data on groundwater depth and salinity were available for 1,797 points throughout the region for the period from 1990 through 2004. The mean values of these point data were spatially interpolated using the Inverse Distance Weighted (IDW) method (Ibrakhimov et al. 2007) and used as additional input factors for the MCA to map the regional distribution of potentially marginal land. In the case of the groundwater table, this means that a low mean table during this period is indicative of insufficient irrigation water supply, because the measurements were generally taken in the months during which agricultural land is irrigated. This explains the classification in table 6.1 (see below).

The access to irrigation infrastructure, represented in the density of the irrigation and drainage network and weighed by its potential capacity (taken from the classification as magistral canals or canals of primary, secondary, or tertiary order) was assumed to reflect water availability for irrigation of crops and options to drain elevated water tables, and thus to reduce the soil salinization. Vector data on irrigation and drainage channels compiled from regional maps from 1960 were integrated. These data were updated using partly available cadastre maps from 2001-2006, and eventually refined using high resolution SPOT images obtained in 2006 (SPOT 2013). The channel capacity was described by its category. Finally, all available vector data were converted to raster layers, adopting the pixel size of the remote sensing-based inputs. Table 6.1 summarizes the input data for the MCA.

6.2.3 Reclassification and weighing of data layers

The data compilation was followed by the classification of the data layer values according to suitability classes and a subsequent weighing of the data layers (table 6.1). Reclassification was achieved by grouping the data layer values and assigning new values ranging between 1 and 5. In the following, the 1-rated conditions are referred to as 'favorable' and the 5-rated as 'unfavorable' for cropping, i.e., the higher the ranking value, the higher the land marginality. The subsequent weighing (in percentage) of the data layers was conducted in collaboration with local experts, and reflects opinions on the importance of any particular layer for the classification of marginal land levels (Dürbeck 2010). All weights summed up to the value 1, which is a prerequisite of the GIS tool. The processed data finally formed the input for the weighted overlay analysis in ArcGIS, and marginality was calculated according to Malczewski (2004) (see section 6.2.1). This resulted in a floating value that ranged between 1 and 5. Next, the values were rounded to the nearest integer to finally obtain a five-class layer, which represented five different degrees of marginality: 'not marginal' (class 1), 'slightly marginal' (class 2), 'moderately marginal' (class 3), 'marginal' (class 4), and 'highly marginal' (class 5).

Table 6.1: Data layers, data ranges, classified values and weights used for the weighted overlay analysis in ArcGIS. * Natural Breaks: This algorithm is implemented in ArcGIS and groups variables according to breaks inherent in the data by maximizing the difference between a given number of classes (ESRI 2012).

Data layer	Data range	Classification	Weight (%)
Cotton yield 2003-2009 ($t \times ha^{-1}$)	0 - 5.6	Natural breaks*	30
Occurrence of fallow/unused land during 2000-2009	0 - 10	0 - 2 = 1 3 - 4 = 2 5 - 6 = 3 7 - 8 = 4 9 - 10 = 5	20
Canal density ($km \times km^{-3}$)	0 - 3.32	Natural breaks*	15
Collector density ($km \times km^{-3}$)	0 - 1.79	Natural breaks*	10
Groundwater depth (m)	0 - 3	$\leq 0.5 = 1$ 0.5 - 1 = 2 1 - 1.5 = 3 1.5 - 2 = 4 2 - 3 = 5	10
Groundwater salinity ($g \times l^{-1}$)	0 - > 4	$\leq 0.5 = 1$ 0.5 - 1.5 = 2 1.5 - 2 = 3 2 - 4 = 4 $> 4 = 5$	10
Soil bonitet	0 - 100	81 - 100 = 1 61 - 80 = 2 41 - 60 = 4 $< 40 = 5$	5

6.2.4 Evaluation of results

Field surveys in 2010 were conducted in four WCAs and consisted of interviews with local experts, farmers and land users, who pointed out locations that they perceived as marginal. These land areas were subsequently mapped and compared with the MCA findings. Marginality of land was calculated within a pixel size of 250 m using the MCA, which rendered validation challenging due to the described limitations. To be able to compare the results of the pixel-based MCA with the field data, the boundaries of the agricultural fields (described in section 4.2.1.3) in the four study WCAs were intersected with the results of the MCA. The average marginality was calculated for each field, and a value higher 1.6 was defined as marginal. Fields correctly identified by the method were subsequently evaluated.

6.3 Results and discussion

The comparison of the local perception and findings of the MCA show that the general tendencies of marginality were, with an accuracy of around 64.4 % (see table 6.2), well captured by the MCA. An example of this comparison is also given in figure 6.2. The accuracy for the different WCAs ranged from 47.8 to 82.5 %. However, the comparison between model results and farmer information also revealed that in addition to the marginal areas indicated by farmers, more areas were characterized as being marginal by the MCA. In fact this could affect up to 61.2 % of all fields in a WCA, although the lower end was 14.5 %. The reasons for the overestimation of the MCA have to be identified by further research. The overarching findings nevertheless show that the MCA approach can be efficient in a rapid assessment of land marginality for cropping practices over larger areas.

Table 6.2: Field-based evaluation of the MCA. Mapped marginal fields were compared to fields identified by the MCA.

WCA name	No. of mapped marginal fields	No. (percent) of fields correctly identified	No. (percent) of fields identified as marginal by the MCA but not mapped as marginal	Total no. of fields
Amirkum	126	82 (65.1)	203 (38.5)	527
Ashirmat	80	66 (82.5)	401 (61.2)	655
Ayran Kul	42	27 (64.3)	316 (49.5)	638
Koramon	92	44 (47.8)	75 (14.5)	518
All	340	219 (64.4)	995 (42.6)	2338

The following results correspond to a total irrigated area of 301,117 ha, and were calculated using the medium resolution MODIS data (from 2003 to 2009). Due to the relatively small field sizes in Khorezm (as compared to the pixel size of MODIS), the results from MODIS tend to overestimate the cropped area. Yet, although the estimated size differs from the official size of 270,000 ha, it is still useful for analyzing the regional distribution of marginal land and trends thereof because the assessment is based on repeatedly measured objective data.

Altogether, 9,767 ha in Khorezm (3.3 % of total irrigated land) were classified as 'slightly marginal'. The classes 'moderately marginal' and 'marginal' accounted for 72,806.9 ha (24.4 %) and 5,253.8 ha (1.8 %), respectively. The class 'highly marginal' only covered 10.7 ha of irrigated land in Khorezm, which is less than 0.01 %. The numbers illustrate that marginal land in Khorezm is mostly 'moderately marginal'. Within the irrigation system of the Khorezm region (the area irrigated between 2003 and 2009), 87,838.3 ha (29.4 %) of marginal land were identi-

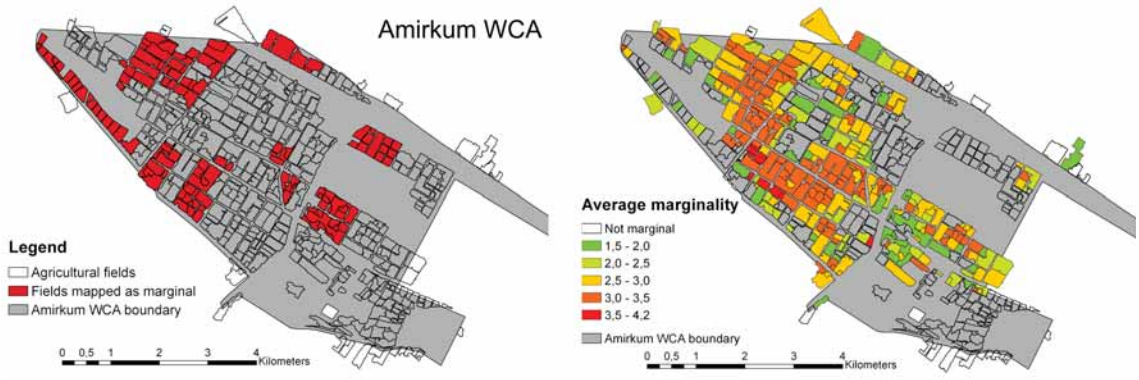

Figure 6.2: Comparison of agricultural fields mapped as being marginal (left) with calculated average marginality (right) for the WCA 'Amirkum'.

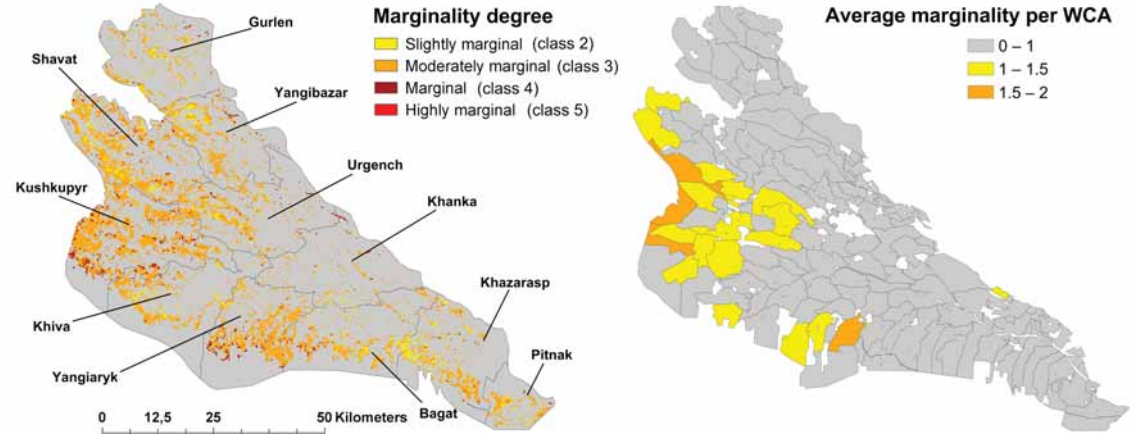

Figure 6.3: Spatial distribution of marginal land in the Khorezm region. Left: Marginality degree at the pixel scale; grey areas indicate land that is not marginal or does not represent agriculture (class 1). Right: average marginality per WCA relative to the total irrigated area.

fied, which was unevenly distributed throughout the region (figure 6.3, left) hence the share of marginal lands differed according to district. Marginal conditions occurred mainly at the desert fringes, especially in the western and southern parts of Khorezm. However, smaller patches of marginality were also detected in the center of the irrigation system.

Figure 6.3 (right) shows the average marginality of agricultural land per WCA. It principally exhibits a similar spatial distribution to that mentioned above, with some noteworthy differences. Due to the fact that the average marginality in figure 6.3 (right) is in relation to the total irrigated area per WCA, the WCAs affected by marginal land are fewer than figure 6.3 (left) might suggest. Still, this illustration can help in spatial planning, because WCAs with a higher average marginality of agricultural land can be viewed as potential 'risk areas', particularly in water-scarce years, thus calling for adjustment of the current management practices. Consequently,

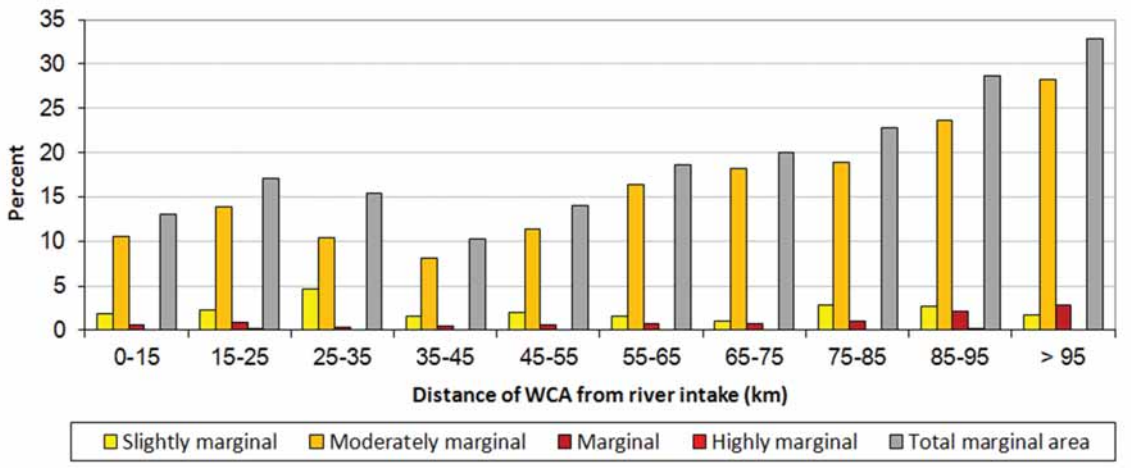

Figure 6.4: Distribution of marginal land, depending on distance to points of water intake from the Amu Darya river.

the identified areas can be prioritized in further investigations by taking additional information into account such as the total irrigated area per WCA. For example, if a high marginality is observed over a large irrigated area, the corresponding WCA should be examined more closely. Thus, mapping the land marginality can serve as an input for more complex indicator systems when combined with additional data.

Occurrence patterns indicate a high correlation between the land marginality and the distance to river water intake points (figure 6.4), which is in line with the results of the yield model. The results of the spatial aggregation of the marginality per WCA, grouped according to the distance from canals to the water intake points from the Amu Darya river (Conrad et al. 2007), suggest that marginality is determined by the location within the irrigation system of Khorezm, i.e. the further away from water intake points, the higher the general occurrence of marginal land. However, figure 6.4 also shows that agricultural land with a better water access (often represented by a closer location to the water intakes) can also be affected by marginality: Even in the class that represents the closest distance to intake points, the total marginal area can reach up to 13 %. The presented methodology can consequently be used to locate such areas.

The results presented in figures 6.3 and 6.4 largely correspond to the trends identified by corresponding research in the Khorezm region. For example, the identified districts with the highest share of marginal land (Kushkupir, Shavat, Yangiarik) were also found to be amongst the ones with the lowest average water productivity in the period 2000 to 2007 (Bekchanov et al. 2010). Furthermore, Conrad et al. (2007) showed that those administrative districts were characterized by a lower seasonal evapotranspiration, which was in contrast to the districts of high crop productivity (e.g., Gurlen and Khanka). Finally, Conrad et al. (2007) also postu-

lated that evapotranspiration decreased with the distance to water intake points. This agrees with the land marginality trend revealed by the adapted MCA approach.

How can the above findings on the spatial distribution of marginal land be utilized? One possibility might be to establish tree plantations on marginalized croplands, which could help to support farmers' livelihoods (Lamers et al. 2009). Such plantings can meliorate the soil via bio-drainage, increase fertility and sequestrate carbon (Khamzina et al. 2012, Hbirkou et al. 2011). Although the combined measures could help to establish viable land uses on marginal land in Khorezm, the existing state order presently limits alternative land use options to smaller areas (Bobojonov et al. 2012); this should be taken into account.

7 Conclusions, synthesis and future research directions

Chapters 4 to 6 presented the methodologies employed to answer the research questions of this study, along with the corresponding results and their discussion. The final chapter will present the main conclusions that can be drawn from those topics. Section 7.1 will focus on the scaling of *in situ* measurements to high resolution satellite data. Section 7.2 reflects on the validation and calibration of MODIS FPAR and NDVI products based on the high resolution FPAR maps derived from RapidEye. Afterwards, section 7.3 concludes on remote sensing-based yield modeling for the Khorezm region using RapidEye and MODIS data. One application of the MODIS-based crop yield maps that was presented was the detection of marginal land. The conclusions that can be drawn from the detection of marginal land and its distribution within the Khorezm region are described in section 7.4. The last two sections will be dedicated to a general synthesis of the presented research (section 7.5) and the description of future research that is required for a better understanding of satellite-based yield modeling as well as yield variations in the study region (section 7.6).

7.1 Scaling FPAR from the field to the RapidEye scale

Scaling data from the ground to high resolution satellite images is the first step for calibration and validation of medium resolution satellite data. Numerous studies have shown that the sampling design is the key to deriving biophysical parameters with high accuracy. Consequently, the sampling design implemented for this study was based on international recommendations and proved to be adequate for the given task. Improvements could likely have been achieved by sampling additional cotton and rice fields. Field measurements with a higher temporal frequency could also contribute to improvements. Yet this also means that additional resources are required, which is not always possible under the given circumstances. FPAR measurements with the AccuPAR device were conducted following general recommendations, with special focus on cotton row measurements. Actual FPAR readings were taken by disregarding the soil and canopy reflecting parts of equation 5.9 (chapter 4.2.1.1). Although the error associated with the simplified equation (4.2) is supposed to be less than 0.05 units of PAR, future experiments should incorporate additional measurements of the soil and canopy reflection for the purpose of comparison. Thus the uncertainty resulting from the simplified equation can be quantified.

As indicated by previous research, the up-scaling of the field measurements should be based on image objects rather than single pixels. For the Khorezm region, Ehammer et al. (2010) showed that the correlation between field-based FPAR and RapidEye-based vegetation indices improves when vegetation indices were first aggregated to image objects. For several reasons the most important requirement for this study was the availability of multi-temporal RapidEye data distributed over the growing season. First, the amount of data is necessary to achieve a robust correlation and regression with *in situ* measurements, which in turn has positive effects on the calibration and validation of MODIS data. If only a single or few RapidEye images were used, calibration and validation of MODIS data would be constrained to a specific period of the season. Consequently, results gained from the analyses would only be valid for this specific period, and applying the results to other time steps would be difficult. Second, coverage of the growing season is a prerequisite for the application of the LUE model, which is improved by a high temporal frequency of satellite imagery. For example, if the peak of the growing season, and consequently maximum FPAR, is not captured by the satellite images this can negatively affect the accuracy of the crop yield model. The regionalization of FPAR is most accurate when field measurements are conducted on multiple crop types and when a crop map is available for regionalization. However, the results of this study showed that the regression equations of different crops are comparable. Related research suggests that this is because soil properties (e.g., color) and the amount of background reflectance has a larger influence on the correlation between FPAR and NDVI than the actual crop type. The implications for regional FPAR mapping are that a crop map can improve the quality of the regionalization process, but is not strictly necessary. However, the general relationship between FPAR and satellite-based vegetation indices should always be calibrated for a specific study area, especially if areas differ strongly in environmental conditions (like soil properties). Furthermore, while a crop map may not be strictly necessary for regionalization of FPAR, it is obviously necessary if the next step is to estimate crop yield from this data (for example by assigning the correct harvest index).

7.2 Optimization of regional FPAR information at the 250 m MODIS scale

The high resolution FPAR maps derived from *in situ* and RapidEye measurements were subsequently used for investigating the accuracy of the collection 5 MODIS FPAR product and for calibration of MODIS NDVI data. Due to the results of this investigation, the subsequent crop yield estimation with MODIS time series was implemented with calibrated 250 m data.

With regard to the validation of the MODIS FPAR product (MOD15A2), the RapidEye FPAR data set did not exhibit any bias concerning ground-measured FPAR. The results of the validation of MODIS data show that there is a general overestimation by MODIS FPAR. The overestimation is within the range of most existing studies on the subject, but partly exceeds

the accuracy of 0.12 FPAR units reported by the MODIS Land Team (NASA 2012). The results demonstrate that overestimation of FPAR is primarily not a result of the misclassification of the underlying MODIS land cover map. The analyses point to sub-pixel heterogeneity as the most important source of error, as even the purest pixels were characterized by a large amount of background influence. There are indications that overestimation decreases with increasing crop cover per pixel for single time steps, but further clarification is prevented by a lack of pure pixels in the region. Uncertainties of the MODIS input reflectances probably contributed to the overall error to some degree, but its quantification needs further research. The large variation in sub-pixel crop composition prevents the use of the MODIS FPAR product for crop-specific analyses. Yet the fact that overall levels of the RMSE vary insignificantly means that errors are quantifiable, and that the product can be used for more general applications. The findings show that product validation is an important step prior to any application. Furthermore, sub-pixel heterogeneity has to be taken into account before MODIS data can be used in similar agricultural environments. More research on the performance of the MODIS FPAR product is needed in order to determine whether the results found here also apply to other agricultural regions with varying configurations of the landscape structure.

Following the validation of the 1 km MODIS FPAR product, this study investigated the correlations between high resolution RapidEye-based FPAR and 250 m MODIS NDVI and EVI products for the purpose of calibrating the medium resolution data. The heterogeneity of 250 m data was furthermore evaluated using the field-based crop map (similar to the 1 km MODIS FPAR product). Analysis of the sub-pixel heterogeneity showed that the 250 m pixel scale is more appropriate for crop studies in Khorezm than the 1 km scale, although a large amount of pixels is still mixed. The fact that the higher resolution data is better suited for crop monitoring in Khorezm was also reflected in a direct visual comparison between the datasets (figure 7.1). The 250 m data allows capturing much finer spatial details, and crop-specific applications are possible at this scale. The number of homogeneous pixels can also be increased by aggregating crop types to classes like broadleaf and cereal crops, as the crop-specific regressions showed that they are only slightly influenced by crop type. However, even if the areas of broadleaf and cereal crops are added for each pixel, more than 40 % of the study region still consists of pixels with less than 30 % agricultural cover. The impact of the mixture of different crop types as well as the amount of background signal (soil, water) on the relationship between VIs and FPAR has to be further quantified. Correlations between MODIS vegetation indices and RapidEye FPAR differed between the investigated products. Daily MODIS data has the advantage that it can be directly used in crop yield models based on satellite data. Yet the MOD09GQ product showed the lowest correlations overall, and the varying observation coverage strongly influences the relations between NDVI and FPAR. The use of composite data promises better results. The 8-day and the 16-day MODIS products showed good correlations, with the 8-day NDVI performing slightly better. Investigation of the 16-day product revealed no significant differences

between MODIS NDVI and EVI, with slightly higher correlations for the NDVI. There were no pronounced differences in the crop-specific regression models, but they depended on pixel homogeneity. Due to the fact that the shorter compositing period of the 8-day product is more suited to the highly dynamic crop growth patterns in Khorezm, it was concluded that it is most useful for crop monitoring in the region. Nevertheless, there are obvious disadvantages of a 250 m calibrated FPAR product, compared to the use of the 1 km MODIS FPAR product. The 250 m product itself is only of empirical nature, meaning that the found relationships have to be thoroughly evaluated before they can be extrapolated to other irrigation systems. Nevertheless, given the overall configuration of the study region and the available data, this seems to be the best approach for now.

7.3 Satellite-based crop yield modeling

Satellite-based light use efficiency modeling is a rather novel approach for crop yield prediction. The study at hand investigated the possibilities for application of such a model in the irrigated Khorezm region at two different scales, driving the model with RapidEye and MODIS data. Despite the fact that both model scales were based on a similar formulation of the Monteith approach, there are specific conclusions that can be drawn from each scale.

The major goal of the presented approach at the RapidEye scale was to model crop biomass accumulation and final yield, and thus to show that a LUE model, based on multi-temporal RapidEye imagery unevenly distributed throughout the season, is able to capture cotton and rice phenology and to identify areas of differing crop growth and yield conditions at field scale. The results showed that this is possible with good accuracy. The yield maps at the RapidEye scale clearly show that cotton and rice yield generally decreases with increasing distance from the river, a fact that was already confirmed by Ruecker et al. (2012). The final crop yield map for cotton and rice can be of high value for land and water managers. It can be used to evaluate the past cropping season in terms of water distribution and crop management. It can also hint at marginal areas where cropping needs special caution or could be replaced by alternative land uses. First and foremost, however, the methodology can be used for crop growth monitoring in the Khorezm region of Uzbekistan or similar environments in Central Asia. In light of these applications, the found error is acceptable.

Validation showed that a water stress factor has to be incorporated in the calculations to result in the highest accuracies. Parameterization of water stress must match the environmental conditions of the study area and the biology of the crops of interest. All crop-specific model parameters like the maximum light use efficiency and the harvest index have to be chosen carefully. The simple sensitivity analysis conducted here indicated that inadequate values can have a high negative impact on final accuracy. Consequently, these parameters cannot simply be taken from

literature and directly used in such a model, but have to be evaluated first.

For this study only a limited amount of field data was used. More data, including biomass from within the season, is required for a thorough validation of the model and to test its potential for similar environments. Future studies should therefore focus on validation and quantification of model uncertainties. The impact of image acquisitions (frequency, date) on model estimates also needs further investigation in order to make the approach more robust. Finally, the maximum spatial extent of the approach, which is a function of spatial coverage and concurrent satellite revisits, remains to be determined.

The crop yield model at the MODIS scale showed that it is able to capture spatial and temporal patterns of cotton and rice yield for the years 2003 to 2009. But this was only possible as the medium resolution MODIS data was calibrated with the high resolution RapidEye FPAR dataset. The use of MODIS-based time series of FPAR was much more straightforward compared to the RapidEye model, due to the inherent imaging characteristics of MODIS. The inclusion of crop phenology in the MODIS-based model was necessary because the start and the end of the season for previous years were unknown. The start and end dates of the season for the different years proved to be rather stable, and a comparison with published values revealed that the start of the season can be accurately determined. The same is true for the end of the season for cotton, but for rice this parameter was underestimated. In general, the question of whether or not the phenological parameters were accurately estimated for a specific pixel depended on the quality of the NDVI time series that was used as input. If there is noise in the curves, it is likely that the estimation of SoS and EoS will fail. Yet this applies mostly to SoS and less to EoS. A novelty of the approach taken here was the use of ET_{act} and ET_c for water stress calculation. The methodology to infer ET_c is more accurate than using ET_0 and will help to better adapt LUE models to cropping systems. In general, the water stress parameter indicated no large differences between years. The only exceptions were the years 2008 and 2009. In 2008, the mean water stress was generally higher compared to other years. In 2009, the overall water stress was the lowest of all investigated years. Exceptional high water stress in 2008 can be explained by the low water availability in that year. In general, however, the total amount of water available for irrigation in the Khorezm region seems to have no significant influence on mean water stress. In contrast to water stress, LUE_{act} was more variable over the years. In general, however, this variation was still at a very low level.

Evaluation of the MODIS model proved that crop yield for cotton and rice can be estimated with reasonable accuracy at Oblast and Rayon level. The overestimation of cotton yield can likely be balanced by further improvements of the model parameters. For example, the estimation of PAR seems to have accounted for a larger part of the errors of the LUE model. An improved procedure is required for this parameter. However, as the overestimation of cotton is rather

systematic, evaluation of model results can account for this fact. A similar conclusion can be drawn for rice yield, albeit the patterns are less clear. In contrast to cotton, modeled rice yield underestimates official statistics. The underestimation, however, varies between years. Further investigation is needed to clarify these patterns. Evaluation at the Rayon level showed that the model was very accurate for some Rayons, but less accurate for others. Although it is unlikely that some Rayons are characterized by agricultural phenomena that are not captured by the model, there is still a small likelihood that high accuracies for some Rayons are the product of chance. However, as there is a high correlation between MODIS and RapidEye-based crop yields it can be assumed that official statistics are less reliable in some Rayons. The quality of the official data needs detailed evaluation. Nevertheless, the presented model also requires a more thorough validation for future applicability. Another unresolved issue is the question why the correlation coefficients between model estimates and official statistics at the Rayon level are partly reversed for cotton and rice.

The crop yield maps for the years 2003 to 2009 and the hot spot analysis revealed specific crop yield patterns in the Khorezm region. Independent of the year, and thus general water availability in the region, the southern and eastern parts of the region always present clusters of low crop yields. In contrast, the Rayons close to the Amu Darya represent hot spots of significantly higher crop yields. In years with low water availability, like 2008, this pattern is even more pronounced. There are high yields in a cold spot region and vice versa, but in general this pattern remains stable.

The relationships between RapidEye and MODIS revealed that there is a high correlation between both datasets. While cotton yield at the MODIS scale overestimates the respective RapidEye-based values, the error is much lower for rice. The data additionally shows that the found errors are independent of the percent coverage of crops for MODIS pixels. This is an interesting result because it highlights that, as long as the MODIS pixel is correctly classified, the associated crop yield in $t \times ha^{-1}$ can be accurately estimated. Yet while this allows for accurate crop yield modeling at the regional scale, the calculation of crop production depends on an estimation of crop area for each pixel. Only if both parameters, crop yield and crop area, are correctly estimated can the presented approach be used to monitor regional crop production.

7.4 Detection of marginal land

An approach for mapping marginal land using remote sensing data and geo-information techniques was presented. Evaluated using *in situ* data, the mean accuracy was 64.4 %. Besides this satisfying accuracy, more fields were identified by the model previously not mapped as marginal land. Whether this is due to different interpretations of marginal land or problems with the model has to be further elaborated. Results showed that around 87,838.3 ha, or 29.4 %, of

the irrigated area of the region was characterized by marginal land. The methodology and the resulting maps are an objective basis for the development of alternative land use options, like the introduction of more drought-tolerant crops or tree plantations, and for discussions amongst local stakeholders and scientists focusing on sustainable land management. The present findings indicate that marginal land is mostly concentrated near desert areas, but it is also scattered as patches throughout the region. General regional patterns differ, but the location of the main irrigation channels as well as the distance to the water intake points also seems to play a decisive role. A GIS aggregation allowed identifying WCAs with a comparatively high marginality of agricultural land. Given a rising water scarcity in the region, this spatial information could help to allocate water resources more efficiently, particularly in drought years. The results represent the scale of MODIS data and can only be an indication of the marginality of actual single fields. This scale represents parts of fields or a mixture of crops and background information, which can always lead to an over or underestimation of the 'true' marginality. However, it helps in delineating risk areas that should be prioritized in designing remedial options, and further investigated using satellite data with a higher resolution.

7.5 Synthesis

Information on agriculture in the irrigated lowlands of the Amu Darya delta is scarce, especially spatial information in the form of maps. Crop yield is often the main determinant of the performance of agricultural systems. The availability of spatial crop yield information on a regional scale is necessary for several purposes:

- The amount of crop yield, combined with the overall crop area, is the decisive information for estimation of regional crop production. In turn, this is important for economic assessments.
- Spatial knowledge on regional crop yield distribution allows identifying fields and areas with sub-optimal crop yield. Thus, action can be taken to identify the reasons for low yields and how they can be improved.
- The availability of crop yield maps for multiple years allows for identifying temporal patterns of high and low crop yields within a region.
- A robust methodology for mapping this kind of information would help in future evaluation procedures and would ideally be usable as a means for within-season crop monitoring.

The main objective of this thesis was to present a methodology that can continuously be used to estimate spatially distributed crop yield in the Khorezm region of Uzbekistan. A remote sensing-based model was identified as the ideal tool to achieve this, due to the spatial and temporal availability of the data, its objectiveness and the general lack of high quality information

in the study region. The results of the study showed that light use efficiency modeling based on remote sensing data is a viable way for regional crop yield prediction. The found accuracies were good within the boundaries of related research. Although additional validation and slight modifications to the model are necessary, it can already be used with its constraints in mind. The model itself was practically tailored to the study area by incorporating parameters that represent the prevailing agricultural and environmental conditions. Many existing studies on LUE-based crop yield modeling incorporate different parameters in their models, and it is important that certain parameterizations are not only copied. For example, Lobell et al. (2003) do not incorporate water stress in their models with reference to the irrigation of the crops in their region. Yet in the case at hand, disregarding the water stress factor would have led to large errors because there are obvious problems of regional water distribution and application. Generally lower accuracies for non-irrigated crops, as compared to irrigated crops, were also shown by Báez-González et al. (2002). The authors were also disregarding a water stress factor in their model. These cases confirm that model parameters have to be adapted to the study region.

From a methodological viewpoint, the work carried out contributed several improvements to satellite-based LUE modeling. These improvements included the use of annual crop yield maps in the modeling process, the calibration of FPAR for the study region using *in situ* and high resolution (RapidEye) imagery, the use of 250 m 8-day MODIS data for crop yield modeling, the incorporation of crop-specific water stress in the calculation and the application for multiple years. Most important of all, this study presented the first application of LUE modeling at the field scale based on RapidEye imagery. New generations of satellite sensors, like RapidEye and the future Sentinel-2 sensor (Drusch et al. 2012), will facilitate novel approaches to field-based crop yield studies. Especially the availability of a band in the SWIR region on board Sentinel-2 will greatly improve applications, as it can be used for water stress detection. The improvements with this new kind of high spatial resolution data are also obvious. Figure 7.1 shows a part of the irrigation system of Khorezm with the crop map indicating cotton (green) and rice fields (blue). The black raster represents MODIS pixels with a resolution of 250 m (thin, dotted lines) and 1 km (thick, solid lines). Figure 7.1 clearly stresses the advantages of the presented model for the study region as compared to models based on MODIS imagery. The 1 km scale is too coarse to adequately capture single crop types. This scale is highly heterogeneous and includes multiple crop types as well as reflectance signals from soil, water and settlements. The 250 m scale is more appropriate for the purpose as it is more homogeneous and shows less crop mixture. Yet even on this scale there is mixture that can compromise the model results. Furthermore, single pixels don't represent single crop fields and decisive information can consequently be lost. The field-based approach is, due to the high spatial resolution of RapidEye data, more capable of accurately capturing canopy FPAR development in the region. This nevertheless comes with the disadvantage of a smaller swath width and repetition rate than medium resolution sensors. Yet this problem might be overcome with the appropriate use of processing chains or new sensor

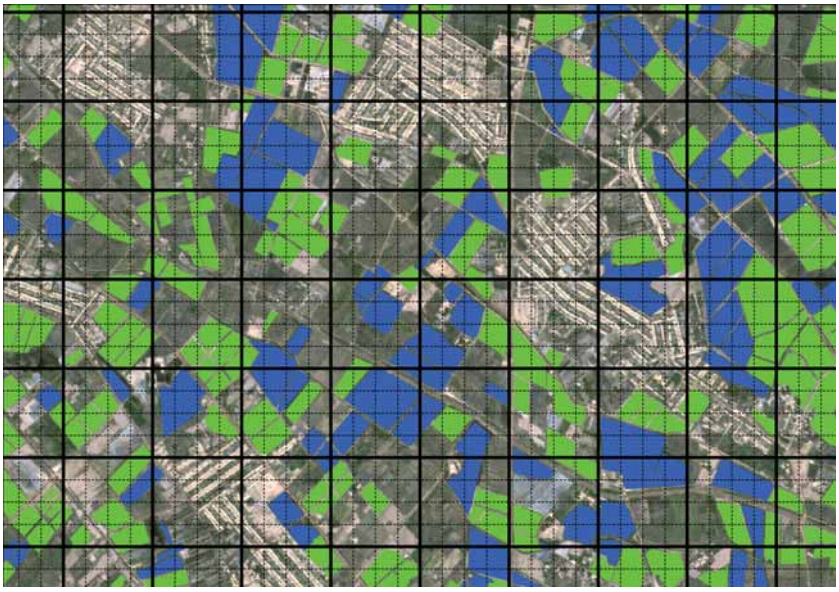

Figure 7.1: A comparison of the RapidEye-based crop map (green: cotton, blue: rice) with MODIS pixels at 250 m (thin dashed lines) and 1 km scale (solid lines).

developments. However, both the RapidEye and the MODIS scale are important for agricultural research. As mentioned above, sensors like RapidEye bring new advantages to the table. But MODIS is still best suited for large-scale investigations, and it additionally allows the view back in time.
The results of the crop yield model at both scales show that there are specific areas in Khorezm that are characterized by comparably lower crop yields over multiple years. Single areas with low crop yields can be explained by several reasons like late sowing, a lack of fertilizers, rainstorms or insufficient water. Yet the large-scale patterns found here are unlikely to be caused by such factors. Although it was not thoroughly investigated in this study, the main reason seems to be the access and large-scale distribution of irrigation water that is responsible for these patterns. One result of these patterns is that there is a large yield gap in the Khorezm region, meaning the difference between lowest and highest crop yields. If this gap is to be closed, future research should investigate the intrinsic reasons for the distribution of crop yields in Khorezm.

A manifestation of repeatedly low crop yields is the occurrence of marginal land. It is a prime example of an application of the developed crop yield model at the MODIS scale. Until now this information was unavailable. Now the information on spatial distribution of marginal land can be used to try to improve the respective land, e.g. by afforestation or by leaving it fallow for a few years. Although this is rather basic information, the data that can be gained by the model developed here can give local authorities a new and better insight into the irrigation system and contribute to an improvement of land and water management in the region.

7.6 Future research directions

The model used to estimate regional crop yield based on RapidEye and MODIS data is in line with previous research on the topic. It was shown that, at both scales, the found accuracy is acceptable and allows for further analysis of the resulting crop yield maps. Despite this, however, there are still open questions and topics that need further investigation. As this study is the first that implemented a LUE model based on multi-temporal RapidEye imagery, this part especially needs further investigation. The following paragraphs summarize the different topics of the study at hand and suggest potential directions for future research.

According to the nature of light use efficiency models, multi-temporal FPAR images are required as the main input. The use of MODIS data for this approach is rather straightforward. RapidEye data, however, requires more attention due to its imaging characteristics. The times series used here adequately covered the growing season 2009. However, it remains to be investigated whether the approach is still feasible in case only few images are available or key stages in crop phenology are not covered by satellite acquisitions. If this is the case, alternative approaches such as presented by Lobell et al. (2003) might be feasible. For most applications, the use of fewer RapidEye images would actually be preferable due to the commercial nature of the data. Besides FPAR, adequate crop maps proved to be another crucial input for the models. Crop maps are mainly used to assign the correct crop-specific parameters to the pixels or fields. Owing to the nature of the remote sensing process, every thematic map has inherent inaccuracies that are evaluated by an accuracy assessment. Obviously, it would be preferable to use crop maps with the highest accuracy possible. There is ongoing research to increase this accuracy (see for example Conrad et al. submitted), but the impact of misclassification on regional yield estimation should be further quantified.

In addition to the input data of the model, the model itself also presents many opportunities for further investigation. One is the formulation of the actual model. Of all the existing studies on crop yield estimation based on LUE models, nearly each one presents a unique version of the original Monteith equation. Of course, this mainly depends on the type of questions that the model is supposed to answer. Some models require parameterization of water stress, others do not. Some models, however, have a more complex formulation because they incorporate more detailed biological processes such as crop respiration and below-ground biomass accumulation. These two exemplary processes were neglected in this study, despite the fact that some authors claim that the incorporation of these processes enhances model accuracy. In the case of crop respiration, it is often only a fixed factor that is applied to convert daily or seasonal GPP to NPP (compare, for example, Brogaard et al. 2005 and Seaquist et al. 2003). It should be investigated whether or not a more complex model formulation actually increases the accuracy of model estimates in the study region. Besides the formulation of the model, the parameters

used in the modeling process also require further investigation. These parameters are mainly the maximum light use efficiency, the harvest index, phenological parameters and water stress. The maximum light use efficiency, as implemented in this study, was taken from existing literature. For future applications, $LUE_{\max}$ should be substituted by values from the study region. It would also be important that these values are based on farmers' fields, and not on experimental treatments. The latter tend to overestimate such parameters, which has a negative impact on model estimates. Another option would be to derive $LUE_{\max}$ directly from remote sensing measurements, an approach that is increasingly investigated (e.g., Sims et al. 2006). Similar research needs apply to the harvest index. Many studies apply literature-based harvest indices to their medium resolution model estimates to derive final crop yield. This procedure seems inaccurate, as H_{i} values reported in the literature are almost exclusively related to field experiments. The application of harvest indices, which were derived by experiment, to medium resolution satellite data is bound to lead to errors as scale influences, and the fact that medium resolution sensors average over a large area, are not accounted for. The dynamic down-scaling of H_{i} in relation to the accumulated water stress over the peak growing season, as adopted in this study, is one option to account for these scale effects. Yet this process also originated from crop models that are applied to field studies. Specific remote sensing-related research is necessary to investigate the scale-dependent behavior of parameters like the harvest index. In comparison to these rather complicated processes, future work towards seasonality in the modeling process is rather straightforward. In this study, the start and end of the growing season was derived by the TIMESAT software and used to constrain the modeling period. Without this constraint, overestimation of estimated crop yield is likely as FPAR (and the NDVI) are mostly greater than zero. Further studies require the involvement of a crop mask in the estimation of phenological parameters and the assignment of separate values for the different TIMESAT parameters for cotton and rice crops. The water stress factor implemented in this study was modified based on existing literature by combining ET_{act} with ET_{c}. This is a rather complicated process, involving extensive processing of satellite imagery and meteorological ground stations. The methods and data are not always available in other regions. Effort should be put into the investigation of alternative approaches to water stress estimation. One such approach is the use of water-sensitive indices like the land surface wetness index (LSWI) that was successfully tested in a crop yield estimation study in India (Patel et al. 2010). This index can also be calculated from MODIS measurements. The substitution of $ET_{\mathrm{act}}/ET_{\mathrm{c}}$ with such an index would greatly simplify the modeling procedure. Finally, it is necessary to investigate the influence of all these parameters, and their respective values, on model estimates. This can for example be achieved with different forms of sensitivity analyses (Cariboni et al. 2007), a simple form of which was already applied here to the parameters of the RapidEye-scale model. A more detailed sensitivity analysis should be conducted targeting all parameters and interdependencies of the crop yield model.

With regard to the results of the crop yield model, further research should be directed towards

the investigation of the spatial and temporal patterns of crop yield as well as their underlying causes. For example, it was shown that there are characteristic patterns of crop yield in the Khorezm region, with high yields clustering near the river and low yields near the desert. But high and low yields can also be found throughout the area. The question of the main determinants for the distribution of crop yields remains. Previous research showed that crop yield correlates for example with soil types and distance to the water intake points (Ruecker et al. 2012), but these factors fail to explain all of the crop yield variability. It is likely that previously disregarded factors such as agricultural practices (fertilization, timing of irrigation, access to pumps etc.) are the causes for a large part of these variations. However, investigation of these factors would require collecting a large amount of data throughout the region, which may not be entirely feasible.

The next question that has to be answered is the question of transferability. Could the model, in its present form, be applied in similar agro-environments in Central Asia? Which parameters need adjustment, and why? And what are the resulting accuracies? These are some of the most important questions, because the comparison of crop yield estimates from different regions in Central Asia would allow taking a big step towards a better understanding of crop yield patterns and variations as well as the underlying causes for Central Asian irrigation systems. Obviously, this approach would also require further validation of the model. More statistical data for evaluation and especially the availability of high quality crop yield data from the field (farmer fields or experimental data) would greatly enhance the confidence one can have in the model estimates.

The presented model, in its current form, can be used to identify spatial and temporal crop yield patterns. Such information was previously non-existent and can help to better understand the irrigation system, for example by trying to raise crop yields on fields and in areas that are characterized by low crop yields over multiple years. With slight modifications, the crop yield model can theoretically also be used to conduct in-season crop yield forecasting. This research would also require more detailed statistical information on crop yields or the collection of field data. To be able to estimate the seasonal crop yield prior to actual harvest would ease the economic planning process, for example by estimating the amount of cotton that can be exported from, or the potential amount of cereals that need to be imported to, the region.

References

Abdullaev, I., De Fraiture, C., Giordano, M., Yakubov, M. & Rasulov, A. (2009): Agricultural Water Use and Trade in Uzbekistan: Situation and Potential Impacts of Market Liberalization. *International Journal of Water Resources Development*, 25(1): 47–63.

Aikman, D. (1989): Potential increase in photosynthetic efficiency from the redistribution of solar radiation in a crop. *Journal of Experimental Botany*, 40(217): 855–864.

Akramkhanov, A., Kuziev, R., Sommer, R., Martius, C., Forkutsa, O. & Massucati, L. (2012): Soils and Soil Ecology in Khorezm. In: C. Martius, I. Rudenko, J.P.A. Lamers & P.L.G. Vlek (Eds.), *Cotton, Water, Salts and Soums - Economic and Ecological Restructuring in Khorezm, Uzbekistan*, 37–58. Springer, Berlin.

Allen, R., Pereira, L., Raes, D. & Smith, M. (1998): Crop evapotranspiration - Guidelines for computing crop water requirements. Tech. rep., FAO, Rome.

Allen, R., Tasumi, M. & Trezza, R. (2007): Satellite-based energy balance for mapping evapotranspiration with internalized calibration (METRIC)-Model. *Journal of Irrigation and Drainage Engineering-ASCE*, 133(4): 380–394.

Arkebauer, T., Weiss, A., Sinclair, T.R. & Blum, A. (1994): In defense of radiation use efficiency: a response to Demetriades-Shah et al.(1992). *Agricultural and Forest Meteorology*, 68(3-4): 221–227.

Asrar, G., Myneni, R. & Choudhury, B. (1992): Spatial heterogeneity in vegetation canopies and remote sensing of absorbed photosynthetically active radiation: a modeling study. *Remote Sensing of Environment*, 41(2-3): 85–103.

Awan, U.K., Ibrakhimov, M., Tischbein, B., Kamalov, P., Martius, C. & Lamers, J.P. (2011): Improving irrigation water operation in the lower reaches of the Amu Darya River - current status and suggestions. *Irrigation and Drainage*, 60(5): 600–612.

Baccini, A., Friedl, M., Woodcock, C.E. & Zhu, Z. (2007): Scaling field data to calibrate and validate moderate spatial resolution remote sensing models. *Photogrammetric Engeneering & Remote Sensing*, 73(8): 945–954.

Báez-González, A.D., Chen, P., Tiscareño López, M. & Srinivasan, R. (2002): Using satellite and field data with crop growth modeling to monitor and estimate corn yield in Mexico. *Crop science*, 42(6): 1943–1949.

Bandyopadhyay, S., Jaiswal, R.K., Hegde, V.S. & Jayaraman, V. (2009): Assessment of land suitability potentials for agriculture using a remote sensing and GIS based approach. *International Journal of Remote Sensing*, 30(4): 879–895.

Baret, F. & Guyot, G. (1991): Potentials and limits of vegetation indices for LAI and APAR assessment. *Remote Sensing of Environment*, 35(2-3): 161–173.

Bastiaanssen, W.G.M. & Ali, S. (2003): A new crop yield forecasting model based on satellite measurements applied across the Indus Basin, Pakistan. *Agriculture, Ecosystems & Environment*, 94: 321–340.

Bastiaanssen, W.G.M., Molden, D.J. & Makin, I.W. (2000): Remote sensing for irrigated agriculture: examples from research and possible applications. *Agricultural Water Management*, 46: 137–155.

Bastiaanssen, W., Menenti, M., Feddes, R. & Holtslag, A. (1998): A remote sensing surface energy balance algorithm for land (SEBAL) 1. Formulation. *Journal of Hydrology*, 212-213: 198–212.

Battisti, D.S. & Naylor, R.L. (2009): Historical warnings of future food insecurity with unprecedented seasonal heat. *Science*, 323: 240–244.

Becker-Reshef, I., Vermote, E., Lindeman, M. & Justice, C. (2010): A generalized regression-based model for forecasting winter wheat yields in Kansas and Ukraine using MODIS data. *Remote Sensing of Environment*, 114(6): 1312–1323.

Bekchanov, M., Karimov, A. & Lamers, J. (2010): Impact of water availability on land and water productivity: a temporal and spatial analysis of the case study region Khorezm, Uzbekistan. *Water*, 2(3): 668–684.

Bernauer, T. & Siegfried, T. (2012): Climate change and international water conflict in Central Asia. *Journal of Peace Research*, 49(1): 227–239.

Bloch, P.C. (2002): Agrarian reform in Uzbekistan and other Central Asian countries. Tech. Rep. 49, Land Tenure Center-University of Wisconsin-Madison, Madison.

Bobojonov, I., Lamers, J.P.A., Djanibekov, N., Ibragimov, N., Begdullaeva, T., Ergashev, A.K., Kienzler, K., Eshchanov, R., Rakhimov, A., Ruzimov, J. & Martius, C. (2012): Crop Diversification in Support of Sustainable Agriculture in Khorezm. In: C. Martius, I. Rudenko, J.P.A. Lamers & P.L.G. Vlek (Eds.), *Cotton, Water, Salts and Soums - Economic and Ecological Restructuring in Khorezm, Uzbekistan*, 219–233. Springer, Berlin.

Bos, M., Burton, M. & Molden, D. (2005): *Irrigation and drainage performance assessment - practical guidelines*. Cromwell Press, Trowbridge, 176 pages.

Boschetti, M., Stroppiana, D., Brivio, P.A. & Bocchi, S. (2009): Multi-year monitoring of rice crop phenology through time series analysis of MODIS images. *International Journal of Remote Sensing*, 30(18): 4643–4662.

Boschetti, M., Stroppiana, D., Confalonieri, R., Brivio, P.A., Crema, A. & Bocchi, S. (2011): Estimation of rice production at regional scale with a Light Use Efficiency model and MODIS time series. *Italian Journal of Remote Sensing*, 43(3): 63–81.

Bouman, B.A.M., Kropff, M.J., Tuong, T.P., Wopereis, M.C.S., ten Berge, H.F.M. & van Laar, H.H. (2001): *ORYZA2000: modeling lowland rice*. International Rice Research Institute, Wageningen University and Research Centre, Los Banos (Philippines), Wageningen, 235 pages.

Box, E.O., Holben, B.N. & Kalb, V. (1989): Accuracy of the AVHRR Vegetation Index as a predictor of biomass, primary productivity and net CO_2 flux. *Vegetatio*, 80: 71–89.

Bradford, J.B., Hicke, J.A. & Lauenroth, W.K. (2005): The relative importance of light-use efficiency modifications from environmental conditions and cultivation for estimation of large-scale net primary productivity. *Remote Sensing of Environment*, 96(2): 246–255.

Breckle, S.W. & Geldyeva, G.V. (2012): Dynamics of the Aral Sea in Geological and Historical Times. In: S.W. Breckle, W. Wucherer, L.A. Dimeyeva & N.P. Ogar (Eds.), *Aralkum - a Man-Made Desert*, 13–36. Springer, Berlin.

Breckle, S.W. & Wucherer, W. (2012): Climatic Conditions in the Aralkum. In: S.W. Breckle, W. Wucherer, L.A. Dimeyeva & N.P. Ogar (Eds.), *Aralkum - a Man-Made Desert*, 49–72. Springer, Berlin.

Breiman, L. (2001): Random Forests. *Machine Learning*, (45): 5–32.

Breiman, L., Friedman, J., Olshen, R. & Stone, C. (1984): *Classification and regression trees*. CRC Press, New York, 368 pages.

Brogaard, S., Runnström, M. & Seaquist, J.W. (2005): Primary production of Inner Mongolia, China, between 1982 and 1999 estimated by a satellite data-driven light use efficiency model. *Global and Planetary Change*, 45(4): 313–332.

Campbell, C.S., Heilman, J.L., McInnes, K.J., Wilson, L.T., Medley, J.C., Wu, G. & Cobos, D.R. (2001): Seasonal variation in radiation use efficiency of irrigated rice. *Agricultural and Forest Meteorology*, 110: 45–54.

Campbell, G.S. & Norman, J.M. (1998): *An Introduction to Environmental Biophysics*. Springer, Berlin, 2 ed., 286 pages.

Cariboni, J., Gatelli, D., Liska, R. & Saltelli, a. (2007): The role of sensitivity analysis in ecological modelling. *Ecological Modelling*, 203(1-2): 167–182.

Cassel-Gintz, M., Lüdeke, M., Petschel-Held, G., Reusswig, F., Plöchl, M., Lammel, G. & Schellnhuber, H. (1997): Fuzzy logic based global assessment of the marginality of agricultural land use. *Climate Research*, 8(2): 135–150.

CAWATER-INFO (2012): Central Asian Water Info. URL: `http://www.cawater-info.net/`. Last accessed: December 2012.

Chapin, F.S., Woodwell, G.M., Randerson, J.T., Rastetter, E.B., Lovett, G.M., Baldocchi, D.D., Clark, D.A., Harmon, M.E., Schimel, D.S., Valentini, R., Wirth, C., Aber, J.D., Cole, J.J., Goulden, M.L., Harden, J.W., Heimann, M., Howarth, R.W., Matson, P.A., McGuire, A.D., Melillo, J.M., Mooney, H.A., Neff, J.C., Houghton, R.A., Pace, M.L., Ryan, M.G., Running, S.W., Sala, O.E., Schlesinger, W.H. & Schulze, E.D. (2006): Reconciling Carbon-cycle Concepts, Terminology, and Methods. *Ecosystems*, 9(7): 1041–1050.

Chen, F., Weber, K., Anderson, J. & Gokhale, B. (2010): Comparison of MODIS fPAR products with Landsat-5 TM-derived fPAR over semiarid rangelands of Idaho. *GIScience & Remote Sensing*, 47(3): 360–378.

Chen, P.Y., Fedosejevs, G., Tiscareño López, M. & Arnold, J. (2006): Assessment of MODIS-EVI, MODIS-NDVI and VEGETATION-NDVI composite data using agricultural measurements: an example at corn fields in western Mexico. *Environmental monitoring and assessment*, 119: 69–82.

Chub, V.E. (2007): *Climate change and its impact on hydro-meteorological processes, agro-climatic and water resources of the Republic of Uzbekistan*. Centre for Hydro-Meteorological Service under Cabinet of Ministers of the Republic of Uzbekistan, Tashkent, 141 pages.

Cohen, W.B., Maiersperger, T.K., Gower, S.T. & Turner, D.P. (2003): An improved strategy for regression of biophysical variables and Landsat ETM+ data. *Remote Sensing of Environment*, 84: 561–571.

Conrad, C., Dech, S., Dubovyk, O., Fritsch, S., Klein, D., Schorcht, G. & Zeidler, J. (submitted): Utilizing crop phenology from RapidEye time series for per-field classifications in large-scale irrigation systems of Central Asia (International Journal of Applied Earth Observation and Geoinformation).

Conrad, C., Dech, S.W., Hafeez, M., Lamers, J., Martius, C. & Strunz, G. (2007): Mapping and assessing water use in a Central Asian irrigation system by utilizing MODIS remote sensing products. *Irrigation and Drainage Systems*, 21(3-4): 197–218.

Conrad, C., Ibragimov, N., Lamers, J. & Martius, C. (in review): Satellite-based analysis of crop rotations in irrigated cotton production systems in Central Asia: How sustainable is post-Soviet land use? (Global and Planetary Change).

Conrad, C., Machwitz, M., Schorcht, G., Löw, F., Fritsch, S. & Dech, S. (2011): Potentials of RapidEye time series for improved classification of crop rotations in heterogenous agricultural landscapes: experiences from irrigation systems in Central Asia. In: *Proc. SPIE 8174*. Prague.

Conrad, C., Schorcht, G., Tischbein, B., Davletov, S., Sultonov, M. & Lamers, J.P.A. (2012): Agro-Meteorological Trends of Recent Climate Development in Khorezm and Implications for Crop Production. In: C. Martius, I. Rudenko, J.P.A. Lamers & P.L.G. Vlek (Eds.), *Cotton, Water, Salts and Soums - Economic and Ecological Restructuring in Khorezm, Uzbekistan*, 25–36. Springer, Berlin.

Conrad, C. (2006): *Fernerkundungsbasierte Modellierung und hydrologische Messungen zur Analyse und Bewertung der landwirtschaftlichen Wassernutzung in der Region Khorezm (Usbekistan)*. Ph.D. thesis, University of Wuerzburg.

Conrad, C., Fritsch, S., Zeidler, J., Rücker, G. & Dech, S. (2010): Per-field irrigated crop classification in arid Central Asia using SPOT and ASTER data. *Remote Sensing*, 2: 1035–1056.

Constable, G.A. & Hearn, A.B. (1981): Irrigation for Crops in a Sub-Humid Environment - VI. Effect of Irrigation and Nitrogen Fertilizer on Growth, Yield and Quality of Cotton. *Irrigation Science*, 3: 17–28.

Cramer, W. & Field, C.B. (1999): Comparing global models of terrestrial net primary productivity (NPP): introduction. *Global Change Biology*, 5: 1–2.

Cramer, W., Kicklighter, D., Bondeau, A., Moore III, B., Churkina, G., Nemry, B., Ruimy, A., Schloss, A. & the participants of the Potsdam NPP model intercomparison (1999): Comparing global models of terrestrial net primary productivity (NPP): overview and key results. *Global Change Biology*, 5: 1–15.

Dalezios, N.R., Domenikiotis, C., Loukas, A., Tzortzios, S.T. & Kalaitzidis, C. (2001): Cotton yield estimation based on NOAA/AVHRR produced NDVI. *Physics and Chemistry of the Earth (B)*, 26(3): 247–251.

de Wit, C.T. (1982): Simulation of living systems. In: F.W.T. Penning de Vries & H.H. van Laar (Eds.), *Simulation of plant growth and crop production*, 3–8. PUDOC, Wageningen.

Deal, J. (2006): The relationship between economically and environmentally marginal land. In: *American Agricultural Economics Association Annual Meeting*, 34. Long Beach.

Decagon Devices Inc. (2010): AccuPAR PAR/LAI ceptometer model LP-80 Operator's Manual Version 10.

Delécolle, R., Maas, S., Guérif, M. & Baret, F. (1992): Remote sensing and crop production models: present trends. *ISPRS Journal of Photogrammetry and Remote Sensing*, 47: 145–161.

Demetriades-Shah, T.H., Fuchs, M., Kanemasu, E.T. & Flitcroft, I. (1992): A note of caution concerning the relationship between cumulated intercepted solar radiation and crop growth. *Agricultural and Forest Meteorology*, 58(3-4): 193–207.

Demetriades-Shah, T., Fuchs, M., Kanemasu, E. & Flitcroft, I. (1994): Further discussions on the relationship between cumulated intercepted solar radiation and crop growth. *Agricultural and Forest Meteorology*, 68(3-4): 231–242.

Devkota, K.P. (2011): *Resource utilization and sustainability of conservation-based rice-wheat cropping systems in Central Asia.* Ph.D. thesis, Rheinische Friedrich-Wilhelms-Universität zu Bonn.

Djumaniyazova, Y., Sommer, R., Ibragimov, N., Ruzimov, J., Lamers, J. & Vlek, P. (2010): Simulating water use and N response of winter wheat in the irrigated floodplains of Northwest Uzbekistan. *Field Crops Research*, 116(3): 239–251.

Dorian, J.P., Abbasovich, U.T., Tonkopy, M.S., Jumabekovich, O.A. & Daxiong, Q. (1999): Energy in central Asia and northwest China: major trends and opportunities for regional cooperation. *Energy Policy*, 27: 281–297.

Dorigo, W.A., Zurita-Milla, R., de Wit, A.J.W., Brazile, J., Singh, R. & Schaepman, M.E. (2007): A review on reflective remote sensing and data assimilation techniques for enhanced agroecosystem modeling. *International Journal of Applied Earth Observation and Geoinformation*, 9(2): 165–193.

Dougherty, T.C., Hall, A.W. & Wallingford, H.R. (1995): Environmental Impact Assessmentf of Irrigation and Drainage Projects - FAO Irrigation and Drainage Paper 53. Tech. rep., FAO, Rome.

Drusch, M., Del Bello, U., Carlier, S., Colin, O., Fernandez, V., Gascon, F., Hoersch, B., Isola, C., Laberinti, P., Martimort, P., Meygret, a., Spoto, F., Sy, O., Marchese, F. & Bargellini, P. (2012): Sentinel-2: ESA's Optical High-Resolution Mission for GMES Operational Services. *Remote Sensing of Environment*, 120: 25–36.

Dürbeck, T. (2010): *Land Suitability Analyse und marginales Land in der Bewässerungsregion Khorezm, Usbekistan.* Magisterarbeit, Würzburg.

Ehammer, A. (2011): *Statistical derivation and regional mapping of fPAR and LAI for irrigated cotton and rice using multi-temporal RapidEye data and ground measurements - A case study for the Khorezm province, Uzbekistan.* Master thesis, University of Innsbruck.

Ehammer, A., Fritsch, S., Conrad, C., Lamers, J. & Dech, S. (2010): Statistical derivation of fPAR and LAI for irrigated cotton and rice in arid Uzbekistan by combining multi-temporal RapidEye data and ground measurements. In: *Proc. SPIE 7824*, vol. 782409, 10.

Eklundh, L. & Jönsson, P. (2010): TIMESAT 3.0 Software Manual. Tech. rep.

Epiphanio, J.C.N. & Huete, A.R. (1995): Dependence of NDVI and SAVI on sun/sensor geometry and its effect on fAPAR relationships in alfalfa. *Remote Sensing of Environment*, 51: 351–360.

ESRI (2012): Webhelp: HotSpot Analysis. URL: `help.arcgis.com`. Last accessed: December 2012.

Fageria, N.K., Baligar, V.C. & Clark, R.B. (2006): *Physiology of Crop Production.* Food Products Press, Binghamton, 345 pages.

FAO (2006): The State of Food Insecurity in the World 2006. Tech. rep., Rome.

FAO (2007): Land evaluation - towards a revised framework. Tech. Rep. 6, FAO.

FAO (2009): Harmonized World Soil Database (version 1.1). URL: `http://www.fao.org/nr/land/soils/harmonized-world-soil-database/en/`. Last accessed: December 2012.

FAO (2011): AQUASTAT. URL: `http://www.fao.org/nr/water/aquastat/main/index.stm`. Last accessed: December 2012.

FAO (2012): FAOSTAT. URL: `http://faostat.fao.org/site/291/default.aspx`. Last accessed: December 2012.

FAO/WFP (2000): Crop and food supply assessment mission to Karakalpakstan and Khorezm regions of Uzbekistan. Tech. rep., Rome.

Fensholt, R., Sandholt, I. & Rasmussen, M.S. (2004): Evaluation of MODIS LAI, fAPAR and the relation between fAPAR and NDVI in a semi-arid environment using in situ measurements. *Remote Sensing of Environment*, 91: 490–507.

Fensholt, R., Sandholt, I., Rasmussen, M.S., Diouf, A. & Stisen, S. (2006): Evaluation of satellite based primary production modelling in the semi-arid Sahel. *Remote Sensing of Environment*, 105: 173–188.

Fensholt, R. & Sandholt, I. (2003): Derivation of a shortwave infrared water stress index from MODIS near- and shortwave infrared data in a semiarid environment. *Remote Sensing of Environment*, 87: 111–121.

Field, C., Randerson, J. & Malmström, C. (1995): Global net primary production: Combining ecology and remote sensing. *Remote Sensing of Environment*, 51: 74–88.

Foley, J.A., Ramankutty, N., Brauman, K.A., Cassidy, E.S., Gerber, J.S., Johnston, M., Mueller, N.D., O'Connell, C., Ray, D.K., West, P.C., Balzer, C., Bennett, E.M., Carpenter, S.R., Hill, J., Monfreda, C., Polasky, S., Rockström, J., Sheehan, J., Siebert, S., Tilman, D. & Zaks, D.P.M. (2011): Solutions for a cultivated planet. *Nature*, 478: 337–342.

Forkutsa, I., Sommer, R., Shirokova, Y.I., Lamers, J.P.A., Kienzler, K., Tischbein, B., Martius, C. & Vlek, P.L.G. (2009): Modeling irrigated cotton with shallow groundwater in the Aral Sea Basin of Uzbekistan: I. Water dynamics. *Irrigation Science*, 27: 331–346.

Forkutsa, I. (2006): *Modeling water and salt dynamics under irrigated cotton with shallow groundwater in the Khorezm region of Uzbekistan.* Ph.D. thesis, University of Bonn.

Friedl, M.A. (1997): Examining the Effects of Sensor Resolution and Sub-Pixel Heterogeneity on Spectral Vegetation Indices: Implications for Biophysical Modeling. In: D.A. Quattrochi & M.F. Goodchild (Eds.), *Scale in Remote Sensing and GIS*, 113–139. Lewis Publishers, Boca Raton.

Friedl, M.A., Davis, F.W., Michaelsen, J. & Moritz, M.A. (1995): Scaling and Uncertainty in the Relationship between the NDVI and Land Surface Biophysical Variables: An Analysis Using a Scene Simulation Model and Data from FIFE. *Remote Sensing of Environment*, 54: 233–246.

Friedl, M., McIver, D., Hodges, J., Zhang, X., Muchoney, D., Strahler, A., Woodcock, C., Gopal, S., Schneider, A., Cooper, A., Baccini, A., Gao, F. & Schaaf, C. (2002): Global land cover mapping from MODIS: algorithms and early results. *Remote Sensing of Environment*, 83: 287–302.

Fritsch, S., Machwitz, M., Conrad, C. & Dech, S. (2011): Relationships between high resolution RapidEye based fPAR and MODIS vegetation indices in a heterogeneous agricultural region. In: *SPIE 8174*. SPIE, Prague.

Fritsch, S., Machwitz, M., Ehammer, A., Conrad, C. & Dech, S. (2012): Validation of the collection 5 MODIS FPAR product in a heterogeneous agricultural landscape in arid Uzbekistan using multitemporal RapidEye imagery. *International Journal of Remote Sensing*, 33(21): 6818–6837.

Gamon, J.A., Penuelas, J. & Field, C.B. (1992): A Narrow-Waveband Spectral Index That Tracks Diurnal Changes in Photosynthetic Efficiency. *Remote Sensing of Environment*, 41: 35–44.

Garbulsky, M.F., Peñuelas, J., Papale, D., Ardö, J., Goulden, M.L., Kiely, G., Richardson, A.D., Rotenberg, E., Veenendaal, E.M. & Filella, I. (2010): Patterns and controls of the variability of radiation use efficiency and primary productivity across terrestrial ecosystems. *Global Ecology and Biogeography*, 19(2): 253–267.

Garbulsky, M.F., Peñuelas, J., Papale, D. & Filella, I. (2008): Remote estimation of carbon dioxide uptake by a Mediterranean forest. *Global Change Biology*, 14: 2860–2867.

Getis, A. & Ord, J.K. (1992): The Analysis of Spatial Association by Use of Distance Statistics. *Geographical Analysis*, 24(3): 189–206.

Ghulam, A., Li, Z.L., Qin, Q., Yimit, H. & Wang, J. (2008): Estimating crop water stress with ETM+ NIR and SWIR data. *Agricultural and Forest Meteorology*, 148: 1679–1695.

Giese, E. (1998): Die ökologische Krise des Aralsees und der Aralseeregion: Ursachen, Auswirkungen, Lösungsansätze. In: *Umweltzerstörungen in Trockengebieten Zentralasiens (West- und Ost-Turkestan) - Ursachen, Auswirkungen, Maßnahmen*, 55–119. Franz Steiner Verlag, Stuttgart.

Gitelson, A.A. (2004): Wide Dynamic Range Vegetation Index for remote quantification of biophysical characteristics of vegetation. *Journal of Plant Physiology*, 161: 165–173.

GKZGK (2009): National report on land resources of Uzbekistan. Tech. rep., State Committee on Land Resources, Geodesy, Cartography and Cadastre.

Glantz, M.H., Rubinstein, A.Z. & Zonn, I. (1993): Tragedy in the Aral Sea basin-Looking back to plan ahead? *Global Environmental Change-Human and Policy Dimensions*, 3(2): 174–198.

Glazirin, G.E., Shanicheva, S.C. & Shub, V.E. (1999): Brief description of Uzbekistan climate. Tech. rep., Tashkent.

Gleick, P.H. (2003): Water Use. *Annual Review of Environment and Resources*, 275–314.

Gobron, N., Pinty, B., Mélin, F., Taberner, M., Verstraete, M.M., Belward, A., Lavergne, T. & Widlowski, J.L. (2005): The state of vegetation in Europe following the 2003 drought. *International Journal of Remote Sensing*, 26(9): 2013–2020.

Gobron, N. & Verstraete, M.M. (2009a): FAPAR - Fraction of Absorbed Photosynthetically Active Radiation (Assessment of the status of the development of the standards for the terrestrial essential climate variables). Tech. rep., FAO, Rome.

Gobron, N. & Verstraete, M.M. (2009b): LAI - Leaf Area Index (Assessment of the status of the development of the standards for the terrestrial essential climate variables). Tech. rep., FAO, Rome.

Goetz, S.J., Prince, S.D., Goward, S.N., Thawley, M.M. & Small, J. (1999): Satellite remote sensing of primary production: an improved production efficiency modeling approach. *Ecological Modeling*, 122: 239–255.

Goward, S.N. & Huemmrich, K.F. (1992): Vegetation Canopy PAR Absorptance and the Normalized Difference Vegetation Index: An Assessment Using the SAIL Model. *Remote Sensing of Environment*, 39: 119–140.

Goward, S., Tucker, C. & Dye, D. (1985): North American vegetation patterns observed with the NOAA-7 advanced very high resolution radiometer. *Vegetatio*, 64: 3–14.

Hakimov, N., Lines, A., Elmuratov, P. & Hakimov, R. (2007): Climate change and water resource alteration in Central Asia: The case of Uzbekistan. In: R. Lal, M. Suleimenov, B.A. Stewart, D.O. Hansen & P. Doraiswamy (Eds.), *Climate Change and Terrestrial Carbon Sequestration in Central Asia*, 75–82. Taylor & Francis, London.

Hall, A.E. (2001): *Crop Responses to Environment*. CRC Press, Boca Raton, 232 pages.

Hanan, N.P., Prince, S.D. & Bégué, A. (1995): Estimation of absorbed photosynthetically active radiation and vegetation net production efficiency using satellite data. *Agricultural and Forest Meteorology*, (76): 259–276.

Hatfield, J.L. (1983): Remote Sensing Estimators of Potential and Actual Crop Yield. *Remote Sensing of Environment*, 13: 301–311.

Hatfield, J.L., Gitelson, A.A., Schepers, J.S. & Walthall, C.L. (2008): Application of Spectral Remote Sensing for Agronomic Decisions. *Agronomy Journal*, 100(3): S117–S131.

Hatfield, J., Asrar, G. & Kanemasu, E. (1984): Intercepted photosynthetically active radiation estimated by spectral reflectance. *Remote Sensing of Environment*, 14(1-3): 65–75.

Hay, R.K.M. (1995): Harvest index: a review of its use in plant breeding and crop physiology. *Annals of Applied Biology*, 126(1): 197–216.

Hay, R.K.M. & Porter, J.R. (2006): *The Physiology of Crop Yield*. Blackwell Publishing Ltd., Oxford, 330 pages.

Hbirkou, C., Martius, C., Khamzina, A., Lamers, J., Welp, G. & Amelung, W. (2011): Reducing topsoil salinity and raising carbon stocks through afforestation in Khorezm, Uzbekistan. *Journal of Arid Environments*, 75: 146–155.

Hertel, T.W. (2011): The global supply and demand for agricultural land in 2050: A perfect storm in the making? *American Journal of Agricultural Economics*, 93(2): 259–275.

Hilker, T., Wulder, M.A., Coops, N.C., Black, T.A. & Guy, R.D. (2008): The use of remote sensing in light use efficiency based models of gross primary production: a review of current status and future requirements. *Science of the Total Environment*, 404(2-3): 411–423.

Hirsch, D. (2008): Problems and perspectives of water user associations in Uzbekistan. In: P. Wehrheim, A. Schoeller-Schletter & C. Martius (Eds.), *Continuity and Change - Land and water use reforms in rural Uzbekistan. Socio-economic and legal analyses for the region Khorezm*, 129–141. Leibniz-Institut für Agrarentwicklung in Mittel- und Osteuropa (IAMO), Halle.

Hornidge, A.K., Oberkircher, L., Tischbein, B., Schorcht, G., Bhaduri, A. & Manschadi, A.M. (2011): Reconceptualizing water management in Khorezm, Uzbekistan. *Natural Resources Forum*, 35(4): 251–268.

Huemmrich, K.F., Privette, J.L., Mukelabai, M., Myneni, R.B. & Knyazikhin, Y. (2005): Time-series validation of MODIS land biophysical products in a Kalahari woodland, Africa. *International Journal of Remote Sensing*, 26(19): 4381–4398.

Huete, A., Didan, K., Miura, T., Rodriguez, E.P., Gao, X. & Ferreira, L.G. (2002): Overview of the radiometric and biophysical performance of the MODIS vegetation indices. *Remote Sensing of Environment*, 83: 195 – 213.

Hufkens, K., Dong, Q.H., Bogaert, J., Huang, C.L., Lu, L., Ma, M.G., Che, T., Li, X., Veroustraete, F. & Ceulemans, R. (2008): Impacts and uncertainties of upscaling of remote-sensing data validation for a semi-arid woodland. *Journal of Arid Environments*, 72(8): 1490–1505.

Ibrakhimov, M., Khamzina, A., Forkutsa, I., Paluasheva, G., Lamers, J.P.A., Tischbein, B., Vlek, P.L.G. & Martius, C. (2007): Groundwater table and salinity: Spatial and temporal distribution and influence on soil salinization in Khorezm region (Uzbekistan, Aral Sea Basin). *Irrigation and Drainage Systems*, 21: 219–236.

Ibrakhimov, M., Martius, C., Lamers, J. & Tischbein, B. (2011): The dynamics of groundwater table and salinity over 17 years in Khorezm. *Agricultural Water Management*, 101: 52–61.

Idso, S., Hatfield, J., Reginato, R. & Jackson, R. (1978): Wheat yield estimation by albedo measurement. *Remote sensing of Environment*, 7: 273–276.

Jones, H.G. & Vaughan, R.A. (2010): *Remote Sensing of Vegetation - Principles, Techniques, and Applications*. Oxford University Press, Oxford, 353 pages.

Jönsson, P. & Eklundh, L. (2002): Seasonality Extraction by Function Fitting to Time-Series of Satellite Sensor Data. *IEEE Transactions on Geoscience and Remote Sensing*, 40(8): 1824–1832.

JRC (2012): Monitoring Agricultural Resources. URL: `http://www.marsop.info/`. Last accessed: December 2012.

Justice, C., Belward, A., Morisette, J., Lewis, P., Privette, J. & Baret, F. (2000): Developments in the 'validation' of satellite sensor products for the study of the land surface. *International Journal of Remote Sensing*, 21(17): 3383–3390.

Justice, C.O. & Becker-Reshef, I. (2007): Developing a strategy for global agricultural monitoring in the framework of Group on Earth Observations (GEO) Workshop Report. Tech. rep., UN FAO, Rome.

Khamzina, A., Lamers, J.P.A. & Vlek, P.L.G. (2012): Conversion of Degraded Cropland to Tree Plantations for Ecosystem and Livelihood Benefits. In: C. Martius, I. Rudenko, J.P.A. Lamers & P.L.G. Vlek (Eds.), *Cotton, Water, Salts and Soums - Economic and Ecological Restructuring in Khorezm, Uzbekistan*, 235–248. Springer, Berlin.

Khamzina, A., Lamers, J.P.A., Worbes, M., Botman, E. & Vlek, P.L.G. (2006): Assessing the potential of trees for afforestation of degraded landscapes in the Aral Sea Basin of Uzbekistan. *Agroforestry Systems*, 66: 129–141.

Kienzler, K.M. (2009): *Improving the nitrogen use efficiency and crop quality in the Khorezm region, Uzbekistan.* Ph.D. thesis, Rheinische Friedrich-Wilhelms-Universität zu Bonn.

Kienzler, K.M., Rudenko, I., Ruzimov, J., Ibragimov, N. & Lamers, J.P.A. (2011): Winter wheat quantity or quality? Assessing food security in Uzbekistan. *Food Security*, 3: 53–64.

Kiniry, J.R. (1994): A note of caution concerning the paper by Demetriades-Shah et al. (1992). *Agricultural and Forest Meteorology*, 68: 229–230.

Kiniry, J., Jones, C., O'Toole, J., Blanchet, R., Cabelguenne, M. & Spanel, D. (1989): Radiation-Use Efficiency in Biomass Accumulation Prior to Grain-filling for Five Grain-Crop Species. *Field Crops Research*, 20: 51–64.

Knöfel, P. (2013): *Conception and adjustment of remote sensing algorithms for acquisition and evaluation of water use efficiency in cotton ecological systems of Central Asia (unpublished).* Ph.D. thesis, University of Wuerzburg.

Koronovsky, N. (2003): Tectonics and Geology. In: M. Shahgedanova (Ed.), *The Physical Geography of Northern Eurasia (Oxford Regional Environments)*, 1–35. Oxford University Press, Oxford.

Kumar, M. & Monteith, J.L. (1981): Remote sensing of crop growth. In: H. Smith (Ed.), *Plants and the daylight spectrum*, 133–144. Academic Press, London.

Lamers, J.P.A., Bobojonov, I., Khamzina, A. & Franz, J. (2009): Financial analysis of small-scale forests in the Amu Darya Lowlands of rural Uzbekistan. *Forests, Trees and Livelihoods*, 18(4): 373–386.

Larcher, W. (2003): *Physiological Plant Ecology - Ecophysiology and Stress Physiology of Functional Groups*. Springer, Berlin, 4 ed., 513 pages.

Leblanc, S.G. & Fernandes, R. (2005): Parametric (modified least squares) and non-parametric (Theil-Sen) linear regressions for predicting biophysical parameters in the presence of measurement errors. *Remote Sensing of Environment*, 95: 303–316.

Létolle, R. & Mainguet, M. (1996): *Der Aralsee - Eine ökologische Katastrophe*. Springer, Berlin, 517 pages.

Li, G., Wang, D., Liu, S., Fan, W., Zhang, H., Xin, X. & Zhang, H. (2010): Validation of MODIS FAPAR products in Hulunber grassland of China. In: *IEEE International Geoscience and Remote Sensing Symposium (IGARSS)*, 30970489, 1047–1050.

Licker, R., Johnston, M., Foley, J.A., Barford, C., Kucharik, C.J., Monfreda, C. & Ramankutty, N. (2010): Mind the gap: how do climate and agricultural management explain the 'yield gap' of croplands around the world? *Global Ecology and Biogeography*, 19: 769–782.

Lioubimtseva, E. (2003): Arid Environments. In: M. Shahgedanova (Ed.), *Physical Geography of Northern Eurasia*, 267–283. Oxford University Press, Oxford.

Lioubimtseva, E., Cole, R., Adams, J.M. & Kapustin, G. (2005): Impacts of climate and land-cover changes in arid lands of Central Asia. *Journal of Arid Environments*, 62: 285–308.

Lioubimtseva, E. & Henebry, G. (2009): Climate and environmental change in arid Central Asia: Impacts, vulnerability, and adaptations. *Journal of Arid Environments*, 73(11): 963–977.

Liu, B.Y. & Jordan, R.C. (1960): The interrelationship and characteristic distribution of direct, diffuse, and total solar radiation. *Solar Energy*, 4: 1–19.

Liu, J. (2009): A GIS-based tool for modelling large-scale crop-water relations. *Environmental Modelling & Software*, 24(3): 411–422.

Liu, J., Pattey, E., Miller, J.R., McNairn, H., Smith, A. & Hu, B. (2010): Estimating crop stresses, aboveground dry biomass and yield of corn using multi-temporal optical data combined with a radiation use efficiency model. *Remote Sensing of Environment*, 114(6): 1167–1177.

Lobell, D.B. & Asner, G.P. (2003): Comparison of Earth Observing-1 ALI and Landsat ETM+ for Crop Identification and Yield Prediction in Mexico. *IEEE Transactions on Geoscience and Remote Sensing*, 41(6): 1277–1282.

Lobell, D.B., Asner, G.P., Ortiz-Monasterio, J.I. & Benning, T.L. (2003): Remote sensing of regional crop production in the Yaqui Valley, Mexico: estimates and uncertainties. *Agriculture, Ecosystems and Environment*, 94: 205–220.

Lobell, D.B., Burke, M.B., Tebaldi, C., Mastrandrea, M.D., Falcon, W.P. & Naylor, R.L. (2008): Prioritizing climate change adaptation needs for food security in 2030. *Science*, 319(5863): 607–610.

Lobell, D.B., Cassman, K.G. & Field, C.B. (2009): Crop Yield Gaps: Their Importance, Magnitudes, and Causes. *Annual Review of Environment and Resources*, 34: 179–204.

Lobell, D.B., Ortiz-Monasterio, J.I. & Lee, A.S. (2010): Satellite evidence for yield growth opportunities in Northwest India. *Field Crops Research*, 118: 13–20.

Lobell, D., Hicke, J., Asner, G., Field, C., Tucker, C. & Los, S. (2002): Satellite estimates of productivity and light use efficiency in United States agriculture, 1982-98. *Global Change Biology*, 8: 722–735.

Lobell, D., Schlenker, W. & Costa-Roberts, J. (2011): Climate trends and global crop production since 1980. *Science*, 333: 616–620.

Maas, S.J. (1988): Using satellite data to improve model estimates of crop yield. *Agronomy Journal*, 80(4): 655–662.

Malczewski, J. (1999): *GIS and Multicriteria Decision Analysis*. John Wiley & Sons, New York, 392 pages.

Malczewski, J. (2004): GIS-based land-use suitability analysis: a critical overview. *Progress in Planning*, 62: 3–65.

Malet, P., Pécaut, F. & Bruchou, C. (1997): Beware of using cumulated variables in growth and development models. *Agricultural and Forest Meteorology*, 88(1-4): 137–143.

Manschadi, A.M., Oberkircher, L., Tischbein, B., Conrad, C., Hornidge, A.K., Bhaduri, A., Schorcht, G., Lamers, J.P.L. & Vlek, P.L.G. (2010): 'White Gold' and Aral Sea disaster - Towards more efficient use of water resources in the Khorezm region, Uzbekistan. *Lohmann Information*, 45(1): 34–47.

Martin, D. & Saha, S.K. (2009): Land evaluation by integrating remote sensing and GIS for cropping system analysis in a watershed. *Current Science*, 96(4): 569–575.

Martius, C., Lamers, J.P.A., Vlek, P.L.G., Eshchanov, R., Rudenko, I. & Salaev, O. (2005): Water, salt, cotton and soums: shedding new light on the Aral Sea problem. In: *Tropentag 2005: The Global Food & Product Chain - Dynamics, Innovations, Conflicts, Strategies.*, 4. Stuttgart.

Martius, C., Rudenko, I., Lamers, J.P.A. & Vlek, P.L.G. (2012): *Cotton, Water, Salts and Soums.* Springer, Berlin, 419 pages.

Maselli, F., Moriondo, M., Angeli, L., Fibbi, L. & Bindi, M. (2011): Estimation of wheat production by the integration of MODIS and ground data. *International Journal of Remote Sensing*, 32(4): 1105–1123.

Mavi, H.S. & Tupper, G.J. (2004): *Agrometeorology - Principles and Applications of Climate Studies in Agriculture.* Food Products Press, Binghamton, 364 pages.

McCallum, I., Wagner, W., Schmullius, C., Shvidenko, A., Obersteiner, M., Fritz, S. & Nilsson, S. (2009): Satellite-based terrestrial production efficiency modeling. *Carbon Balance and Management*, 4(8): 1–14.

McCree, K.J. (1972a): The action spectrum, absorptance and quantum yield of photosynthesis in crop plants. *Agricultural Meteorology*, 9: 191–216.

McCree, K.L. (1981): Photosynthetically active radiation. In: O.L. Lange (Ed.), *Encyclopedia of Plant Physiology*, 41–55. Springer, Berlin.

McCree, K. (1972b): Test of current definitions of photosynthetically active radiation against leaf photosynthesis data. *Agricultural Meteorology*, 10(6): 443–453.

Micklin, P. (2002): Water in the Aral Sea Basin of Central Asia: Cause of Conflict or Cooperation? *Eurasian Geography and Economics*, 43(7): 505–528.

Micklin, P. (2007): The Aral Sea Disaster. *Annual Review of Earth and Planetary Sciences*, 35: 47–72.

Micklin, P. (2010): The past, present, and future Aral Sea. *Lakes & Reservoirs: Research & Management*, 15: 193–213.

Middleton, N. (2003): The Aral Sea. In: M. Shahgedanova (Ed.), *Physical Geography of Northern Eurasia*, 497–510. Oxford University Press, Oxford.

Monteith, J.L. (1969): Light interception and radiative exchange in crop stands. In: J. Eastin (Ed.), *Physiological aspects of crop yield*, 89–111. Lincoln.

Monteith, J.L. (1972): Solar radiation and productivity in tropical ecosystems. *Journal of Applied Ecology*, 9(3): 747–766.

Monteith, J.L. (1977): Climate and efficiency of crop production in Britain. *Philosophical Transactions of the Royal Society of London. Series B- Biological Sciences*, 281(980): 277–294.

Monteith, J. (1965): Light distribution and photosynthesis in field crops. *Annals of Botany*, 29(113): 17.

Monteith, J. (1994): Validity of the correlation between intercepted radiation and biomass. *Agricultural and Forest Meteorology*, 68(3-4): 213–220.

Moriondo, M., Maselli, F. & Bindi, M. (2007): A simple model of regional wheat yield based on NDVI data. *European Journal of Agronomy*, 26: 266–274.

Morisette, J.T., Baret, F., Privette, J.L., Myneni, R.B., Nickeson, J.E., Garrigues, S., Shabanov, N., Weiss, M., Fernandes, R.A., Leblanc, S.G., Kalacska, M., Sanchez-Azofeifa, G.A., Chubey, M., Rivard, B., Stenberg, P., Rautiainen, M., Voipio, P., Manninen, T., Pilant, A.N., Lewis, T.E., Iiames, J.S., Colombo, R., Meroni, M., Busetto, L., Cohen, W.B., Turner, D.P., Warner, E.D., Peterson, G.W., Seufert, G. & Cook, R. (2006): Validation of global moderate-resolution LAI products: a framework proposed within the CEOS Land Product Validation subgroup. *IEEE Transactions on Geoscience and Remote Sensing*, 44(7): 1804–1817.

Morisette, J.T., Privette, J.L. & Justice, C.O. (2002): A framework for the validation of MODIS Land products. *Remote Sensing of Environment*, 83: 77–96.

Morton, J.F. (2007): The impact of climate change on smallholder and subsistence agriculture. *Proceedings of the National Academy of Sciences of the United States of America*, 104(50): 19680–19685.

Moulin, S., Bondeau, A. & Delecolle, R. (1998): Combining agricultural crop models and satellite observations: from field to regional scales. *International Journal of Remote Sensing*, 19(6): 1021–1036.

Myneni, R., Knyazikhin, Y., Glassy, J., Votava, P. & Shabanov, N. (2003): User's Guide FPAR, LAI (ESDT: MOD15A2) 8-day Composite NASA MODIS Land Algorithm. Tech. rep., NASA.

Myneni, R.B., Hoffman, S., Knyazikhin, Y., Privette, J.L., Glassy, J., Tian, Y., Wang, Y., Song, X., Zhang, Y., Smith, G.R., Lotsch, A., Friedl, M., Morisette, J.T., Votava, P., Nemani, R.R. & Running, S.W. (2002): Global products of vegetation leaf area and fraction absorbed PAR from year one of MODIS data. *Remote Sensing of Environment*, 83(1-2): 214–231.

Myneni, R. & Williams, D. (1994): On the relationship between FAPAR and NDVI. *Remote Sensing of Environment*, 49(3): 200–211.

Nakaji, T., Ide, R., Oguma, H., Saigusa, N. & Fujinuma, Y. (2007): Utility of spectral vegetation index for estimation of gross CO_2 flux under varied sky conditions. *Remote Sensing of Environment*, 109(3): 274–284.

NASA (2012): MODIS Land Team Validation. URL: `http://landval.gsfc.nasa.gov/`. Last accessed: December 2012.

Nouvellon, Y., Seen, D.L., Rambal, S., Bégué, A., Moran, M.S., Kerr, Y. & Qi, J. (2000): Time course of radiation use efficiency in a shortgrass ecosystem: consequences for remotely sensed estimation of primary production. *Remote Sensing of Environment*, 71: 43–55.

OBLSTAT (2010): Official Statistical Data on Agricultural Crop Production and Yields (2003-2009). Tech. rep., Khorezm Regional Department of the Ministry of Macro-Economics and Statistics of the Republic of Uzbekistan in Khorezm, Urgench.

O'Hara, S.L. (2000): Lessons from the past: water management in Central Asia. *Water Policy*, 2: 365–384.

Ord, J.K. & Getis, A. (1995): Local spatial autocorrelation statistics: distributional issues and an application. *Geographical Analysis*, 27(4): 286–306.

Ososkova, T., Gorelkin, N. & Chub, V. (2000): Water resources of Central Asia and adaptation measures for climate change. *Environmental Monitoring and Assessment*, 61: 161–166.

Pan, G., Sun, G.J. & Li, F.M. (2009): Using QuickBird imagery and a production efficiency model to improve crop yield estimation in the semi-arid hilly Loess Plateau, China. *Environmental Modelling & Software*, 24(4): 510–516.

Parry, M.L., Canziani, O.F., Palutikof, J.P., van der Linden, P.J. & Hanson, C.E. (2007): *Climate Change 2007 - Impacts, Adaptation and Vulnerability - Contribution of Working Group II to the Fourth Assessment Report of the Intergovernmental Panel on Climate Change*. Cambridge University Press, Cambridge, 982 pages.

Patel, N.R., Bhattacharjee, B., Mohammed, A.J., Tanupriya, B. & Saha, S.K. (2006): Remote sensing of regional yield assessment of wheat in Haryana, India. *International Journal of Remote Sensing*, 27(19): 4071–4090.

Patel, N.R., Dadhwal, V.K., Saha, S.K., Garg, A. & Sharma, N. (2010): Evaluation of MODIS data potential to infer water stress for wheat NPP estimation. *Tropical Ecology*, 51(1): 93–105.

Pinter, P.J., Hatfield, J.L., Schepers, J.S., Barnes, E.M., Moran, M.S., Daughtry, C.S.T. & Upchurch, D.R. (2003): Remote Sensing for Crop Management. *Photogrammetric Engineering & Remote Sensing*, 69(6): 647–664.

Pinter, P., Jackson, R., Idso, S. & Reginato, R. (1981): Multidate spectral reflectance as predictors of yield in water stressed wheat and barley. *International Journal of Remote Sensing*, 2(1): 43–48.

Potter, C.S., Randerson, J.T., Field, C.B., Matson, P.A., Vitousek, P.M., Mooney, H.A. & Klooster, S.A. (1993): Terrestrial ecosystem production: a process model based on global satellite and surface data. *Global Biogeochemical Cycles*, 7(4): 811–841.

Prentice, I.C., Cramer, W., Harrison, S.P., Leemans, R., Monserud, R.A. & Solomon, A.M. (1992): A global biome model based on plant physiology and dominance, soil properties and climate. *Journal of Biogeography*, 19(2): 117–134.

Prince, S.D. (1991): A model of regional primary production for use with coarse resolution satellite data. *International Journal of Remote Sensing*, 12(6): 1313–1330.

Prince, S.D. & Goward, S. (1995): Global primary production: A remote sensing approach. *Journal of Biogeography*, 22(4-5): 815–835.

Prishchepov, A.V., Radeloff, V.C., Baumann, M., Kuemmerle, T. & Müller, D. (2012): Effects of institutional changes on land use: agricultural land abandonment during the transition from state-command to market-driven economies in post-Soviet Eastern Europe. *Environmental Research Letters*, 7(2): 1–13.

R Core Team (2012): R: A Language and Environment for Statistical Computing. URL: `http://www.r-project.org`. Last accessed: December 2012.

Rabus, B., Eineder, M., Roth, A. & Bamler, R. (2003): The shuttle radar topography mission-a new class of digital elevation models acquired by spaceborne radar. *ISPRS Journal of Photogrammetry and Remote Sensing*, 57(4): 241–262.

Ragab, R. & Prudhomme, C. (2002): Climate change and water resources management in arid and semi-arid regions: Prospective and challenges for the 21st century. *Biosystems Engineering*, 81: 3–34.

RapidEye (2011): Satellite Imagery Product Specifications (Version 3.2). Tech. rep., Brandenburg an der Havel.

Reddy, S.J. (1995): Over-emphasis on energy terms in crop yield models. *Agricultural and Forest Meteorology*, 77: 113–120.

Reeves, M.C., Zhao, M. & Running, S.W. (2005): Usefulness and limits of MODIS GPP for estimating wheat yield. *International Journal of Remote Sensing*, 26(7): 1403–1421.

Richter, R. (2009): Atmospheric/Topographic Correction for Satellite Imagery (ATCOR-2/3 User Guide, Version 7.0, January 2009). Tech. rep., German Aerospace Agency (DLR)/German Remote Sensing Data Center (DFD), Wessling.

Roll, G., Alexeeva, N., Aladin, N., Plotnikov, I., Sokolov, V., Sarsembekov, T. & Micklin, P. (2006): Aral Sea - Experience and Lessons Learned Brief. Tech. rep., International Lake Environment Committee - Lake Basin Management Initiative (LBMI).

Roujean, J.L. & Breon, F.M. (1995): Estimating PAR absorbed by vegetation from bidirectional reflectance measurements. *Remote Sensing of Environment*, 51: 375–384.

Rudenko, I., Nurmetov, K. & Lamers, J.P.A. (2012): State Order and Policy Strategies in the Cotton and Wheat Value Chains. In: C. Martius, I. Rudenko, J.P.A. Lamers & P.L.G. Vlek (Eds.), *Cotton, Water, Salts and Soums - Economic and Ecological Restructuring in Khorezm, Uzbekistan*, 371–387. Springer, London.

Ruecker, G., Conrad, C., Ibragimov, N., Kienzler, K., Ibrakhimov, M., Martius, C. & Lamers, J.P.A. (2012): Spatial Distribution of Cotton Yield and its Relationship to Environmental, Irrigation Infrastructure and Water Management Factors on a Regional Scale in Khorezm, Uzbekistan. In: C. Martius, I. Rudenko, J.P.A. Lamers & P.L.G. Vlek (Eds.), *Cotton, Water, Salts and Soums - Economic and Ecological Restructuring in Khorezm, Uzbekistan*, 59–68. Springer, Berlin.

Ruimy, A., Saugier, B. & Dedieu, G. (1994): Methodology for the estimation of terrestrial net primary production from remotely sensed data. *Journal of Geophysical Research-Atmospheres*, 99(D3): 5263–5283.

Running, S.W., Thornton, P.E., Nemani, R. & Glassy, J.M. (2000): Global Terrestrial Gross and Net Primary Productivity from the Earth Observing System. In: O.E. Sala, R.B. Jackson, H.A. Mooney & R.W. Howarth (Eds.), *Methods in Ecosystem Science*, 44–57. Springer, Berlin.

Running, S.W., Nemani, R.R., Heinsch, F.A., Zhao, M., Reeves, M. & Hashimoto, H. (2004): A Continuous Satellite-Derived Measure of Global Terrestrial Primary Production. *BioScience*, 54(6): 547–560.

Runyon, J., Waring, R.H., Goward, S.N. & Welles, J.M. (1994): Environmental limits on net primary production and light-use efficiency across the Oregon transect. *Ecological Applications*, 4(2): 226–237.

Saiko, T.A. & Zonn, I.S. (2000): Irrigation expansion and dynamics of desertification in the Circum-Aral region of Central Asia. *Applied Geography*, 20: 349–367.

Schmidhuber, J. & Tubiello, F. (2007): Global food security under climate change. *Proceedings of the National Academy of Sciences*, 104(50): 19703–19708.

Schorcht, G., Conrad, C., Dech, S., Lamers, J., Rücker, G. & Fritsch, S. (2009): Field based FAO-56 dual crop coefficient method for water demand estimations using remote sensing and geodata management approaches. In: *Proceedings of the GISCA 2009 - GIScience for Environmental and Emergency Management in Central Asia*. Bishkek.

Schulze, E.D., Beck, E. & Müller-Hohenstein, K. (2005): *Plant Ecology*. Springer, Berlin, 702 pages.

Seaquist, J.W., Olsson, L. & Ardö, J. (2003): A remote sensing-based primary production model for grassland biomes. *Ecological Modelling*, 169: 131–155.

Seckler, D., Amarasinghe, U., Molden, D., de Silva, R. & Barker, R. (1998): World water demand and supply, 1990 to 2025: Scenarios and issues. Tech. rep., International Water Management Institute, Colombo.

Sellers, P.J. (1985): Canopy reflectance, photosynthesis and transpiration. *International Journal of Remote Sensing*, 6(8): 1335–1372.

Seong, J., Mulcahy, K. & Usery, E. (2002): The sinusoidal projection: a new importance in relation to global image data. *The Professional Geographer*, 54(2): 218–225.

Severskiy, I., Chervanyov, I., Ponomarenko, Y., Novikova, N.M., Miagkov, S.V., Rautalahti, E. & Daler, D. (2005): Global International Water Assessment - Aral Sea (GIWA Regional Assessment 24). Tech. rep., University of Kalmar on behalf of United Nations Environment Programme (UNEP), Kalmar.

Shi, Z., Ruecker, G.R., Mueller, M., Conrad, C., Ibragimov, N., Lamers, J.P.A., Martius, C., Strunz, G., Dech, S. & Vlek, P.L.G. (2007): Modeling of Cotton Yields in the Amu Darya River Floodplains of Uzbekistan Integrating Multitemporal Remote Sensing and Minimum Field Data. *Agronomy Journal*, 99(5): 1317–1326.

Siebert, S. & Döll, P. (2010): Quantifying blue and green virtual water contents in global crop production as well as potential production losses without irrigation. *Journal of Hydrology*, 384(3-4): 198–217.

Siegfried, T., Bernauer, T., Guiennet, R., Sellars, S., Robertson, A.W., Mankin, J., Bauer-Gottwein, P. & Yakovlev, A. (2012): Will climate change exacerbate water stress in Central Asia? *Climatic Change*, 112(3-4): 881–899.

Sims, D.A., Rahman, A.F., Cordova, V.D., El-Masri, B.Z., Baldocchi, D.D., Flanagan, L.B., Goldstein, A.H., Hollinger, D.Y., Misson, L., Monson, R.K., Oechel, W.C., Schmid, H.P., Wofsy, S.C. & Xu, L. (2006): On the use of MODIS EVI to assess gross primary productivity of North American ecosystems. *Journal of Geophysical Research*, 111: 1–16.

Sinclair, T.R. & Seligman, N.G. (1996): Crop modeling: From infancy to maturity. *Agronomy Journal*, 88(5): 698–704.

Sjöström, M., Ardö, J., Arneth, A., Boulain, N., Cappelaere, B., Eklundh, L., de Grandcourt, A., Kutsch, W., Merbold, L., Nouvellon, Y., Scholes, R., Schubert, P., Seaquist, J. & Veenendaal, E. (2011): Exploring the potential of MODIS EVI for modeling gross primary production across African ecosystems. *Remote Sensing of Environment*, 115(4): 1081–1089.

Smit, B., Bray, J. & Keddie, P. (1991): Identification of marginal agricultural areas in Ontario, Canada. *Geoforum*, 22(3): 333–346.

Smith, P.C., De Noblet-Ducoudré, N., Ciais, P., Peylin, P., Viovy, N., Meurdesoif, Y. & Bondeau, A. (2010): European-wide simulations of croplands using an improved terrestrial biosphere model: Phenology and productivity. *Journal of Geophysical Research*, 115(G1): 1–14.

Solano, R., Didan, K., Jacobson, A. & Huete, A. (2010): MODIS Vegetation Indices (MOD13) C5 User's Guide (Version 1.00). Tech. rep., Terrestrial Biophysics and Remote Sensing Lab - The University of Arizona.

Sommer, R., Kienzler, K., Conrad, C., Ibragimov, N., Lamers, J., Martius, C. & Vlek, P. (2008): Evaluation of the CropSyst model for simulating the potential yield of cotton. *Agronomy for Sustainable Development*, 28(2): 345–354.

Spitters, C.J.T. (1990): Crop growth models: their usefulness and limitations. *Acta Horticulturae*, 267: 349–368.

Spoor, M. (1998): The Aral Sea Basin Crisis: Transition and Environment in Former Soviet Central Asia. *Development and Change*, 29: 409–435.

SPOT (2013): SPOT Image. URL: `www.spotimage.fr`. Last accessed: December 2012.

Steinberg, D.C. & Goetz, S. (2009): Assessment and extension of the MODIS FPAR products in temperate forests of the eastern United States. *International Journal of Remote Sensing*, 30(1): 169–187.

Steinberg, D., Goetz, S. & Hyer, E. (2006): Validation of MODIS FPAR products in boreal forests of Alaska. *IEEE Transactions on Geoscience and Remote Sensing*, 44(7): 1818–1828.

Steinmetz, S., Guerif, M., Delecolle, R. & Baret, F. (1990): Spectral estimates of the absorbed photosynthetically active radiation and light-use efficiency of a winter wheat crop subjected to nitrogen and water deficiencies. *International Journal of Remote Sensing*, 11(10): 1797–1808.

Stöckle, C., Donatelli, M. & Nelson, R. (2003): CropSyst, a cropping systems simulation model. *European Journal of Agronomy*, 18(3-4): 289–307.

Strahler, A.H., Woodcock, C.E. & Smith, J.A. (1986): On the nature of models in remote sensing. *Remote Sensing of Environment*, 20(2): 121–139.

Suits, G.H. (1972): The Calculation of the Directional Reflectance of a Vegetative Canopy. *Remote Sensing of Environment*, 2: 117–125.

Tan, B., Hu, J., Zhang, P., Huang, D., Shabanov, N., Weiss, M., Knyazikhin, Y. & Myneni, R.B. (2005): Validation of Moderate Resolution Imaging Spectroradiometer leaf area index product in croplands of Alpilles, France. *Journal of Geophysical Research*, 110: 1–15.

Tao, F., Yokozawa, M., Zhang, Z., Xu, Y. & Hayashi, Y. (2005): Remote sensing of crop production in China by production efficiency models: models comparisons, estimates and uncertainties. *Ecological Modelling*, 183(4): 385–396.

Tewolde, H., Sistani, K.R., Rowe, D.E., Adeli, A. & Tsegaye, T. (2005): Estimating cotton leaf area index nondestructively with a light sensor. *Agronomy Journal*, 97(4): 1158–1163.

Tian, Y., Zhang, Y., Knyazikhin, Y., Myneni, R., Glassy, J., Dedieu, G. & Running, S. (2000): Prototyping of MODIS LAI and FPAR algorithm with LASUR and LANDSAT data. *IEEE Transactions on Geoscience and Remote Sensing*, 38(5): 2387–2401.

Tian, Y.H., Wang, Y.J., Zhang, Y., Knyazikhin, Y., Bogaert, J. & Myneni, R.B. (2003): Radiative transfer based scaling of LAI retrievals from reflectance data of different resolutions. *Remote Sensing of Environment*, 84: 143–159.

Tucker, C.J. (1979): Red and photographic infrared linear combinations for monitoring vegetation. *Remote Sensing of Environment*, 8: 127–150.

Tucker, C.J., Holben, B.N., Elgin Jr., J.H. & McMurtrey III, J.E. (1981): Remote Sensing of Total Dry-Matter Accumulation in Winter Wheat. *Remote Sensing of Environment*, (11): 171–189.

Tucker, C. & Sellers, P. (1986): Satellite remote sensing of primary production. *International Journal of Remote Sensing*, 7(11): 1395–1416.

Tucker, C., Vanpraet, C., Sharman, M. & van Ittersum, G. (1985): Satellite remote sensing of total herbaceous biomass production in the Senegalese Sahel: 1980-1984. *Remote Sensing of Environment*, 17(3): 233–249.

Turner, D.P., Ritts, W.D., Cohen, W.B., Gower, S.T., Running, S.W., Costa, M.H., Zhao, M., Kirschbaum, A.A., Ham, J.M., Saleska, S.R. & Ahl, D.E. (2006): Evaluation of MODIS NPP and GPP products across multiple biomes. *Remote Sensing of Environment*, 102(3-4): 282–292.

Turner, D.P., Gower, S.T., Cohen, W.B., Gregory, M. & Maiersperger, T.K. (2002): Effects of spatial variability in light use efficiency on satellite-based NPP monitoring. *Remote Sensing of Environment*, 80: 397–405.

Turner, D.P., Ritts, W.D., Cohen, W.B., Maeirsperger, T.K., Gower, S.T., Kirschbaum, A.A., Running, S.W., Zhao, M., Wofsy, S.C., Dunn, A.L., Law, B.E., Campbell, J.L., Oechel, W.C., Kwon, H.J., Meyers, T.P., Kurc, S.A., Small, E.E. & Gamon, J.A. (2005): Site-level evaluation of satellite-based global terrestrial gross primary production and net primary production monitoring. *Global Change Biology*, 11(4): 666–684.

Turner, D.P., Urbanski, S., Bremer, D., Wofsy, S.C., Meyers, T., Gower, S.T. & Gregory, M. (2003): A cross-biome comparison of daily light use efficiency for gross primary production. *Global Change Biology*, 9: 383–395.

Tyc, G., Tulip, J., Schulten, D., Krischke, M. & Oxfort, M. (2005): The RapidEye mission design. *Acta Astronautica*, 56(1-2): 213–219.

USGS (2012): Land processes distributed active archive center (LP DAAC). URL: `https://lpdaac.usgs.gov/`. Last accessed: December 2012.

Veldwisch, G.J. (2007): Changing patterns of water distribution under the influence of land reforms and simultaneous WUA establishment - Two cases from Khorezm, Uzbekistan. *Irrigation and Drainage Systems*, 21(3-4): 265–276.

Veldwisch, G.J.A. & Spoor, M. (2008): Contesting rural resources: Emerging 'forms' of agrarian production in Uzbekistan. *Journal of Peasant Studies*, 35(3): 424–451.

Vina, A. & Gitelson, A.A. (2005): New developments in the remote estimation of the fraction of absorbed photosynthetically active radiation in crops. *Geophysical Research Letters*, 32(17).

Vlek, P.L.G., Martius, C., Wehrheim, P., Schoeller-Schletter, A. & Lamers, J. (2001): Economic Restructuring of Land and Water Use in the Region Khorezm (Uzbekistan; Project Proposal for Phase I). Tech. Rep. September 2001, Center for Development Research, Bonn.

von Grebmer, K., Fritschel, H., Nestorova, B., Olofinbiyi, T., Pandya-Lorch, R. & Yohannes, Y. (2008): Global Hunger Index: The Challenge of Hunger 2008. Tech. rep., Welthungerhilfe, International Food Policy Research Institute IFPRI, CONCERN worldwide, Bonn, Washington D.C., Dublin.

Wallach, D. (2006): Evaluating crop models. In: D. Wallach, D. Makowski & J. Jones (Eds.), *Working with Dynamic Crop Models - Evaluation, Analysis, Parameterization, and Applications*, 11–53. Elsevier, Amsterdam.

Wang, H., Jia, G., Fu, C., Feng, J., Zhao, T. & Ma, Z. (2010): Deriving maximal light use efficiency from coordinated flux measurements and satellite data for regional gross primary production modeling. *Remote Sensing of Environment*, 114(10): 2248–2258.

Wang, Y.J., Tian, Y.H., Zhang, Y., El-Saleous, N., Knyazikhin, Y., Vermote, E. & Myneni, R.B. (2001): Investigation of product accuracy as a function of input and model uncertainties - Case study with SeaWiFS and MODIS LAI/FPAR algorithm. *Remote Sensing of Environment*, 78(3): 299–313.

Wang, Y.J., Woodcock, C.E., Buermann, W., Stenberg, P., Voipio, P., Smolander, H., Häme, T., Tian, Y.H., Hu, J.N., Knyazikhin, Y. & Myneni, R.B. (2004): Evaluation of the MODIS LAI algorithm at a coniferous forest site in Finland. *Remote Sensing of Environment*, 91(1): 114 – 127.

Wegerich, K. (2004): Organizational Problems of Water Distribution in Khorezm, Uzbekistan. *Water International*, 29(2): 130–137.

Wehrheim, P. & Martius, C. (2008): Farmers, cotton, water, and models - Introduction and overview. In: P. Wehrheim, A. Schoeller-Schletter & C. Martius (Eds.), *Continuity and Change - Land and water use reforms in rural Uzbekistan. Socio-economic and legal analyses for the region Khorezm*, 1–15. Leibniz-Institut für Agrarentwicklung in Mittel- und Osteuropa (IAMO), Halle.

Weiss, M., Beaufor, L., Baret, F., Allard, D., Bruguier, N. & Marloie, O. (2001): Leaf area index measurements at different scales for the validation of large swath satellite sensors: first results of the VALERI project. In: *Proceedings of the 8th International Symposium on Physical Measurements and Signature in Remote Sensing*, 125–130. CNES, Aussois.

WFP (2008): Poverty and Food insecurity in Uzbekistan. Tech. rep., World Food Program.

Wiegand, C., Anderson, G., Lingle, S. & Escobar, D. (1996): Soil Salinity Effects on Crop Growth and Yield - Illustration of an Analysis and Mapping Methodology for Sugarcane. *Journal of Plant Physiology*, 148(3-4): 418–424.

Wolfe, R., Roy, D. & Vermote, E. (1998): MODIS land data storage, gridding, and compositing methodology: Level 2 grid. *IEEE Transactions on Geoscience and Remote Sensing*, 36(4): 1324–1338.

Wu, C., Munger, J.W., Niu, Z. & Kuang, D. (2010): Comparison of multiple models for estimating gross primary production using MODIS and eddy covariance data in Harvard Forest. *Remote Sensing of Environment*, 114(12): 2925–2939.

Xiao, X., Zhang, Q., Braswell, B., Urbanski, S., Boles, S., Wofsy, S., Moore III, B. & Ojima, D. (2004): Modeling gross primary production of temperate deciduous broadleaf forest using satellite images and climate data. *Remote Sensing of Environment*, 91(2): 256–270.

Yan, H., Fu, Y., Xiao, X., Huang, H.Q., He, H. & Ediger, L. (2009): Modeling gross primary productivity for winter wheat-maize double cropping system using MODIS time series and CO_2 eddy flux tower data. *Agriculture, Ecosystems & Environment*, 129(4): 391–400.

Yang, P., Shibasaki, R., Wu, W., Zhou, Q., Chen, Z., Zha, Y., Shi, Y. & Tang, H. (2007): Evaluation of MODIS land cover and LAI products in cropland of North China Plain using in situ measurements and Landsat TM images. *IEEE Transactions on Geoscience and Remote Sensing*, 45(10): 3087–3097.

Yang, W., Tan, B., Huang, D., Rautiainen, M., Shabanov, N., Wang, Y., Privette, J., Huemmrich, K., Fensholt, R., Sandholt, I., Weiss, M., Ahl, D.E., Gower, S.T., Nemani, R.R., Knyazikhin, Y. & Myneni, R.B. (2006): MODIS leaf area index products: From validation to algorithm improvement. *IEEE Transactions on Geoscience and Remote Sensing*, 44(7): 1885–1898.

Yoshida, S. (1981): *Fundamentals of Rice Crop Science*. The International Rice Research Institute, Los Banos, Manila, 269 pages.

ZEF (2012): Sustainable management of land and water resources in Uzbekistan. URL: `http://www.khorezm.zef.de/`. Last accessed: December 2012.

Zeileis, A. & Grothendieck, G. (2005): zoo: S3 Infrastructure for Regular and Irregular Time Series. *Journal of Statistical Software*, 14(6): 1–27.

Zhang, Y., Yu, Q., Jiang, J. & Tang, Y. (2008): Calibration of Terra/MODIS gross primary production over an irrigated cropland on the North China Plain and an alpine meadow on the Tibetan Plateau. *Global Change Biology*, 14: 757–767.

Zhao, M., Heinsch, F.A., Nemani, R.R. & Running, S.W. (2005): Improvements of the MODIS terrestrial gross and net primary production global data set. *Remote Sensing of Environment*, 95(2): 164–176.

Zhao, M. & Running, S.W. (2010): Drought-induced reduction in global terrestrial net primary production from 2000 through 2009. *Science*, 329: 940–943.

Zomer, R.J., Trabucco, A., Bossio, D.A. & Verchot, L.V. (2008): Climate change mitigation: A spatial analysis of global land suitability for clean development mechanism afforestation and reforestation. *Agriculture, Ecosystems & Environment*, 126(1-2): 67–80.

A Appendix

A.1 Calculation of the global radiation ($Glob_{rad}$)

The following steps for calculating the incoming solar radiation are taken from Campbell & Norman (1998). The required components are: equation of time, time of solar noon, solar declination, the zenith angle of the sun and the direct and diffuse parts of the radiation.

The equation of time (ETi) is calculated as (equation 11.4 in Campbell & Norman 1998):

$$ETi = \frac{-104.7sinf + 596.2sin2f + 4.3sin3f - 12.7sin4f - 429.3cosf - 2.0cos2f + 19.3cos3f}{3600} \tag{A.1}$$

Where $f = 279.575 + 0.9856J$ in degrees, and J is the (Julian) calendar day with J =1 at January 1.

The time of solar noon (t_0) is modeled as (equation 11. 3 in Campbell & Norman 1998):

$$t_0 = 12 - LC - ETi \tag{A.2}$$

LC is a longitude correction that amounts to 1/15th of an hour for each degree east and west of the standard meridian. It is positive for locations east of the standard meridian and negative for locations west of it.

The solar declination is then calculated as (equation 11.2 in Campbell & Norman 1998):

$$sin\delta = 0.39785sin\left[278.97 + 0.9856J + 1.9165sin\left(356.6 + 0.9856J\right)\right] \tag{A.3}$$

The calculation of the sun's zenith angle needs an estimation of t_0 and has the form (equation 11.1 in Campbell & Norman 1998):

$$cos\psi = sin\beta = sin\phi\ sin\delta + cos\phi\ cos\delta\ cos\left[15\left(t - t_0\right)\right] \tag{A.4}$$

Where ϕ is the latitude, δ is the solar declination and t is time.

For an estimation of the direct solar radiation, the direct irradiance on a surface perpendicular

to the beam (S_p) is required. It is calculated according to (equation 11.11 in Campbell & Norman 1998):

$$S_p = S_{po}\tau^m \tag{A.5}$$

Here, S_{po} is the incoming extraterrestrial radiation, τ is the atmospheric transmittance and m is the optical air mass number. m can also be referred to as 'the ratio of slant path length through the atmosphere to zenith path length' (Campbell & Norman 1998, pp. 172-173), and is calculated as (equation 11.12 in Campbell & Norman 1998):

$$m = \frac{p_a}{101.3cos\psi} \tag{A.6}$$

$p_a/101.3$ describes the atmospheric pressure at the investigated site divided by the sea level atmospheric pressure. This term corrects for altitude effects. The ratio can be approximated by (equation 3.7 in Campbell & Norman 1998):

$$p_a = 101.3exp\left(\frac{-A}{8200}\right) \tag{A.7}$$

A is the altitude above sea level (in meters).

The term τ describes the atmospheric transmissivity, which depends on the cloudiness. According to Liu & Jordan (1960), it ranges between 0.75 and 0.45 on clear days. Values around 0.4 describe overcast skies. For this thesis, a value of 0.69 was assumed, which reflects the general clear sky conditions in the study area.

Afterwards, direct radiation (S_b) can be approximated as (equation 11.8 in Campbell & Norman 1998):

$$S_b = S_p cos\psi \tag{A.8}$$

The diffuse radiation (S_d) on clear days can be modeled with an empirical approximation adopted from Liu & Jordan (1960) (equation 11.13 in Campbell & Norman 1998):

$$S_d = 0.3\left(1 - \tau^m\right) S_{po} cos\psi \tag{A.9}$$

Finally, the incoming global radiation (S_t) can be calculated as (equation 11.9 in Campbell & Norman 1998):

$$S_t = S_b + S_d \tag{A.10}$$

A.2 Studies on crop yield prediction based on satellite-driven LUE modeling

The subsequent table summarizes the relevant studies on LUE-based crop yield modeling mentioned in this dissertation. The used abbreviations are as follows:

LUE_{max} = Maximum Light Use Efficiency, LUE_{act} = Actual Light Use Efficiency, T_s = Temperature Stress, W_s = Water Stress, $SEBAL$ = Surface Energy Balance Algorithm for Land, $FPAR$ = Fraction of Absorbed Photosynthetically Active Radiation, PAR = Photosynthetically Active Radiation, H_i = Harvest Index, T_{min} = Minimum Temperature, T_{max} = Maximum Temperature, VPD = Vapor Pressure Deficit, $SIWSI$ = Shortwave Infrared Water Stress Index, $CWSI$ = Crop Water Stress Index, $MTVI$ = Modified Triangular Vegetation Index, ET_{act} = Actual Evapotranspiration, ET_c = Crop Evapotranspiration.

Table A.1: An overview of studies on regional crop yield prediction based on satellite-driven LUE modeling.

Study	Sensor	Spatial, temporal res.	FPAR from	LUE_{max}	LUE_{act}	T_s	W_s	Crops	Land use	Region	Validation	Year(s)
Lobell et al. 2002	AVHRR	8 km, 14 day	NDVI	Biome-specific	Down-regulation	Deviation from T_{opt} and 20 °C	Soil moisture	Corn, soybean, wheat	County statistics	North America	Statistical data	1982-1998
Bastiaanssen & Ali 2003	AVHRR	1.1 km, bi-monthly (irregular)	NDVI	Crop-specific	Down-regulation	Low T; deviation from T_{opt}	Evaporative fraction (SEBAL)	Wheat, rice, cotton, sugar-cane	Classification	Indus Basin, Pakistan	Statistical data	1993-1994
Lobell et al. 2003	Landsat	30 m, 7 acquisitions	NDVI, SR	Constant, based on field studies		-	-	Maize, wheat, soybean	Classification	Yaqui valley, Mexico	Statistical data	1993-1994; 1999-2000
Reeves et al. 2005	MODIS	1 km, 8 day	MOD17	Biome-specific	Down-regulation	T_{min}	VPD	Wheat	MODIS land cover	North America	Statistical data	2001, 2002
Tao et al. 2005	AVHRR		Comparison of CASA and GLO-PEM2 (see text)					Maize	Crop map	China	Statistical data, experimental stations	1999, 2000
Fensholt et al. 2006	MODIS	1 km, 8 day	Customized MOD17	Biome-specific	Down-regulation	T_{min}	VPD, SIWSI	MODIS cropland biome	MODIS land cover	Sahel	Field sites	2001
Patel et al. 2006	MODIS	250 m, 8 day	NDVI	LUE depends on growth stage, T and W stress via field measurements				Wheat	Two AWIFS scenes	Haryana state, India	Statistical data	2003-2004
Moriondo et al. 2007	AVHRR	0.01°, 10 day	NDVI	Static for all growth stages		H_i from NDVI ranges		Wheat	Statistical data, AVHRR NDVI	Italy	Statistical data	1986-2003/2004
Shi et al. 2007	MODIS	250 m, 16 day	FPAR down-scaling via NDVI	Crop-specific	Down-regulation	T_{min}	VPD	Cotton	Classification	Khorezm, Uzbek-istan	Statistical data	2002
Pan et al. 2009	Landsat	30 m, 2 acquisitions	NDVI, SR	LUE calibrated for season		-	-	Cereal crops, alfalfa	Quickbird	China	Statistical and field data	2005
Liu et al. 2010	Landsat, CASI	30 m, 8 acquisitions	MTVI; calibration of canopy model	Empirical determination of seasonal LUE		-	CWSI	Corn	Site-specific	Canada	Biomass at field site	2001, 2006
Maselli et al. 2011	MODIS	250 m, 16 day	NDVI	Static for all growth stages		H_i from NDVI ranges		Wheat	Statistical data, MODIS NDVI	Tuscany, Italy	Statistical data	2001-2007
This study - high resolution	Rapid Eye	Field (6.5 m aggregated), 10 acquisitions	NDVI (calibrated)	Crop-specific	Down-regulation	T_{min}, T_{max}	$\frac{ET_{act}}{ET_c}$	Cotton, rice	Classification	Khorezm, Uzbek-istan	Harvest information	2009
This study - medium resolution	MODIS	250 m, 8 day	NDVI (calibrated)	Crop-specific	Down-regulation	T_{min}	$\frac{ET_{act}}{ET_c}$	Cotton, rice	Classification	Khorezm, Uzbek-istan	Statistical data, RapidEye results	2003-2009

A.3 Hot spot analysis for rice (2003 to 2009) at the MODIS scale

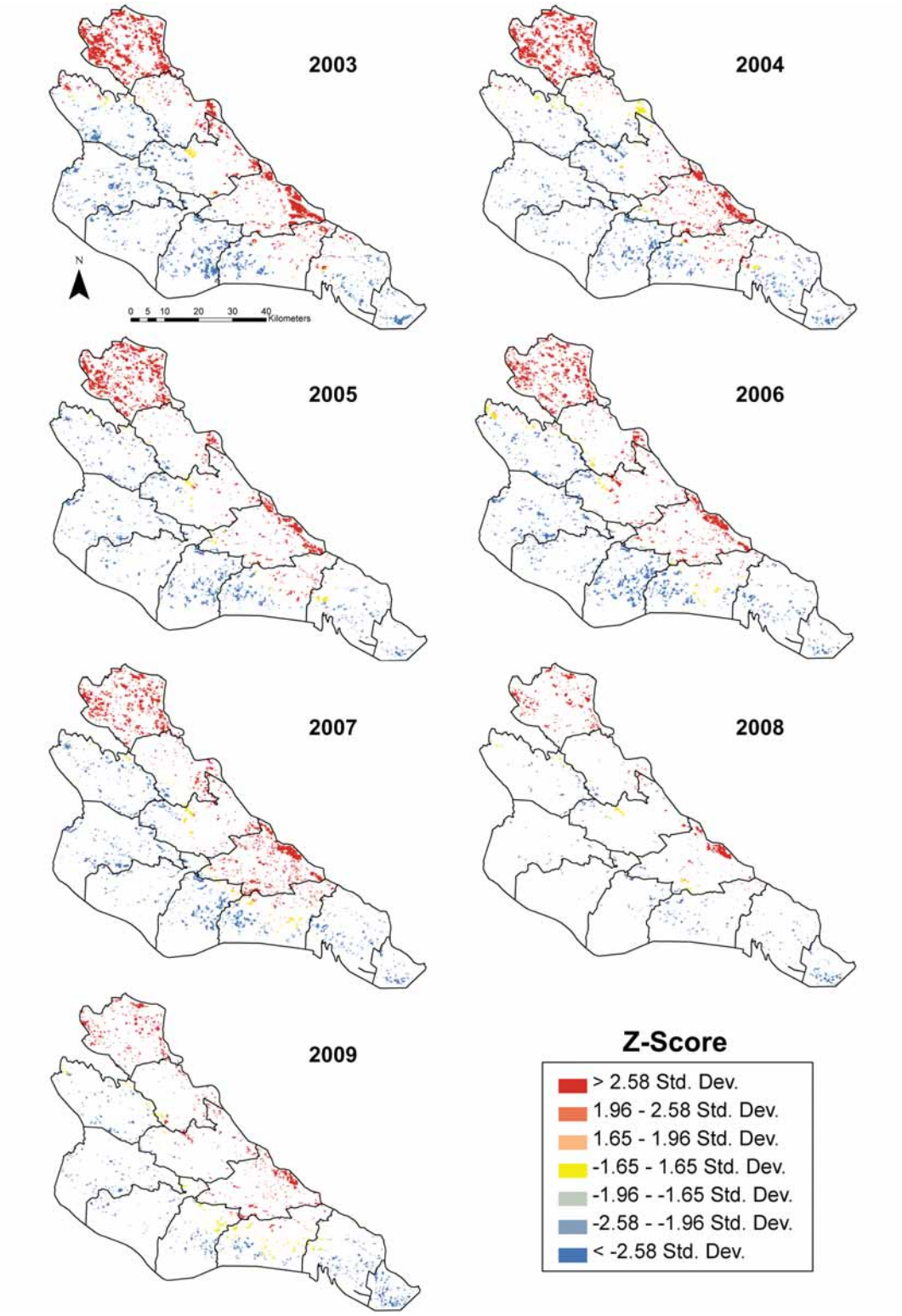

Figure A.1: Hot spot analysis for rice from 2003 to 2009 at the MODIS scale.

Acknowledgments

This thesis would not exist without the guidance and support of many people. First and foremost I would like to thank Prof. Christopher Conrad for supervising my thesis. He supported me in the development of my own ideas and guided me whenever I was confronted with problems. I am also grateful for everything I learned during my time at the Department of Remote Sensing in Würzburg. That's also why I especially would like to express my gratitude to Prof. Stefan Dech, who was always supportive of my work. Furthermore I want to thank Prof. Dr. Heiko Paeth for accepting to be the second advisor of my thesis. His critical questions and ideas helped me to refine my work. Dr. Gerd Rücker was mentoring me during the first one and a half years of my time as a doctoral student. His ideas, and our discussions in Germany and Uzbekistan, helped me to find the right direction of my research.

Mentors are one thing, but equally important are the colleagues one shares his daily life with. That's why I want to thank my friends and members of the remote sensing unit in Würzburg for creating a unique working atmosphere. I especially want to thank:

- Miriam for being a great office/roommate (and for Fin!).
- Gunther for help in all the little things, and for being crazy enough to be part of the 'other' project.
- Sarah, Fabian and Patrick for an unforgettable time in the office, for running sessions and for the occasional night out.
- Julian for being an essential help in all things programming-related.

Of course I want to thank all people who took the time to read this thesis and gave me helpful advice for its improvement.

On the part of the Khorezm project, special thanks go to Dr. John Lamers for the support during my field work in Khorezm and for valuable feedback during my presentations in Urgench and Bonn. Without his never-ending willingness to deal with problems great and small, my field work (and those of everyone else) would have been impossible. I am also grateful to Dr. Ahmad Manschadi for positive feedback and for co-authoring some of my work. His presence at the guest house in Urgench always ensured that people would not get rusty and field trips organized. Special credit goes to Liliana for a great job in organizing daily life in Urgench.

There were many more people involved in this daily routine, but one must definitely mention 'Totja Galja' for the best Plov in Urgench and for keeping people well fed in the guest house. The guest house was a very important location during the stays in Urgench, and I want to thank all my friends and colleagues for some memorable months in that house. I remember the special 'guest house cinema', outdoor sit-ins and one or two parties very gladly (and let's not forget our adventures into Uzbek nightlife).

Furthermore I want to thank Andrea Ehammer, for letting me mentor her master thesis and for greatly helping me out during the field work in Khorezm. Large parts of this data were the foundation of chapter 4 of this dissertation and of the journal article mentioned there. Here, I would also like to acknowledge that chapter 6 of this thesis is based on the work of Teresa Dürbeck, who wrote her M.A. thesis in the framework of the Khorezm project. Lastly, I want to mention that all RapidEye data used in this study was provided by the RapidEye Science Archive (RESA), which is hosted by the German Aerospace Agency (DLR).

I especially want to thank Claudia and Björn for helping me with the English corrections of this dissertation.

Last but not least, I want to thank my friends for being what they are. I am also very grateful to my parents, who always supported me in the decisions I made. Finally, I want to thank Andrea for sharing all the highs and lows during the time it took to complete this thesis.

Erklärung zur selbständigen Verfassung der vorliegenden Arbeit

Hiermit erkläre ich, dass ich die vorliegende Arbeit mit dem Titel "Spatial and temporal patterns of crop yield and marginal land in the Aral Sea Basin: derivation by combining multi-scale and multi-temporal remote sensing data with a light use efficiency model" selbständig und nur unter Verwendung der angegebenen Quellen und Hilfsmittel angefertigt habe.

Würzburg, 15. Februar 2013 Sebastian Fritsch